
Modified gravity and cosmology with two extra dimensions

Robert Schneider



München, 2016

Modified gravity and cosmology with two extra dimensions

Robert Schneider

Dissertation
an der Fakultät für Physik
der Ludwig-Maximilians-Universität München

vorgelegt von
Robert Schneider
aus München

München, den 24. Februar 2016

Erstgutachter: Prof. Dr. Stefan Hofmann
Zweitgutachter: Prof. Dr. Georgi Dvali

Datum der mündlichen Prüfung: 20. April 2016

As far as the laws of
mathematics refer to reality,
they are not certain; and as
far as they are certain, they
do not refer to reality.

(Albert Einstein)

CONTENTS

Zusammenfassung	xi
Abstract	xiii
Conventions	xv
Acronyms	xvii
1 Introduction	1
1.1 Concordance cosmology	3
1.1.1 Theory	3
1.1.2 Observations	5
1.1.3 Inflation	9
1.2 The cosmological constant problem	9
1.2.1 Weinberg's no-go theorem	12
1.3 Braneworlds and Degravitation	13
1.3.1 Other reasons to modify gravity	15
1.4 DGP model	16
1.4.1 Theory	16
1.4.2 Cosmology	17
1.5 Outline and Summary	26
2 Interpretation of the Weyl tensor	31
2.1 Summary	32
2.2 Introduction	32
2.3 Standard Interpretation of Weyl components	33
2.4 Examples where the standard interpretation works	37
2.4.1 Static plane	37
2.4.2 Schwarzschild	39
2.4.3 Plane wave	39
2.4.4 Spherical wave	40
2.5 Examples where the standard interpretation fails	41
2.5.1 Static cylinder	43
2.5.2 Einstein-Rosen waves	45



2.6	Pirani's criterion	48
2.7	Thorne's C-energy	48
2.8	Conclusion	51
3	Nonreflecting boundary condition for cylindrical waves	53
3.1	Definition of the problem	53
3.2	Prelude: Plane waves	54
3.3	Cylindrical waves	57
3.4	Evaluating the kernel	59
3.4.1	Summary and discussion	62
3.5	Numerical example	64
3.5.1	Discretization	65
3.5.2	Result and discussion	66
4	The universe as a cosmic ring	69
4.1	Setup	70
4.2	Deriving modified Friedmann equations	71
4.2.1	Cosmological ansatz and field equations	71
4.2.2	On-brane equations	73
4.2.3	Excluding incoming bulk waves	75
4.2.4	Excluding Newton-like bulk fields	78
4.3	Solutions and comparison to observations	80
4.3.1	Vanishing azimuthal pressure	81
4.3.2	Stabilized fifth dimension	86
4.4	Summary and outlook	87
	Appendices	91
4.A	Full bulk solution	91
4.B	Fixing the residual gauge	95
5	The universe as a cosmic string	97
5.1	Static deficit angle solution	100
5.2	Regularization	102
5.3	Cosmology	106
5.3.1	Coordinates and field equations	107
5.3.2	Generalized static solution	115
5.3.3	Boundary and initial conditions	116
5.3.4	Numerical algorithm	119
5.3.5	Numerical solutions	121
5.3.6	Scanning parameter space	127
5.4	Ghost or no ghost? Resolving the tension	132
5.4.1	The problem with ghosts and tachyons	134
5.4.2	Linear stability analysis	135

5.5	Discussion	146
5.5.1	EFT perspective	147
5.5.2	Phenomenology	149
Appendices		157
5.A	Non-stabilized circumference	157
5.A.1	Nonlinear cosmology	157
5.A.2	Linear ghost analysis	159
5.B	Numerical errors and consistency checks	162
6	Super-critical cosmic strings	165
6.1	Summary	165
6.2	Introduction and outline	166
6.3	Coordinates and geometry	169
6.3.1	Induced geometry	170
6.3.2	Super-criticality	171
6.3.3	Junction conditions	172
6.4	Static solution	174
6.5	Numerical results	175
6.5.1	Sub-critical tension	175
6.5.2	Super-critical tension	177
6.5.3	Radial geometry	178
6.6	Analytic results	182
6.7	Removing the conical singularity	187
6.8	Parameter plot	189
6.9	Braneworld in 6D	190
6.10	Conclusion and outlook	192
Appendices		195
6.A	Classification of exterior geometries	195
6.A.1	Changes of character in vacuum	196
6.A.2	Changes of character across the shell	197
6.B	Co-moving coordinates	198
6.C	Validity of EFT	199
7	The universe on a rugby ball	201
7.1	Introduction and summary	201
7.1.1	Conventions and notation	204
7.2	Delta branes with BLF	204
7.2.1	Ansatz	205
7.2.2	Maxwell sector	205
7.2.3	Counter term	207
7.2.4	Dilaton sector	208
7.2.5	Gravitational sector	209



7.2.6	Condition for 4D flatness	210
7.2.7	Explicit 4D flat solutions	211
7.2.8	Fine-tuning	212
7.2.9	Constraint	213
7.3	Breaking scale invariance on thick branes	214
7.3.1	Ring regularization	215
7.3.2	Angular pressure and 4D curvature	216
7.3.3	Volume dependence	217
7.3.4	Phenomenology	218
7.3.5	Numerical results and fine-tuning	219
7.4	Conclusion	228
Appendices		231
7.A	Agreement with a specific UV model	231
Bibliography		233
Acknowledgments		249

ZUSAMMENFASSUNG

In dieser Dissertation untersuchen wir die gravitativen Konsequenzen von Theorien, in denen die vier Raumzeit Dimensionen unseres Universums um zwei räumliche Extradimensionen erweitert werden. Insbesondere liegt der Fokus auf Branen-Konstruktionen, die davon ausgehen, dass unsere Welt auf einer Hyperebene im höherdimensionalen Bulk eingebettet ist, was große oder gar unendlich ausgedehnte Extradimensionen ermöglicht. Unsere Motivation, solche Modelle zu studieren, rührt hauptsächlich von deren prinzipieller Möglichkeit, das Kosmologische Konstanten (KK) Problem mittels Degravitation zu lösen: Die KK krümmt nur die Extradimensionen und lässt die Branengeometrie flach.

Ein Hauptunterschied zum einfacheren Fall einer Kodimension eins Brane ist, dass hier Gravitationswellen in den Bulk emittiert werden können—selbst für 3D homogene und isotrope Geometrien, wie sie für Kosmologie Fragestellungen relevant sind. Daher analysieren wir zunächst die Frage, wie eine Randbedingung für auslaufende Wellen implementiert werden kann, was notwendig ist um ein geschlossenes System modifizierter Friedmann Gleichungen zu erhalten, das die Branen-Evolution vorhersagt. Wir finden, dass ein potenzielles Werkzeug aus der Literatur, das auf einer bestimmten Zerlegung des Weyl-Tensors beruht—während es für ebene Gravitationswellen anwendbar ist—für zylindrische Wellen versagt. Dieses Versagen steht im Zusammenhang mit der Tatsache, dass es bereits unmöglich ist, ein- und auslaufende lineare zylindrische Wellen (auf einer flachen Raumzeit) lokal zu trennen; dies demonstrieren wir, indem wir die entsprechende nichtreflektierende Randbedingung explizit herleiten, welche nichtlokal in der Zeit ist.

Anschließend betrachten wir eine Verallgemeinerung des Dvali-Gabadadze-Porrati (DGP) Modells, die zusätzlich zu der einen unendlichen Kodimension eine weitere, kompakte Branen-Dimension enthält. Da die 3D maximal symmetrische Brane hier ebene Wellen emittiert, können wir das Weyl-Tensor Kriterium verwenden um einlaufende Bulk-Wellen auszuschließen, und so die resultierenden Friedmann Gleichungen herzuleiten. Wenn die kompakte Dimension stabilisiert wird, reproduzieren wir DGP Kosmologie, finden jedoch Indikationen dafür, dass die Stabilisierung versagen sollte wenn die KK dominiert, was zusätzliche, potenziell interessante Modifikationen zu späten Zeiten zur Folge hätte. Wenn die kompakte Richtung hingegen frei expandieren kann, gibt es dynamisch degravitierende Lösungen—die allerdings kein 4D Regime aufweisen und daher ausgeschlossen sind, was wir durch einen Fit an Supernova



Daten demonstrieren.

Danach wenden wir uns der Kodimension zwei Version des DGP Modells zu. Indem wir das volle nichtlineare gekoppelte Bulk-Branen System für kosmologische Symmetrien auf der (regularisierten) Brane numerisch lösen, zeigen wir, dass in einer Region des Parameterraums eine KK—aber auch jede andere Fluid Komponente—dynamisch degravitiert wird, und eine statische Geometrie unter Aussendung von Einstein-Rosen Wellen angenähert wird. Für andere Modellparameter beobachten wir pathologische, super-beschleunigende Lösungen. Der Ursprung dieses instabilen Verhaltens lässt sich auf eine tachyonische Geist Mode zurückführen, die wir in diesem Parameterbereich durch die Analyse linearer Metrik-Fluktuationen um einen nicht-trivialen reinen Tensions-Hintergrund identifizieren. Während wir damit das Geist-Resultat auf Minkowski aus der Literatur bestätigen, gewinnen wir die wichtige Einsicht, dass der Geist verschwindet wenn die Branenspannung groß genug ist, wodurch das Modell mit der physikalischen Erwartung einer gesunden effektiven Theorie bei niedrigen Energien in Einklang gebracht wird. Leider ist der gesunde Bereich wieder nicht mit einem adäquaten 4D Gravitationsregime kompatibel und daher phänomenologisch ausgeschlossen.

Die vorhergehende Analyse beschränkte sich auf sub-kritische Branenspannungen, für die der Defizitwinkel der konischen Außenraumgeometrie kleiner als 2π ist. Im darauf folgenden Kapitel untersuchen wir super-kritische Spannungen (zunächst in 4D) und finden, dass die (regularisierte) statische Lösung nicht mehr stabil ist. Stattdessen dehnt sich die axiale Richtung mit einer asymptotisch konstanten Expansionsrate aus, und die Außenraumgeometrie (die notwendigerweise kompakt ist) nimmt die Form einer wachsenden Zigarre an. Es gelingt uns, eine analytische Relation zwischen Expansionsrate und Branenspannung herzuleiten, welche—auf das 6D Setup übertragen—lediglich die KK um einen (kleinen) konstanten Betrag verschiebt, und daher für das KK Problem nicht hilfreich ist.

Zuletzt analysieren wir den Fall von zwei endlichen Kodimensionen innerhalb des “supersymmetric large extra dimensions” (SLED) Modells. Zuerst zeigen wir, dass—entgegen Behauptungen in der jüngeren Literatur—ein Branen-lokalisierter Fluss nicht helfen kann, die Feinabstimmung zu verhindern, die für 4D flache Lösungen nötig ist (und hier durch die Flussquantisierung erzwungen wird); dies liegt im Wesentlichen daran, dass nur skaleninvariante Branen-Kopplungen eine flache Brane garantieren. Danach adressieren wir die Frage, ob ein realistischeres Modell mit einer endlichen Branen-Dicke sowie Skaleninvarianz brechenden Kopplungen dennoch erfolgreich sein könnte, indem es eine zwar nicht-verschwindende, aber hinreichend kleine 4D Krümmung vorhersagt, finden jedoch eine negative Antwort: Falls das Volumen der Extradimensionen innerhalb seiner derzeit erlaubten Grenzen liegt, liefern beide Effekte einen viel zu großen Krümmungsbeitrag, es sei denn die Branen-Dicke wäre viele Größenordnungen kleiner als die Bulk Planck Länge, und eine Art von Feinabstimmung wäre wieder im Spiel.

ABSTRACT

In this thesis, we investigate the gravitational consequences of theories in which the four spacetime dimensions of our universe are augmented by two spatial extra dimensions. More specifically, the focus is on braneworld scenarios, where our world is confined on a hypersurface in the higher-dimensional bulk, allowing the extra dimensions to be large or even infinite. Our main motivation for studying such models is that they could in principle be able to solve the cosmological constant (CC) problem via degravitation: the CC only curves the extra space, leaving the brane geometry flat.

A major difference to the simpler case of a codimension-one brane is that here, gravitational waves can be emitted into the bulk, even at the 3D homogeneous and isotropic level, as is relevant for cosmology. Therefore, we first analyze the question how an outgoing wave boundary condition can be implemented, which is necessary in order to obtain a closed set of modified Friedmann equations predicting the cosmological on-brane evolution. We find that a potential tool from the literature, provided by a certain decomposition of the Weyl tensor—while being applicable to plane gravitational waves—fails for cylindrical waves. This failure is related to the fact that it is already impossible to locally separate incoming from outgoing linear cylindrical waves (on flat spacetime), as we demonstrate by explicitly deriving the corresponding nonreflecting boundary condition, which is nonlocal in time.

We then consider a generalization of the Dvali-Gabadadze-Porrati (DGP) model, containing an additional compact on-brane dimension on top of the one infinite codimension. Since here the 3D maximally symmetric brane emits plane waves, the Weyl tensor criterion can be used to exclude incoming bulk waves, and we derive the resulting Friedmann equations. If the compact dimension is stabilized, DGP cosmology is recovered, but we find indications that the stabilization should break down when the CC starts to dominate, which would lead to additional, potentially interesting late time modifications. If, on the other hand, the compact direction is allowed to expand freely, there are dynamically degravitating solutions—which, however, lack a 4D regime and are thus ruled out, as we demonstrate by fitting to supernova data.

Next, we turn to the codimension-two version of the DGP model. By numerically solving the full nonlinear coupled bulk-brane system for cosmological symmetries on the (regularized) brane, we show that in some region of parameter space, a CC—but also any other fluid component—gets degravitated dynamically, and a static geometry is approached via the emission of Einstein-Rosen waves. For other model parameters,



pathological super-accelerating solutions are encountered. The origin of this unstable behavior is traced back to a tachyonic ghost mode which is identified in this parameter region by studying linear metric perturbations around a nontrivial pure tension background. While confirming the ghost result on Minkowski from the literature, we gain the important insight that the ghost disappears if the brane tension is large enough, thereby reconciling the model with the physical expectation of a healthy low energy effective theory. Unfortunately, the healthy region is again incompatible with an appropriate 4D gravity regime, and therefore ruled out phenomenologically.

The preceding analysis only covered sub-critical brane tensions, meaning that the deficit angle of the exterior conical geometry is less than 2π . In the following chapter, we investigate super-critical tensions (first in 4D), and find that the (regularized) static solution is no longer stable. Instead, the axial direction expands at an asymptotically constant rate, and the exterior geometry (which is necessarily compact) takes the form of a growing cigar. We are able to derive an analytic relation between the expansion rate and the tension, which—when adapted to the 6D setup—only yields a (small) constant shift in the CC, and can therefore not help with the CC problem.

Finally, the case of two finite codimensions is analyzed within the model of supersymmetric large extra dimensions (SLED). First, we show that—contrary to recent claims in the literature—a brane-localized flux cannot help avoiding the fine-tuning (which is here imposed by flux quantization) in order to obtain 4D flat solutions, basically because only scale invariant brane couplings ensure a flat brane. Next, we ask if a more realistic model with a finite brane width and scale invariance breaking couplings could still be successful by predicting a small enough (albeit nonzero) 4D curvature, but find a negative answer: If the extra-dimensional volume is within its currently allowed range, both effects give way too large contributions to the curvature, unless the brane width were many orders of magnitude below the bulk Planck length, and again some sort of fine-tuning were invoked.

CONVENTIONS

The following conventions will be used throughout this thesis:

- We work in units in which $\hbar = c = 1$. The reduced Planck mass M_{Pl} is thus related to Newton's constant G_{N} via $M_{\text{Pl}}^2 \equiv 1/(8\pi G_{\text{N}})$.
- Apart from Chap. 7, our sign conventions for the metric, Riemann and Einstein tensor are “+++” as defined (and adopted) in [MTW73]; thus, in particular, the metric is “mostly plus”. In Chap. 7, we use Weinberg's convention “+−−”, where the Riemann and Einstein tensor have the opposite signs as in “+++”.
- The total dimension of spacetime is denoted by $d = 4 + n$, with n being the number of extra dimensions.
- Capital Latin indices M, N, \dots denote d -dimensional, Greek indices μ, ν, \dots four-dimensional spacetime indices.
- Greek indices α, β, \dots refer to five-dimensional spacetime indices on the brane with one compact extra dimension.
- Small Latin indices i, j, \dots label the three-dimensional spatial coordinates (except for Chap. 2, where they denote the two perpendicular tetrad components).
- Tensor (or vector) fields, when suppressing their indices, are written in boldface, e.g. \mathbf{g} for the metric with components $g_{\mu\nu}$.
- The Minkowski metric is denoted by $\boldsymbol{\eta}$.
- The determinant of the metric \mathbf{g} is abbreviated by g .
- The Riemann tensor is denoted by \mathbf{R} , the Weyl tensor by \mathbf{C} , the Ricci tensor by \mathcal{R} , the Ricci scalar by \mathcal{R} , the Einstein tensor by \mathbf{G} and the energy momentum tensor by \mathbf{T} .
- Mathematical constants are written in roman type to distinguish them from variable names or indices, e.g. “e” and “i” for Euler's number and the imaginary unit, respectively.
- 6D is short for “6-dimensional”, etc; whether the dimensions are all spacelike or contain time will be clear from the context.



ACRONYMS

Here is a list of the frequently used acronyms:

BIG	Brane induced gravity
CC	Cosmological constant
CDM	Cold dark matter
CMB	Cosmic microwave background
DGP	Dvali-Gabadadze-Porrati
DOF	Degree of freedom
EFT	Effective field theory
EOS	Equation of state
ER	Einstein-Rosen
FRW	Friedmann-Robertson-Walker
GGP	Gibbons-Gueven-Pope
GR	General relativity
LLR	Lunar laser ranging
NEC	Null energy condition
NO	Nielsen-Olesen
ODE	Ordinary differential equation
PDE	Partial differential equation
SI	Scale invariance
SN	Supernova



CHAPTER 1

INTRODUCTION

The modern theory of cosmology is in a very paradoxical situation: On the one hand, the current concordance model, called Λ CDM, which has emerged over the past few decades, is in astonishing agreement with a plethora of high precision observations, and draws a consistent picture of our universe from a minuscule fraction of a second after the big bang until today. On the other hand, the perhaps simplest ingredient of the model, which is completely characterized by one single number—the cosmological constant Λ —presents the worst mismatch between theoretical expectation and actual observation in the entire history of science. To be clear, this does not mean that the model is inconsistent; after choosing a certain value for Λ , the model works perfectly well and matches practically all observations. Furthermore, the precise value of Λ cannot even be *calculated* from first principles, since we do not know the (hypothetical) fundamental theory that would be valid up to arbitrarily high energy scales. Without such a theory of everything, the best we can do is regard our quantum field theories (like the Standard Model) as effective field theories (EFT), valid only up to some energy cutoff M . Then, like any other parameter of a quantum field theory that undergoes renormalization, the actual value of Λ can only be obtained by *measuring* it at some renormalization scale; only the renormalization group flow¹ of Λ then is a robust theoretical prediction. Since there is only one true measurement² of Λ —through the observed accelerated expansion of our universe—there can be no inconsistency between theoretical prediction and experiment. This is why, above, we deliberately referred to the problem as a tension between observation and theoretical *expectation*, not prediction. This expectation, as will be discussed in more detail in Sec. 1.2, comes from our experience that the smallness of some parameter in a theory can usually be understood in a *natural* way. On the contrary, when raising the cutoff M of our EFT, the observed smallness of Λ can only be understood by a more and more severe *fine-*

¹Here, we mean the change of Λ as the masses are varied, not a physical change with energy.

²In fact, radiative corrections do not even lead to a momentum dependent, physical running of Λ ; therefore, since we cannot change the masses of particles and repeat the measurement of Λ , its RG flow is not testable even in principle.



tuning of the bare parameter appearing in the resulting more fundamental theory. If we take the Standard Model EFT to be valid up to the Planck scale (which is certainly an upper bound), the required fine-tuning spans ~ 118 decimal places.³ If, instead, the cutoff is only just above the electroweak scale (that is the lower bound), still a fantastic number of ~ 54 decimal places have to be tuned. But even if we take only the electron into account, there is a discrepancy of ~ 32 orders of magnitude. This, in short, is the cosmological constant (CC) problem.

In the Standard Model, there is a closely related problem, called the (gauge, or electroweak) hierarchy problem. It asks why the observed Higgs mass is so much smaller than the maximum Planckian cutoff (or than yet unobserved heavy particles between the electroweak and the Planck scale). However, in that case new physics beyond the Standard Model (like supersymmetry) provides a potential way out. This is not the case for the CC problem because, as discussed above, it is already present at much lower energies, up to which we have already tested the Standard Model. Therefore, the CC problem cannot be addressed by UV physics—it is, instead, an IR problem.

Another fundamental difference between the hierarchy and CC problem is that the latter only arises once gravity is included. In fact, without gravity, only energy differences are physically relevant, and so the zero point (or vacuum) energy is not observable. However, according to general relativity (GR), every source of energy inevitably curves spacetime, hence so does the vacuum energy. Consequently, the only way to measure Λ is in fact by measuring the spacetime curvature of our universe and then inferring the value of Λ using the Einstein equations.

In the same way as the hierarchy problem motivates going beyond the Standard Model, and putting a lot of effort into finding signs of such new physics at particle accelerators, the CC problem therefore naturally suggests to come up with IR modifications of GR and pin down their observational consequences. More specifically, one would like to build a theory of gravity in which spacetime curvature is insensitive to the vacuum energy,⁴ but which does not spoil the success of GR in the regime where it has been tested so successfully. This rather ambitious goal turns out to be notoriously difficult to achieve. As will be discussed in Sec. 1.3, a promising framework in this regard is provided by the braneworld paradigm, in particular if our universe is assumed to be embedded into a six-dimensional bulk. The main subject of this thesis is to study particular models within this class (primarily codimension-two brane-induced gravity), and to test them for theoretical consistency, their potential to address the CC problem, as well as their phenomenological viability.

But before turning to these modifications of GR, it is worthwhile to briefly review Λ CDM—the state of the art model for the cosmological evolution of our universe. This is done in Sec. 1.1, where we also sketch the main observational probes that give us great confidence in the correctness of this model. Then, in Sec. 1.2, we will discuss the CC problem in more detail, and Sec. 1.3 explains why extra dimensions

³The numbers refer to the tuning of the corresponding vacuum energy density $\rho_{\text{vac}} \equiv M_{\text{Pl}}^2 \Lambda$, cf. Sec. 1.2.

⁴This idea goes under the name of “degravitation”, see Sec. 1.3.

(and in particular two of them) could help. Since we will be especially interested in the case of infinite extra dimensions, the 5D prototype—called the DGP model—will be reviewed in Sec. 1.4, with emphasis on the geometrical aspects which are important when deriving the cosmological brane evolution. This introductory chapter will be concluded in Sec. 1.5 with an outline of the rest of this thesis, as well as a summary of the main results.

1.1 Concordance cosmology

1.1.1 Theory

The Λ CDM model assumes that gravity is described by GR [Ein16a] on all relevant scales. GR can be defined by a variational principle with the following action:

$$S = S_{\text{EH}} + S_{\text{m}} = \int d^4x \sqrt{-g} \left(\frac{M_{\text{Pl}}^2}{2} \mathcal{R} + \mathcal{L}_{\text{m}} \right). \quad (1.1.1)$$

The first term is usually called the Einstein-Hilbert action [Hil15, Ein16b]. Here, g is the determinant of the metric $g_{\mu\nu}$, \mathcal{R} is the Ricci scalar (i.e. the trace of the Ricci tensor $\mathcal{R}_{\mu\nu}$) constructed from $g_{\mu\nu}$, and \mathcal{L}_{m} denotes the Lagrangian density of all the matter (i.e. non-gravitational) degrees of freedom. Varying this action with respect to $g^{\mu\nu}$ gives Einstein's field equations:⁵

$$M_{\text{Pl}}^2 G_{\mu\nu} = T_{\mu\nu}, \quad (1.1.2)$$

where $G_{\mu\nu} := \mathcal{R}_{\mu\nu} - g_{\mu\nu} \mathcal{R}/2$ is the Einstein tensor and

$$T_{\mu\nu} := -\frac{2}{\sqrt{-g}} \frac{\partial(\sqrt{-g} \mathcal{L}_{\text{m}})}{\partial g^{\mu\nu}} = g_{\mu\nu} \mathcal{L}_{\text{m}} - 2 \frac{\partial \mathcal{L}_{\text{m}}}{\partial g^{\mu\nu}} \quad (1.1.3)$$

is the energy-momentum tensor. Note that we assume the cosmological constant Λ to be included in \mathcal{L}_{m} , i.e. $\mathcal{L}_{\text{m}} \supset -M_{\text{Pl}}^2 \Lambda$. Classically, it is equivalent to the minimum of the potential energy of all the matter degrees of freedom. For non-gravitational physics, this absolute value is irrelevant, because only energy differences matter. With gravity, however, this is not the case because according to the Einstein equations (1.1.2), every form of energy—including vacuum energy $\rho_{\text{vac}} \equiv M_{\text{Pl}}^2 \Lambda$ —inevitably curves spacetime.

⁵If the spacetime has a boundary, on which variations of the first (orthogonal) derivatives of $g_{\mu\nu}$ are not required to vanish, one has to add the York-Gibbons-Hawking boundary term [Yor72, GH77] to the action (1.1.1) in order to arrive at the correct Einstein equations (see also [Wal84, Appendix E]).



Background evolution

The other main assumption, usually referred to as the cosmological principle, is that our universe is spatially homogeneous and isotropic on large scales.⁶ As a consequence of these symmetries, one can choose coordinates in which the metric takes the Friedmann-Robertson-Walker (FRW) form:

$$ds^2 \equiv g_{\mu\nu} dx^\mu dx^\nu = -dt^2 + a(t)^2 \left(\frac{dr^2}{1 - kr^2} + r^2 d\Omega^2 \right). \quad (1.1.4)$$

Here, $d\Omega^2 \equiv d\theta^2 + \sin^2 \theta d\phi^2$ is the line element of the unit 2-sphere, and $k \in \{0, +1, -1\}$ corresponding to a (three-dimensional) spatially flat, closed and open geometry, respectively. The entire dynamics of this metric is encoded in the single function of time $a(t)$, called the scale factor, the evolution of which is determined by the Einstein equations (1.1.2). The energy-momentum tensor is also restricted by the assumed symmetries and has to take the form

$$T^\mu{}_\nu = \text{diag}(-\rho, p, p, p), \quad (1.1.5)$$

corresponding to a perfect fluid with energy density ρ and pressure p .

Plugging (1.1.4) and (1.1.5) into (1.1.2) results in two independent equations of motion for the scale factor, the Friedmann equations [Fri22, Fri24]:

$$3M_{\text{Pl}}^2 \left[\left(\frac{\dot{a}}{a} \right)^2 + \frac{k}{a^2} \right] = \rho, \quad (1.1.6a)$$

$$-M_{\text{Pl}}^2 \left[2\frac{\ddot{a}}{a} + \left(\frac{\dot{a}}{a} \right)^2 + \frac{k}{a^2} \right] = p, \quad (1.1.6b)$$

where we introduced the short hand notation of a dot representing a derivative with respect to t . Energy conservation $\nabla_\mu T^\mu{}_\nu = 0$, which is implied by the Einstein equations due to the Bianchi identity $\nabla_\mu G^\mu{}_\nu \equiv 0$, yields one further nontrivial equation:

$$\dot{\rho} + 3\frac{\dot{a}}{a}(\rho + p) = 0. \quad (1.1.7)$$

This equation, together with the first (or constraint) Friedmann equation (1.1.6a) already implies the second Friedmann equation (1.1.6b). Therefore, the complete set of dynamical equations is given by Eqs. (1.1.6a) and (1.1.7). Since there are three unknown functions of time— $a(t)$, $\rho(t)$ and $p(t)$ —this only constitutes a closed system, determining the evolution, after one imposes an equation of state (EOS) $p = p(\rho)$; this is usually taken to be a linear relation $p = w\rho$. In this case, Eq. (1.1.7) can immediately be integrated, yielding

$$\rho \propto a^{-3(1+w)}. \quad (1.1.8)$$

⁶Originally a philosophical assumption, the cosmological principle has now in fact been confirmed observationally, cf. Sec. 1.1.2.

In the Λ CDM model, one assumes the cosmic fluid to be composed of three different components: radiation with EOS parameter $w = 1/3$, non-relativistic matter (or dust) for which $w = 0$, and a cosmological constant Λ (or, equivalently, vacuum energy $\rho_{\text{vac}} \equiv M_{\text{Pl}}^2 \Lambda$, cf. Sec. 1.2) corresponding to $w = -1$. In these cases the energy conservation equation can easily be integrated giving $\rho_{\text{rad}} \propto a^{-4}$, $\rho_{\text{m}} \propto a^{-3}$ and $\rho_{\text{vac}} \propto a^0 = \text{const.}$

The only equation left is the first Friedmann equation (1.1.6a), which can now conveniently be rewritten in the form

$$\Omega_{\Lambda} + \Omega_k \left(\frac{a_0}{a}\right)^2 + \Omega_{\text{m}} \left(\frac{a_0}{a}\right)^3 + \Omega_{\text{rad}} \left(\frac{a_0}{a}\right)^4 = \frac{H^2}{H_0^2}. \quad (1.1.9)$$

Here we introduced the Hubble parameter $H := \dot{a}/a$, the subscript “0” denotes evaluation at $t = t_0$ (today), and the dimensionless constants Ω_i are defined as the density ratios $\Omega := \rho_0/(3M_{\text{Pl}}^2 H_0^2)$ for each fluid component, as well as the spatial curvature term $\Omega_k := -k/(H_0^2 a_0^2)$. Evaluating Eq. (1.1.9) today, it simply becomes

$$\sum_i \Omega_i = 1. \quad (1.1.10)$$

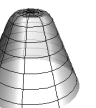
1.1.2 Observations

Several independent observational probes show that our universe can very well be described by the Λ CDM model with a spatially flat geometry ($k = 0$), and with the cosmic fluid today made up of $\Omega_{\Lambda} \approx 0.7$ and $\Omega_{\text{m}} \approx 0.3$, with the matter part consisting of only $\Omega_{\text{b}} \approx 0.05$ baryons and $\Omega_{\text{DM}} \approx 0.25$ non-baryonic, so-called (cold) “dark matter”. Let us now summarize the main observational tests⁷ that lead to this well-established picture.

Type Ia supernovae

For a given choice of parameters Ω_i , Eq. (1.1.9) allows us to calculate the expansion history of the universe. In fact, since H only enters quadratically, its sign is not fixed, and so the theory does not tell us whether the universe is expanding or contracting. Therefore, only observations can tell us which branch to choose, and it turns out that we live in an expanding universe. This was famously first discovered by Hubble, who observed that distant galaxies show a redshift that linearly grows with their distance [Hub29]. Interpreting this redshift as the Doppler-shift due to the recessional velocity of the galaxies, one arrives at a linear distance-velocity relation, the constant of proportionality—the Hubble constant—given by $H_0 > 0$.

⁷Note that the list given here is not complete; for instance, we do not elaborate on weak lensing, cluster counts, or galaxy rotation curves, just to name a few. Since this would be beyond the scope of this thesis, we instead refer to the literature for more comprehensive and detailed discussions of other observational probes [Wei08, A+06, BHS05].



Extending this idea to higher redshifts, the primary tool of astronomers has for a long time been to look for “standard candles”, i.e. objects of known absolute luminosity L . Measuring their redshift $z \equiv a_0/a - 1$ and apparent luminosity⁸ ℓ —or, equivalently, luminosity distance d_L , defined by $\ell = L/(4\pi d_L^2)$ —and fitting to the theoretical prediction [Wei08]

$$d_L(z) = a_0 (1+z) r(z) = (1+z) \int_0^z \frac{dz'}{H(z')} \quad (1.1.11a)$$

$$= \frac{(1+z)}{H_0 \Omega_k^{1/2}} \sinh \left[\Omega_k^{1/2} \int_{1/(1+z)}^1 \frac{dx}{x^2 \sqrt{\Omega_\Lambda + \Omega_k x^{-2} + \Omega_m x^{-3}}} \right], \quad (1.1.11b)$$

one can determine the cosmological parameters. Note that in the second line, we dropped Ω_{rad} because the contribution of radiation is negligible⁹ in the relevant redshift range. Furthermore, due to the constraint (1.1.10), only two of the remaining three Ω s determining the shape of $d_L(z)$ are independent.

The most successful class of standard candles is provided by Type Ia supernovae (SNe). They all have roughly the same absolute luminosity because the star explosion is triggered by the universal Chandrasekhar limit. Furthermore, the intrinsic scatter in luminosities can be corrected by an empirically established relation between the peak brightness and width of the corresponding light curves. Finally, SNe are bright enough to be observable up to relatively high redshifts, making them ideal candidates to directly test the expansion history of our universe. The latest observations are compatible with the flat Λ CDM model, require cosmic acceleration at 99.999% confidence [C⁺11], and yield the best fit parameter $\Omega_m = 0.295 \pm 0.034$ [B⁺14], implying $\Omega_\Lambda = 0.705 \pm 0.034$.

Since the cosmological parameters Ω_i only affect the shape of $d_L(z)$ (and not its overall normalization), the relative magnitudes of SNe are enough to determine the Ω_i . The Hubble constant H_0 , on the other hand, only enters as an overall factor, and is therefore sensitive to the absolute magnitudes. Consequently, H_0 can only be measured by building up a cosmic distance ladder, starting from standard candles in our local universe,¹⁰ e.g. Cepheid variables. The most recent analysis along these lines gives $H_0 = (73.8 \pm 2.4) \text{ km s}^{-1} \text{ Mpc}^{-1}$ [R⁺11]. Since the systematic errors lead to rather large uncertainties in H_0 , it is customary to quote results for other cosmological parameters which are independent of H_0 , and indicate the dependence on H_0 in terms of the parameter $h := H_0/(100 \text{ km s}^{-1} \text{ Mpc}^{-1}) \approx 0.7$.

⁸For historical reasons, astronomers use the apparent *magnitude* m instead of luminosity, related by $\ell \propto 10^{-2m/5}$, and similarly for the absolute magnitude. The luminosity distance is then given by $d_L = 10^{1+(m-M)/5} \text{ pc}$ [Wei08].

⁹From the CMB temperature (see below), one finds $\Omega_{\text{rad}} = 4.15 \times 10^{-5} h^{-2}$ (with $h \approx 0.7$, see below) [Wei08].

¹⁰Another intriguing possibility would be to calculate the absolute luminosity of SNe from first principles. However, this is a rather ambitious goal, because the stellar explosions involve very complicated, nonlinear physics; therefore, this method can so far not be used to replace primary distance indicators [Wei08, HGLM03].

Big bang nucleosynthesis

Following the universe’s expansion backwards in time, Eq. (1.1.9) usually¹¹ implies that there is an initial moment of time $t = 0$ at which the scale factor vanishes, implying a diverging expansion rate and energy density. This singularity—known as the big bang—signals a breakdown of classical GR, and it ultimately would have to be resolved by some theory of quantum gravity, the effects of which become important at Planckian energies $\sim 10^{19}$ GeV.

However, we can safely trust this backward extrapolation up to energies of order 10 TeV, up to which the Standard Model has been tested in accelerator experiments. In particular, one can calculate the abundances of light elements that were formed during big bang nucleosynthesis (BBN) at a temperature of order 0.1 MeV [Muk05]. Using the Standard Model to determine the various reaction rates, the light element abundances after BBN can be calculated as a function of the baryon to photon ratio. Therefore, astrophysical measurements of these abundances can be used to test the hot big bang hypothesis, and to infer the baryon density Ω_b . The predicted abundances are in very good agreement with observations, thus giving very strong confidence in the correctness of the hot big bang scenario, and imply a baryon density today of $\Omega_b h^2 = 0.021 \pm 0.001$ [Ste03, IMM⁺09]. With $h \approx 0.7$, this gives $\Omega_b \approx 0.04$; together with the SNe measurement of $\Omega_m = 0.27$, this means that the main part of the matter density must be non-baryonic, dark matter with $\Omega_{DM} \approx 0.23$.

Cosmic microwave background

After BBN, the universe was filled with a hot dense plasma of electrons and baryons. The temperature was so high that electrons could not be bound by nuclei to form atoms, and the photons were in thermal equilibrium with the hot dense baryonic matter. When the temperature became low enough to allow for neutral Hydrogen to form, the photons decoupled and started propagating freely, preserving their black body distribution. This cosmic background radiation still pervades the universe today, with a temperature that has decreased according to the expansion since recombination, resulting in a photon spectrum that is now peaked around microwave scales. This robust prediction of the hot big bang scenario was first observed by Penzias and Wilson [PW65], which can be viewed as the major turning point opening the door to today’s precision cosmology. Since then, there were several ground based as well as space experiments refining the measurement of the cosmic microwave background (CMB) over a large range of frequencies to ever higher precision. They unambiguously show that the CMB radiation has a perfect black body spectrum of temperature $T_{CMB} = (2.725\,48 \pm 0.000\,57)$ K [Fix09], which is (after subtracting the dipole due to the solar system’s peculiar motion) extremely isotropic, and only shows fluctuations of order 10^{-5} . These anisotropies are an

¹¹For a closed universe ($k > 0$) with Ω_Λ large enough, there are parameter choices for which there is no big bang singularity and the universe instead bounces and re-expands. However, this region of parameter space is excluded at very high significance by basically all relevant observations.



imprint of the density fluctuations at recombination and provide a unique opportunity to constrain cosmological parameters. However, the mere existence of the CMB radiation is already extremely valuable, as it gives unsurmountable empirical evidence for the hot big bang paradigm, as well as the assumption of isotropy.

The oscillations in the baryon-photon fluid before recombination leave a characteristic imprint of peaks and troughs in the angular power spectrum of the CMB temperature anisotropies. The concrete positions and relative heights of these peaks are, in particular, sensitive to the baryon and dark matter densities, and so these parameters can be measured by fitting the Λ CDM predictions to the observed power spectrum. Assuming a flat geometry, the best fit values of the Planck 2015 data [A⁺15a]—presenting the latest and most accurate CMB measurements to date—are $\Omega_\Lambda = 0.692 \pm 0.012$ (and thus $\Omega_m = 0.308 \pm 0.012$), $\Omega_b h^2 = 0.02226 \pm 0.00023$ and $\Omega_{\text{DM}} h^2 = 0.1186 \pm 0.0020$. The Hubble constant can also be obtained from the CMB data alone, and was determined from the Planck data as $H_0 = (67.81 \pm 0.92) \text{ km s}^{-1} \text{ Mpc}^{-1}$. Furthermore, the base Λ CDM model provided an excellent fit, and no extensions of this model were favored by the data. The Planck results are in excellent agreement with the standard theory of BBN, and in good agreement with observations of SNe and BAO¹² (see next section). The low value for H_0 , however, is in slight tension ($\sim 2\sigma$) with direct astrophysical measurements. This might be a sign for new physics, but could as yet still turn out to be caused by an underestimation of systematic errors.

Furthermore, the CMB data can be used to constrain the initial conditions of the primordial fluctuations. The observations show that the scalar perturbations are given by a Gaussian, nearly scale invariant, but slightly red-tilted spectrum. Since this is a very generic prediction of inflationary models (see Sec. 1.1.3), the CMB temperature anisotropies provide strong evidence in favor of cosmic inflation.

Large scale structure and baryon acoustic oscillations

The cosmological principle, assuming homogeneity and isotropy, is clearly violated on small scales. After all, there are planets, stars, galaxies, galaxy clusters, etc. However, observations of the large scale structure in our universe show that when averaged over the cosmic web—consisting of walls, filaments and voids—at $\sim 100 \text{ Mpc}$ scales [SYPB09, S⁺12], the universe does indeed become homogeneous.

Furthermore, the statistical distribution of galaxies is sensitive to the angular diameter distance $d_A(z) = d_L(z)(1+z)^{-2}$ and thus to the history of the Hubble parameter, i.e. $H(z)$, which in turn depends on the Ω s. The regular, periodic features in the corresponding power spectrum, caused by sound waves in the baryonic plasma in the early universe, are referred to as baryon acoustic oscillations (BAO) and provide another useful standard ruler for cosmology, see [BH10] for a review. A great advantage over standard candles like SNe is that BAO are dominated on relatively large scales, on which inhomogeneities can still be treated linearly today, and so they are only sub-

¹²There is, however, a slight tension ($\sim 3\sigma$) with recent high redshift BAO measurements [A⁺15a].

ject to well understood, linear physics. They are particularly useful for constraining cosmological parameters when combined with measurements of the CMB anisotropies. In particular, allowing for spatial curvature, the combination of CMB and BAO measurements yields $\Omega_k = 0.000 \pm 0.005$ [A⁺15a], i.e. our universe is now observed to be spatially flat to better than one percent accuracy. Furthermore, allowing the equation of state of dark energy to differ from a pure CC, for instance parametrized in the form $w(a) = w_0 + (1 - a)w_a$, the current observations give the constraints $w_0 = -1.04^{+0.72}_{-0.69}$ and $w_a < 1.32$ [A⁺14], in very good agreement with a CC.

1.1.3 Inflation

It is now widely believed that the era of radiation domination was preceded by a period of accelerated expansion, called cosmic inflation. The benefit of this scenario is twofold: First, it solves three major puzzles of the standard big bang scenario: the flatness, horizon and monopole problem; This was the original motivation to study inflationary models [Gut81, Lin82, AS82]. Second, it provides a natural mechanism to generate the primordial fluctuations in the CMB, from which all the structure in the present universe originates—via quantum fluctuations in the inflaton field, which get magnified during the inflationary expansion [MC81, Haw82, GP82, Sta82, BST83]. While the first reason is more or less a philosophical one,¹³ the second one allows to make rather robust and falsifiable predictions which can be tested by CMB measurements. This fact has given inflation the status of a scientific theory, the test of which is now a major subject of observational cosmology. Current state of the art measurements of the CMB are in perfect agreement with the simplest slow-roll inflationary models [A⁺15b].

1.2 The cosmological constant problem

The wealth of observational evidence clearly shows that the energy budget our universe is currently dominated by “dark” components: roughly 70% dark energy, and 25% dark matter, whereas only an embarrassingly small amount of about 5% can be attributed to known Standard Model (SM) particles. From a purely cosmological point of view, there is no problem with the dark components: they are perfectly fine sources in the Einstein equations, and the ability of the simple Λ CDM model to fit this huge amount of different observations with just a few parameters is highly nontrivial and a great success of cosmology. However, there is more to physics than cosmology, and one would certainly like to understand the dark side of the universe from a microscopic

¹³Regarding the flatness and horizon problem, one could always argue that the initial conditions of the universe were either fine-tuned, or controlled by the as yet unknown theory of quantum gravity, whereas the monopole problem assumes a grand unified theory (GUT), for which there is no direct experimental evidence yet. However, inflation is preferred by most physicists as it resolves these puzzles in a natural way without relying on unknown quantum gravity, and prevents cosmology from ruling out GUTs.



point of view.

Regarding dark matter, there are several—in fact rather natural, or independently supported—extensions of the SM that provide good candidates for dark matter particles, in particular:¹⁴ (i) weakly interacting massive particles (WIMPs) that arise as lightest super-partners in supersymmetric extensions of the SM; (ii) axions, which are inevitable if the strong CP problem is to be solved by a mechanism à la Peccei-Quinn [PQ77b, PQ77a].

On the other hand, for dark energy there already exists an apparently ideal candidate, even within the SM: vacuum energy, i.e. the energy of the vacuum state of quantum field theory. Local Lorentz invariance implies that it has to take the form $T_{\mu\nu}^{(\text{vac})} = -\rho_{\text{vac}} g_{\mu\nu}$, and is hence equivalent to a cosmological constant $\Lambda \equiv \rho_{\text{vac}}/M_{\text{Pl}}^2$. So one might think that there is no mystery with dark energy, it is simply vacuum energy. However, in this case the opposite problem occurs: we would expect the contribution from vacuum energy to be much *larger* than what is observed in cosmology.

To verify this statement, let us first estimate the cosmologically measured value of $\rho_{\text{vac}} \equiv 3\Omega_{\Lambda}M_{\text{Pl}}^2H_0^2$. Plugging in the numbers $\Omega_{\Lambda} \approx 0.7$, $H_0 \approx 70 \text{ km s}^{-1} \text{ Mpc}^{-1} \sim 10^{-33} \text{ eV}$ and $M_{\text{Pl}} \sim 10^{27} \text{ eV}$, we arrive at $\rho_{\text{vac}} \sim 10^{-12} \text{ eV}^4$.

Next, we should say something about the theoretical expectation for ρ_{vac} . Classically, there would in fact be no expectation at all; it represents a single free parameter in the theory, the value of which simply has to be inferred from experiment. Quantum mechanically, however, things are quite different. The reason is that in quantum field theory (QFT), there are loop Feynman diagrams that contribute to the vacuum energy.¹⁵ For instance, summing up all the zero modes of a single scalar field ϕ of mass m would give a contribution

$$\rho_{\phi} = \int_0^{\infty} \frac{4\pi k^2 dk}{(2\pi)^3} \frac{1}{2} \sqrt{k^2 + m^2}. \quad (1.2.1)$$

This integral is divergent, so to get a finite result one has to introduce a cutoff $M \gg m$, yielding the leading contribution

$$\rho_{\phi} \approx \frac{M^4}{16\pi^2}. \quad (1.2.2)$$

Now the CC problem is often phrased in the following way [Wei89]: If we trust our field theory up to the Planck scale, we should choose for the cutoff $M \sim M_{\text{Pl}}$, giving an estimate for the vacuum energy of $\rho_{\phi} \sim 10^{106} \text{ eV}^4$, which is 118 orders of magnitude larger than the observed value. However, this argument is rather problematic, because we used the cutoff dependent result (1.2.2) to make this estimate; but from QFT we know very well that, while it is usually necessary to introduce a cutoff (or some other

¹⁴See [Wei08, Chapter 3.4], and [BHS05] for a more extensive review on DM candidates.

¹⁵They are usually taken to be bubble diagrams with no external legs. More accurately, they should be thought of as coupling to external graviton lines, since gravity provides the probe by which they are measured.

sort of regulator) during a loop calculation, in the end no physical observable can depend on this cutoff.

Thus, if we want to make any reasonable statement about the observable vacuum energy, it should better be independent of an arbitrarily chosen cutoff. This can indeed be done in an effective field theory (EFT) framework [BvN13]: In the modern, Wilsonian interpretation, any QFT should be regarded as an EFT that is only valid up to some high energy scale M , that arises from a more fundamental (possibly unknown) UV theory by integrating out all degrees of freedom above M . One can then systematically investigate how the parameters in the EFT change as the cutoff M is raised or lowered. But the crucial point is that, again, any physical observables that can be calculated will be independent of the cutoff. After all, we can choose M completely arbitrarily, thereby conveniently dividing the world into low energy degrees of freedom, which are resolved dynamically, and high energy degrees of freedom, the complete effect of which has been absorbed in the EFT parameters. The outcome of an experiment can clearly not depend on this arbitrary choice.

Now imagine that we choose the cutoff just above m , and calculate the vacuum energy in this EFT. Since the ϕ field is included in the dynamical content of the theory, it again adds a one-loop contribution

$$\rho_\phi = \int_0^M \frac{4\pi k^2 dk}{(2\pi)^3} \frac{1}{2} \sqrt{k^2 + m^2} \quad (1.2.3a)$$

$$= \frac{1}{16\pi^2} \left[M^4 + m^2 M^2 + \frac{m^4}{8} + \frac{m^4}{2} \ln\left(\frac{m}{2M}\right) + m^4 \mathcal{O}\left(\frac{m^2}{M^2}\right) \right]. \quad (1.2.3b)$$

Note that this time we kept all the sub-leading terms that were neglected before in Eq. (1.2.2). This is crucial because, as we said, the physical result can not depend on M , and so all M -dependent contributions in (1.2.3b) have to be canceled by appropriate counter-terms. But now we see that there is also an M -independent contribution $\propto m^4$, which survives after renormalization and enters into the physically observable vacuum energy.¹⁶ Therefore, we can conclude that

$$\rho_{\text{phys}} = \rho_{\text{bare}} + \frac{m^4}{128\pi^2}, \quad (1.2.4)$$

where $\rho_{\text{bare}} \equiv M_{\text{Pl}}^2 \Lambda_{\text{bare}}$ is the bare value of the vacuum energy in our EFT. Applying this line of reasoning for example to the electron, which has a mass $m_e \approx 0.5$ MeV, we see that the observed value of the vacuum energy in an EFT with cutoff just above m_e implies a cancellation between ρ_{bare} and m_e^4 to a precision of about 32 decimal places! Of course, as we raise the EFT cutoff just above the electroweak scale to include the whole SM, the required fine-tuning becomes even worse; after including for instance the Higgs boson with mass $m_H \approx 125$ GeV, the required cancellation already spans a fantastic number of 54 orders of magnitude. This very unnatural “explanation” of the

¹⁶This could also have been anticipated by dimensional analysis.



smallness of the vacuum energy constitutes the CC problem.¹⁷

The fact that the amount of fine-tuning increases as we raise the cutoff is particularly worrisome, because standard EFT reasoning suggests that by doing so, the theory becomes more and more fundamental. In particular, this means that the CC problem cannot be solved by modifying the theory in the UV. For instance, supersymmetry cannot help because it has to be broken at least up to the electroweak scale, so it could at best dispose of a need for fine-tuning above this scale. But the 53 orders of magnitude certainly remain. Instead, we are faced with a low energy problem, indicating that it might be addressable by new physics in the IR. Furthermore, since the empiric value of ρ_{vac} can only be inferred gravitationally, a promising route might be to modify the theory of gravity in the IR. The hope would be to come up with some sort of “degravitation” mechanism, i.e. a modification that renders the curvature of spacetime (which is what we observe to be small) insensitive to vacuum energy (which is what we expect to be large). We will now briefly review why the most straightforward implementation of this idea, only supplementing 4D GR by additional degrees of freedom which should dynamically cancel the CC, is bound to fail. Afterwards, we will explain what can be learned from this when seeking for successful degravitation mechanisms, and in particular why extra dimensions could provide a promising window of opportunity.

1.2.1 Weinberg’s no-go theorem

Before trying to come up with ways to tackle the CC problem, it is helpful to know what has already been tried and failed. Perhaps the most powerful insight in this regard was gained by Weinberg [Wei89],¹⁸ who proved a very general no-go theorem which we shall briefly review. It rules out a broad class of potential solutions, namely those in which gravity is a 4D covariant metric theory, and additional fields lead to an automatic cancellation of the CC. This idea is usually called an *adjustment* or *self-tuning* mechanism. The proof can be sketched as follows. (For simplicity, we focus on the case with one additional scalar field ϕ , but it can in fact be generalized to an arbitrary—but finite—field content [Wei89].) The goal is to obtain flat equilibrium solutions, i.e. solutions for which both the metric and the scalar field are constant throughout spacetime. The corresponding field equations thus simplify to¹⁹

$$\frac{\partial L}{\partial \phi} = 0, \quad \frac{\partial L}{\partial g_{\mu\nu}} = 0. \quad (1.2.5)$$

¹⁷For a slightly different modern perspective on the CC problem (and the suggestion of a potential solution) see [KP14]. There, it is pointed out that higher loop corrections also usually give contributions of order m^4 , making the vacuum energy radiatively unstable.

¹⁸For more recent reviews, see e.g. [Wei96, Bur13, KP14]

¹⁹Here, L denotes the total Lagrangian density without the metric determinant factor, i.e. the action is $S = \int d^4x L$.

Using the GL(4) symmetry which constant solutions inherit from general covariance, one can show that they imply (on-shell)

$$L = c\sqrt{-g}, \quad (1.2.6)$$

where c is independent of $g_{\mu\nu}$. The trouble is that then there are only solutions to the metric field equations if c is tuned to zero. Now the adjustment idea is to promote this tuning to a self-tuning, thus allowing for natural solutions. This could in principle be achieved by assuming the trace of the gravitational field equations to be proportional to the scalar field equations,

$$g_{\mu\nu} \frac{\partial L}{\partial g_{\mu\nu}} \propto \frac{\partial L}{\partial \phi}. \quad (1.2.7)$$

In this case, flat spacetime solutions would be guaranteed by the existence of a solution to the scalar field equations with constant ϕ . The problem is that—without fine-tuning—no such solution exists. This can be seen by noticing that (1.2.7), after a suitable scalar field redefinition, translates into the symmetry requirement

$$\delta g_{\mu\nu} = 2\epsilon g_{\mu\nu}, \quad \delta\phi = -\epsilon, \quad (1.2.8)$$

which is nothing but a scale invariance. It demands that the Lagrangian for constant fields takes the form

$$L = c_0 \sqrt{-g} e^{4\phi}, \quad (1.2.9)$$

with c_0 independent of both ϕ and $g_{\mu\nu}$ (but it could depend on other degrees of freedom which we are neglecting here). Hence, for $c_0 \neq 0$, there is no minimum for the scalar potential and thus no constant solution. In other words, flat spacetime solutions are again only achieved by fine-tuning $c_0 = 0$ (which would ultimately again be spoiled by quantum corrections due to massive loops). One might hope that the problem could still be solved by allowing for the non-constant runaway solutions $\phi \rightarrow -\infty$. However, while this would indeed dynamically adjust $\mathcal{R} \rightarrow 0$, it would also make all masses vanish by approaching the scale invariant point [Bur13, KP14]. In this case we have gained nothing because the CC problem would not exist without massive particles in the first place, and—more importantly—this is obviously not the world we live in.

1.3 Braneworlds and Degravitation

The above no-go result is very useful because it applies to a very general class of models; hence, when seeking for a solution to the CC problem, we should better relax at least one of the assumptions that went into its derivation. One assumption was that gravity is described by a 4D metric; to some extent, the problem can be phrased by saying that the 4D vacuum energy inevitably curves 4D spacetime. But this rigid relation can be relaxed if we consider a braneworld scenario, according to which our universe is merely a 4D hypersurface (a *brane*) embedded in a higher-dimensional spacetime (the *bulk*) [RS83, AHDD98, RS99a, RS99b, AHDKS00, KSS00]. In this case, it is



possible that also the extra space gets curved by the vacuum energy on the brane, thereby reducing the intrinsic 4D curvature $\mathcal{R}^{(4)}$ which we observe—or, equivalently, the corresponding *effective* 4D CC Λ_{eff} that we would ascribe to it—thus allowing for degravitation [DGS03, DGS02, AHDDG02, DHK07, dRHKT08].

A particularly promising setup is provided by two extra bulk dimensions: In this case, the brane-tension (i.e. 4D CC) of our codimension-two universe *only* curves the extra space into a cone, leaving the 4D brane spacetime completely flat [Sun99, CLP00, CG03], just like a usual cosmic string in 4D GR [Vil81, His85]. In other words, Λ_{eff} is exactly zero, irrespective²⁰ of the value of Λ , i.e. the 4D CC is completely degravitated.

Therefore, a codimension-two braneworld seems like the ideal candidate for addressing the CC problem. But this proposal also confronts us with an immediate problem: in our universe gravity obeys the Newtonian $1/r^2$ force law, at least on all length scales where we have tested it. But if gravitational field lines would spread out equally through all six bulk dimensions, we would obtain a $1/r^4$ scaling instead. So any realistic codimension-two model must be equipped with some mechanism which ensures that the field lines cannot leak too far into the bulk, so that the inverse square law is recovered (at least approximately) on all relevant scales. At the moment, there are basically two known mechanisms that can achieve this:

- (i) *Compact extra dimensions*: In this (more traditional) approach the extra space has a finite extent, which prevents the field lines from spreading out too far into the bulk. This effect only becomes negligible once a brane observer probes distances small enough so that all directions start to look the same locally. Hence, these models yield a UV modification, where gravity becomes higher dimensional at distances smaller than the size of the extra space.
- (ii) *Brane induced gravity (BIG)*: The bulk volume is infinite, and the idea is to add a brane-localized 4D Einstein-Hilbert term to the action. If its coefficient is identified with the 4D Planck mass M_{Pl} , the correct Newtonian force law is recovered for small enough distances. Pictorially speaking, the gravitational field lines are pulled onto the brane by the additional induced gravity term. A certain ratio of M_{Pl} to the corresponding bulk gravity scale defines a crossover length, above which the field lines start leaking and gravity becomes six dimensional. This model thus provides a genuine IR modification of gravity. Originally, it was developed with one extra-dimension [DGP00] and dubbed the DGP model, which will be reviewed in Sec. 1.4; but in principle, the mechanism can be generalized to arbitrary higher codimensions [DG01, DGHS03], in particular to the auspicious 6D case.

One of the main goals of this thesis (achieved in Chap. 5) is to study proposal (ii), i.e. codimension-two BIG, in great detail: to derive its (nonlinear) cosmological pre-

²⁰This only holds for *sub-critical* tensions $M_{\text{Pl}}^2\Lambda < 2\pi M_6^4$, meaning that the deficit angle is less than 2π . The *super-critical* case will also be studied in this thesis (Chap. 6), revealing inflating backgrounds as the correct geometries.

dictions in the presence of FRW matter on the brane, thereby in particular testing its potential to dynamically degravitate, and to investigate its theoretical as well as phenomenological consistency.

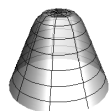
The virtue of infinite extra dimensions to address the CC problem has already been pointed out in the literature [DG01, DGS02, DGS03, AHDDG02]. One crucial difference to compact scenarios is that one cannot write down a local effective low energy theory with a finite number of degrees of freedom. Either, one has to work with the full higher-dimensional theory, or one ends up with nonlocal effective interactions. Hence, Weinberg’s no-go theorem is not applicable to the effective 4D theory. This is in contrast to option (i) above, because there the theory always admits the usual Kaluza-Klein reduction [Kal21, Kle26], leading to a local 4D EFT with finitely many degrees of freedom. Therefore, Weinberg’s argument applies, and one expects that perfect degravitation can only be achieved by some sort of fine-tuning. This was indeed confirmed explicitly since the earliest attempts [Sun99, CG03, NPT04, GP04]. Nonetheless, there have been claims in the recent literature that this problem could be avoided in the concrete compact model of supersymmetric large extra dimensions (SLED) [ABPQ04, BvN11, BvN13]. Another major part (Chap. 7) of this thesis is thus devoted to the tuning issue within the SLED proposal.

1.3.1 Other reasons to modify gravity

Even though the idea to degravitate the CC is one of the major motivations to modify general relativity, it is of course not the only one. For instance, in addition to the “old” CC problem (why is Λ_{eff} so small?), the observational detection of a dark energy component in our universe adds to this a “new” CC problem (why is Λ_{eff} not zero?). This of course only becomes a problem if we were to come up with a solution to the old problem that would predict Λ_{eff} to be exactly zero (as e.g. expected for the codimension-two BIG scenario). But taking this point of view, one can start to think about modifications of GR which could explain the accelerated expansion without the need of a cosmological constant. In fact, this is one of the main reasons why the DGP cosmology attracted a lot of attention in the literature: it contains a self-accelerating branch, on which a de Sitter phase is realized despite $\Lambda = 0$, cf. the end of Sec. 1.4.2.

Another motivation is that even though the cosmological concordance model does a very good job at fitting a large number of observations, it might still be that there is an alternative theory that would provide a better fit.²¹ Or even if it does not, it would be useful to see other models failing because this would give us even more confidence in the concordance model. Of course, if dark matter particles will not be detected, Λ CDM will face yet another problem that will motivate the search for alternatives.

²¹It should also be mentioned that there are indeed some shortcomings of the Λ CDM model on small (i.e. galactic) scales, like the core-cusp problem [dB10], missing satellites [MGG⁺99], or a lack of explaining the Tully-Fisher relation [MSBdB00] (for further problems, see [K⁺10] and the discussion in [CFPS12]). However, some of them hinge on numerical studies and might still turn out to be low-resolution artifacts.



Finally, GR has at some point to be reconciled with the framework of quantum field theory, which describes all non-gravitational physics so successfully. While this can be done at low energies by treating perturbative quantum gravity as an EFT (which is a predictive theory) [Don94b, Don94a, Bur04], problems arise at high energies due to the non-renormalizability of GR. At present, the most prominent candidate for a UV completion of quantum gravity is string theory (or M theory), which requires ten (or eleven) dimensions for consistency, and thus motivates studying extra-dimensional scenarios. Furthermore, branes are naturally incorporated in string theory as objects on which open strings can end (D-branes), and so it is conceivable that some successful braneworld modification of GR could ultimately be embedded within string theory. In this work, however, we will not worry about this question but rather follow a top-down approach by first investigating the gravitational consequences of certain braneworld models treated as EFTs. If interesting models were found this way, one could subsequently ask whether they can also arise as the low energy limits of certain UV completions of quantum gravity.

1.4 DGP model

In this section, we give a short review of codimension-one BIG, better known as the Dvali-Gabadadze-Porrati (DGP) model [DGP00]. After defining the theory, the main focus will be on the derivation of the cosmological solutions, and why they can be derived in such a straightforward manner—without assumptions about the bulk geometry other than 4D FRW symmetries. These insights will be important in pinning down the main obstacle when generalizing this procedure to the codimension-two setup, which is one of the main objectives of this thesis.

1.4.1 Theory

In the DGP model, our 4D universe is a codimension-one brane in a five-dimensional bulk. The corresponding action reads

$$\mathcal{S} = \frac{M_5^3}{2} \int d^5 X \sqrt{-g^{(5)}} \mathcal{R}^{(5)} + \int d^4 x \sqrt{-g} \left(\mathcal{L}_m + \frac{M_{\text{Pl}}^2}{2} \mathcal{R} \right), \quad (1.4.1)$$

where M_5 is the 5D Planck mass (i.e. bulk gravity scale), and $\mathcal{R}^{(5)}$ denotes the Ricci scalar that is constructed from the bulk metric $\mathbf{g}^{(5)}$. In other words, the first term is simply the 5D Einstein-Hilbert action describing pure gravity in the bulk. The second term is the brane action, with \mathcal{L}_m incorporating all matter degrees of freedom (ultimately the Standard Model), which are localized on the codimension-one defect and minimally coupled to gravity; and, crucially, there is also a brane-localized 4D Einstein-Hilbert term, i.e. the 4D Ricci \mathcal{R} built from the induced metric \mathbf{g} . In fact, this last term should in principle always be included from an EFT point of view, because it arises naturally if heavy degrees of freedom on the brane are integrated out.

It is therefore usually referred to as the *brane induced gravity* (BIG) term, and is the vital ingredient to achieve a 4D gravity regime in the DGP setup, even though the extra dimensions are neither compact nor warped (as in other braneworld scenarios like [AHDD98, RS99a, ABPQ04]). In order for the model to be phenomenologically viable, its coefficient M_{Pl} has to be identified with the 4D Planck mass.

By studying linear perturbations around Minkowski (brane and bulk), one can explicitly show that this 4D regime is indeed realized for small enough distances, where the gravitational potential of a point source goes like $\sim 1/r$, and turns to a 5D scaling $\sim 1/r^2$ at large distances. The transition occurs at the *crossover scale*²²

$$r_c := \frac{M_{\text{Pl}}^2}{2M_5^3}. \quad (1.4.2)$$

There is, however, a difference to 4D GR at the linear level: the tensor structure of the on-brane graviton propagator differs from the GR form, and is instead that of (linear) 4D massive gravity, which would lead to light bending predictions incompatible with observations. However, this vDVZ discontinuity [vDV70, Zak70] was shown to be an artifact of the linear treatment, and is in fact absent in the full nonlinear theory [DDGV02, Gru05, Por02]. This is the analogue of the *Vainshtein mechanism* [Vai72] in massive gravity, saying that the linear perturbation theory breaks down close to heavy sources, at the so-called Vainshtein radius, and the nonlinear corrections ensure that the correct GR limit is recovered.

The vDVZ discontinuity and the Vainshtein mechanism in the DGP model can be traced to a helicity-0 mode that exists in the effective 4D description of the theory, but gets screened due to nonlinearities close to a source. However, this scalar mode also leads to a strong coupling problem [LPR03, Rub03, Dva06]: for $r_c \sim H_0$, quantum fluctuations around Minkowski become strongly coupled at ~ 1000 km. While it has been argued that this scale can be reduced (to ~ 1 cm on the surface of the earth) and the observational effects sufficiently screened [NR04], there are also doubts whether this would actually happen in a specific UV completion [KPSS15].

1.4.2 Cosmology

The cosmological solutions for a codimension-one brane, describing the evolution of the on-brane scale factor in terms of a *modified Friedmann equation*, were first derived in [BDL00, BDEL00], and later generalized to include BIG terms, i.e. to the case of DGP cosmology, in [Def01]. Since one of the main goals in this thesis is to derive the analogous equations in generalizations of the DGP model, it is worthwhile to review the (rather simple) derivation in the DGP case here in this introduction.

²²Throughout this chapter, r_c refers to the 5D crossover scale. In later chapters, r_c will be used for the analogous 6D crossover scale, and the 5D one will be denoted by r_c^{DGP} .



Derivation

To this end, we assume the bulk to be empty, and the brane to be filled with a perfect fluid in a 3D homogeneous and isotropic way.²³ The most general bulk metric compatible with these symmetries can be written as

$$ds^2 = -e^{2N(t,y)} dt^2 + f(t,y) dt dy + e^{2A(t,y)} \delta_{ij} dx^i dx^j + e^{2B(t,y)} dy^2. \quad (1.4.3)$$

This can further be simplified by adopting *Gaussian normal coordinates*²⁴ in y direction. They are constructed by using the proper distance along brane-orthogonal geodesics as the new coordinate. As a consequence, the metric then takes the form²⁵

$$ds^2 = -e^{2N(t,y)} dt^2 + e^{2A(t,y)} \delta_{ij} dx^i dx^j + dy^2, \quad (1.4.4)$$

and the brane is located at $y = 0$. Hence, the induced metric is simply (1.4.4) evaluated at $y = 0$,

$$ds_{(4)}^2 = -dt^2 + e^{2A_0(t)} \delta_{ij} dx^i dx^j, \quad (1.4.5)$$

where $A_0(t) := A(t, 0)$, and we used a global rescaling of time to set $N(t, 0) = 0$, so that t measures proper (cosmological) time on the brane. From Eq. (1.4.5), the on-brane scale factor, and the corresponding Hubble parameter can be identified as

$$a(t) \equiv e^{A_0(t)} \quad \text{and} \quad H(t) \equiv \frac{dA_0(t)}{dt}, \quad (1.4.6)$$

respectively. Like in standard cosmology (at the homogeneous and isotropic level), the entire cosmological dynamics that an on-brane observer can measure is encoded in this single function, and the goal is to derive the modified Friedmann equation determining its evolution.

The above construction of Gaussian normal coordinates is always possible, at least in a neighborhood of the brane,²⁶ which is sufficient for our purposes. In addition to simplifying the metric, this choice of coordinates also simplifies the equations of motion: Instead of needing to use Israel's junction conditions [Isr66, Isr67], the equations of motion can be written in a concise way with a delta function,

$$M_5^3 G_{MN}^{(5)} = \delta(y) \delta_M^\mu \delta_N^\nu (T_{\mu\nu} - M_{\text{Pl}}^2 G_{\mu\nu}) \quad \Leftrightarrow \quad G_{MN}^{(5)} = \delta(y) \delta_M^\mu \delta_N^\nu \tilde{T}_{\mu\nu}, \quad (1.4.7)$$

where we defined the *effective* energy momentum tensor

$$\tilde{T}_{\mu\nu} := \frac{1}{M_5^3} (T_{\mu\nu} - M_{\text{Pl}}^2 G_{\mu\nu}). \quad (1.4.8)$$

²³Furthermore, for simplicity, we restrict ourselves to 3D spatially flat geometries and set the bulk CC to zero. For the general case of nonzero 3D curvature and bulk CC, the interested reader is referred to the literature [Def01].

²⁴See, e.g. [Car04, Appendix D].

²⁵By a slight abuse of notation, we use the same names for the coordinates and metric functions as before. This will not lead to any confusion, as the metric (1.4.3) will not be used anymore.

²⁶The geodesics could cross at some finite distance, leading to a coordinate singularity.

It represents the source (rescaled by M_5 for convenience) which is “seen” from a 5D GR point of view, i.e. which sources the 5D Einstein tensor, as is clear from the field equations (1.4.7). Note, however, that the DGP model is not a mere source- or *potential* modification, because the BIG terms $G_{\mu\nu}$ contain time derivatives of the metric, implying a *kinetic* modification of GR. This should always be kept in mind when using the shorthand notation $\tilde{T}_{\mu\nu}$.

For the cosmological setup, the energy momentum tensor has the form of a perfect fluid,

$$T^\mu{}_\nu = \text{diag}(-\rho, p, p, p), \quad (1.4.9)$$

with the pressure being related to the energy density via an EOS, $p = w\rho$. Using the induced metric (1.4.5) to calculate $G_{\mu\nu}$, one finds that $\tilde{T}^\mu{}_\nu$ has the same form, but with the *effective* fluid components

$$\tilde{\rho} := \frac{1}{M_5^3} (\rho - 3M_{\text{Pl}}^2 H^2), \quad (1.4.10a)$$

$$\tilde{p} := \frac{1}{M_5^3} \left[p + M_{\text{Pl}}^2 (2\dot{H} + 3H^2) \right]. \quad (1.4.10b)$$

Explicitly, the complete set of nontrivial components of the equations of motion (1.4.7) then read

$$\begin{aligned} \binom{t}{t} : \quad & e^{-2N} \left(3\dot{A}^2 \right) - 3 \left(2A'^2 + A'' \right) = \delta(y) \tilde{\rho}, \end{aligned} \quad (1.4.11a)$$

$$\begin{aligned} \binom{x}{x} : \quad & -e^{-2N} \left(3\dot{A}^2 - 2\dot{A}\dot{N} + 2\ddot{A} \right) + 3A'^2 + 2A'N' + N'^2 + 2A'' + N'' = \delta(y) \tilde{p}, \end{aligned} \quad (1.4.11b)$$

$$\binom{y}{y} : \quad -e^{-2N} \left(2\dot{A}^2 - \dot{A}\dot{N} + \ddot{A} \right) + A'^2 + A'N' = 0, \quad (1.4.11c)$$

$$\binom{t}{y} : \quad A'\dot{A} - N'\dot{A} + \dot{A}' = 0, \quad (1.4.11d)$$

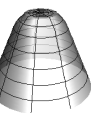
where dot and prime were introduced as shorthand for ∂_t and ∂_y , respectively. The junction conditions across the brane can now be obtained by integrating Eqs. (1.4.11a) and (1.4.11b) over a small region around the brane, viz. $y \in [-\epsilon, \epsilon]$, and taking the limit $\epsilon \rightarrow 0^+$. Using the continuity of the metric functions and their first r -derivatives, this yields²⁷

$$[A'] = -\frac{1}{3}\tilde{\rho} \quad \text{and} \quad [N'] = \frac{2}{3}\tilde{\rho} + \tilde{p}, \quad (1.4.12)$$

where the square brackets denote the *jump* across the brane, i.e.

$$[f] := \lim_{\epsilon \rightarrow 0^+} [f(y + \epsilon) - f(y - \epsilon)], \quad (1.4.13)$$

²⁷Of course, the same equations would have been obtained by calculating the brane’s extrinsic curvature and implementing Israel’s junction conditions.



for some function $f(y)$.

Note that $\tilde{\rho} = 0$ and $\tilde{p} = 0$ are nothing but the standard 4D Friedmann equations, cf. Eqs. (1.1.6a) and (1.1.6b). Thus, the junction conditions (1.4.12) can formally already be regarded as the modified Friedmann equations, with modification terms proportional to²⁸ $M_5^3 [A']$ and $M_5^3 [N']$. But a priori, these jumps are unknown functions of t , which depend on the bulk geometry via (1.4.11)—a complicated system of nonlinear, coupled partial differential equations (PDE). However, we are in fact not interested in the full bulk solution. Everything that can be measured by an on-brane observer is encoded in the induced metric (1.4.5), and so it would be desirable to obtain a closed set of ordinary differential equations (ODE) for the two on-brane functions $a(t)$ and $\rho(t)$, like in standard cosmology.

As it turns out, this is indeed possible in the DGP model. The idea [BDL00] is to use the bulk equations (1.4.11) for $y \neq 0$, but in the limit $y \rightarrow 0^\pm$. Equivalently, one can take the jump (1.4.13), as well as the *mean*

$$\langle f \rangle := \frac{1}{2} \lim_{\epsilon \rightarrow 0^+} [f(y + \epsilon) + f(y - \epsilon)] \quad (1.4.14)$$

of the bulk equations. From Eqs. (1.4.11a) and (1.4.11b), one thus obtains four equations that determine the jumps and means of the second y -derivatives A'' and N'' , which are of no interest. But Eqs. (1.4.11c) and (1.4.11d) only contain first y -derivatives. Using the identities

$$[fg] = [f] \langle g \rangle + \langle f \rangle [g] \quad \text{and} \quad \langle fg \rangle = \langle f \rangle \langle g \rangle + \frac{1}{4} [f] [g], \quad (1.4.15)$$

as well as the continuity of the metric functions themselves, this yields four equations for the four jumps and means of the first y -derivatives N' and A' . Explicitly, one obtains

$$\left[\frac{y}{y} \right] : \quad [A'] \left(2 \langle A' \rangle + \langle N' \rangle \right) + [N'] \langle A' \rangle = 0, \quad (1.4.16a)$$

$$\left\langle \frac{y}{y} \right\rangle : \quad 2H^2 + \dot{H} - \frac{1}{4} [A'] \left([A'] + [N'] \right) - \langle A' \rangle \left(\langle A' \rangle + \langle N' \rangle \right) = 0, \quad (1.4.16b)$$

$$\left[\frac{t}{y} \right] : \quad H \left([A'] - [N'] \right) + [\dot{A}'] = 0, \quad (1.4.16c)$$

$$\left\langle \frac{t}{y} \right\rangle : \quad H \left(\langle A' \rangle - \langle N' \rangle \right) + \langle \dot{A}' \rangle = 0. \quad (1.4.16d)$$

Equation (1.4.16c) only contains jumps, which can be replaced via the junction conditions (1.4.12), giving

$$\dot{\tilde{\rho}} + 3H (\tilde{\rho} + \tilde{p}) = 0. \quad (1.4.17)$$

²⁸Incidentally, this shows that one recovers standard 4D cosmology in the limit $M_5^3 \rightarrow 0$. This is of course how the DGP model was designed to work in the first place, and can already be anticipated from the form of the action (1.4.1) or the equations of motion (1.4.7).

Due to the 4D Bianchi identities, the tildes can be dropped, and one recovers the standard 4D energy conservation equation (1.1.7).²⁹

We will now restrict ourselves to Z_2 symmetric configurations, i.e. the solution is assumed to be invariant under $y \mapsto -y$. This is usually³⁰ done in the literature [BDEL00, Def01, DDG02], and is quite a natural assumption in the codimension-one setup. In this case, $\langle A' \rangle = \langle N' \rangle = 0$, and so (1.4.16a) as well as (1.4.16d) are identically fulfilled.³¹ The only nontrivial remaining equation is (1.4.16b), which—after using the junction conditions—becomes

$$2H^2 + \dot{H} + \frac{1}{36}\tilde{\rho}(\tilde{\rho} + 3\tilde{p}) = 0. \quad (1.4.18)$$

Now this equation only contains intrinsic on-brane functions, i.e. no information about the bulk geometry is needed anymore. Hence, it constitutes the local modified Friedmann equation we were looking for. To be precise, since it contains second time derivatives of the scale factor, it is the *second* modified Friedmann equation, analogous to (1.1.6b). The corresponding *first* modified Friedmann equation can, however, be obtained analytically as well. To this end, note that after using (1.4.17) to eliminate \tilde{p} it can easily be integrated,

$$\frac{d}{dt} \left(H^2 - \frac{\tilde{\rho}^2}{36} \right) = -4H \left(H^2 - \frac{\tilde{\rho}^2}{36} \right) \quad \Rightarrow \quad \frac{\tilde{\rho}^2}{36} - H^2 = \mathcal{C}a^{-4}, \quad (1.4.19)$$

where \mathcal{C} is a constant of integration. Plugging in the definition of $\tilde{\rho}$, the explicit form of the (first) modified Friedmann equation finally reads

$$\boxed{3M_{\text{Pl}}^2 H^2 = \rho + 6M_5^3 \sigma \sqrt{H^2 + \mathcal{C}a^{-4}}}, \quad (1.4.20)$$

with $\sigma = \pm 1$. This is the equation derived in [Def01] (specialized to our choice of zero 3D curvature and bulk CC). It is the standard Friedmann equation (1.1.6a) plus a modification term, the size of which is controlled by the bulk gravity scale M_5 .

One can already see that for $\sigma = +1$, it admits solutions with $\rho = 0$ —i.e. without any source—but $H \neq 0$ (in particular $H = r_c = \text{const}$ for $\mathcal{C} = 0$). Therefore, this is usually called the *self-accelerating* branch, while $\sigma = -1$ is referred to as the *normal* branch.

In turn, it is tempting to infer from (1.4.20) the existence of degravitating ($p = -\rho$ but $H = 0$) solutions in the normal branch with $\mathcal{C} > 0$. However, this is not the case because (1.4.18) shows that $H \equiv 0$ requires the EOS $p = -\rho/3$. (Note that for $H = 0$, the second Friedmann equation cannot be replaced by the energy conservation equation,

²⁹Alternatively, this follows (more abstractly) from the Gauss-Codazzi relation, which—together with the vacuum field equations and the 4D Bianchi identity implies $\nabla_\mu T^\mu_\nu = 0$.

³⁰See however [Pad05a, Pad05b, OGP09].

³¹Without assuming Z_2 symmetry, these equations can be used to eliminate the means $\langle A' \rangle$ and $\langle N' \rangle$, and Eq. (1.4.16b) would also yield the modified Friedmann equation. It would modify the Z_2 symmetric counterpart (1.4.18) by an additional term $\propto \exp(-8a)(\tilde{\rho} + 3\tilde{p})/\tilde{\rho}^3$.



as its derivation assumes $H \neq 0$.) However, there is indeed *some* degravitation— H is smaller than in standard GR—although this effect is too small to help with the CC problem, cf. the phenomenology discussion below.

Bulk geometry

Before reviewing the phenomenology of the DGP cosmology, let us discuss a crucial physical property of the codimension-one setup, which allowed for this simple derivation of a modified Friedmann equation, but which will not apply to higher dimensional generalizations. It is quite remarkable that the entire dependence of the on-brane evolution described by (1.4.20) on the bulk geometry is encoded in the single constant \mathcal{C} . In order to better understand how this is possible, let us investigate the complete bulk solution.

Incidentally, it turns out that here in the codimension-one case, the full nonlinear bulk field equations can even be solved exactly [BDEL00]. Indeed, Eq. (1.4.11d) can immediately be integrated, giving

$$N(t, y) = A(t, y) - A_0(t) + \ln \left(\frac{\dot{A}(t, y)}{H(t)} \right), \quad (1.4.21)$$

where the boundary condition $N_0 = 0$ was already implemented, and we assumed $H \neq 0$ in order to have a nontrivial cosmology. After plugging this into (1.4.11a), it can be integrated as well, yielding³²

$$A(t, y) = A_0 + \frac{1}{2} \ln \left(1 \pm 2y\sqrt{H^2 + \mathcal{C}a^{-4}} + y^2 H^2 \right), \quad (1.4.22)$$

where \mathcal{C} is a constant of integration (which will turn out to be the same as the \mathcal{C} introduced above), and the sign of the square-root can be chosen freely. In order to have a nonvanishing jump $[A']$ (and thus a nontrivial modification to the Friedmann equation), either the integration constant or the sign (or both) has to be chosen differently in the half-spaces $y > 0$ and $y < 0$.

Assuming again Z_2 symmetry across the brane, the constant \mathcal{C} must be identical on both sides, and the sign must be opposite. However, we can still choose whether it is the plus (minus) sign for $y > 0$ ($y < 0$), or vice versa. The corresponding solution can thus be written as

$$A(t, y) = A_0 + \frac{1}{2} \ln \left(1 + 2\sigma|y|\sqrt{H^2 + \mathcal{C}a^{-4}} + y^2 H^2 \right), \quad (1.4.23)$$

where $\sigma = \pm 1$ chooses the branch. From this we can, as a consistency check, calculate the jump

$$[A'] = 2\sigma\sqrt{H^2 + \mathcal{C}a^{-4}}, \quad (1.4.24)$$

³²Strictly speaking, Eq. (1.4.11c) also needs to be used to eliminate one otherwise arbitrary function of y , because it is only first order in ∂_y . Equation (1.4.11b) is then already fulfilled, as is guaranteed by the Bianchi identities.

which, after using the junction condition (1.4.12) indeed reproduces the modified Friedmann equation (1.4.20).

Now we have learned that also the full bulk solution (1.4.21), (1.4.23), is completely determined by one single *constant* \mathcal{C} (and a choice of sign). This implies that there can not be any propagating degrees of freedom in the bulk: those would require the freedom to specify initial conditions, and hence arbitrary *functions* in the general solution. In other words, even though the solution (1.4.21), (1.4.23) depends on t , this time-dependence can in fact not be physical, but must be a mere coordinate artifact. This can be seen more explicitly by transforming to new coordinates $(t, y) \mapsto (T, Y)$ as follows (for $\mathcal{C} \neq 0$): Defining $T(t, y)$ as the solution of the differential equations³³

$$\dot{T} = \sigma_1 \left(\frac{\dot{A}^2}{\mathcal{C}} e^{4A} + e^{2N} \right)^{1/2} e^A, \quad T' = \sigma_2 \left(\frac{A'^2}{\mathcal{C}} e^{4A} - 1 \right)^{1/2} e^A, \quad (1.4.25)$$

with the signs $\sigma_{1,2}$ chosen such that $\sigma_1 \sigma_2 = \text{sgn}(\dot{A}A')$, and $Y(t, y)$ as

$$Y := \frac{1}{\alpha} (1 - e^{2A}), \quad \alpha := \pm 2\sqrt{\mathcal{C}}, \quad (1.4.26)$$

the bulk metric takes the form

$$ds^2 = - (1 - \alpha Y)^{-1} dT^2 + (1 - \alpha Y) \delta_{ij} dx^i dx^j + dY^2. \quad (1.4.27)$$

This is the 5D generalization of the 4D vacuum solution with 2D planar symmetry, first found by Levi-Civita [Lev18] (see also Sec. 2.4.1), to a 3D hyperplane. From this form it is obvious that the bulk geometry is indeed static. The entire dynamics on the brane comes from the fact that it is not located at $Y = \text{const}$, but moves³⁴ through the static bulk geometry at a nonvanishing speed $dY_0/dt = 2Ha^2/\alpha$.

The fact that the most general plane-symmetric vacuum solution is static means that there exists a version of Birkhoff's theorem for the case of planar symmetry. In 4D, this was discovered by Taub [Tau51]:

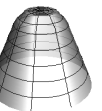
“A space-time with plane symmetry with $R_{\mu\nu} = 0$ admits a coordinate system where the line element is independent of x^0 , that is, is static.”

Here, “plane symmetry” refers to translational and rotational symmetry in the two directions of the plane.³⁵ Above, we have explicitly shown that Taub's theorem also

³³The integrability condition of those is fulfilled, as can be checked explicitly by plugging in the solutions (1.4.21), (1.4.23) for N and A .

³⁴Equivalently, from the brane point of view, the static bulk geometry is pulled towards (or pushed away from) the brane.

³⁵As an aside, note that the theorem does not rule out plane gravitational waves, i.e. waves propagating in one direction through space. Indeed, exact vacuum solutions describing plane waves are known [Bri25], see also Sec. 2.4.3. But those always dependent differently on the two plane directions, i.e. they are not *plane symmetric*. A similar statement also holds for spherical gravitational waves, cf. Sec. 2.4.4.



holds in the generalized case of a three-dimensional (spatially flat) homogeneous and isotropic hyperplane in a 5D spacetime.

For positive 3D spatial curvature, the brane has the topology of a 3-sphere, and the corresponding solution would be 5D Schwarzschild [Def01, GKMP07]. (This is why the constant \mathcal{C} is usually referred to as the *Schwarzschild mass parameter* in the literature. For vanishing 3D spatial curvature, however, the name *Levi-Civita mass parameter* is more adequate.) Hence, the statement that the symmetries imply a static bulk geometry also holds in this case, where the appropriate generalization of the actual Birkhoff theorem to a 3-sphere applies.

Note that the case $\mathcal{C} = 0$ was actually excluded above, as the coordinate transformation (1.4.26), (1.4.25) would then be ill-defined. However, one can find another coordinate transformation in that case, bringing the line element to canonical Minkowski form [DD00].³⁶ Thus, for $\mathcal{C} = 0$ the solution is not only static, but in fact flat spacetime. This can also be checked in the original coordinates (1.4.4) by calculating the Riemann tensor, which vanishes for $\mathcal{C} = 0$.

For $\mathcal{C} \neq 0$, spacetime is not flat, as can for instance be verified by calculating the Kretschmann scalar, i.e. the square of the Riemann tensor, $\mathcal{K} := R_{MNPQ}R^{MNPQ}$. Explicitly, one finds

$$\mathcal{K} = \frac{9\alpha^4}{2(1 - \alpha Y)^4} = 72\mathcal{C}^2 e^{-8A}. \quad (1.4.28)$$

Furthermore, this shows that (for $\mathcal{C} \neq 0$) there is a physical (curvature) singularity at $Y = 1/\alpha$. However, geodesic motion of massive particles cannot reach this point, and photons undergo an infinite redshift along geodesics towards the singularity [AG83]. In this sense, the singularity lies “at infinity” and is thus not part of the physically accessible spacetime.

The Z_2 symmetric DGP cosmology solution is obtained by only keeping the part $Y > Y_0(T)$ of the bulk spacetime (1.4.27), and gluing it together with its mirror image on the other side. One can easily check that the sign σ , which chooses the DGP branch, cf. Eq. (1.4.20), is related to the sign of α via $\sigma = -\text{sgn}(\alpha)$. Hence, the normal branch $\sigma = -1$ corresponds to keeping the part of the bulk geometry which contains the boundary singularity at $Y = 1/\alpha$, while for the self-accelerating branch $\sigma = +1$ the opposite, asymptotically flat half-space is kept, see Fig. 1.1. Moreover, the kink at the brane is such as if it were created by a *positive* energy density for $\sigma = -1$, and by a *negative* one for $\sigma = +1$. This can already be inferred from the DGP Friedmann equation (1.4.20), which implies $\text{sgn}(\tilde{\rho}) = -\sigma$. Hence, the self-accelerating branch—from the bulk point of view—corresponds to a negative energy density localized on the brane, suggesting that this solution might not be stable [Def01]. This is indeed the

³⁶One might therefore think that the coordinates (T, Y) are still valid in that case (even though the transformation (1.4.26), (1.4.25) are ill-defined), as the metric (1.4.27) also reduces to Minkowski for $\alpha \rightarrow 0$. However, this is not quite true: in the correct coordinates X^A the brane is not located at, say, $X^4 = X^4(X^0)$ like in (1.4.27), but rather given by some hyperplane defined by $f(X^A) = 0$, where the function f depends on *all* spatial coordinates [DD00]. Otherwise, the metric (1.4.27) would immediately imply $H = 0$.

case, as will be discussed below.

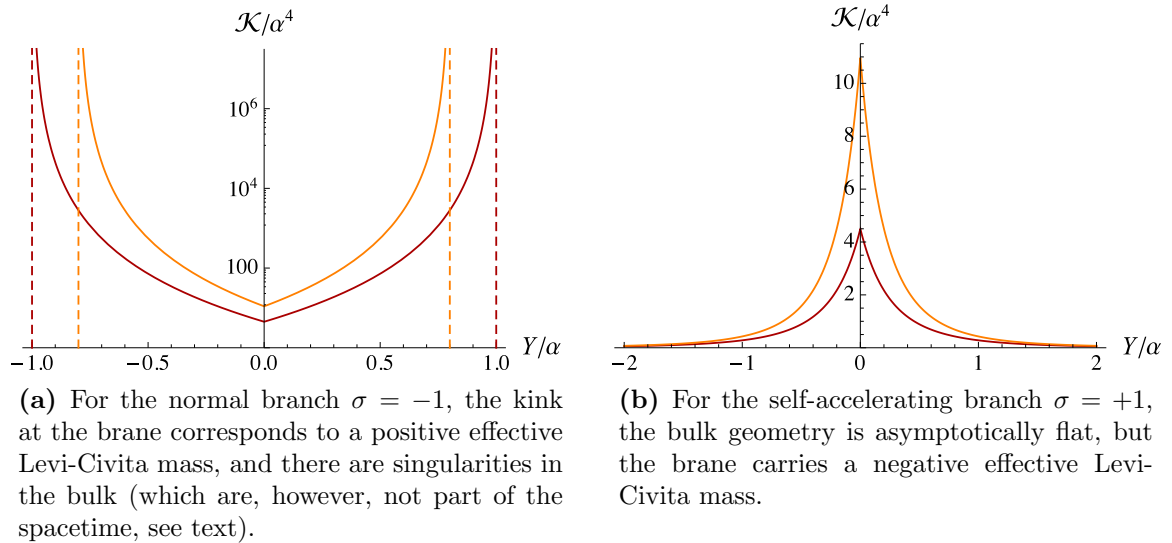


Figure 1.1: Visualization of the bulk geometry for the DGP cosmology with $\mathcal{C} \equiv \alpha^2/4 \neq 0$. The plots show the 5D Kretschmann scalar $\mathcal{K} \equiv R_{MNPQ}R^{MNPQ}$ in the static coordinates (1.4.27) at two different moments of (on-brane) time, with Y shifted such that the brane stays at $Y = 0$. Larger \mathcal{K} corresponds to a smaller scale factor a , cf. (1.4.28).

In summary, the main message of this section is that *the cosmological symmetries (3D homogeneity and isotropy) imply a static bulk geometry for a codimension-one brane*. This is the reason why it was possible at all to derive a local 4D (modified) Friedmann equation, describing the on-brane evolution in a closed way, without making any further assumptions. If the bulk geometry could contain propagating degrees of freedom (i.e. gravitational waves), such a derivation would have been impossible: one could always have prepared gravitational bulk waves propagating towards the brane, by choosing appropriate initial conditions in the bulk. When they arrived at the brane, they would have influenced its dynamics in some arbitrary way. But no such waves are possible in the codimension-one setup, thanks to Taub's theorem on plane symmetric vacuum solutions, which generalizes to 3D (hyper-)planar symmetry in five spacetime dimensions. Hence, one simply cannot freely choose initial conditions in the bulk which would respect the symmetries, and so the only impact of the bulk geometry on the on-brane evolution is encoded in one single constant \mathcal{C} , corresponding to the Levi-Civita mass of the bulk spacetime. In particular, the constant can be set to zero, corresponding to the brane being embedded in a Minkowski bulk.

As it turns out, no generalization of Taub's (or Birkhoff's) theorem holds in the case of a codimension-two brane, as will be discussed in more detail in Chap. 5. Consequently, the on-brane evolution generally depends on gravitational waves coming from the bulk, and it will be necessary to exclude such incoming waves in order to arrive at a unique on-brane evolution. Therefore, a large part of this thesis (Chaps. 2 and 3) is devoted to the question if (and how) such an *outgoing wave condition* can be realized.



Phenomenology

Let us now briefly discuss the phenomenological status of the DGP cosmology; for more details we refer to the review [MK10] and references therein. We will only consider the case $\mathcal{C} = 0$, where the brane is embedded into Minkowski space, as is usually done in the literature. The modified Friedmann equation (1.4.20) can then conveniently be written as

$$H^2 = \frac{\rho}{3M_{\text{Pl}}^2} + \frac{\sigma}{r_c} |H|, \quad (1.4.29)$$

where r_c is the crossover scale (1.4.2). Obviously, the cosmological evolution is always close to standard 4D GR at early times when $H \gg r_c$, but will exhibit a late-time modification at $H \sim r_c$.

The self-accelerating branch ($\sigma = +1$), with the vacuum solution $H = r_c$, has attracted quite some attention, because it could in principle have provided an alternative to dark energy as the origin of the observed accelerated expansion. (That is, it was a candidate for addressing the new CC problem—of course without saying anything about the old one.) However, it was soon realized that linear perturbations around the self-accelerating branch contain a mode with a negative kinetic term (“ghost”) [LPR03, NR04, Koy05, GKS06, CGKP06], rendering this branch pathological. There were, however, arguments that the linear analysis is not conclusive, due to the strong coupling [DGI06, Dva06], as well as arguments against these arguments [Pad07, KS07]. In any case, the self-accelerating cosmology—without an additional CC—has in the meantime also been ruled out at $\sim 5\sigma$ with respect to Λ CDM [FWH+08].

In the (ghost free) normal branch ($\sigma = -1$), there is no self-acceleration, and so one has to assume a nonzero brane CC in order to be compatible with observations. In fact, there is even partial degravitation taking place, because the BIG terms shield some of the CC’s gravitational impact, leaving an *effective* CC

$$\Lambda_{\text{eff}} = \Lambda - \frac{3}{r_c} |H|. \quad (1.4.30)$$

However, since $r_c \gtrsim 1/H_0$ in order to achieve a viable cosmology, this can at most reduce Λ by an amount $\sim H_0^2$ and is therefore irrelevant with respect to the CC problem. Since the cosmological evolution always reduces to Λ CDM for r_c large enough, this model cannot be ruled out, and observations only place increasing lower bounds on r_c . But there is clearly no evidence in favor of the DGP modifications, and current data (including Planck 2013) yields $H_0 r_c > 12$ [Xu14].

1.5 Outline and Summary

We will now present an outline of the rest of this thesis, as well as a brief summary of the main results that will be obtained.

First, we will investigate the question how an outgoing wave condition can be implemented for gravitating codimension-two objects. A promising tool is provided by a

certain decomposition of the Weyl tensor into components with a clear physical interpretation. In particular, it is sometimes claimed in the literature that incoming and outgoing wave components of the gravitational field could be unambiguously identified this way. This claim will be scrutinized in Chap. 2, where we will find that while this identification does work in some cases (e.g. for plane waves), it fails in general—and in particular in the case of cylindrical waves which we are interested in. Therefore, this Weyl decomposition cannot be used to derive a local Friedmann equation for a codimension-two brane.

Physically, the origin of this failure can be traced back to the impossibility of *locally* distinguishing incoming from outgoing cylindrical waves—even for a linear wave equation on a flat background. This will be discussed in detail in Chap. 3, where the actual nonreflecting boundary condition will be derived, and shown to take the form of a convolution with a nontrivial retarded integral kernel. In other words, the outgoing cylindrical wave condition at some fixed radial position is nonlocal in time. As discovered by Einstein and Rosen, the exact vacuum solution describing cylindrical waves in GR is—surprisingly—also determined by a function satisfying the exact same *linear* wave equation as a scalar field on Minkowski. Therefore, this outgoing wave kernel also yields the correct boundary condition for codimension-two branes, implying that the corresponding Friedmann equation also has to be nonlocal. While making the cosmology of a codimension-two braneworld much more difficult on a technical level, this observation also shows that Weinberg’s 4D argument is not applicable here, suggesting that these models could indeed be able to incorporate a dynamical adjustment mechanism that cancels the CC.

But before turning to the actual codimension-two setup, an alternative generalization of the DGP model will be studied in Chap. 4. In this theory, which we will refer to as the “cosmic ring”, the DGP model is augmented by an additional *compact* on-brane dimension. This setup is the simplest member of the class of hybrid models containing both compact and infinite extra dimensions. It will be shown that in this case the Weyl criterion of Chap. 2 *is* applicable, since instead of cylindrical, plane waves are emitted. The corresponding (local) Friedmann equations only provide a closed system once an equation of state for the angular pressure in the compact direction is specified. We will consider two cases: If this pressure is used to stabilize the compact dimension, DGP cosmology is reproduced. However, we find that when the brane enters the CC dominated era, the stabilizing pressure violates the null energy condition, suggesting that the stabilization should brake down, thus leading to additional late time modifications. While potentially interesting, the consequences of an explicit UV model are beyond the scope of this thesis. In the second case we set the pressure to zero. Most interestingly, we will find degravitating attractor solutions, serving as a proof of principle; however, this model does not allow for a 4D regime and is thus ruled out phenomenologically, as will be demonstrated by fitting to SN data.

Chapter 5 finally turns to the actual codimension-two BIG model. To smooth out the (generically) divergent bulk metric at the brane position, the pointlike defect will be replaced by a ring of finite circumference, stabilized by a suitable angular pressure. The cosmological evolution of the brane will then be obtained by numerically integrat-



ing the full bulk-brane system forward in time.³⁷ Depending on the model parameters (on-brane energy density and crossover scale), two qualitatively different behaviors will be found: In the first class of solutions, all brane sources are degravitated, and—by emitting Einstein-Rosen waves into the bulk—the geometry quickly approaches the corresponding static, 4D flat solution which is only curved in the transverse bulk dimension. This confirms the realization of a dynamical degravitation mechanism at the fully nonlinear level. In the second class, the solutions behave pathological: the on-brane geometry super-accelerates, i.e. the Hubble parameter grows unbounded; furthermore, the effective brane energy (= energy + BIG term) which sources bulk gravitons becomes negative, and even tends to $-\infty$. In the subsequent section, by studying linear fluctuations around the static deficit angle background, a tachyonic ghost mode is identified as the origin of this unstable behavior. This confirms previous results on a Minkowski background in the literature,³⁸ but extends the analysis to nonzero values of the brane tension. Most importantly, it reconciles the codimension-two BIG model with the physical expectation of a healthy low energy EFT in the following way: The ghost disappears if the tension is large enough, i.e. it is caused by assuming a large BIG scale, but keeping the brane tension (unnaturally) small. Finally, the phenomenological viability of the model is investigated: unfortunately, the healthy parameter regime is in conflict with the requirement of a successful 4D behavior, and so the model is ruled out.

The preceding analysis was restricted to *sub-critical* brane tensions, for which the deficit angle of the static geometry is less than 2π . Chapter 6 addresses the *super-critical* case, for simplicity first in 4D GR. Using the same regularization as before, we find (numerically) that the corresponding static configuration—which here closes up in a conical singularity—is unstable. Instead, the expansion rate in axial string direction asymptotically approaches a constant nonzero value, and the exterior geometry (which is necessarily compact) takes the form of a growing cigar. Furthermore, the conical singularity can be avoided in these solutions, and a horizon is formed outside the string. Moreover, we are able to derive an analytic relation between the string tension and the axial expansion rate. When generalized to 6D BIG, this yields a Friedmann equation whose only (leading) modification is a small constant shift in the CC. Therefore, this model cannot help with the CC problem.

In the final part of this thesis, Chap. 7, we study the SLED model, in which 4D gravity on the codimension-two brane (without BIG terms) is achieved by compactifying the extra space into a rugby-ball. In the recent literature, this model was claimed to solve the CC problem if a brane-localized flux (BLF) is included. We show that (and why) this assertion was wrong, and that the BLF cannot help avoiding a fine-

³⁷Unfortunately, the outgoing wave condition of Chap. 3 will not be helpful here, because the brane with constant proper circumference has a nonvanishing coordinate-speed in the Einstein-Rosen frame, cf. Sec. 5.3.1.

³⁸Those were argued to be wrong in another recent publication [BHN12]; we will only briefly comment on the errors that led to this wrong conclusion, for more details see the appendix of our publication [ENS15].

tuning that is necessary to obtain 4D flat solutions, in accordance with Weinberg's no-go result (which is applicable to compact extra dimensions). The model could still be relevant if it naturally led to a nonzero, but small enough 4D curvature. The fact that the observed vacuum energy scale is of the same order as the Kaluza-Klein scale corresponding to the largest allowed size of the extra dimensions suggests that this might indeed be possible. However, by constructing explicit bulk solutions (again using the ring regularization), we find that this is not the case: For a nonzero brane width, there are contributions to the 4D Ricci scalar which are way too large to be phenomenologically viable, unless the brane width were allowed to be much smaller than the fundamental Planck length. Furthermore, even if this were tolerated, a scale invariance breaking brane tension (as should be expected for a realistic setup containing the Standard Model on the brane), would make either the bulk volume or the brane curvature (or both) much larger than phenomenologically allowed, unless again some sort of fine-tuning is assumed. In summary, we thus find that the SLED model cannot solve the CC problem either.



CHAPTER 2

INTERPRETATION OF THE WEYL TENSOR

Note: This chapter is to large extent a verbatim reproduction of the publication [HNS13], which arose in collaboration with Stefan Hofmann and Florian Niedermann.

In braneworld scenarios it is in general¹ necessary to impose boundary conditions at the brane that exclude incoming gravitational bulk waves, in order to obtain a unique time evolution for given on-brane initial data. This important point will be discussed in more detail in Chaps. 4 and 5, where the cosmologies of explicit brane world models are studied. Here, we focus on a tool known from the literature, which might be helpful in formulating such an outgoing wave boundary condition. The idea is to identify incoming and outgoing gravitational waves as certain components of the Weyl tensor. It applies to standard GR in d spacetime dimensions.

In this chapter, the notational conventions are the following: Capital Latin indices A, B, \dots denote d -dimensional spacetime indices (in the examples considered in this chapter, $d = 4$), boldface symbols denote d -dimensional vector- (or tensor-)fields, and small Latin indices a, b, \dots are tetrad indices. Small Latin indices i, j, \dots are those tetrad indices which run only over the $d - 2$ spatial tetrad vectors orthogonal to the privileged spatial direction (see below), whereas tetrad indices evaluated as 0 or 1 always correspond to the two null tetrad vectors, cf. Eq. (2.3.4). A dot is shorthand for the scalar product with respect to the metric \mathbf{g} , e.g. $\mathbf{x} \cdot \mathbf{y} \equiv g_{AB}x^Ay^B$ for vectors \mathbf{x} and \mathbf{y} . Antisymmetrization of indices is denoted by square brackets, i.e.

$$T_{[AB]} := \frac{1}{2} (T_{AB} - T_{BA}),$$

¹The codimension-one case is exceptional in this regard, at least when cosmological symmetries are imposed, because they exclude bulk waves thanks to Taub's (or Birkhoff's) theorem, cf. Sec 1.4.2.



and we also use the notation

$$T_{\{ABCD\}} := \frac{1}{2} (T_{[AB][CD]} + T_{[CD][AB]}).$$

For convenience, we work in units in which $M_{\text{Pl}} = 1$ in the present chapter.

2.1 Summary

According to folklore in general relativity, the Weyl tensor can be decomposed into parts corresponding to Newton-like, incoming and outgoing wavelike field components. It is shown here that this one-to-one correspondence does not hold for spacetime geometries with cylindrical isometries. This is done by investigating some well-known exact solutions of Einstein's field equations with whole-cylindrical symmetry, for which the physical interpretation is very clear, but for which the standard Weyl interpretation would give contradictory results. For planar or spherical geometries, however, the standard interpretation works for both, static and dynamical spacetimes. It is argued that one reason for the failure in the cylindrical case is that for waves spreading in two spatial dimensions there is no local criterion to distinguish incoming and outgoing waves already at the linear level. It turns out that Thorne's local energy notion, subject to certain qualifications, provides an efficient diagnostic tool to extract the proper physical interpretation of the spacetime geometry in the case of cylindrical configurations.

2.2 Introduction

Newton's theory of a gravitational force is given by the pair (\mathcal{G}, Φ) , where \mathcal{G} denotes Galilean space and Φ is the gravitational potential. In Einstein's theory of general relativity, the pair (\mathcal{G}, Φ) is superseded by (\mathcal{M}, g) , where \mathcal{M} denotes spacetime, modeled as a pseudo-Riemannian manifold with a local geometry represented by a metric field g . While in the classical theory the interpretation of Φ is completely clear—its gradient simply gives (minus) the acceleration that a test particle would undergo—an analogous interpretation of g and its derivatives is far from obvious in the relativistic theory. This is mainly due to the equivalence principle, saying that the affine connection (which is basically the first derivative of the metric, and thus analogue to the Newtonian force field) can be set to zero locally at any point $p \in \mathcal{M}$ by an appropriate choice of coordinates. A real gravitational effect is only present at p , if this cannot be done in a whole neighborhood of p simultaneously, or equivalently if the Riemann tensor at p does not vanish. Outside sources, the Riemann tensor reduces to the Weyl tensor \mathbf{C} . Thus, the physical content of the metric field in vacuum should be somehow encoded in \mathbf{C} . Moreover, instead of having only one static field component Φ , there are new dynamical degrees of freedom, corresponding to gravitational waves. It would thus be desirable to have a decomposition of the Weyl tensor into Newton-like parts and wavelike parts.

Since Einstein’s field equations are nonlinear and coupled, the possibility of a clear separation between Newton-like and wavelike contributions might be doubtful. However, Szekeres [Sze65] showed that such a decomposition can in fact be found, by following Pirani’s approach [Pir56] and studying the geodesic deviation for nearby freely falling test particles. More recently, this program has been generalized by Podolsky and Svarc [PS12] to spacetimes of arbitrary dimensions.

The main result of these investigations is that \mathbf{C} can be deconstructed into components corresponding to Newton-like² components and, in addition, to contributions corresponding to transverse and longitudinal, outgoing and incoming gravitational waves. We will refer to this result as the *standard interpretation* of the Weyl tensor. The standard interpretation is frequently quoted and used in the literature, see e. g. [SKM⁺03, Wan91, BB02, Nol04, NBBR06, NE08].

Here we show that, although the standard interpretation works very well in certain cases, there are other cases where it fails. This is done by studying two explicit examples of exact solutions of Einstein’s field equations, for which the true physical interpretation is evident, but where the standard interpretation would give contradictory results. To be more specific, we show that a nonzero component of the Weyl tensor does not imply the corresponding physical effect to be present. The correct physical interpretation can, however, still be deduced from the *asymptotic* falloff behavior of those components.

The rest of this chapter is organized as follows: In Sec. 2.3 we review the standard interpretation of the Weyl tensor, introduced by Pirani [Pir56, Pir09] and Szekeres [Sze65] using the concept of geodesic deviation. Section 2.4 is devoted to the discussion of planar and spherical geometries, both static and dynamical, for which the interpretation works very well. Then, in Sec. 2.5 we turn to solutions of Einstein’s equations with cylindrical isometries, again static as well as dynamical, and show that the standard interpretation breaks down. In Sec. 2.6 we note that the static cylindrically symmetric solution also invalidates Pirani’s wave criterion [Pir57], and in Sec. 2.7 we check that Thorne’s C-energy [Tho65] provides a good tool for cylindrical setups. Finally, we conclude in Sec. 2.8.

2.3 Standard Interpretation of Weyl components

Let us first briefly review the technique originally used by Szekeres [Sze65] to extract the physical meaning of the various components of the Weyl tensor, before we apply it to some concrete solutions of Einstein’s field equations.

Consider a timelike geodesic with unit tangent vector \mathbf{t} , and a neighboring timelike geodesic separated by the vector \mathbf{y} (parametrized such that $\mathbf{t} \cdot \mathbf{y} = 0$). Then, the geodesic deviation equation, governing the change of \mathbf{y} at linear order, in vacuum

²We will use the more appropriate name “Newton-like”, instead of Szekeres’ “Coulomb-like” [Sze65], which has become standard terminology. Some authors also choose the compromise “Newton-Coulomb-like” [PS12].



reads

$$\frac{D^2 y^A}{d\tau^2} = C^A{}_{BCD} t^B t^C y^D =: M^A{}_D y^D, \quad (2.3.1)$$

where $D/d\tau$ denotes covariant differentiation along the geodesic and $C^A{}_{BCD}$ is the Weyl tensor, i.e. the traceless part of the Riemann tensor:

$$C_{ABCD} = R_{ABCD} - \frac{2}{d-2} (R_{A[C} g_{B]D} - R_{B[C} g_{D]A}) + \frac{2}{(d-1)(d-2)} R g_{A[C} g_{D]B}. \quad (2.3.2)$$

Now complement \mathbf{t} with $d-1$ orthonormal spacelike vectors $\mathbf{x}_1, \dots, \mathbf{x}_{d-1}$ to obtain an orthonormal tetrad

$$\mathbf{e}_a = (\mathbf{t}, \mathbf{x}_1, \dots, \mathbf{x}_{d-1}), \quad \mathbf{e}_a \cdot \mathbf{e}_b = \eta_{ab}. \quad (2.3.3)$$

This tetrad defines a frame which an observer along the geodesic would use to make physical measurements. It is further convenient to define a null tetrad, but instead of working with a complex null tetrad, as is usually done in $d=4$, we will use the conventions of Podolsky and Svarc [PS12] and take a real null tetrad, or *mixed tetrad*, since this approach has the advantage of being applicable in any number of dimensions. The complexification of the two remaining spatial dimensions is in fact of no importance for the discussion, and the results will of course be completely equivalent. Therefore, we define

$$\mathbf{m}_a = (\mathbf{m}_0, \mathbf{m}_1, \mathbf{m}_i) := (\mathbf{k}, \mathbf{l}, \mathbf{m}_i) \quad (i = 2, \dots, d-1), \quad (2.3.4)$$

by combining one of the spacelike vectors, say $\mathbf{x}_1 =: \mathbf{x}$, with \mathbf{t} to form two appropriately normalized null vectors, and leaving the other vectors unchanged:

$$\mathbf{k} := \frac{1}{\sqrt{2}} (\mathbf{t} + \mathbf{x}), \quad \mathbf{l} := \frac{1}{\sqrt{2}} (\mathbf{t} - \mathbf{x}), \quad (2.3.5a)$$

$$\mathbf{m}_i := \mathbf{x}_i \quad (i = 2, \dots, d-1). \quad (2.3.5b)$$

This frame now satisfies the quasi-orthonormality relations

$$\mathbf{k} \cdot \mathbf{k} = \mathbf{l} \cdot \mathbf{l} = 0, \quad \mathbf{k} \cdot \mathbf{l} = -1, \quad (2.3.6a)$$

$$\mathbf{m}_i \cdot \mathbf{k} = \mathbf{m}_i \cdot \mathbf{l} = 0, \quad \mathbf{m}_i \cdot \mathbf{m}_j = \delta_{ij}, \quad (2.3.6b)$$

or, in matrix notation

$$\mathbf{m}_a \cdot \mathbf{m}_b = \tilde{\eta}_{ab} := \begin{pmatrix} 0 & -1 & 0 \\ -1 & 0 & 0 \\ 0 & 0 & \delta_{ij} \end{pmatrix}, \quad (2.3.7)$$

and the metric can be written as

$$g_{AB} = -k_A l_B - l_A k_B + m_A^2 m_B^2 + \dots + m_A^{d-1} m_B^{d-1}. \quad (2.3.8)$$

Note that here, and in what follows, all evaluated indices (and indices i, j, \dots) are to be understood as mixed tetrad indices, as defined in (2.3.4). Space-time indices will always remain unevaluated and denoted by A, B, \dots . The mixed tetrad indices are raised and lowered with $\tilde{\eta}_{ab}$ (and its inverse), in particular

$$\mathbf{m}^a = (\mathbf{m}^0, \mathbf{m}^1, \mathbf{m}^i) = (-l, -\mathbf{k}, \mathbf{m}_i). \quad (2.3.9)$$

The Weyl tensor can now be expressed in terms of its mixed tetrad components

$$C_{ABCD} = C_{abcd} m_A^a m_B^b m_C^c m_D^d, \quad (2.3.10)$$

which, using its symmetries $C_{ABCD} = C_{\{ABCD\}}$, can be expanded as

$$\begin{aligned} C_{ABCD} = & 4C_{0i0j} l_{\{A} m_B^i l_C m_D^j\} \\ & - 8C_{010i} l_{\{A} k_B l_C m_D^i\} - 4C_{0ijk} l_{\{A} m_B^i m_C^j m_D^k\} \\ & + 4C_{0101} l_{\{A} k_B l_C k_D\} + 4C_{01ij} l_{\{A} k_B m_C^i m_D^j\} \\ & + 8C_{0i1j} l_{\{A} m_B^i k_C m_D^j\} + C_{ijkl} m_{\{A}^i m_B^j m_C^k m_D^l\} \\ & - 8C_{101i} k_{\{A} l_B k_C m_D^i\} - 4C_{1ijk} k_{\{A} m_B^i m_C^j m_D^k\} \\ & + 4C_{1i1j} k_{\{A} m_B^i k_C m_D^j\}. \end{aligned} \quad (2.3.11)$$

Here, the terms have been ordered according to their *boost weights* [CMPP04], where some quantity Q is said to have boost weight b , if it transforms under a Lorentz boost with velocity v in direction \mathbf{x} as

$$Q \mapsto \lambda^b Q, \quad \lambda := \sqrt{\frac{1+v}{1-v}} > 1. \quad (2.3.12)$$

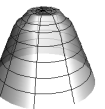
The physical interpretation of each term is then found by inserting (2.3.11) into (2.3.1) and using the various orthogonality relations. The corresponding contributions to the matrix M_{AD} in (2.3.1) are (the notation follows [DPPR10]):

(i) boost weight +2:

$$C_{0i0j} =: \Omega_{ij} \longrightarrow -\frac{1}{2} \Omega_{ij} m_A^i m_D^j \quad (2.3.13)$$

This gives rise to a deviation y^D of the neighboring geodesic into the hyperplane³ spanned by the \mathbf{m}^i , i.e. orthogonal to \mathbf{x} . Furthermore, since the matrix Ω_{ij} is symmetric and traceless, a sphere of test particles in this hyperplane will be deformed into an ellipsoid. This is the characteristic effect of a gravitational wave, and so Ω_{ij} is usually interpreted as (the modes of) a *transverse gravitational wave propagating in the direction $-\mathbf{x}$* . The direction of propagation can for instance be

³We use the terms “hyperplane”, “sphere” and “ellipsoid” in order to include higher-dimensional spacetimes. In $d = 4$, these terms can be replaced by “plane”, “circle” and “ellipse”.



inferred from the boost weight, which is +2 for Ω_{ij} . This means that a Lorentz boost in the direction $+\mathbf{x}$ will enhance this term, in accordance with the interpretation of a wave traveling in the opposite direction. Alternatively, inserting a plane wave traveling in direction $+\mathbf{x}$ shows that this term actually vanishes, cf. Sec. 2.4.3.

(ii) boost weight +1:

$$C_{010i} =: \Psi_i \longrightarrow \frac{1}{\sqrt{2}} \Psi_i (x_A m_D^i + m_A^i x_D) \quad (2.3.14)$$

This term is similar to the first one, but this time the deflection occurs in the $\mathbf{x}\text{-}\mathbf{m}^i$ hyperplane. Therefore, it is usually identified as a *longitudinal gravitational wave propagating in the direction $-\mathbf{x}$* .

(iii) boost weight 0:

$$C_{0101} =: \Phi, \quad C_{0i1j} =: \Phi_{ij} \longrightarrow -(\Phi x_A x_D + \Phi_{(ij)} m_A^i m_D^j) \quad (2.3.15)$$

Due to the traceless condition, $\Phi + \Phi^i_i = 0$, this term will stretch a sphere of test particles in the \mathbf{x} direction, while leading to contractions in the directions $\mathbf{m}^i \perp \mathbf{x}$ (or vice versa). Thus, it represents the (higher-dimensional) analogue of the tidal forces caused by localized, static sources, and can, therefore, be interpreted as a *Newton-like* part of the Weyl tensor.

(iv) boost weight -1:

$$C_{101i} =: \Psi'_i \longrightarrow \frac{1}{\sqrt{2}} \Psi'_i (x_A m_D^i + m_A^i x_D) \quad (2.3.16)$$

In complete analogy to case (ii), this term is interpreted as a *longitudinal gravitational wave propagating in the direction $+\mathbf{x}$* .

(v) boost weight -2:

$$C_{1i1j} =: \Omega'_{ij} \longrightarrow -\frac{1}{2} \Omega'_{ij} m_A^i m_D^j \quad (2.3.17)$$

In analogy to case (i), this term is interpreted as a *transverse gravitational wave propagating in the direction $+\mathbf{x}$* .

All other terms, i.e. those standing on the right in (2.3.11), only give vanishing contributions to (2.3.1). This does by no means imply that these components of the Weyl tensor have no physical effect, it only says that they give no linear order contribution to the relative acceleration of freely falling nearby test particles.

The privileged spatial vector \mathbf{x} , which is the direction of propagation of the gravitational wave components, can be chosen arbitrarily. In the general case it is of course possible to have superpositions of waves traveling in any direction. The geometries

considered by us explicitly, however, have sufficient isometries to single out a unique direction of propagation. This means that the two null vectors \mathbf{k} and \mathbf{l} are uniquely determined, apart from Lorentz boosts in the direction of wave propagation, a point which we will come back to later. There is also some freedom in choosing the remaining orthogonal tetrad vectors \mathbf{m}_i , corresponding to rotations in the plane orthogonal to the wave direction. This will however not affect any of our results.

2.4 Examples where the standard interpretation works

Let us first look at some exact vacuum solutions of Einstein's field equations, which support the standard interpretation of the Weyl components.

2.4.1 Static plane

The general plane-symmetric, static solution of Einstein's field equations in vacuum was first found by Levi-Civita [Lev18] (see also [AG83] for a more recent discussion), and can be written in the form

$$ds^2 = -a^{-2/3} dt^2 + dx^2 + a^{4/3} (dy^2 + dz^2), \quad (2.4.1a)$$

$$a(x) = 1 - \alpha x, \quad (2.4.1b)$$

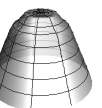
where α is some constant, and we used the gauge freedom to set $a(x=0) = 1$. As a source which gives rise to this geometry, we consider a thin layer of matter located at $x=0$, and so according to the symmetries of the set-up, the energy-momentum tensor has the form

$$T^A_B = \text{diag}(-\rho, 0, p, p) \delta(x). \quad (2.4.2a)$$

For $x \neq 0$, the metric is of the form (2.4.1). By choice, it is continuous across $x=0$ and accommodates different constants α in the half-spaces $x > 0$ and $x < 0$, say $\alpha_>$ and $\alpha_<$. These constants are not arbitrary, however, and must be chosen such that the discontinuity in the first derivative of the metric with respect to x implies, upon taking one more x derivative, the correct δ -like contribution, as given by (2.4.2a). This procedure corresponds to implementing Israel's junction conditions [Isr66, Isr67]. We will further assume the full metric to be symmetric across the plane, i.e. under $x \mapsto -x$, implying $\alpha_> = -\alpha_< =: \alpha$. Then, the junction conditions yield

$$\frac{8\alpha}{3} = \rho, \quad \frac{2\alpha}{3} = -p \quad \Rightarrow p = -\frac{\rho}{4}. \quad (2.4.3)$$

The matter source has to fulfill this EOS (implying a negative pressure) in order to allow for a static solution. Note that $\alpha > 0$ for a physically reasonable source with positive energy density.



The symmetry of this geometry suggests that we choose $\boldsymbol{x} = \boldsymbol{\partial}_x$ as the privileged direction, with respect to which we calculate the Weyl components. The corresponding mixed tetrad is

$$\boldsymbol{k} = \frac{1}{\sqrt{2}} (a^{1/3} \boldsymbol{\partial}_t + \boldsymbol{\partial}_x), \quad \boldsymbol{l} = \frac{1}{\sqrt{2}} (a^{1/3} \boldsymbol{\partial}_t - \boldsymbol{\partial}_x), \quad (2.4.4a)$$

$$\boldsymbol{m}_i = a^{-2/3} \boldsymbol{\partial}_i, \quad (i = y, z). \quad (2.4.4b)$$

However, there is a problem with this choice of tetrad: for the interpretation discussed above to apply, the timelike vector must be tangent to a geodesic. But $a^{1/3} \boldsymbol{\partial}_t$ is in fact *not* parallel transported along its integral curves (except for the trivial case $\alpha = 0$), so the frame (2.4.4) can actually not be used. However, since the metric (2.4.1) admits the Killing vectors \boldsymbol{m}_i , it is clear that geodesics exist with tangent vectors of the form $\boldsymbol{t} = f \boldsymbol{\partial}_t + g \boldsymbol{\partial}_x$ with some functions $f(x)$ and $g(x)$. The corresponding null vectors have the form $h^{\pm 1} (a^{1/3} \boldsymbol{\partial}_t \pm \boldsymbol{\partial}_x)$ with some function $h(x)$, which can be seen by requiring the various orthonormality relations among the vectors to hold. Therefore, the Weyl components in the frame (2.4.4) only differ from the ones for which the physical interpretation was derived by the overall factors $h^{\pm b} \neq 0$, where b is the corresponding boost weight. Hence, since it is sufficient for our purpose to identify the vanishing components, we might as well use the frame (2.4.4).

Having established the frame, it is straightforward to compute the various Weyl components. It turns out that all of the wave components vanish identically:

$$\Omega_{ij} = \Psi_i = 0 = \Omega'_{ij} = \Psi'_i, \quad (2.4.5)$$

and the only nonzero components are the Newton-like terms

$$\Phi = \frac{4\alpha^2}{9(1 - \alpha|x|)^2}, \quad \Phi_{ij} = -\frac{1}{2} \Phi \delta_{ij}. \quad (2.4.6)$$

This result is in perfect agreement with the standard interpretation of the various Weyl components.

For completeness, it should be mentioned that there are also some nonvanishing Weyl components in the non-observable sector of Sec. 2.3. They are again all of boost weight 0 and are given by

$$C_{ijkl} = -\frac{1}{2} \Phi (\delta_{ik} \delta_{jl} - \delta_{jk} \delta_{il}), \quad (2.4.7)$$

yielding no further independent components. Their appearance is implied by the Newton-like terms (2.4.6) by the traceless condition $C^i_{jik} = C_{0j1k} + C_{1j0k} = 2\Phi_{(jk)}$. Similar comments will also apply in the following examples, but we will not explicitly reiterate on this.

As an aside, note that there are spacetime singularities at $x = \pm 1/\alpha$, as can be seen by calculating the Kretschmann scalar $R^{ABCD} R_{ABCD} = 12\Phi^2$. However, as already remarked in the 5D analog in Sec. 1.4.2, geodesic motion of massive particles cannot reach them, and photons undergo an infinite redshift along geodesics towards the singularities [AG83]. As a consequence, the physically accessible spacetime only covers the open interval $x \in (-1/\alpha, 1/\alpha)$.

2.4.2 Schwarzschild

In the static Schwarzschild geometry, we expect that again only the Newton-like field components are present. Let us now verify that this is indeed the case. The metric outside the Schwarzschild radius r_s is given by

$$ds^2 = -f dt^2 + f^{-1} dr^2 + r^2 [d\theta^2 + \sin(\theta)^2 d\phi^2], \quad (2.4.8a)$$

$$f(r) = 1 - \frac{r_s}{r}. \quad (2.4.8b)$$

This time, the symmetry allows us to identify $\mathbf{x} \propto \partial_r$ as the privileged spatial direction, and so the corresponding mixed tetrad reads

$$\mathbf{k} = \frac{1}{\sqrt{2}} (f^{-1/2} \partial_t + f^{1/2} \partial_r), \quad (2.4.9a)$$

$$\mathbf{l} = \frac{1}{\sqrt{2}} (f^{-1/2} \partial_t - f^{1/2} \partial_r), \quad (2.4.9b)$$

$$\mathbf{m}_1 = \frac{1}{r} \partial_\theta, \quad \mathbf{m}_2 = \frac{1}{r \sin(\theta)} \partial_\phi. \quad (2.4.9c)$$

As before, $f^{-1/2} \partial_t$ is not tangent to a geodesic, but a discussion completely analogous to the corresponding situation in the example of a static plane applies, and so we can in fact use this frame. And again, all of the wave components vanish, the only nonzero components being the Newton-like terms

$$\Phi = -\frac{r_s}{r^3}, \quad \Phi_{ij} = -\frac{1}{2} \Phi \delta_{ij}. \quad (2.4.10)$$

As a result, also in the case of a spherically symmetric geometry, the standard interpretation of the Weyl components works perfectly well.

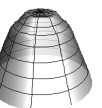
2.4.3 Plane wave

Next, we consider the complementary case: instead of a static field configuration which only has Newton-like components, we investigate a geometry that corresponds to pure plane gravitational waves. In this case, only the wavelike components are expected to be nonzero. Specifically, consider the well-known pp-wave vacuum solution [Bri25] (see also [SKM⁺03, chap. 24.5])

$$ds^2 = -2h du^2 - 2dudv + dy^2 + dz^2, \quad (2.4.11a)$$

with

$$h(u, y, z) = a(u) (y^2 - z^2) / 2 + b(u) y z, \quad (2.4.11b)$$



where $a(u)$ and $b(u)$ are some arbitrary functions. The exact solution (2.4.11) represents a plane gravitational wave with wave vector $\boldsymbol{\partial}_v$, and the corresponding mixed tetrad frame reads

$$\mathbf{k} = \boldsymbol{\partial}_v, \quad \mathbf{l} = \boldsymbol{\partial}_u - h\boldsymbol{\partial}_v, \quad (2.4.12a)$$

$$\mathbf{m}_i = \boldsymbol{\partial}_i, \quad (i = y, z). \quad (2.4.12b)$$

Note that this time, the vector \mathbf{k} is tangent to a *null* geodesic. However, this poses no conceptual problem, since the standard interpretation of the Weyl tensor as discussed in section 2.3 can analogously be applied to null geodesics instead of timelike geodesic, cf. [Wan91].

And indeed, in the frame (2.4.12) the only nonvanishing Weyl components are

$$\Omega'_{ij} = \begin{pmatrix} a(u) & b(u) \\ b(u) & -a(u) \end{pmatrix}, \quad (2.4.13)$$

while, in particular, $\Omega_{ij} = 0$. Hence, the standard interpretation of the Weyl tensor correctly identifies the purely wavelike field character, as well as the direction of propagation of the wave. Evidently, the two arbitrary functions a and b are precisely the two modes of the gravitational wave.

2.4.4 Spherical wave

Let us finally investigate the Robinson-Trautman spacetime [RT60] (see also [SKM⁺03, chap. 28]), which can be interpreted as describing spherical (but of course not spherically symmetric) gravitational waves. The metric has the form

$$ds^2 = -2Hdu^2 - 2dudr + \frac{r^2}{p^2} (d\xi^2 + d\eta^2), \quad (2.4.14)$$

where p is a function of (u, ξ, η) and

$$H(u, r, \xi, \eta) = \frac{1}{2}\Delta \ln p - r (\ln p)' - \frac{m(u)}{r}, \quad (2.4.15)$$

with $\Delta := p^2 (\partial_\xi^2 + \partial_\eta^2)$ and the prime denoting differentiation with respect to u . With this choice, the vacuum Einstein equations reduce to the single fourth order differential equation

$$\Delta \Delta \ln(p) + 12m (\ln p)' - 4m' = 0. \quad (2.4.16)$$

Here u is a retarded time coordinate and $\boldsymbol{\partial}_r$ is tangent to a null geodesic. We can therefore choose the mixed tetrad frame

$$\mathbf{k} = \boldsymbol{\partial}_r, \quad \mathbf{l} = \boldsymbol{\partial}_u - H\boldsymbol{\partial}_r, \quad (2.4.17a)$$

$$\mathbf{m}_i = \frac{p}{r} \boldsymbol{\partial}_i \quad (i = \xi, \eta), \quad (2.4.17b)$$

in which the nonzero, independent components of the Weyl tensor become

$$\Phi_{ij} = \frac{m}{r^3} \delta_{ij}, \quad (2.4.18a)$$

$$\Psi'_i = -\frac{p}{2r^2} \partial_i \Delta \ln p, \quad (2.4.18b)$$

$$\Omega'_{ij} = \frac{1}{2r} \begin{pmatrix} A_{11} - A_{22} & A_{12} + A_{21} \\ A_{21} + A_{12} & -A_{11} + A_{22} \end{pmatrix}, \quad (2.4.18c)$$

with

$$A_{ij} := \partial_i \left\{ p^2 \partial_j \left[\frac{1}{2} \Delta \ln p - r (\ln p)' \right] \right\}. \quad (2.4.18d)$$

The main result is that indeed all the incoming (i.e. in the direction opposite to u) components Ψ_i and Ω_{ij} vanish, and only Newton-like and outgoing wavelike components are present in general. (Note that “pure wave” solutions without Newton-like admixture can be constructed by setting $m = 0$.) Therefore, this example is also in perfect agreement with the standard interpretation.

The explicit form of the Weyl components depends on the particular solution of (2.4.16), one example being [RT60]

$$m(u) = m_0 = \text{const}, \quad p(u, \xi, \eta) = \xi^{3/2}, \quad (2.4.19)$$

for which

$$\Phi_{ij} = \frac{m_0}{r^3} \delta_{ij}, \quad \Psi'_\xi = -\frac{3\xi^{3/2}}{4r^2}, \quad \Omega'_{ij} = \frac{9\xi^2}{8r^2} \begin{pmatrix} -1 & 0 \\ 0 & 1 \end{pmatrix}. \quad (2.4.20)$$

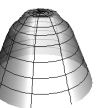
These terms have the correct falloff behavior $\sim 1/r^3$ and $\sim 1/r^2$ for Newton-like and wavelike components, respectively, expected in a spatially three-dimensional, spherical setup.⁴ The scaling $\sim 1/r^2$ of the wave components is also in agreement with the asymptotic criterion for outgoing waves put forward in [ADM61].

2.5 Examples where the standard interpretation fails

In this section we prove that the standard interpretation of the Weyl tensor is not applicable to all spacetime geometries. The focus will be on geometries with whole-cylinder symmetry, i.e. those with azimuthal ϕ symmetry and symmetry along a z direction perpendicular to ϕ , for which the metric can most conveniently be written in the form (see e.g. [Tho65] or [SKM⁺03, chap. 22])

$$ds^2 = e^{2(\eta-\alpha)} (-dt^2 + dr^2) + e^{2\alpha} dz^2 + e^{-2\alpha} W^2 d\phi^2, \quad (2.5.1)$$

⁴Note that the Weyl tensor is basically the second derivative of the metric, so the Newtonian $\sim 1/r$ potential of a spherical symmetric source in three space dimensions would manifest itself as a $\sim 1/r^3$ contribution to the Weyl tensor.



where η, α and W are functions of (t, r) . Note that (2.5.1) only describes a cylindrical geometry, if there is an axis (which we will assume to be located at $r = 0$), on which the norm of the Killing vector associated with ϕ symmetry $\sigma = \partial_\phi$ vanishes:

$$\sigma^2 \equiv \sigma_A \sigma^A = W^2 e^{-2\alpha} \xrightarrow{r \rightarrow 0} 0. \quad (2.5.2)$$

Furthermore, requiring the metric not to have a conical singularity at $r = 0$ leads to the following *regularity condition* on the axis [MS93]:

$$\frac{\nabla_A(\sigma^2)\nabla^A(\sigma^2)}{4\sigma^2} = W^2 e^{-2\eta} \left[-\left(\frac{\dot{W}}{W} - \dot{\alpha}\right)^2 + \left(\frac{W'}{W} - \alpha'\right)^2 \right] \xrightarrow{r \rightarrow 0} 1. \quad (2.5.3)$$

In these coordinates, the Einstein field equations read:

$$\frac{W''}{W} - \frac{\ddot{W}}{W} = \mathcal{T}_t^t + \mathcal{T}_r^r, \quad (2.5.4a)$$

$$\alpha'' + \frac{W'}{W}\alpha' - \ddot{\alpha} - \frac{\dot{W}}{W}\dot{\alpha} = 2\left(\mathcal{T}_t^t + \mathcal{T}_r^r - \mathcal{T}_z^z + \mathcal{T}_\phi^\phi\right), \quad (2.5.4b)$$

$$\alpha'^2 + \dot{\alpha}^2 - \frac{W'}{W}\eta' - \frac{\dot{W}}{W}\dot{\eta} + \frac{\ddot{W}}{W} = -\mathcal{T}_r^r, \quad (2.5.4c)$$

$$\alpha'^2 - \dot{\alpha}^2 + \eta'' - \ddot{\eta} = \mathcal{T}_\phi^\phi, \quad (2.5.4d)$$

$$2\alpha'\dot{\alpha} - \frac{W'}{W}\dot{\eta} - \frac{\dot{W}}{W}\eta' + \frac{\dot{W}'}{W} = \mathcal{T}_r^t, \quad (2.5.4e)$$

where we defined

$$\mathcal{T}^A_B := e^{2(\eta-\alpha)} T^A_B, \quad (2.5.5)$$

with T^A_B being the energy momentum tensor.

The symmetry of the metric (2.5.1) allows us to identify $\mathbf{x} \propto \partial_r$ as the direction of wave propagation, and the corresponding mixed null tetrad is

$$\mathbf{k} = \frac{e^{\alpha-\eta}}{\sqrt{2}} (\partial_t + \partial_r), \quad \mathbf{l} = \frac{e^{\alpha-\eta}}{\sqrt{2}} (\partial_t - \partial_r), \quad (2.5.6a)$$

$$\mathbf{m}_1 = e^{-\alpha} \partial_z, \quad \mathbf{m}_2 = \frac{e^\alpha}{W} \partial_\phi. \quad (2.5.6b)$$

Again, the vector $e^{\alpha-\eta} \partial_t$ is in general not tangent to a geodesic, but due to the symmetries of the metric (2.5.1), the same argument as presented below equation (2.4.4) in the static planar case applies here as well. Thus, according to the standard interpretation, the primed components of the Weyl tensor (Ψ' and Ω') evaluated in the frame (2.5.6) should correspond to *outgoing* waves, and the unprimed ones (Ψ and Ω) to *incoming* waves.

2.5.1 Static cylinder

Let us first discuss the static solution, i.e. all metric functions depend only on r , and choose a cylindrical shell of matter located at $r = r_0$ as a source:

$$T^A_B = \text{diag}(-\rho, 0, p_z, p_\phi) \frac{1}{W} \delta(r - r_0). \quad (2.5.7a)$$

The metric outside such a static cylinder was first derived by Levi-Civita [Lev19] (see also, e.g. [Tho65]). Like in the planar case, the full solution of Einstein's field equations can be obtained by first solving the homogeneous equations inside and outside the cylinder, and then matching the solutions such that the metric is continuous across the cylinder, but the first r derivatives are discontinuous in order for the second r derivatives on the left-hand side to produce the correct δ -like contribution (2.5.7a) on the right-hand side. By further implementing the regularity conditions (2.5.2) and (2.5.3), we arrive at

$$W(r) = \begin{cases} r & (r < r_0) \\ r_0 + W_1(r - r_0) & (r > r_0), \end{cases} \quad (2.5.8a)$$

$$\alpha(r) = \begin{cases} 0 & (r < r_0) \\ \alpha_1 \ln [W(r)/r_0] & (r > r_0), \end{cases} \quad (2.5.8b)$$

$$\eta(r) = \begin{cases} 0 & (r < r_0) \\ \alpha_1^2 \ln [W(r)/r_0] & (r > r_0), \end{cases} \quad (2.5.8c)$$

where α_1 and W_1 are constants of integration. Inside the cylinder the metric is just that of Minkowski space, and outside it has the form

$$ds^2_{>} = \left(\frac{W(r)}{r_0}\right)^{2\alpha_1(\alpha_1-1)} (-dt^2 + dr^2) + \left(\frac{W(r)}{r_0}\right)^{2\alpha_1} dz^2 + \left(\frac{W(r)}{r_0}\right)^{2(1-\alpha_1)} r_0^2 d\phi^2. \quad (2.5.9)$$

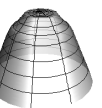
The junction conditions across $r = r_0$ imply that the constants α_1 and W_1 are related to the source localized on the cylindrical shell by

$$W_1 = 1 - \rho, \quad \alpha_1 W_1 = -\frac{1}{2} (\rho + p_z - p_\phi), \quad (2.5.10)$$

as well as the following relation between the energy-momentum components,

$$4(1 - \rho) p_\phi = (\rho + p_z - p_\phi)^2. \quad (2.5.11)$$

Physically, this EOS again originates from the requirement for the source to be in hydrostatic equilibrium, since otherwise the solution would not be static. Note that for $p_\phi = 0$ these relations imply the EOS $p_z = -\rho$ as well as $\alpha_1 = 0$, and the solution becomes the geometry of a cosmic string [Vil81, His85], which only produces a deficit angle in the outside geometry, and has a vanishing Weyl tensor for $r > r_0$. If $p_\phi \neq$



0, however, the parameter α_1 can in principle take any value, leading to an outside geometry that is not Riemann flat. The Weyl components for the solution (2.5.8) become, for $r > r_0$,

$$\Phi = \Phi_0 e^{2(\alpha-\eta)}, \quad \Phi_{ij} = -\frac{1}{2}\Phi_0 e^{2(\alpha-\eta)} \delta_{ij}, \quad (2.5.12a)$$

$$\Omega_{ij} = \Omega'_{ij} = \Omega e^{2(\alpha-\eta)} \begin{pmatrix} 1 & 0 \\ 0 & -1 \end{pmatrix}, \quad (2.5.12b)$$

with

$$\Omega := \frac{\alpha_1}{2}(\alpha_1 - 1)(2\alpha_1 - 1) \left(\frac{W_1}{W(r)} \right)^2, \quad (2.5.12c)$$

$$\Phi_0 := -\alpha_1(\alpha_1 - 1) \left(\frac{W_1}{W(r)} \right)^2. \quad (2.5.12d)$$

Incidentally, this shows that the geometry is always asymptotically (locally) flat for $r \rightarrow \infty$ because

$$e^{2(\alpha-\eta)} W(r)^{-2} = r_0^2 W(r)^{-2(\alpha_1^2 - \alpha_1 + 1)} \quad (2.5.13)$$

and

$$2(\alpha_1^2 - \alpha_1 + 1) > \frac{3}{2} \quad \forall \alpha_1, \quad (2.5.14)$$

and we assume $W_1 > 0$ in order to avoid a second axis outside the cylinder, where $W(r)$ would be zero.⁵ Moreover, all Weyl components have the same falloff behavior which is $\sim r^{-2}$ for Φ_0 and Ω .

The problem with the standard interpretation is now manifest: if the standard interpretation of the individual components were correct, we would conclude that (except for the special cases $\alpha_1 \in \{0, 1, 1/2\}$) there are incoming and outgoing waves present in this solution. The geometry, however, is in fact *static*, so we know for sure that there are actually no waves at all. This shows that the Ω parts of the Weyl tensor are not only due to gravitational wave components, but also due to static, i.e. Newton-like field components. There is no contradiction to the discussion of the geodesic deviation in Sec. 2.3, because the tidal forces in the z and ϕ directions, acting on a freely falling observer in the cylindrical geometry (2.5.9), will in general not be equal, and, therefore, can produce an elliptical deformation of test particles precisely in the same way as discussed in Sec. 2.3. As a result, the Ω parts of the Weyl tensor cannot be used to extract the purely wavelike content of the spacetime geometry.

It should be noted that this also provides a counter-example for a more recent suggestion of a ‘‘radiation scalar’’ [BB02], which was defined as the product of the complex Weyl scalars Ψ_0 and Ψ_4 , in a tetrad frame in which Ψ_1 and Ψ_3 are zero.⁶ Using our

⁵According to (2.5.10), this is equivalent to requiring $\rho < 1$. Larger energy densities would be *super-critical*; the special case of a super-critical cosmic string ($p_z = -\rho$, $p_\phi = 0$) will be studied in Chap. 6.

⁶The relation between the complex Weyl scalars, usually used in four spacetime dimensions, and the real ones that we use, can be found in [PS12]

variables, the latter requirement translates to $\Psi = \Psi' = 0$, and is thus satisfied by our static solution. Furthermore, in this solution the radiation scalar becomes Ω^2 , which is in general nonvanishing. This shows that the following claim in [BB02],

“[the radiation scalar] vanishes in regions of space-time which can be said unambiguously to contain no gravitational radiation”,

is not true.

However, one might still hope that even though the interpretation of the Ω terms fails for static geometries, it could still be valid for pure wave solutions, and in particular the distinction between incoming and outgoing waves could still be rigorously made for those cases. Unfortunately, this is also not true, as we will show in the next section.

2.5.2 Einstein-Rosen waves

To this end, consider cylindrically symmetric gravitational waves, first discovered by Einstein and Rosen [ER37] (see also, e.g. [Mar58]). The metric for this class of vacuum solutions is obtained from (2.5.1) by setting $W = r$:

$$ds^2 = e^{2(\eta-\alpha)} (-dt^2 + dr^2) + e^{2\alpha} dz^2 + e^{-2\alpha} r^2 d\phi^2. \quad (2.5.15)$$

We refrain from specifying the energy-momentum tensor that would give rise to the cylindrical waves and simply assume that there is some time-dependent source distributed in accordance with the cylindrical symmetry over a bounded region around the axis at $r = 0$. Thus, we only consider the vacuum Einstein equations outside this region, which take the simple form

$$-\ddot{\alpha} + \alpha'' + \frac{\alpha'}{r} = 0, \quad (2.5.16a)$$

$$\eta' = r (\alpha'^2 + \dot{\alpha}^2), \quad \dot{\eta} = 2r\alpha'\dot{\alpha}. \quad (2.5.16b)$$

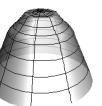
The first equation is nothing but the linear cylindrical wave equation in flat space, and given any solution α of this equation, the other two—which are consistent on account of the first one—can simply be integrated to obtain η .

Since this system is so simple, but still represents exact solutions of Einstein’s field equations with a clear physical interpretation, it is a perfect candidate to test the standard interpretation of the Weyl components. For the metric (2.5.15), the nonzero, independent components of the Weyl tensor become, after some simplifications using the vacuum equations (2.5.16),

$$\Omega_{ij} = \Omega^{(\text{in})} e^{2(\alpha-\eta)} \begin{pmatrix} 1 & 0 \\ 0 & -1 \end{pmatrix}, \quad (2.5.17a)$$

$$\Phi = \Phi_0 e^{2(\alpha-\eta)}, \quad (2.5.17b)$$

$$\Omega'_{ij} = \Omega^{(\text{out})} e^{2(\alpha-\eta)} \begin{pmatrix} 1 & 0 \\ 0 & -1 \end{pmatrix}, \quad (2.5.17c)$$



with

$$\Omega^{(\text{in})} := -\frac{1}{2} \left\{ [3 - 2r(\alpha' + \dot{\alpha})] (\alpha' + \dot{\alpha})^2 + \alpha'' + 2\dot{\alpha}' + \ddot{\alpha} \right\}, \quad (2.5.17d)$$

$$\Phi_0 := \left(\frac{1}{r} - \alpha' \right) \alpha' + \dot{\alpha}^2, \quad (2.5.17e)$$

$$\Omega^{(\text{out})} := -\frac{1}{2} \left\{ [3 - 2r(\alpha' - \dot{\alpha})] (\alpha' - \dot{\alpha})^2 + \alpha'' - 2\dot{\alpha}' + \ddot{\alpha} \right\}. \quad (2.5.17f)$$

Now consider, for example, a solution of (2.5.16a) corresponding to a purely outgoing⁷ wave with frequency ω :

$$\begin{aligned} \alpha(t, r) &= \text{Re} \left[e^{-i\omega t} H_0^{(1)}(\omega r) \right] \\ &= \cos(\omega t) J_0(\omega r) + \sin(\omega t) Y_0(\omega r), \end{aligned} \quad (2.5.18)$$

where $H_0^{(1)}$ denotes the Hankel function of the first kind, and J_0 and Y_0 are the Bessel functions of the first and second kind, respectively. Plugging (2.5.18) into (2.5.17) yields some complicated expressions for the three components, containing trigonometric and Bessel functions, the explicit form of which is not of great interest. The main point is that they are all nonvanishing, even though their magnitude and falloff behavior with r is different, cf. Fig. 2.1. Furthermore, they all behave like outgoing waves, in accordance with our choice (2.5.18), confirming that the geometry only contains outgoing wave components.

The observation that the component Φ is nonzero is not too disturbing, because an outgoing wave could also induce Newton-like contributions—even though the solution (2.5.18) does not contain a static, Newton-like part $\propto \ln(r)$. But the fact that $\Omega^{(\text{in})}$ is nonzero, and furthermore also behaves like an outgoing wave, clearly shows that the interpretation of $\Omega^{(\text{in})}$ as an incoming gravitational wave is not correct.

Even though the interpretation that $\Omega^{(\text{in})}$ corresponds to incoming gravitational waves is wrong, there is still a difference between the different Weyl components: they all have a distinct falloff behavior as $r \rightarrow \infty$. Only $\Omega^{(\text{out})}$ falls asymptotically off like a cylindrical wave, viz. $\sim r^{-1/2}$, whereas all other components fall off faster. So in the case of pure cylindrical waves, the interpretation still works asymptotically far away from the source. This can physically be understood because for $r \rightarrow \infty$ cylindrical waves look like plane waves, for which we saw that the decomposition into incoming and outgoing wave components is successful.

This might be considered a window of opportunity, indicating that the standard interpretation of the Weyl components might in general still hold asymptotically far away from the source. However, for the static solution discussed in Sec. 2.5.1, all the

⁷That outgoing modes of cylindrical waves are indeed represented by $\exp(-i\omega t)$ times a Hankel function of the first kind will be discussed in more detail in Chap. 3. Here, it can already be seen in a qualitative way from the plots in Fig. 2.1.

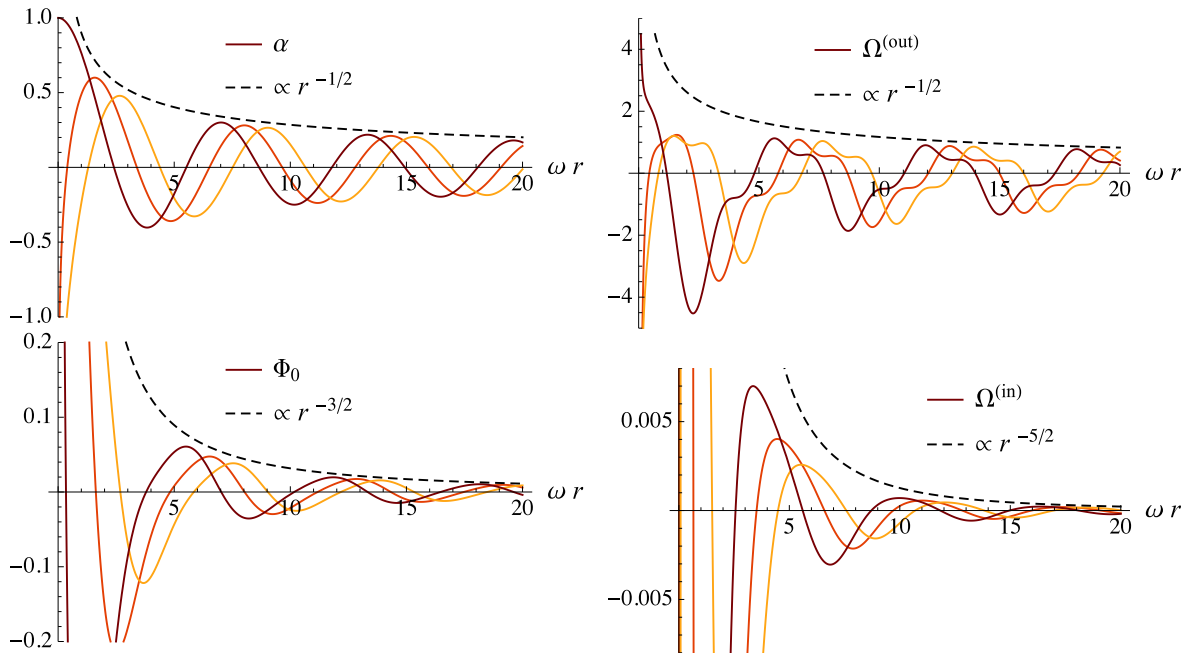
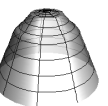


Figure 2.1: Plots of the metric function α and all the independent components of the Weyl tensor for the outgoing Einstein-Rosen wave solution (2.5.18). The dark red lines correspond to $t = 0$, whereas the orange and yellow lines are evaluated at times $t = 1/\omega$ and $t = 2/\omega$, respectively. Evidently, all functions behave like waves propagating outwards. All the Weyl terms have different falloff behavior with r , $\Omega^{(\text{out})}$ being the only component with the same behavior $\propto 1/\sqrt{r}$ as a linear cylindrical wave, but they are all nonvanishing.

components have exactly the same falloff behavior,⁸ cf. Eq. (2.5.12). Thus, it is *not true* in general that the decomposition into Newton- and wavelike components gets better and better in the limit $r \rightarrow \infty$. Physically, the key difference between the pure wave and the static case is, of course, that while waves look like plane waves far away from the source, the cylinder does not look like a plane from far away.

On the other hand, as shown in Sec. 2.5.1, the wave components that are due to such a static field always fall off like $\Omega \sim r^{-2}$, i.e. faster than $\sim r^{-1/2}$ which is the characteristic falloff behavior of the actual gravitational waves. Therefore, the correct statement is the following: in the case of a cylindrical geometry, those parts of the wave components $\Omega^{(\text{in})}$ and $\Omega^{(\text{out})}$ that fall off like $\sim r^{-1/2}$ are due to incoming and outgoing gravitational waves, respectively. Thus, the standard interpretation still applies to cylindrically symmetric geometries in the weaker sense that the presence and distinction of incoming and outgoing radiation can be inferred from the asymptotic falloff behavior

⁸As discussed below equation (2.4.4) the different Weyl components could get overall factors if one took the true geodesic tetrad, which could change the falloff behavior. But these factors come with powers of the boost weight of the corresponding components, and so it is not possible that both Ω and Ω' could both become suppressed relative to Φ for the static cylindrically symmetric solution. If one of them is suppressed, the other one will always be enhanced.



of the respective wave components of the Weyl tensor. But our result unambiguously shows that these components cannot be used as a local criterion, i.e. by evaluating them at some fixed value of r , for the presence or absence of gravitational waves.

2.6 Pirani's criterion

In [Pir57], Pirani suggested a slightly different criterion for deciding whether a given geometry contains gravitational waves or not, depending on its Petrov type:⁹

“At any event in empty spacetime, gravitational radiation is present if the Riemann tensor is of Type II or Type III, but not if it is of Type I.”

(Note that here type D and N should be understood as subclasses included in type I and II, respectively.) The difference to the Weyl component criterion is that a Petrov type I spacetime can have nonvanishing components Ω and Ω' [SKM+03, Chap. 4.2]. However, they must be equal, and so Pirani would correctly classify the static example of Sec. 2.5.1 as one without waves, because it is of type I. However, it turns out that the dynamical solution of Einstein-Rosen waves can in fact be of type I. Actually, this example was also discussed by Pirani in [Pir57], claiming that it is of type II and thus in accordance with his definition. But this statement is false: even though they *can* be of type II, they can *also* be of type I [SKM+03, p. 352], as is for example the case for our outgoing wave solution. Therefore, Pirani's diagnostic tool also does not work in general.

2.7 Thorne's C-energy

For whole-cylindrically symmetric spacetime geometries, like the ones discussed in Sec. 2.5, Thorne was able to define a physically well-motivated notion of local energy, the so called “C-energy” [Tho65]. It is given by a covariantly conserved four-vector \mathbf{P} , which can be viewed as the flux vector of gravitational energy. For an (accelerated) observer localized at constant spatial coordinates, P^t is thus the energy density, and P^r corresponds to the flux of energy in radial direction. Therefore, P^r could be used as a diagnostic tool, which should be nonzero only if gravitational waves are present, and the sign of which should determine the direction of propagation.

Let us, for convenience, briefly recall the definition from [Tho65]. The C-energy flux vector \mathbf{P} is defined as

$$P^A := \frac{\epsilon^{ABCD}}{\sqrt{-g}} (\partial_B E) \frac{\xi_{(z)C} \xi_{(\phi)D}}{|\xi_{(z)}|^2 |\xi_{(\phi)}|^2}, \quad (2.7.1)$$

where $\epsilon^{ABCD} = +1$ when $(ABCD)$ are even permutations of $(trz\phi)$, $\xi_{(z)}$ and $\xi_{(\phi)}$ are the two Killing vectors of the whole cylindrical geometry (normalized such that

⁹For a discussion of the Petrov classification, see [SKM+03, Chap. 4] and references therein.

$|\boldsymbol{\xi}_{(z)}| = 1$ on the symmetry axis when there is no gravitational radiation present, and $|\boldsymbol{\xi}_{(\phi)}|$ measures the proper circumference around the axis), and E denotes the “potential function” for C-energy:

$$E := -\pi \ln \left[\frac{\partial_A (|\boldsymbol{\xi}_{(z)}| |\boldsymbol{\xi}_{(\phi)}|) \partial^A (|\boldsymbol{\xi}_{(z)}| |\boldsymbol{\xi}_{(\phi)}|)}{4\pi^2 |\boldsymbol{\xi}_{(\phi)}|^2} \right]. \quad (2.7.2)$$

In the coordinates (2.5.1), the Killing vectors have the components

$$\xi_{(z)}^A = h_z \delta_z^A, \quad \xi_{(\phi)}^A = 2\pi \delta_\phi^A, \quad (2.7.3)$$

where h_z is some positive constant (which is fixed by requiring the proper normalization of $\boldsymbol{\xi}_{(z)}$). The potential function then becomes

$$E = 2\pi \left[\eta - \frac{1}{2} \ln (W'^2 - \dot{W}^2) \right], \quad (2.7.4)$$

and the nonvanishing components of the flux vector are

$$P^t = + \frac{1}{2\pi h_z} \frac{e^{2(\alpha-\eta)}}{W} E', \quad (2.7.5a)$$

$$P^r = - \frac{1}{2\pi h_z} \frac{e^{2(\alpha-\eta)}}{W} \dot{E}. \quad (2.7.5b)$$

Inserting (2.7.4) in (2.7.5), and using the Einstein field equations (2.5.4) in vacuum, the flux vector can be written as

$$P^t = \kappa \frac{W'(\dot{\alpha}^2 + \alpha'^2) - 2\dot{W}\dot{\alpha}\alpha'}{W'^2 - \dot{W}^2}, \quad (2.7.6a)$$

$$P^r = \kappa \frac{\dot{W}(\dot{\alpha}^2 + \alpha'^2) - 2W'\dot{\alpha}\alpha'}{W'^2 - \dot{W}^2}, \quad (2.7.6b)$$

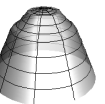
where κ denotes the manifestly positive—and thus for our purposes irrelevant—factor $\kappa := \exp[2(\alpha - \eta)]/h_z$.

From (2.7.5b) it follows immediately that the energy flux P^r indeed vanishes for the static solution (2.5.8), which has the only nonzero component

$$P^t = \frac{\kappa \alpha_1^2 W_1}{W(r)^2}. \quad (2.7.7)$$

So this time the static, Newton-like character of the spacetime is correctly reproduced. Furthermore, P^t is non-negative,¹⁰ which is of course necessary for it to be interpreted as an energy density.

¹⁰Here, we are restricting ourselves to the sub-critical case $\rho < 1$, which according to (2.5.10) implies $W_1 > 0$. In the super-critical case, which will be considered in Chap. 6, positivity is still ensured by the switch of radial orientation.



For the Einstein-Rosen geometry (2.5.15), the flux vector in vacuum simplifies to

$$P^t = \kappa \left(\dot{\alpha}^2 + \alpha'^2 \right), \quad (2.7.8a)$$

$$P^r = -2\kappa\dot{\alpha}\alpha', \quad (2.7.8b)$$

which for the outgoing wave (2.5.18) gives

$$P^t = \kappa\omega^2 \left[(J_1 \cos + Y_1 \sin)^2 + (Y_0 \cos - J_0 \sin)^2 \right], \quad (2.7.9a)$$

$$P^r = 2\kappa\omega^2 (Y_0 \cos - J_0 \sin) (J_1 \cos + Y_1 \sin), \quad (2.7.9b)$$

where the arguments ωr for the Bessel functions, and ωt for the trigonometric functions should be understood. First of all, note that P^t is again manifestly non-negative, as is required for its interpretation as an energy density. Furthermore, the flux in r direction does not vanish, in agreement with the presence of gravitational waves. As can be seen from the plot in Fig. 2.2, it is *not* strictly positive, though; in the region close to the axis at $r = 0$, it becomes negative. This effect, however, disappears if the flux averaged over one period $T \equiv 2\pi/\omega$ is considered:

$$\langle P^r \rangle := \frac{1}{T} \int_0^T dt P^r = \frac{2\kappa\omega}{\pi r}. \quad (2.7.10)$$

This has exactly the form expected for a stationary flux of outgoing cylindrical waves. Purely incoming Einstein-Rosen waves, for which $\alpha = \text{Re} \left[\exp(-i\omega t) H_0^{(2)}(\omega r) \right]$ instead of (2.5.18), yield the same result, but with opposite sign.

Let us emphasize that, on the other hand, $\langle \Omega^{(\text{in})} \rangle \neq 0$ and so this averaging cannot be used to circumvent the failure of the standard Weyl interpretation.

As a result, Thorne's C-energy passes all tests in our two examples, where the standard interpretation of the Weyl tensor fails, apart from the subtlety that the radial flux P^r can locally (both in space and time) have the opposite sign than the actual direction of wave propagation. This could be due the well-known fact [Had52] that waves in two spatial dimensions do not obey the principle of Huygens and Fresnel, meaning that signals do not propagate exclusively with the speed of light, but also slower. (This can directly be seen from the fact that the retarded Green's function for the wave operator in $2 + 1$ dimensions has support not only *on* the backward light cone, but also *inside*.) A possible interpretation is based on backscattering processes taking place, because if we still demand propagation to mean propagation with the fundamental velocity, then an outgoing wave in two spatial dimensions must be viewed as the superposition of a part propagating outwards and some (smaller) part that propagates inwards. Provided the C-energy flux measures energy propagating with the speed of light, backscattering processes could explain the unexpected behavior of P^r . Only for large distances from the axis, where the waves asymptotically become one-dimensional, the backscattering effect becomes negligible. This would also explain why the "wrong" sign of P^r is only found close to the axis, where backscattering is still efficient.

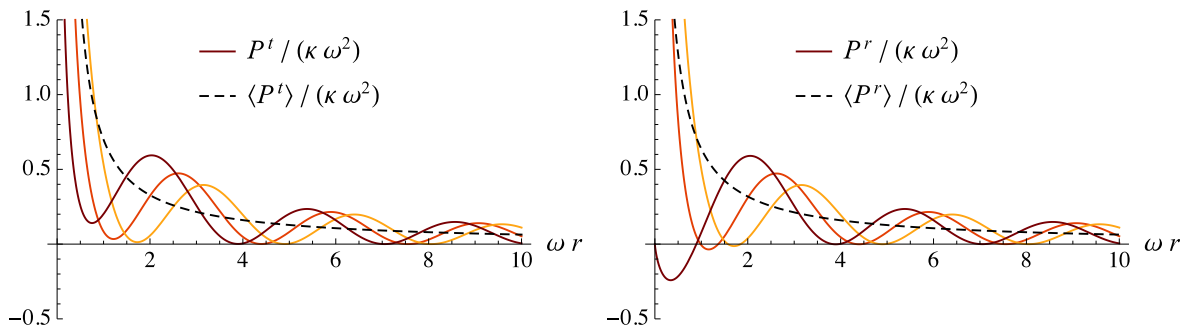


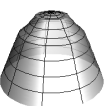
Figure 2.2: Plots of the nonvanishing components of the C-energy flux vector for the outgoing Einstein-Rosen wave solution (2.5.18). The dark red lines correspond to $t = 0$, whereas the orange and yellow lines are evaluated at times $t = 1/(2\omega)$ and $t = 1/\omega$, respectively. The dashed lines are the corresponding time-averaged quantities, which (asymptotically) fall off like $1/r$.

This observation suggests that the same effect might also be responsible for the failure of the Weyl-criterion when applied to cylindrical waves. In this case there is also a further, independent argument: if Ω really corresponded to the purely incoming gravitational wave component, then this term, when set equal to zero, would constitute a *local* outgoing-wave condition. However, no such local condition exists even for *linear* cylindrical waves, as will be discussed in detail in Chap. 3. It would thus be quite surprising if the much more complicated nonlinear wave phenomena of general relativity would in general allow for such a local condition. Note that this argument is also supported by the observation that the standard interpretation works for plane and spherical waves, but fails for cylindrical waves.

2.8 Conclusion

The main scientific objective of this chapter was to prove that the standard interpretation of the Weyl tensor [Sze65, SKM⁺03, PS12] does not hold in general. This has been achieved by investigating explicitly two exact vacuum solutions of Einstein's equations with whole-cylinder symmetry: first, a static solution has been shown to admit nonvanishing wave components according to the standard interpretation, which does not make sense. In addition, this example invalidates a more recent suggestion for a local criterion indicating the presence of gravitational waves [BB02]. Second, purely outgoing Einstein-Rosen waves were considered, and it was shown that according to the standard interpretation, they have not only nonzero outgoing wave- and Newton-components, but also *incoming* wave components. Moreover, they are of Petrov Type I, which also shows that a further instrument to diagnose the presence of gravitational waves put forward by Pirani [Pir57] does not work.

The only way in which the standard interpretation can still be used in the case of cylindrical symmetry is by considering only those parts of the Weyl components which have the correct asymptotic falloff behavior as $r \rightarrow \infty$: $\sim r^{-2}$ for the Newton-like



component Φ_0 , and $\sim r^{-1/2}$ for the transverse wave components $\Omega^{(\text{in})}$ and $\Omega^{(\text{out})}$. But it can not be used as a spatially *local* criterion. This is the most relevant insight with respect to the codimension-two braneworld model studied in Chap. 5. Otherwise, such a local Weyl criterion (generalized to 6D) could have been used to obtain a local modified Friedmann equation (like in the DGP model).

Furthermore, we showed that the standard interpretation *does* work for plane wave and spherical wave geometries. This will be used to derive a local modified Friedmann equation for the braneworld model in Chap. 4, which also has two extra dimensions, but with a different topology which leads to plane instead of cylindrical waves.

Based on these findings, we argued that the failure of the wave interpretation might be due to the more fundamental inability to locally distinguish between incoming and outgoing wave components for cylindrical waves, which is even true for a linear scalar field on Minkowski spacetime, as will be discussed in Chap. 3.

Therefore, the standard interpretation of the Weyl tensor is not applicable to space-time geometries with whole-cylinder symmetry. Instead, for those systems, Thorne's local energy concept, called C-energy, is an appropriate tool to diagnose the presence or absence of gravitational waves. It is, however, not possible to locally distinguish between incoming and outgoing waves, for the very same reason stated before. At least, Thorne's concept works for periodic waves when the time-averaged C-energy flux is considered. This gives a spatially local criterion¹¹ with the correct interpretation.

Note that the above explanation actually addresses only the distinction between incoming and outgoing wavelike components, but does not resolve the shortcoming that a static solution can admit nonzero wavelike Weyl components. However, it was also shown that the wave components in fact *do* vanish for *static* plane-symmetric and spherically symmetric geometries. This gives prominence to the cylinder symmetry as the cause for the standard interpretation to fail.

Finally, let us stress that our results do not invalidate the Gedankenexperiment to measure components of the Weyl tensor by observing the relative acceleration of nearby freely falling test particles. Our work rather shows that it is in general not possible to classify these components as Newton-like, or as incoming or outgoing gravitational waves.

¹¹This criterion is that there are outgoing (incoming) gravitational waves if $\langle P^r \rangle$ is positive (negative). Hence, it has the form of an *inequality*, and could therefore not be used as a local boundary condition to exclude incoming waves. This boundary condition will be the subject of Chap. 3.

CHAPTER 3

NONREFLECTING BOUNDARY CONDITION FOR CYLINDRICAL WAVES

In the previous chapter we learned that the “standard” decomposition of the Weyl tensor into static, and incoming- and outgoing wave components is in general not applicable. The failure was explicitly demonstrated for vacuum spacetime geometries with whole-cylinder symmetry, and it was argued that it is (at least partly) due to the impossibility to separate incoming and outgoing cylindrical waves by means of a local criterion. In this chapter, we will confirm this claim by explicitly deriving the outgoing cylindrical wave boundary condition, which turns out to be manifestly nonlocal.¹

3.1 Definition of the problem

Consider a scalar field α which is subject to the (flat spacetime) homogeneous wave equation in $D + 1$ dimensions,

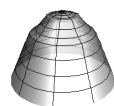
$$-\partial_t^2 \alpha + \Delta_D \alpha = 0. \quad (3.1.1)$$

We call the field “cylindrically symmetric”² if it is independent of $(D - 2)$ of the spatial coordinates \boldsymbol{x} —the direction of the (generalized) cylinder axis—and depends on the remaining two space-coordinates (y_1, y_2) only via their Euclidean distance $r = \sqrt{y_1^2 + y_2^2}$ from the axis. In this case, the Laplace operator reduces to $\Delta_{\text{cyl}} = \partial_r^2 + (1/r)\partial_r$, and the wave equation becomes

$$-\partial_t^2 \alpha + \partial_r^2 \alpha + \frac{1}{r} \partial_r \alpha = 0. \quad (3.1.2)$$

¹For discussions of nonreflecting boundary conditions in the literature see [KG89, Giv91, AGH00] and references therein.

²Sometimes, in particular in a GR context, the name “whole cylinder symmetry” is used to emphasize the symmetry in axial direction. We will drop the adjective “whole” for the sake of brevity.



Next, assume that the field is sourced (in a cylindrically symmetric way), but only inside some region bounded by $r = r_0$, so that Eq. (3.1.2) holds for $r > r_0$. We then might want to restrict the computational domain for solving the initial value problem to the inner region ($r < r_0$). However, in order for the time evolution therein to be unique, we must specify some boundary conditions for the field at $r = r_0$. For instance, we could simply impose the fixed boundary condition $\alpha|_0 = 0$. Physically, this would correspond to a perfectly reflecting boundary; no waves could leave the domain $r < r_0$, and the exterior solution $\alpha_{>}(t, r)$ would be the trivial one, $\alpha_{>} = 0$. We are now interested in the opposite case, in which the boundary is perfectly transparent. In other words, the boundary condition should lead to a time evolution in the interior which is the same as if there was no boundary at all, and the exterior field only contains outgoing waves. The purpose of this chapter is to find the corresponding “nonreflecting”, or “outgoing wave” boundary condition for cylindrical waves.

Note that by “boundary condition” we mean a spatially local condition on α at r_0 : If it were not local in r , we could as well just include the exterior domain into the initial value problem, which is exactly what we would like to get rid of. However, we cannot expect it to be a restriction on $\alpha|_0$ alone, because it should be possible to choose for $\alpha|_0$ a completely arbitrary function of t , but still only have outgoing waves in the exterior. Therefore, the desired relation will not be ultra-local, but also involve r -derivatives of α . The adjective “local” then means that it should only involve finitely many of them.

Remark:

Incidentally, the whole analysis also applies to *exact* cylindrically symmetric gravitational waves (Einstein-Rosen waves). This is due to the miracle that the corresponding metric function α fulfills exactly the *linear* wave equation (3.1.2), cf. Sec. 2.5.2. Furthermore, Einstein-Rosen waves can trivially be generalized to an axis with an arbitrary number of dimensions > 1 , which is exactly the situation relevant for studying cosmology in a codimension-two braneworld model, see Chap. 5.

Therefore, we are in fact not only addressing a scalar field model, but also deriving the exact nonreflecting boundary condition for cylindrical gravitational waves (in arbitrary spacetime dimensions $d \geq 4$). Using the metric function α as the proper tool for this purpose is in line with Thorne’s concept of C-energy [Tho65], which was already observed to work very well in Chap. 2.

3.2 Prelude: Plane waves

Before turning to the actual case of cylindrical waves, let us start with the much simpler example of plane waves. Those are waves which only depend on one of the spatial coordinates y , for which the wave equation is simply

$$-\partial_t^2 \alpha + \partial_y^2 \alpha = 0. \quad (3.2.1)$$

The analogue problem here is to find a “right-moving” boundary condition at some $y = y_0$. As is well known, the general solution of Eq. (3.2.1) can be written as

$$\alpha(t, y) = \alpha_R(t - y) + \alpha_L(t + y). \quad (3.2.2)$$

The reason for that is the fact that the plane wave d’Alembert operator factorizes,

$$-\partial_t^2 + \partial_y^2 = (\partial_t + \partial_y)(-\partial_t + \partial_y) =: \mathcal{O}_R \mathcal{O}_L. \quad (3.2.3)$$

The parts α_R and α_L are annihilated by \mathcal{O}_R and \mathcal{O}_L , and readily recognized as right- and left-moving waves, respectively. Hence, the requirement that there only be right-moving waves for $y > y_0$ reads $\mathcal{O}_R \alpha_{>} = 0$, and taking the limit $y \rightarrow y_0^+$ yields the desired boundary condition

$$\partial_y \alpha|_0(t) = -\partial_t \alpha|_0(t). \quad (3.2.4)$$

Note that it is local not only in space, but also in time.

Even though this derivation was quite simple, it turns out that the same trick does not work for cylindrical waves. The reason is that the cylindrical wave d’Alembert operator does *not* factorize. One could insist on a factorization by formally writing

$$-\partial_t^2 + \Delta_{\text{cyl}} = (\partial_t + \sqrt{\Delta_{\text{cyl}}})(-\partial_t + \sqrt{\Delta_{\text{cyl}}}). \quad (3.2.5)$$

But since $\sqrt{\Delta_{\text{cyl}}}$ is a nonlocal operator, the resulting criterion would not meet our requirement of a spatial locality. (It would be local in time, though.)

Let us, therefore, give an alternative derivation of the nonreflecting boundary condition (3.2.4), which seems like overkill in the case of plane waves, but will have the great advantage of being applicable to cylindrical waves as well. The general solution of (3.2.1) can, alternatively, be obtained by Fourier transformation. In terms of the temporal Fourier transform of α ,

$$\hat{\alpha}(\omega, y) := \int dt \alpha(t, y) e^{i\omega t}, \quad (3.2.6)$$

the wave equation turns into

$$\omega^2 \hat{\alpha} + \partial_y^2 \hat{\alpha} = 0, \quad (3.2.7)$$

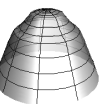
the general solution of which reads

$$\hat{\alpha}(\omega, y) = a(\omega) e^{i\omega y} + b(\omega) e^{-i\omega y}. \quad (3.2.8)$$

Inverting the Fourier transform then gives the general solution

$$\alpha(t, y) = \int \frac{d\omega}{2\pi} [a(\omega) e^{i\omega y} + b(\omega) e^{-i\omega y}] e^{-i\omega t} \quad (3.2.9a)$$

$$= \int \frac{d\omega}{2\pi} [a(\omega) e^{-i\omega(t-y)} + b(\omega) e^{-i\omega(t+y)}]. \quad (3.2.9b)$$



At this stage we see that we again arrived at a sum of a general right- and left-moving wave, described by the Fourier coefficients $a(\omega)$ and $b(\omega)$, respectively. In fact, we could just call them α_R and α_L and recover Eq. (3.2.2). But this is not the point. Instead, we can now implement the right-moving wave condition by setting $b(\omega) = 0$, giving

$$\alpha_{>}(t, y) = \int \frac{d\omega}{2\pi} a(\omega) e^{-i\omega(t-y)}. \quad (3.2.10)$$

We can evaluate this at the boundary by letting $y \rightarrow y_0$,

$$\alpha|_0(t) = \int \frac{d\omega}{2\pi} a(\omega) e^{-i\omega(t-y_0)}. \quad (3.2.11)$$

But we can also first take the y -derivative, and then let $y \rightarrow y_0$, yielding

$$\partial_y \alpha|_0(t) = \int \frac{d\omega}{2\pi} i\omega a(\omega) e^{-i\omega(t-y_0)}. \quad (3.2.12)$$

These last two equations can now be used to derive the desired relation between $\alpha|_0$ and $\partial_y \alpha|_0$: Using the inverse Fourier transform of the former to eliminate $a(\omega)$ in the latter leads to

$$\partial_y \alpha|_0(t) = \int \frac{d\omega}{2\pi} i\omega \int dt' \alpha|_0(t') e^{-i\omega(t-t')} \quad (3.2.13a)$$

$$=: \int dt' \mathcal{K}(t-t') \alpha|_0(t'). \quad (3.2.13b)$$

At first sight, this looks like a nonlocal relation in time. But taking a closer look at the outgoing plane wave kernel \mathcal{K} , we find

$$\mathcal{K}(t) \equiv \int \frac{d\omega}{2\pi} i\omega e^{-i\omega t} = -\partial_t \int \frac{d\omega}{2\pi} e^{-i\omega t} = -\delta'(t). \quad (3.2.14)$$

Using this in (3.2.13b) and integrating by parts, we finally recover the local nonreflecting boundary condition (3.2.4). Even though this seems like an unnecessarily complicated way to derive this simple relation, we will now prove the power of this method by applying it to cylindrical waves. The nontrivial part was of course to realize that one of the fundamental solutions in Fourier space, see Eq. (3.2.8), corresponds to purely right-moving, and the other to purely left-moving modes. Luckily, we will see that such a clean separation is also possible in the cylindrically symmetric case.

Finally, it should be mentioned that the nonreflecting boundary condition excludes the static solutions of (3.2.1), viz. $\alpha \propto y$. This is clear as, according to the separation (3.2.2), those represent a sum of left- and right-moving waves. Accordingly, the boundary condition (3.2.4) implies $\partial_y \alpha_0 = 0$ for a static solution. In a concrete application, it might be desirable not to exclude static fields in the exterior domain. But this is of course no problem, because the general solution can be obtained by linear superposition. To be specific, suppose that at the initial time of integration,

the exterior field should not be the trivial solution $\alpha = 0$, but the general static solution $\alpha_{\text{stat}} = c_1 + c_2 y$ with some constants c_1, c_2 . Then, the correct exterior solution is $\alpha_{>} = \alpha_{\text{R}}(t - y) + \alpha_{\text{stat}}(y)$, and the boundary condition (3.2.4) simply has to be modified into

$$\partial_y \alpha|_0(t) = -\partial_t \alpha|_0(t) + c_2. \quad (3.2.15)$$

3.3 Cylindrical waves

Let us now come to the actual case of interest—cylindrical waves. Defining, as before, the (temporal) Fourier transform

$$\hat{\alpha}(\omega, r) := \int dt \alpha(t, r) e^{i\omega t}, \quad (3.3.1)$$

the cylindrical wave equation (3.1.2) takes the form

$$\omega^2 \hat{\alpha} + \partial_r^2 \hat{\alpha} + \frac{1}{r} \partial_r \hat{\alpha} = 0. \quad (3.3.2)$$

Its general solution is given by [AS65]

$$\hat{\alpha}(\omega, r) = A(\omega) J_0(\omega r) + B(\omega) Y_0(\omega r), \quad (3.3.3)$$

where J_n and Y_n denote the Bessel functions of the first and second kind, respectively. They are real-valued, and (3.3.3) is analogous to writing the solution for plane waves, cf. Eq. (3.2.7), in terms of cos and sin. However, in the derivation in Sec. 3.2 it was crucial to write the fundamental solutions in the complexified form (3.2.8). Only then did the corresponding Fourier coefficients correspond to left- and right-moving waves, cf. Eq. (3.2.9). Guided by this analogy, we should now also use the complex combinations $H_n^{(1)} = J_n + iY_n$ and $H_n^{(2)} = J_n - iY_n$, known as the Hankel functions of the first and second kind, respectively. Thus, we rewrite Eq. (3.3.3) as

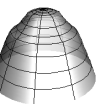
$$\hat{\alpha}(\omega, r) = a(\omega) H_0^{(1)}(\omega r) + b(\omega) H_0^{(2)}(\omega r), \quad (3.3.4)$$

without loss of generality, and so the solution for α is given by

$$\alpha(t, r) = \int \frac{d\omega}{2\pi} \left[a(\omega) H_0^{(1)}(\omega r) + b(\omega) H_0^{(2)}(\omega r) \right] e^{-i\omega t}. \quad (3.3.5)$$

If the analogy to plane waves is to hold, then the first term should correspond to outgoing, and the second term to incoming waves. That this is indeed the case, can be checked by noting that, asymptotically far away, the asymptotic form of the Hankel functions for large arguments is [AS65, p. 364]

$$H_0^{(1)}(x) \sim \sqrt{\frac{2}{\pi x}} e^{i(x-\pi/4)}, \quad H_0^{(2)}(x) \sim \sqrt{\frac{2}{\pi x}} e^{-i(x-\pi/4)} \quad (x \rightarrow \infty). \quad (3.3.6a)$$



Now there is a slight subtlety here because the integral (3.3.5) requires integrating not only over positive, but also over negative ω . However, the Hankel functions have a branch cut along the negative real axis. Thus, in order for α to be well defined, we must specify which branch is to be used. This can for instance be done by replacing $\omega \rightarrow \omega \pm i\epsilon$ in the arguments of the Hankel functions, with the limit $\epsilon \rightarrow 0$ (from above) to be understood. Using the analytic properties of the Bessel functions [AS65, p. 361], one can then easily check that the asymptotic formula (3.3.6) generalizes to ($x \rightarrow -\infty$) if and only if we choose the “ $+i\epsilon$ ” prescription for $H_0^{(1)}$, and the “ $-i\epsilon$ ” prescription for $H_0^{(2)}$.

We will therefore *adopt this prescription from now on*. Consequently, the cylindrical waves at asymptotically large radii take the form

$$\alpha(t, r) \sim \int \frac{d\omega}{2\pi} \frac{1}{\sqrt{\omega r}} [a(\omega) e^{-i\omega(t-r)} + b(\omega) e^{-i\omega(t+r)}] \quad (r \rightarrow \infty), \quad (3.3.7)$$

where we dropped some irrelevant constant factors. Evidently, these correspond to outgoing and incoming waves, respectively. Thus, requiring α to contain only outgoing waves is indeed equivalent to setting $b(\omega)$ equal to zero, leading to the exterior solution

$$\alpha_{>}(t, r) = \int \frac{d\omega}{2\pi} a(\omega) H_0^{(1)}(\omega r) e^{-i\omega t}. \quad (3.3.8)$$

We can now proceed exactly as in the case of plane waves to obtain the desired boundary condition,

$$\partial_r \alpha|_0(t) = \int \frac{d\omega}{2\pi} (-\omega) \frac{H_1^{(1)}(\omega r_0)}{H_0^{(1)}(\omega r_0)} \int dt' \alpha|_0(t') e^{-i\omega(t-t')}, \quad (3.3.9)$$

where we used $dH_0^{(1)}(z)/dz = -H_1^{(1)}(z)$, and $|_0$ denotes evaluation at $r = r_0$. Changing to the dimensionless variables $x := \omega r_0$ and $y := (t - t')/r_0$, this can be written as the convolution

$$\partial_r \alpha|_0(t) = \frac{1}{r_0} \int dy \mathcal{H}(y) \alpha|_0(t - yr_0), \quad (3.3.10)$$

with the outgoing cylindrical wave kernel

$$\mathcal{H}(y) := - \int \frac{dx}{2\pi} \frac{x H_1^{(1)}(x)}{H_0^{(1)}(x)} e^{-ixy}. \quad (3.3.11)$$

Note that here the $+i\epsilon$ prescription, as discussed above, still has to be understood. Without a prescription the integral would be ill-defined, and for the $-i\epsilon$ prescription this kernel would not produce solely outgoing waves.

Just like in the case of plane waves, the nonreflecting boundary condition (3.3.10) excludes any static fields in the exterior. Therefore, a time independent boundary value $\alpha|_0$ should imply $\partial_r \alpha|_0 = 0$, which translates into the consistency requirement

$$\int dy \mathcal{H}(y) = 0. \quad (3.3.12)$$

This can readily be confirmed analytically, since after courageously interchanging the order of integrations, we get

$$\int dy \mathcal{H}(y) = - \int dx \frac{xH_1^{(1)}(x)}{H_0^{(1)}(x)} \delta(x) = - \frac{xH_1^{(1)}(x)}{H_0^{(1)}(x)} \Big|_{x=0} = 0. \quad (3.3.13)$$

If needed, the most general static exterior field configuration $\alpha(r) = c_1 + c_2 \ln(r)$ could again be included by adding c_2/r_0 to the right hand side of Eq. (3.3.10).

3.4 Evaluating the kernel

Written in this formal way, Eq. (3.3.10) is not yet particularly useful—not only if we would like to use it for actual calculations, but even to infer qualitative features; in particular, we would like to know whether this boundary condition is local (in time), like in the case of plane waves.

Therefore, we would now like to explicitly perform the integral in (3.3.11), i.e. calculate the inverse Fourier transform of

$$\hat{\mathcal{H}}(x) := - \frac{xH_1^{(1)}(x)}{H_0^{(1)}(x)}, \quad (3.4.1)$$

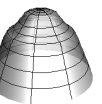
keeping in mind the $+i\epsilon$ prescription. This turns out to be quite a formidable task, and we will in the end resort to a numerical integration for obtaining the final quantitative result. But the integrand will only be amenable to a numerical investigation after some preparatory work. This is because, as we will see below, the kernel is not a smooth function, but contains distributional pieces, which are hard to obtain directly by a numerical evaluation. One of these distributional parts can already be anticipated from the knowledge that at large radii the plane wave criterion should be recovered, which is only possible if \mathcal{H} again contains the part $-\delta'(y)$. In fact, we can even be a bit more precise. At asymptotically large argument, the integrand can be expanded in a Laurent series around $1/x = 0$ as

$$\hat{\mathcal{H}}(x) = ix - \frac{1}{2} + \frac{i}{8x} + \frac{1}{8x^2} - \frac{25i}{128x^3} + \mathcal{O}\left(\frac{1}{x^4}\right). \quad (3.4.2)$$

Performing the $+i\epsilon$ inverse Fourier transform, this yields

$$\mathcal{H}(y) = \underbrace{-\delta'(y) - \frac{1}{2}\delta(y)}_{=: \mathcal{H}^{(\text{dis})}(y)} + \Theta(y) \left[\frac{1}{8} - \frac{y}{8} + \frac{25}{256}y^2 + \mathcal{O}(y^3) \right]. \quad (3.4.3)$$

In this way, we indeed recover the term corresponding to the plane wave criterion, but also a second distributional part that will lead to another local contribution in the boundary condition. As for the remainder, the overall Heaviside step function $\Theta(y)$



can be inferred from the $+i\epsilon$ prescription and the fact that the integrand is analytic in the upper complex half-plane, see Fig. 3.1. This means that \mathcal{H} is a *retarded* kernel;³ it evaluates α in the boundary condition (3.3.10) only at times earlier than t . This is physically reasonable and makes the kernel especially applicable to the integration of initial value problems.

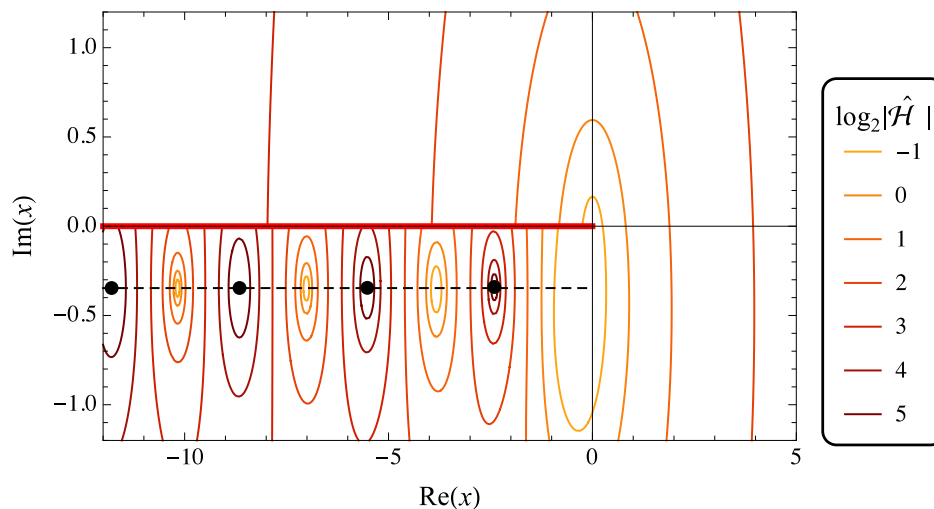


Figure 3.1: Analytic structure of the integrand $\hat{\mathcal{H}}(x)$: It has a branch cut (thick red line) on the negative real axis, and poles (black dots) in the lower left quadrant, whose imaginary parts approach $-\ln(2)/2$ (dashed line) as $\text{Re}(x) \rightarrow -\infty$ [AS65, p. 373]. The $+i\epsilon$ prescription demands that the Fourier integration is to be performed right above the real axis.

It is tempting to try to determine the remaining function

$$\mathcal{H}^{(\text{reg})}(y) := \mathcal{H}(y) - \mathcal{H}^{(\text{dis})}(y) \quad (3.4.4)$$

by proceeding in a similar fashion term by term, extending the series in brackets in (3.4.3) and hoping that it converges. However, its radius of convergence turns out to be only 2, see Fig. 3.2. Nevertheless, the convergence for $y < 2$ already provides some important information:

- (i) There are no further local δ -contributions to the kernel other than $-\delta'(y) - \delta(y)/2$.
- (ii) The kernel contains a nonlocalized (retarded) part and hence, *the outgoing wave boundary condition for cylindrical waves is nonlocal*.

³One might have expected that there is some freedom of choice here, and that one could equally well have defined an *advanced* outgoing wave kernel. But this is not the case, since the $+i\epsilon$ prescription was forced upon us in order to obtain purely outgoing waves, as discussed below Eq. (3.3.6). On the other hand, imposing an *incoming* wave condition would have unambiguously led to an *advanced* kernel; indeed, the corresponding kernel would simply be $\mathcal{H}(-y)$, as can be seen immediately by reversing time.

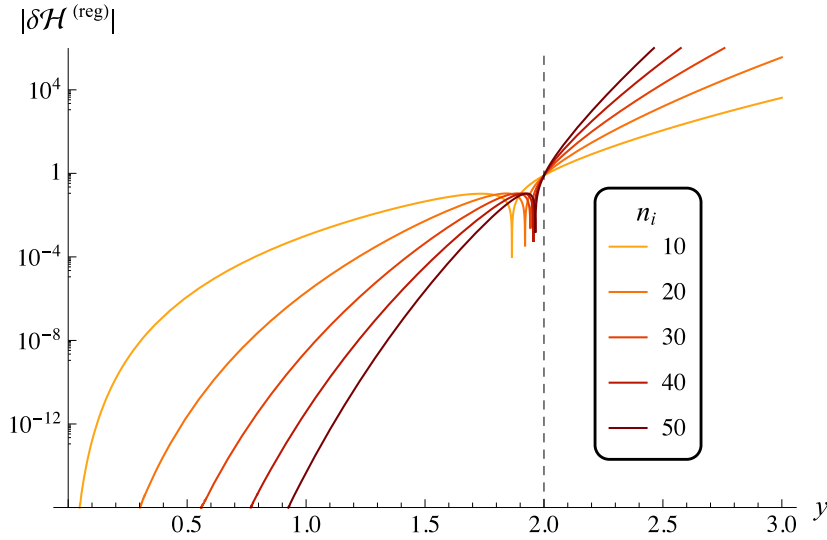


Figure 3.2: Testing convergence of the series expansion of $\mathcal{H}^{(\text{reg})}$ around $y = 0$, as obtained by expanding $\hat{\mathcal{H}}$ around $x = \infty$, see Eq. (3.4.3). The plot shows (the absolute value of) the difference of two truncated series ending at orders y^{n_i} and y^{n_i+1} , respectively. Evidently, the series converges for $y < 2$, but diverges for $y > 2$.

It remains to determine the function $\mathcal{H}^{(\text{reg})}(y)$ for arguments $y \geq 2$. Since it seems impossible to derive it in a closed analytic form, we will content ourselves with evaluating it numerically. To this end, it is useful to first rewrite Eq. (3.3.11) in a manifestly real form. Using the analytic properties of the Bessel functions [AS65, pp. 360–361], it is straightforward to obtain

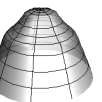
$$\mathcal{H}(y) = - \int_0^\infty \frac{dx}{\pi} \frac{1}{J_0^2 + Y_0^2} \left[x(J_0 J_1 + Y_0 Y_1) \cos(xy) - \frac{2}{\pi} \sin(xy) \right], \quad (3.4.5)$$

where, for brevity, the arguments x of all the Bessel functions were suppressed. The great advantage of writing the kernel in this way is that, since the integration runs only over positive x , the integrand is unambiguous, and so there is no need for an $i\epsilon$ prescription anymore. Next, we can get rid of the distributional parts of $\mathcal{H}(y)$ by subtracting the first two terms in (3.4.2) from the integrand. In the real representation, those are

$$\mathcal{H}^{(\text{dis})}(y) = - \int_0^\infty \frac{dx}{\pi} \left[\frac{1}{2} \cos(xy) - x \sin(xy) \right]. \quad (3.4.6)$$

However, the remaining function $\mathcal{H}^{(\text{reg})}$ is still not continuous, but has a jump of size $1/8$ at $y = 0$, see Eq. (3.4.3). When evaluating the integral numerically (with an appropriate cutoff), this leads to oscillatory artifacts near $y = 0$, the size of which increases with the cutoff. This can be avoided by further subtracting

$$\Theta(y) \frac{e^{-y}}{8} = \int_0^\infty \frac{dx}{\pi} \frac{\cos(xy) + x \sin(xy)}{8(1+x^2)}. \quad (3.4.7)$$



From the series expansion (3.4.3), one can see that this subtracts not only the discontinuity from the kernel, but also the discontinuity in its first derivative. Hence, the residual part of the kernel, which we will call $\mathcal{H}^{(\text{res})}$, will be continuously differentiable and go like $\mathcal{O}(y^2)$. In the real cos-sin-representation, it is given by

$$\mathcal{H}^{(\text{res})}(y) = \int_0^\infty \frac{dx}{\pi} \left[\hat{\mathcal{H}}_c^{(\text{res})}(x) \cos(xy) + \hat{\mathcal{H}}_s^{(\text{res})}(x) \sin(xy) \right], \quad (3.4.8a)$$

$$\hat{\mathcal{H}}_c^{(\text{res})}(x) := -\frac{x(J_0 J_1 + Y_0 Y_1)}{J_0^2 + Y_0^2} - \frac{1}{8(1+x^2)} + \frac{1}{2}, \quad (3.4.8b)$$

$$\hat{\mathcal{H}}_s^{(\text{res})}(x) := \frac{2}{\pi(J_0^2 + Y_0^2)} - \frac{x}{8(1+x^2)} - x, \quad (3.4.8c)$$

where the arguments x of the Bessel functions were again omitted. Before finally evaluating this integral numerically, there is another simplification that can be made. We already know that $\mathcal{H}^{(\text{res})}$ vanishes for $y < 0$. Since the two terms in the integrand of (3.4.8a) are even and odd functions of y , respectively, we can use this information to rewrite the residual kernel as⁴

$$\boxed{\mathcal{H}^{(\text{res})}(y) = \Theta(y) \frac{2}{\pi} \int_0^\infty dx \hat{\mathcal{H}}_s^{(\text{res})}(x) \sin(xy)}. \quad (3.4.9)$$

At last, this integral is well suited for numerical evaluation. The resulting function is plotted in Fig. 3.3. For asymptotically large arguments ($y \rightarrow \infty$), it falls off like $\mathcal{H}^{(\text{res})}(y) \sim 1/[y \ln^2(y)]$. Furthermore, Eq. (3.3.12), implies that the integral over $\mathcal{H}^{(\text{res})}$ equals $3/8$, which can also be confirmed numerically.

3.4.1 Summary and discussion

To summarize, the outgoing cylindrical wave kernel is given by

$$\mathcal{H}(y) = -\delta'(y) - \frac{1}{2}\delta(y) + \Theta(y) \mathcal{H}^{(\text{reg})}(y), \quad (3.4.10)$$

with $\mathcal{H}^{(\text{reg})}(y) = \Theta(y) \exp(-y)/8 + \mathcal{H}^{(\text{res})}(y)$, which is plotted in Fig. 3.4. As a result, the nonreflecting boundary condition for cylindrical waves (3.3.10) finally becomes

$$\boxed{\partial_r \alpha|_0(t) = -\partial_t \alpha|_0(t) - \frac{1}{2r_0} \alpha|_0(t) + \frac{1}{r_0} \int_0^\infty dy \mathcal{H}^{(\text{reg})}(y) \alpha|_0(t - yr_0)}. \quad (3.4.11)$$

The difference to the corresponding boundary condition for plane waves, viz. (3.2.4), is a second local non-derivative term and, more importantly, a (retarded) *nonlocal* term. Both of them scale like $1/r_0$ and thus vanish in the limit $r_0 \rightarrow \infty$. This is intuitively

⁴One could just as well express it in terms of $\mathcal{H}_c^{(\text{res})}$, but this would be more costly to evaluate numerically because it involves more Bessel function terms.

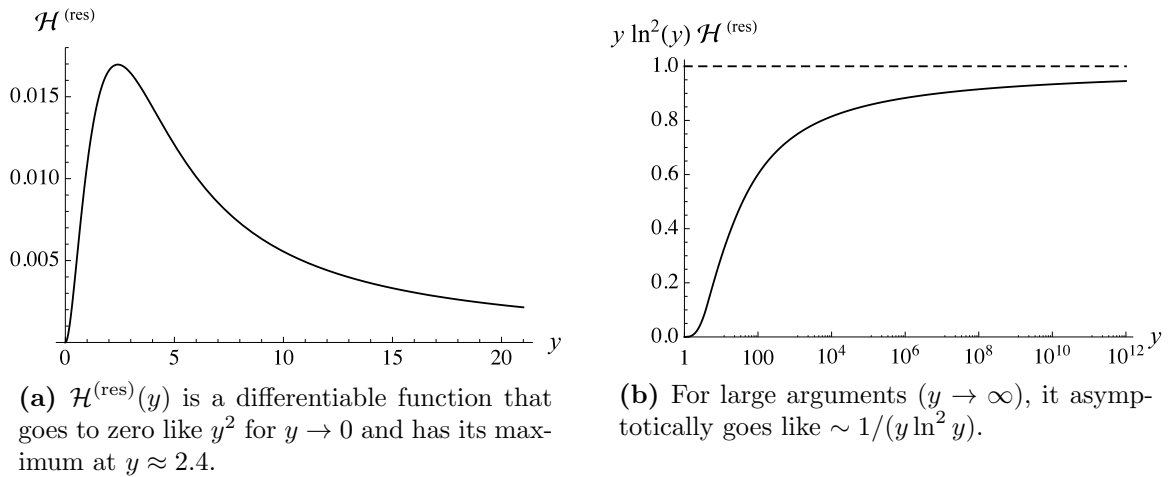


Figure 3.3: Numerical evaluation of the residual part (3.4.9) of the cylindrical outgoing wave kernel.

reasonable, because cylindrical waves look locally more and more like plane waves as they approach radial infinity.

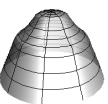
The second local term $\alpha/(2r)$ simply accounts for the correct fall-off behavior $\sim 1/\sqrt{r}$ of the outgoing cylindrical wave. Indeed, the differential equation that is obtained by dropping the nonlocal term from (3.4.11) has the general solution $\alpha_{\text{out}}(t-r)/\sqrt{r}$.

Let us finally discuss the physical origin of the nonlocality. It is well known [Had52] that waves in two spatial dimensions do not obey the principle of Huygens and Fresnel,⁵ meaning that signals do not propagate exclusively with the speed of light, but also slower. Mathematically, this can directly be seen from the fact that the retarded Green’s function for the d’Alembert operator in $2+1$ dimensions has support not only *on* the backward light cone, but also *inside*. This is another manifestation of the same nonlocality that enters the nonreflecting boundary condition (3.4.11). Physically, the failure of Huygens’ principle in two spatial dimensions can be understood as a consequence of the fact that the principle holds in three dimensions:⁶ The wave equation (3.1.2) can be thought of as describing waves in an intrinsically 2D world,⁷ in which Huygen’s principle fails. But it also describes cylindrical waves in 3D which do not depend on the axial coordinate. From this point of view, a cylindrical wave pulse is created by an infinitely long straight line source, located at the symmetry axis. The 2D world is simply a plane perpendicular to the axis in 3D, where the 3D line source becomes a 2D point source. Now, if Huygens’ principle holds in 3D, then a short pulse sent out by the line source can be thought of as a collection of infinitely many 3D point sources along the axis, each sending out a 3D spherical wave pulse. As a consequence, the 2D observer at some distance r_0 will first see the pulse coming

⁵In the following, we will call it “Huygens’ principle” for short.

⁶This illustrative explanation is due to John Baez [Bae06].

⁷In this section, “ n D” refers to n spatial dimensions.



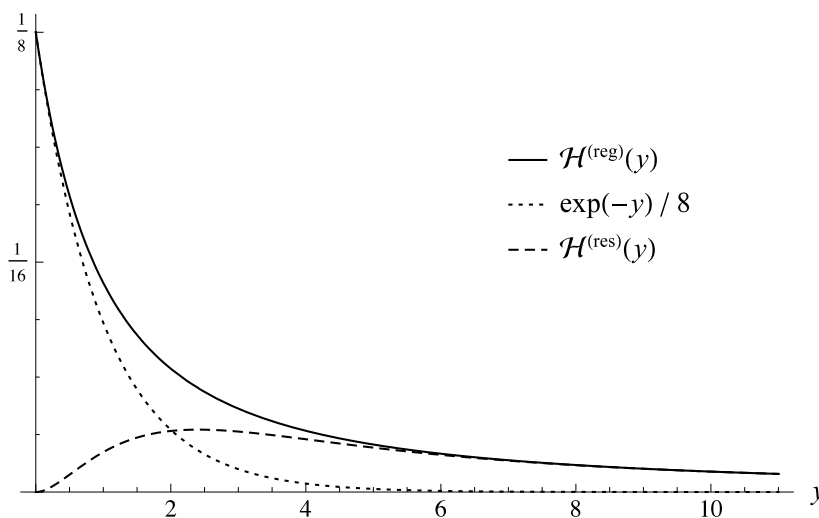


Figure 3.4: The nonlocal part $\mathcal{H}^{(\text{reg})}(y)$ of the outgoing cylindrical wave kernel entering the boundary condition (3.4.11) is the sum of $\Theta(y) \exp(-y)/8$ and $\mathcal{H}^{(\text{res})}(y)$. Asymptotically, it falls off like $1/(y \ln^2 y)$, and its total integral equals $1/2$.

from the closest point of the 3D axis, corresponding to propagation “on the light cone”. But afterwards, she receives the spherical wave fronts from all the points lying further and further away along the axis, getting dimmer and dimmer. From the 2D perspective, those correspond to a tail of the wave pulse, propagating “inside the light cone”, which only asymptotically settles back to zero. This tail will be nicely visualized in the numerical example below.

Incidentally, it turns out that this pattern generalizes to arbitrary even and odd dimensions [Bro15]: Huygens’ principle fails (holds) in every even (odd) number of spatial dimensions. Accordingly, we expect the corresponding outgoing wave criterion to be nonlocal (local) in all even (odd) dimensions. For the case of 3D spherical waves, this can easily be confirmed by noting that the d’Alembert operator again factorizes,

$$-\partial_t^2 + \frac{2}{R} \partial_R + \partial_R^2 = \left(\partial_t + \frac{1}{R} + \partial_R \right) \left(-\partial_t + \frac{1}{R} + \partial_R \right). \quad (3.4.12)$$

Hence, the corresponding nonreflecting boundary condition is indeed local and reads

$$\partial_R \alpha|_0(t) = -\partial_t \alpha|_0(t) - \frac{1}{R_0} \alpha|_0(t). \quad (3.4.13)$$

3.5 Numerical example

In order to gain more confidence in the derived boundary condition, and to show how it can actually be applied in a numerical calculation, let us consider a concrete example. (This toy example also serves as a warm-up exercise for the more complicated case of BIG cosmology, which will be studied numerically in Sec. 5.3.) Let the scalar field α

at time $t = 0$ be subject to the initial data

$$\alpha(t = 0, r) = \Theta(r_0 - 4r) \exp\left(-\frac{4r^2}{r_0^2 - 4r^2}\right), \quad (3.5.1a)$$

$$\partial_t \alpha(t = 0, r) = 0, \quad (3.5.1b)$$

i.e. it has nonzero field values for $r < r_0/4$ which go to zero smoothly at $r \rightarrow r_0/4$, and is initially at rest. The task is to determine the future evolution of α in the region $r \in [0, r_0]$. For this evolution to be unique, boundary conditions at $r = 0$ and $r = r_0$ have to be given. Regularity at the axis $r = 0$ demands that $\partial_r \alpha(t, r = 0) = 0$; at $r = r_0$ the field should satisfy the nonreflecting boundary condition (3.4.11).

3.5.1 Discretization

To solve this problem numerically, we introduce an equidistant spacetime lattice, i.e. we replace the continuous variables (t, r) by a finite number of points $(t^{(i)}, r_{(n)})$ with an equidistant spacing

$$\Delta t = \Delta r =: \epsilon. \quad (3.5.2)$$

Note that this choice satisfies the ‘‘Courant condition’’ $\Delta t/\Delta r \leq 1$, and so the resulting scheme will be numerically stable [PTVF92]. The spacetime grid is then given by

$$t^{(i)} = i\epsilon \quad (i = 0, 1, \dots, I), \quad r_{(n)} = n\epsilon \quad (n = 0, 1, \dots, N), \quad (3.5.3)$$

with its boundaries located at $t^{(0)} \equiv 0$, $r_{(0)} \equiv 0$ and $r_{(N)} \equiv r_0$. Away from the boundaries, the derivatives of α can be approximated by the (symmetric) differences

$$\partial_t \alpha(t, r) \rightarrow \frac{1}{2\epsilon} (\alpha_n^{i+1} - \alpha_n^{i-1}), \quad \partial_t^2 \alpha(t, r) \rightarrow \frac{1}{\epsilon^2} (\alpha_n^{i+1} - 2\alpha_n^i + \alpha_n^{i-1}), \quad (3.5.4a)$$

$$\partial_r \alpha(t, r) \rightarrow \frac{1}{2\epsilon} (\alpha_{n+1}^i - \alpha_{n-1}^i), \quad \partial_r^2 \alpha(t, r) \rightarrow \frac{1}{\epsilon^2} (\alpha_{n+1}^i - 2\alpha_n^i + \alpha_{n-1}^i). \quad (3.5.4b)$$

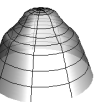
where α_n^i is shorthand for $\alpha(t^{(i)}, r_{(n)})$. The cylindrical wave differential equation (3.1.2) then turns into the difference equation

$$\alpha_n^{i+1} = -\alpha_n^{i-1} + \alpha_{n+1}^i + \alpha_{n-1}^i + \frac{1}{2n} (\alpha_{n-1}^i - \alpha_{n+1}^i), \quad (3.5.5)$$

from which the scalar field (in the interior domain) at time t^{i+1} can be calculated given its values at the two preceding time steps t^i and t^{i-1} . At the boundaries of the domain of integration, i.e. at $i = 0$, $n = 0$ and $n = N$, this equation cannot be used, because it would require values of the scalar field *outside* the domain. In these cases, we will instead use the asymmetric differences

$$\partial_t \alpha(t = 0, r) \rightarrow \frac{1}{\epsilon} (\alpha_n^1 - \alpha_n^0), \quad (3.5.6a)$$

$$\partial_r \alpha(t, r = 0) \rightarrow \frac{1}{\epsilon} (\alpha_1^i - \alpha_0^i), \quad \partial_r \alpha(t, r = r_0) \rightarrow \frac{1}{\epsilon} (\alpha_N^i - \alpha_{N-1}^i), \quad (3.5.6b)$$



together with the corresponding initial and boundary conditions. With the initial data (3.5.1), this implies that the discretized field at $i = 0$ and $i = 1$ is simply given by (3.5.1a), evaluated at the grid points $r_{(n)}$. Regularity at $r = 0$ yields $\alpha_0^i = \alpha_1^i$, and the nonreflecting boundary condition at $r = r_0$ turns, after some rearrangements, into⁸

$$\left(1 + \frac{\xi}{2}\right) \alpha_N^{i+1} = \alpha_{N-1}^i + \xi^2 \sum_{j=0}^i \mathcal{H}^{(\text{reg})}[(i+1-j)\xi] \alpha_N^j, \quad (3.5.7)$$

where $\xi := \epsilon/r_0$, and the integral was replaced by the corresponding Riemann sum. This nonlocal part requires the values of the kernel function $\mathcal{H}^{(\text{reg})}(y)$ in the range $y \in [0, t_{\text{max}}/r_0]$, sampled at $I + 1$ points. They can be obtained beforehand by numerically evaluating (3.4.9) to the required precision. The system of equations is now complete, and it is straightforward to implement the corresponding algorithm.

Before presenting the results, let us discuss how the numerical errors can be estimated. One way is to check how much the calculated field values change when the grid-spacing decreases. For instance, one can define an error estimate $\delta\alpha$, for α calculated with grid-spacing ϵ , as $\delta\alpha(\epsilon) := \alpha(2\epsilon) - \alpha(\epsilon)$. If $\alpha(\epsilon)$ converged to its true value linearly in ϵ as $\epsilon \rightarrow 0$, this would give exactly the correct error, for a faster convergence the true error would even be smaller. This requires running the numerics twice, to obtain both $\alpha(\epsilon)$ and $\alpha(2\epsilon)$. On the other hand, we can also use this additional information to obtain an even better estimate for α , by linearly extrapolating to $\epsilon \rightarrow 0$, viz. $\alpha_{\text{ext}} = 2\alpha(\epsilon) - \alpha(2\epsilon)$.

3.5.2 Result and discussion

The result of the numerical integration for $t \in [0, 2r_0]$ is shown in Fig. 3.5. One can see that the wave packet indeed moves outward through the boundary $r = r_0$, as it should. Furthermore, unlike a plane wave, it leaves a tail behind and the field only asymptotically settles back to zero. This tail is the physical origin of the nonlocal part in the boundary condition (3.4.11), cf. the discussion at the end of the preceding section.

Due to this tail, it is hard to see if there is still a small artificial reflection produced at r_0 . Therefore, in order to get a more quantitative statement about how well the nonreflecting boundary condition works, we have to subtract the “true” nonreflected result. This can be obtained by doubling the spatial domain of integration, but keeping $t_{\text{max}} = 2r_0$, because then the initial wave packet will only reach the new boundary at $t = 2r_0$, and any reflections that occur there can not yet have propagated back to r_0 .

After this subtraction, we obtain α_{ref} , which is a direct measure of the reflection that occurs at r_0 . It is plotted in Fig. 3.6 (blue) at time $t = 2r_0$ —when the reflected part at $r = 0$ is maximal—and is indeed zero within the numerical uncertainties. For

⁸There is some arbitrariness in choosing whether the r -difference is evaluated at time i or $i - 1$. Both choices would work, but we use the latter because then two terms cancel, and so the number of required calculations reduces.

comparison, we also plotted (red) the same quantity for the case when only the two local parts in the boundary condition (3.4.11) are used, i.e. the sum in (3.5.7) is dropped. Then, about 0.01% of the initial amplitude are reflected back to the axis, confirming the necessity of the nonlocal part in the correct nonreflecting boundary condition.

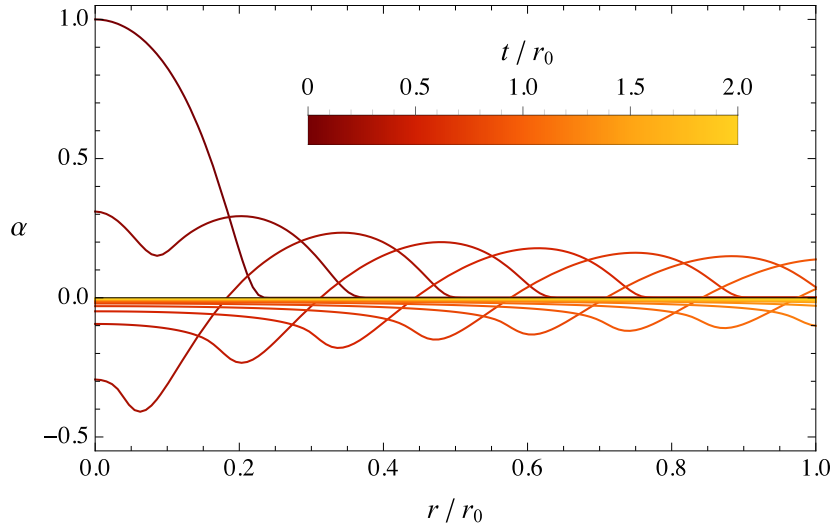
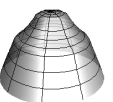


Figure 3.5: Radial profile of the cylindrically symmetric scalar field α , as obtained by numerically integrating the initial data (3.5.1), using the outgoing wave boundary condition (3.4.11) at $r = r_0$. The field excitation, which is initially localized in a compact region near the axis, propagates outward and passes through the boundary without reflection. It leaves a tail behind, which is the origin of the nonlocal part in the boundary condition (3.4.11).



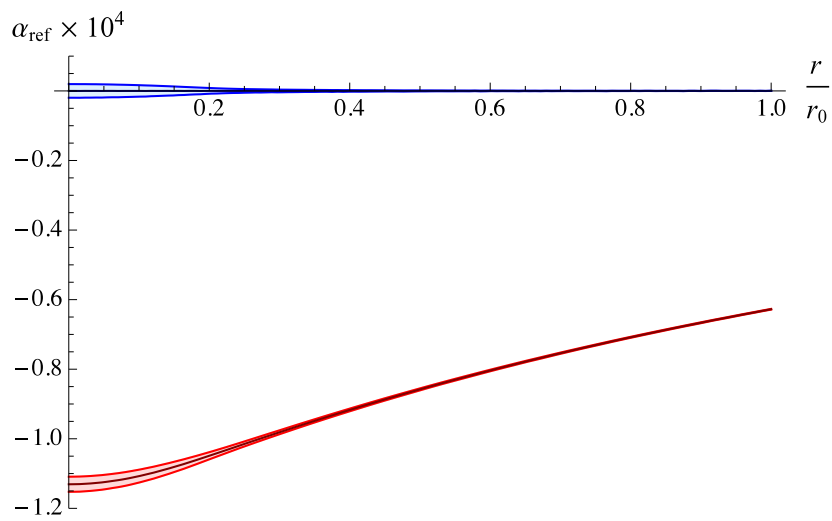


Figure 3.6: The part of the field that gets reflected at $r = r_0$, evaluated at $t = 2r_0$ when the maximum of the reflected wave packet has reached the axis at $r = 0$. The filled bands indicate the numerical uncertainties. The red curve shows the result when only the local terms in the nonreflecting boundary condition are used, leading to about 0.01% reflection. This residual reflection is completely removed with the full nonlocal boundary condition, as shown by the blue curve.

CHAPTER 4

THE UNIVERSE AS A COSMIC RING

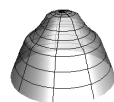
Note: The results presented in this chapter arose in collaboration with Florian Niedermann, and were published in [NS15a].

As discussed in the introduction, any theory with more than three spatial dimensions has to address the question why we have not yet seen them. In order not to be ruled out immediately, they must provide some sort of mechanism which hides the extra dimensions, at least at the length (or energy) scales that we have been able to probe. There are basically two known mechanisms which can achieve this: Either, following Kaluza and Klein [Kal21, Kle26], the extra dimensions are assumed to be compact with very small circumferences—so small that the energies required to probe them are somewhere above the current collider limits. The other paradigm is the braneworld scenario, claiming that all matter is confined to a $(3 + 1)$ -dimensional brane. In that case, only gravity is able to probe the bulk dimensions, and so one also has to rely on an additional mechanism which provides a way of restoring 4D GR on the scales where it has been tested. One possibility is to include BIG terms with appropriate coefficients on the brane, as in the DGP model.

In this chapter, we will investigate an extension of the DGP model which, in addition to the one infinite bulk extra dimension, has another *compact* brane dimension.¹ This represents the simplest prototype of the whole class of models which have *both* compact and infinite extra dimensions, and the primary goal of this chapter is to derive its modified Friedmann equations, describing the cosmological evolution on the brane.

The key new qualitative feature, which is also expected to occur in more elaborate higher-dimensional extensions, is the possibility to emit gravitational waves into the bulk, already at the 3D homogeneous and isotropic background level. Technically, this confronts us with the problem that the on-brane evolution is only unique after incoming waves have been excluded. We will see that the decomposition of the Weyl tensor, as described in Chap. 2, provides a successful tool for doing so. Therefore, the

¹We will always implicitly assume the compact dimension to be much larger than the fundamental Planck length, so that it can be described by classical (higher-dimensional) GR.



current model is still simple enough to investigate the cosmological consequences in an analytic² way.

Two (a posteriori) features make the model especially interesting: First, we find degravitating attractor solutions at the full nonlinear level, i.e. 4D flat solutions despite the presence of a 4D CC, where all curvature is deposited into the extra dimensions. However, they turn out not to be phenomenologically viable, and thus mainly serve as a proof of principle (or perhaps as a motivation to come up with similar but more successful variants). Second, the model could provide phenomenologically interesting late time modifications other than just the DGP ones. As we will see, they are expected to occur because of a breakdown of the stabilization of the compact dimension's size modulus. Hence, the same effect might occur in other models of the Kaluza-Klein type, which could open the window to a whole new category of late time modifications that could be tested against GR. However, the details of this mechanism depend on the concrete realization of the stabilization mechanism, which is beyond the scope of the current work and is left for future research.

4.1 Setup

The model under consideration is defined by the action

$$\mathcal{S} = \frac{M_6^4}{2} \int d^6 X \sqrt{-g^{(6)}} \mathcal{R}^{(6)} + \int d^5 x \sqrt{-g^{(5)}} \left(\mathcal{L}_m + \frac{M_5^3}{2} \mathcal{R}^{(5)} \right). \quad (4.1.1)$$

The first part is the six-dimensional (6D) Einstein-Hilbert action, describing standard gravity in the bulk, with corresponding Planck scale M_6 . The bulk is assumed to be source-free,³ and all matter sources, encoded in the Lagrangian \mathcal{L}_m , are confined on the five-dimensional (5D) brane with induced metric tensor $\mathbf{g}^{(5)}$. The final ingredient is the brane induced gravity (BIG) term, i.e. the five-dimensional Einstein-Hilbert term derived from $\mathbf{g}^{(5)}$, the size of which is controlled by the induced Planck scale M_5 . It can be thought of as arising from integrating out heavy brane degrees of freedom, just like in the DGP model.

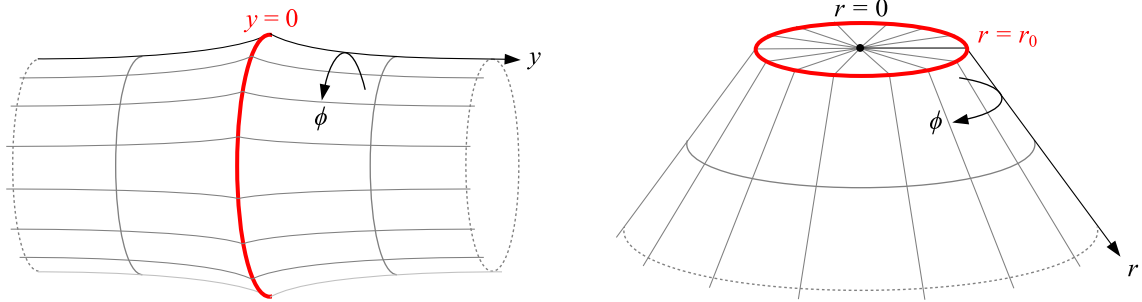
The *topology* of the full 6D manifold is $\mathcal{M}_5 \times \mathbb{R}$, and that of the 5D brane is $\mathcal{M}_5 = \mathcal{M}_4 \times \mathcal{S}_1$, where $\mathcal{M}_4 = \mathbb{R}^{(1,3)}$ denotes Minkowski spacetime and \mathcal{S}_1 is the unit circle. Physically, the four infinite brane dimensions correspond to the familiar dimensions that we see at low energies, whereas the fifth compact dimension is assumed to be microscopically small, and therefore unobservable at low energies. Its proper circumference will be denoted by $2\pi c$, cf. Eqs. (4.2.2) and (4.2.3). The sixth (bulk) dimension is again infinitely large, but also hidden from low energy observations because

²The Friedmann equations will, in some cases, be solved numerically; but since they are just a system of ordinary differential equations, this is completely trivial, as opposed to the numerical treatment of the full Einstein PDEs in Chap. 5.

³In particular, the bulk cosmological constant is set to zero for simplicity.

all matter (in particular any observer) is confined to \mathcal{M}_5 . The extra-dimensional topology is visualized in Fig. 4.1a. The infinite extra dimension is labeled by $y \in (-\infty, \infty)$, and the compact one by $\phi \in [0, 2\pi)$.

Note that the action (4.1.1) could as well describe a codimension-two brane, regularized by blowing the brane up to a circle of finite radius. However, the present setup is topologically distinct from such a scenario, in which the 6D manifold would have topology $\mathcal{M}_4 \times \mathbb{R}^2$. This topology is depicted in Fig. 4.1b, and the corresponding model will be studied in Chap. 5. The correct topology will then be implemented by requiring the azimuthal metric coefficient to vanish at the axis $r = 0$. We will refer to that model as the “cosmic string”, due to its similarity to the geometry of a (regularized) cosmic string in GR. Here, instead, there is no axis on the manifold, and it is natural to assume Z_2 symmetry around the brane (like in the DGP model), as will be done below. This model will be named “cosmic ring”.



(a) “Cosmic ring”—cylindrical topology: the symmetry axis does not lie on the manifold, and it is natural to assume reflection symmetry around $y = 0$.

(b) “Cosmic string”—radial topology: $r = 0$ is the symmetry axis and the brane can create a defect angle in the exterior. There is no reflection symmetry around $r = r_0$ in this case.

Figure 4.1: Illustration of two possible bulk geometries that can locally be described by the same metric ansatz, but are topologically different. Only the two extra dimensions are depicted, embedded into a fictitious three-dimensional space. The 5D brane is drawn in red, and is located at $y = 0$ and $r = r_0$, respectively. In this chapter, we are considering the cylindrical topology (a); the radial topology will be the subject of Chap. 5, where (regularized) codimension-two BIG is studied.

4.2 Deriving modified Friedmann equations

4.2.1 Cosmological ansatz and field equations

The aim of the present section is to derive the modified Friedmann equations describing the cosmological evolution of the brane in the model (4.1.1), similarly to the DGP case discussed in Sec. 1.4.2. To this end, we assume the brane to be filled with a perfect fluid in a ϕ -independent, as well as 3D homogeneous and isotropic way. The



assumption of azimuthal symmetry is justified if we restrict ourselves to energies much below the corresponding Kaluza-Klein scale $\sim 1/c$, as we do when addressing (late time) cosmological questions corresponding to energies of order today's Hubble scale H_0 . Furthermore, for simplicity, we restrict ourselves to 3D spatially flat geometries; the generalization to nonvanishing 3D curvature would be straightforward. The most general metric compatible with these symmetries can be written as

$$ds^2 = -e^{2N(t,y)} dt^2 + e^{2A(t,y)} \delta_{ij} dx^i dx^j + dy^2 + e^{2C(t,y)} d\phi^2, \quad (4.2.1)$$

where we adopted Gaussian normal coordinates in y -direction, like in the DGP case, cf. Sec. 1.4.2. In these coordinates, the brane is located at $y = 0$, and thus the 5D induced metric is simply

$$ds_{(5)}^2 = -dt^2 + e^{2A_0(t)} \delta_{ij} dx^i dx^j + e^{2C_0(t)} d\phi^2, \quad (4.2.2)$$

where $A_0(t) := A(t, 0)$, $C_0(t) := C(t, 0)$, and we used a local rescaling of t at the brane to set $N(t, 0) = 0$, so that proper (cosmological) time on the brane is measured by t . Hence, the scale factors in x - and ϕ -direction are recognized as

$$a(t) := e^{A_0(t)} \quad \text{and} \quad c(t) := e^{C_0(t)}, \quad (4.2.3)$$

respectively, and the corresponding expansion rates are measured by the ‘‘Hubble’’ parameters

$$H_a(t) := \frac{\dot{a}(t)}{a(t)} \equiv \dot{A}_0(t) \quad \text{and} \quad H_c(t) := \frac{\dot{c}(t)}{c(t)} \equiv \dot{C}_0(t), \quad (4.2.4)$$

with the dot denoting d/dt . The entire cosmological dynamics that an on-brane observer can measure is encoded in these two functions, and it is the main goal of this section to derive the corresponding ‘‘Friedmann’’ equations, which determine their time evolution for a given matter content.

As discussed in Sec. 1.4.2, the use of Gaussian normal coordinates allows to implement Israel's junction conditions by simply inserting delta functions in Einstein's field equations. In complete analogy to (1.4.7), the equations of motion thus read

$$M_6^4 G_{MN}^{(6)} = \delta(y) \delta_M^\alpha \delta_N^\beta \left(T_{\alpha\beta} - M_5^3 G_{\alpha\beta}^{(5)} \right). \quad (4.2.5)$$

Here, $T_{\alpha\beta}$ is the 5D energy momentum tensor that follows from \mathcal{L}_m . It is not necessary to specify this Lagrangian, since due to the symmetries of our cosmological ansatz the energy momentum tensor must take the form of a perfect fluid,

$$T^\alpha_\beta = \text{diag}(-\rho, p, p, p, p_\phi). \quad (4.2.6)$$

The azimuthal component p_ϕ , measuring the pressure in direction of the compact extra dimension, can be used to stabilize the brane circumference. We will come back to this point later.

Explicitly, the complete set of nontrivial components of the field equations (4.2.5) then become

$$\begin{aligned} (t) : \quad e^{-2N} \left(-3\dot{A}^2 - 3\dot{A}\dot{C} \right) + 6A'^2 + 3A'C' + C'^2 + 3A'' + C'' = -\delta(y) \tilde{\rho}, \end{aligned} \quad (4.2.7a)$$

$$\begin{aligned} (x) : \quad e^{-2N} \left(-3\dot{A}^2 - 2\dot{A}\dot{C} - \dot{C}^2 + 2\dot{A}\dot{N} + \dot{C}\dot{N} - 2\ddot{A} - \ddot{C} \right) + 3A'^2 \\ + 2A'C' + C'^2 + 2A'N' + C'N' + N'^2 + 2A'' + C'' + N'' = \delta(y) \tilde{p}, \end{aligned} \quad (4.2.7b)$$

$$\begin{aligned} (\phi) - (y) : \quad e^{-2N} \left(3\dot{A}\dot{C} + \dot{C}^2 - \dot{C}\dot{N} + \ddot{C} \right) \\ + 3A'^2 - 3A'C' - C'N' + N'^2 + 3A'' + N'' = \delta(y) \tilde{p}_\phi, \end{aligned} \quad (4.2.7c)$$

$$\begin{aligned} (y) : \quad e^{-2N} \left(-6\dot{A}^2 - 3\dot{A}\dot{C} - \dot{C}^2 + 3\dot{A}\dot{N} + \dot{C}\dot{N} - 3\ddot{A} - \ddot{C} \right) \\ + 3A'^2 + 3A'C' + 3A'N' + C'N' = 0, \end{aligned} \quad (4.2.7d)$$

$$(t) : \quad e^{-2N} \left(3A'\dot{A} - 3N'\dot{A} + C'\dot{C} - N'\dot{C} + 3\dot{A}' + \dot{C}' \right) = 0, \quad (4.2.7e)$$

where dot and prime are again shorthand for ∂_t and ∂_y , respectively. Furthermore, for notational convenience, the BIG terms were again absorbed into the *effective* fluid components

$$\tilde{\rho} := \frac{1}{M_6^4} \left[\rho - 3M_5^3 (H_a^2 + H_a H_c) \right], \quad (4.2.8a)$$

$$\tilde{p} := \frac{1}{M_6^4} \left[p + M_5^3 \left(2\dot{H}_a + \dot{H}_c + 3H_a^2 + H_c^2 + 2H_a H_c \right) \right], \quad (4.2.8b)$$

$$\tilde{p}_\phi := \frac{1}{M_6^4} \left[p_\phi + 3M_5^3 \left(\dot{H}_a + 2H_a^2 \right) \right]. \quad (4.2.8c)$$

When set to zero, those would correspond to the Friedmann equations of 5D (spatially flat) Kaluza-Klein cosmology [Fre82], which in the limit $H_c \ll H_a$ reproduces the standard 4D GR result. Due to the sixth dimension, those will here get modified by extrinsic curvature contributions from the bulk geometry, like in the DGP model.

4.2.2 On-brane equations

In order to go from the PDEs (4.2.7) to a system of on-brane ODEs, we can now proceed just like in the DGP case: First, perform a delta-matching of Eqs. (4.2.7a)–(4.2.7c), giving (after solving for the jumps)

$$[A'] = \frac{1}{4} (\tilde{p}_\phi - \tilde{p} - \tilde{\rho}), \quad [C'] = \frac{1}{4} (3\tilde{p} - 3\tilde{p}_\phi - \tilde{\rho}), \quad [N'] = \frac{1}{4} (\tilde{p}_\phi + 3\tilde{p} + 3\tilde{\rho}). \quad (4.2.9)$$



And second, take the jump and mean of the other⁴ Eqs. (4.2.7d) and (4.2.7e), yielding

$$[y] : 3[A'] \left(2\langle A' \rangle + \langle C' \rangle + \langle N' \rangle \right) + [C'] \left(3\langle A' \rangle + \langle N' \rangle \right) + [N'] \left(3\langle A' \rangle + \langle C' \rangle \right) = 0, \quad (4.2.10a)$$

$$\langle y \rangle : \frac{3}{4} [A'] \left([A'] + [C'] + [N'] \right) + \frac{1}{4} [C'] [N'] + 3\langle A' \rangle \left(\langle A' \rangle + \langle C' \rangle + \langle N' \rangle \right) + \langle C' \rangle \langle N' \rangle - 6H_a^2 - 3H_a H_c - H_c^2 - 3\dot{H}_a - \dot{H}_c = 0, \quad (4.2.10b)$$

$$[t] : 3H_a \left([A'] - [N'] \right) + H_c \left([C'] - [N'] \right) + 3[\dot{A}'] + [\dot{C}'] = 0, \quad (4.2.10c)$$

$$\langle t \rangle : 3H_a \left(\langle A' \rangle - \langle N' \rangle \right) + H_c \left(\langle C' \rangle - \langle N' \rangle \right) + 3\langle \dot{A}' \rangle + \langle \dot{C}' \rangle = 0. \quad (4.2.10d)$$

In this way, we have again extracted all the local on-brane information from the bulk equations of motion. As before, inserting the jumps (4.2.9) into the $[t]$ equation yields the energy conservation equation. This time, however, it is not the 4D standard one, but gets modified due to the dynamics of the compact extra dimension,⁵

$$\dot{\rho} + 3H_a (\rho + p) + H_c (\rho + p_\phi) = 0. \quad (4.2.11)$$

Let us now come to the crucial difference of this system of ODEs, as compared to the DGP case. There, the corresponding system provided enough equations to solve for all the means,⁶ thus ultimately leading to a closed evolution equation for the scale factor $a(t)$. But here, the counting does not add up: Energy conservation (4.2.11) determines $\rho(t)$ (while p and p_ϕ are determined by some equations of state), leaving us—after eliminating the jumps via (4.2.9)—with the *three* equations (4.2.10a), (4.2.10b) and (4.2.10d) for *five* unknown functions $\langle A' \rangle(t)$, $\langle C' \rangle(t)$, $\langle N' \rangle(t)$, $a(t)$ and $c(t)$. Hence, two equations are missing for a closed system which would yield a unique time evolution given initial conditions on the brane.

Assuming Z_2 symmetry helps a bit, but is not enough: In this case $\langle A' \rangle = \langle C' \rangle = \langle N' \rangle = 0$, so that Eqs. (4.2.10a) and (4.2.10d) are identically fulfilled, and we are left with Eq. (4.2.10b), which simplifies to

$$\frac{3}{4} [A'] \left([A'] + [C'] + [N'] \right) + \frac{1}{4} [C'] [N'] = 6H_a^2 + 3H_a H_c + H_c^2 + 3\dot{H}_a + \dot{H}_c, \quad (4.2.12)$$

⁴Again, taking the jump and mean of the first three equations (which contain second y -derivatives) would give six additional equations, but also six additional variables—the jump and mean of the second y -derivatives—and would thus not provide any additional information for the on-brane system.

⁵This is readily recognized as (the only nontrivial component of) $\nabla_m^{(5)} T^m_n = 0$, which follows (more abstractly) from the Gauss-Codazzi relation, together with the vacuum field equations and the 5D Bianchi identity.

⁶Or, after assuming Z_2 symmetry, implying vanishing means, there was still one equation left determining $a(t)$.

and constitutes only *one* equation for the *two* functions $a(t)$ and $c(t)$. Therefore, the on-brane system is still not closed, and consequently allows for *completely arbitrary* cosmological evolutions on the brane. [One could, for instance, require c to have some arbitrary time-dependence, and then use (4.2.10b) to infer the corresponding form of a .]

In the DGP case this did not happen and, as discussed in Sec. 1.4.2, the reason was that there Taub's (or Birkhoff's) theorem applied and enforced a static bulk geometry due to the imposed symmetries. The reason for the failure in the present case should thus be clear: There is no such theorem which would forbid gravitational bulk waves in this six-dimensional setup. Accordingly, the arbitrariness in the on-brane solution is inherited from the freedom to freely choose initial wave profiles in the bulk and let them propagate towards the brane.⁷ In other words, instead of the one constant of integration that appeared in the DGP Friedmann equation due to the one free parameter of the static bulk solution, there are now infinitely many “constants of integration”, which would be necessary to specify the initial wave data, rendering the on-brane system undetermined.

The inapplicability of Taub's theorem is due to the fact that the geometry under investigation is not (hyper-)plane-symmetric. As already mentioned, “planar symmetry” in the theorem refers to translational *and rotational* symmetry in the plane directions. The metric (4.2.1) shows that rotational symmetry between the x - and ϕ -directions is broken, because the functions A and C are generally different. Indeed, requiring them to be equal would restore planar symmetry, and the theorem would strike again: the three equations (4.2.10a), (4.2.10b) and (4.2.10d) would again yield a closed system for the remaining three functions $\langle A' \rangle$, $\langle N' \rangle$ and a .⁸

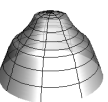
4.2.3 Excluding incoming bulk waves

When gravitational waves are present in the bulk, the only way to obtain a closed system of on-brane ODEs is by imposing outgoing wave boundary conditions on both sides of the brane. Note that this is in accordance with the counting of equations in the preceding section: Without Z_2 symmetry across the brane, those would add the two additional equations that are needed to close the system; with Z_2 symmetry there would only be one outgoing wave boundary condition, also matching the one missing equation in that case. For simplicity, we will from now on restrict ourselves to the Z_2 symmetric case, which is a natural assumption in the current bulk topology, cf. Fig. 4.1a.

Since those waves, according to the required symmetries, are plane waves, we expect the standard interpretation of the components of the Weyl tensor to apply, as discussed

⁷This also explains why enforcing Z_2 symmetry decreases the number of undetermined functions by one: without the symmetry, one could prepare different bulk waves on the left and right bulk half-spaces.

⁸Alternatively, in the Z_2 symmetric case, Eq. (4.2.12) would be the one equation determining the time evolution of the single function a .



Comp.	Name	Identities	Interpretation
C_{0p0q}	Ω_{pq}	$\Omega_{pq} = \Omega_{qp}$ $\Omega^p_p = 0$	Transverse gravitational wave propagating in the direction $-y$
C_{010p}	Ψ_p		Longitudinal gravitational wave propagating in the direction $-y$
C_{0101} C_{0p1q}	Φ Φ_{pq}	$\Phi + \Phi^p_p = 0$	Newton-like part of the gravitational field
C_{101p}	Ψ'_p		Longitudinal gravitational wave propagating in the direction $+y$
C_{1p1q}	Ω'_{pq}	$\Omega'_{pq} = \Omega'_{qp}$ $\Omega'^p_p = 0$	Transverse gravitational wave propagating in the direction $+y$

Table 4.1: The standard interpretation of the components of the Weyl tensor, cf. Chap. 2. The indices $\{0, 1, p\}$ refer to the mixed tetrad components $\{\mathbf{k}, \mathbf{l}, (\mathbf{m}_i, \mathbf{m}_\phi)\}$, respectively, as defined in Eq. (4.2.13). The listed identities follow directly from the symmetries and tracelessness of the Weyl tensor.

in Chap. 2. The desired outgoing wave condition can then be realized by setting to zero the Weyl components corresponding to outgoing gravitational waves.

To calculate the Weyl components, we proceed as described in Chap. 2: First, we set up the mixed orthonormal tetrad⁹ for the metric (4.2.1),

$$\mathbf{k} = \frac{1}{\sqrt{2}} (e^{-N} \partial_t + \partial_y), \quad \mathbf{l} = \frac{1}{\sqrt{2}} (e^{-N} \partial_t - \partial_y), \quad \mathbf{m}_i = e^{-A} \partial_i, \quad \mathbf{m}_\phi = e^{-C} \partial_\phi. \quad (4.2.13)$$

The null vectors \mathbf{k} and \mathbf{l} were chosen such that the Weyl components will measure gravitational wave propagation relative to the y -direction, i.e. perpendicular to the brane, as required. In this frame, one can calculate the components of the Weyl tensor \mathbf{C} , as defined in Sec. 2.3.

For convenience, we list their definitions and interpretations here in Table 4.1. The straight forward calculation then yields

$$\Omega_{ij} = \Omega^- \delta_{ij}, \quad \Omega_{\phi\phi} = -3\Omega^-, \quad \Omega_{i\phi} = 0, \quad (4.2.14a)$$

$$\Psi_i = 0, \quad (4.2.14b)$$

$$\Phi_{ij} = \Phi^{(x)} \delta_{ij}, \quad \Phi_{\phi\phi} = \Phi^{(\phi)}, \quad \Phi = -3\Phi^{(x)} - \Phi^{(\phi)}, \quad (4.2.14c)$$

$$\Psi'_i = 0, \quad (4.2.14d)$$

$$\Omega'_{ij} = \Omega^+ \delta_{ij}, \quad \Omega'_{\phi\phi} = -3\Omega^+, \quad \Omega'_{i\phi} = 0, \quad (4.2.14e)$$

⁹Note that, like in the examples of Chap. 2, the timelike vector $e^{-n} \partial_t$ is in general not tangent to a geodesic. However, the discussion below Eqs. (2.4.4) applies here analogously, so that this only changes the Weyl components by some overall factors, which are irrelevant for our purposes.

with

$$\Omega^- := \frac{e^{-2N}}{6} \left(3\dot{A}\dot{C} + 2\dot{C}^2 - 2\dot{C}\dot{N} + 2\ddot{C} \right) + \frac{e^{-N}}{3} \left(\dot{C}C' - \dot{C}N' + \dot{C}' \right) - \frac{A'C'}{2} - \frac{C'N'}{3}, \quad (4.2.15a)$$

$$\Phi^{(x)} := \frac{e^{-2N}}{2} \left(2\dot{A}^2 + \dot{A}\dot{C} \right) - A'^2 - \frac{A'C'}{2}, \quad \Phi^{(\phi)} := \frac{3}{2} \left(e^{-2N} \dot{A}\dot{C} - A'C' \right), \quad (4.2.15b)$$

$$\Omega^+ := \frac{e^{-2N}}{6} \left(3\dot{A}\dot{C} + 2\dot{C}^2 - 2\dot{C}\dot{N} + 2\ddot{C} \right) - \frac{e^{-N}}{3} \left(\dot{C}C' - \dot{C}N' + \dot{C}' \right) - \frac{A'C'}{2} - \frac{C'N'}{3}, \quad (4.2.15c)$$

These terms were simplified by using the vacuum field equations to eliminate all second y -derivatives as well as \ddot{A} and \dot{A}' . If the bulk were not empty, there would thus be additional source terms in these expressions, like e.g. in the case of a nonvanishing bulk $\mathcal{C}\mathcal{C}$.¹⁰

The bulk Weyl tensor is thus completely characterized by the four independent terms given in (4.2.15). According to the standard interpretation—which, as discussed before, is expected to apply to the current planar setup—they correspond to transverse gravitational waves Ω^- propagating in direction $-y$, and Ω^+ in direction $+y$, as well as Newton-like field components $\Phi^{(x)}$ and $\Phi^{(\phi)}$.

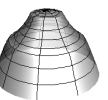
As an important consistency check, one can do the same calculation in the DGP setup. There, it turns out that only the Newton-like components are nonzero, while all the wave components vanish identically; moreover, the Newton-like terms contain only one independent component, which vanishes if and only if the constant \mathcal{C} in the DGP cosmology solution is set to zero [NS15a]. Since we already know that this constant corresponds to the Levi-Civita (or Schwarzschild) mass parameter, measuring the static bulk curvature, this is an explicit confirmation that the standard interpretation of the Weyl components indeed works correctly in this case.

Furthermore, one can check that when enforcing planar symmetry in the metric ansatz (4.2.1) by setting $A = C$, again all the wave components Ω, Ω' would vanish,¹¹ in accordance with Taub's theorem, which then guarantees a static bulk geometry.

Finally, note that Ω^+ and Ω^- interchange their roles upon time-reversal, as they should, while the Newton-like terms are invariant. Thus, the identification of the wave components via the standard Weyl decomposition passes all the nontrivial consistency checks, and so we can be confident that it provides the correct tool to implement the

¹⁰For completeness, it should be mentioned that there are also some nonvanishing Weyl components in the “non-observable” sector, cf. Sec. 2.3. They are all proportional to the Newton-like terms $\Phi^{(x)}$ and $\Phi^{(\phi)}$, and their appearance follows from the tracelessness condition, cf. also the discussion in Sec. 2.4.1.

¹¹This is not apparent from their form given in (4.2.15), because there the vacuum field equations were used in an A - C -asymmetric way. But one can explicitly check that they indeed vanish after the field equations are used again in the symmetric case $A = C$.



outgoing wave condition in the present setup. To this end, we set $\Omega^- = 0$ for $y > 0$, and $\Omega^+ = 0$ for $y < 0$. In order to translate this into appropriate on-brane conditions, we can simply take the the respective limits $y \rightarrow 0^\pm$. Due to the Z_2 symmetry, this yields one nontrivial condition, namely

$$\frac{1}{4} [C'] \left(3 [A'] + 2 [N'] \right) = H_c \left([C'] - [N'] \right) + [\dot{C}'] + 3H_a H_c + 2H_c^2 + 2\dot{H}_c. \quad (4.2.16)$$

This provides the missing equation which, together with (4.2.12) [and the junction conditions (4.2.9)], constitutes a closed system of ODEs determining the cosmological evolution of the scale factors $a(t)$ and $c(t)$.

Note that those equations contain the time derivatives of both Hubble parameters H_a and H_c (in linearly independent combinations), and are thus two second order differential equations for the scale factors. Thus, we have only obtained the ‘‘second’’ Friedmann equations, and no constraint equation. The same thing happened also in the DGP case, cf. Eq. (1.4.18), where the analogous equation could be integrated once analytically, to obtain the first Friedmann equation (1.4.20) containing the integration constant \mathcal{C} , corresponding to the static bulk field. The subsequent analysis was then simplified by setting this constant to zero. In the present case, Eqs. (4.2.12) and (4.2.16) cannot be integrated analytically. Still, physically, we expect one of the initial conditions to correspond to the static part of the bulk curvature, in analogy to the DGP scenario. We could of course study the solutions of the system (4.2.12), (4.2.16) for different initial conditions, treating them as free parameters. However, for simplicity, we prefer to reduce the parameter space by setting to zero the static part of the bulk geometry, just like in the DGP case. Here, this can be achieved by setting to zero the Newton-like Weyl components $\Phi^{(x)}$ and $\Phi^{(\phi)}$. Due to Z_2 symmetry, this adds *two* further on-brane equations. One might thus worry that this assumption could be too restrictive, leading to an overdetermined system (even if no assumptions about the wave components are made). We shall see below that this is not the case: One of the equations will be redundant, allowing for consistent, nontrivial cosmological solutions. Furthermore, it turns out that one can, in addition, still require to have no incoming waves, making those solutions consistent with our physical assumption of a source-free bulk.

4.2.4 Excluding Newton-like bulk fields

Setting the Newton-like field components (4.2.15b) to zero in the bulk is equivalent to the two conditions¹²

$$e^{-N} \dot{A} = \sigma A', \quad e^{-N} \dot{C} = \sigma C', \quad (4.2.17)$$

where $\sigma = \pm 1$. Interestingly, it turns out that then the wave components reduce to

$$\Omega^- = -(1 + \sigma) \left(A'' + A'^2 \right), \quad \Omega^+ = (1 - \sigma) \left(A'' + A'^2 \right), \quad (4.2.18)$$

¹²Note that we divided by \dot{A} to derive the second equation, so it would be absent for a static solution.

where the vacuum field equations were again employed. Irrespective of the sign σ , one of them will thus always vanish. In other words, we found that the absence of Newton-like field components implies that the bulk contains either solely left-moving or solely right-moving waves. In particular, we can choose $\sigma = -\text{sgn}(y)$, so that there are only bulk waves propagating away from the brane. Thus, the outgoing wave condition is already fulfilled with this choice, as advertised above.

However, we still have to check whether the two on-brane conditions that follow from Eqs. (4.2.17) in a Z_2 symmetric setup lead to an overdetermined system. They read

$$[A'] = -2H_a, \quad [C'] = -2H_c, \quad (4.2.19)$$

and one can check that after using them in (4.2.12), this equation becomes equivalent to (4.2.10c), and thus to energy conservation (4.2.11). Therefore, the system is not overdetermined, and the two equations (4.2.19) provide a closed, consistent system of on-brane ODEs for the two scale factors $a(t)$ and $c(t)$. Explicitly, after plugging in the junction conditions (4.2.9) and the definitions of the effective fluid components (4.2.8), these modified Friedmann equations read

$$3H_a + H_c = \frac{1}{2M_6^4} [\rho - 3M_5^3 (H_a^2 + H_a H_c)], \quad (4.2.20a)$$

$$H_c = \frac{1}{8M_6^4} \left[\rho - 3p + 3p_\phi + 3M_5^3 (\dot{H}_a - \dot{H}_c + 2H_a^2 - 3H_a H_c - H_c^2) \right]. \quad (4.2.20b)$$

The first equation was obtained by taking a suitable linear combination of the two original equations, in such a way that all second time derivatives \dot{H}_a and \dot{H}_c dropped out,¹³ which was possible because they entered only in the single combination $\dot{H}_a - \dot{H}_c$. Hence, it represents a first order (or constraint) equation, like the first Friedmann equation (1.4.20) in DGP cosmology. Accordingly, the system (4.2.20) requires one less initial condition than the more general outgoing wave system (4.2.12), (4.2.16), and its solutions form a subspace in the corresponding full parameter space. In this sense, it is completely analogous to the DGP cosmology (1.4.20) with the constant \mathcal{C} set equal to zero.

However, there is also a qualitative difference: whereas setting $\mathcal{C} = 0$ in the DGP model implied a Minkowski bulk, here the bulk spacetime in general consists of purely outgoing gravitational waves. They are measured by the Weyl component Ω^\pm (for $y \gtrless 0$) which can, evaluated at the brane, be expressed solely in terms of the scale factors as

$$\Omega^+(0^+) = \Omega^-(0^-) = \frac{2(\dot{a}\ddot{c} - \dot{c}\ddot{a})}{3\dot{a}c + \dot{c}a}. \quad (4.2.21)$$

¹³Not that, without the BIG terms $\propto M_5$, also the second equation would not contain any second time derivatives, and one would thus have two constraint equations.



This term vanishes only in the special case $\dot{c} \propto \dot{a}$ (including $\dot{a} = 0$ or $\dot{c} = 0$), then leading to a Minkowski bulk. Even though this is not the generic case, we will see below that the corresponding solutions represent attractors in a broader class of solutions.

In Appendix 4.A we will see that it is even possible to derive the full (nonlinear) bulk solution in the case of vanishing Newton-like Weyl components, thereby confirming that it indeed corresponds to outgoing gravitational bulk waves, as expected from the Weyl analysis. The bulk geometry is completely determined once the on-brane evolution of the scale factors a and c is known, and can be given in closed analytic form expressed in terms of a and c . In the remaining main part of this chapter, we discuss the solutions of the system of modified Friedmann equations (4.2.20), as well as their phenomenological status.

4.3 Solutions and comparison to observations

Another difference to the DGP setup is that here, in addition to appropriate initial conditions, one also needs to specify an EOS determining the pressure p_ϕ in direction of the compact extra dimension. Ultimately, this EOS should be determined by the more fundamental microscopic theory that gave rise to the brane in the first place, like e.g. string theory. As this is beyond the scope of the present work, we shall content ourselves with an effective description in which the EOS is added by hand. We will consider two cases:

- (i) $p_\phi = 0$, corresponding to a freely expanding (or collapsing) compact extra dimension. This choice is not very well motivated on physical grounds, but rather serves as an illustration of how the dynamics of the compact extra dimension can influence the 4D behavior. Furthermore, we will see that it provides a concrete example of a dynamical degravitation mechanism, making it conceptually interesting. However, we will find—not surprisingly—that this choice does not lead to phenomenologically viable solutions.
- (ii) p_ϕ is defined implicitly by requiring the proper size of the compact dimension to be constant. Technically, this is simply achieved by setting $H_c = 0$, and using the second Friedmann equation (4.2.20b) to read off the required form of p_ϕ a posteriori. Physically, this should be realizable in some concrete UV model in which the size modulus of the ϕ -dimension is stabilized by some additional degree of freedom, for instance by an wrapping a scalar field around the compact dimension as in [KK07]. Setting $H_c = 0$ exactly, corresponds to the limit of making this degree of freedom infinitely heavy.

Let us now discuss these two scenarios in turn. The EOS for p , i.e. the pressure in x -direction, will always be assumed to be given by a linear EOS parametrized by w , i.e. $p = w\rho$ (or a sum $\rho = \sum \rho_i$ of different fluid components with different w_i) like in standard cosmology.

4.3.1 Vanishing azimuthal pressure

After setting $p_\phi = 0$, the energy conservation equation (4.2.11) can be integrated to obtain

$$\rho \propto a^{-3(1+w)} c^{-1}. \quad (4.3.1)$$

Since c measures the proper circumference of the compact ϕ -dimension, the dimensionally reduced 4D energy density is given by $\rho^{(4)} := (2\pi c) \rho$, which consequently scales like¹⁴

$$\rho^{(4)} \propto a^{-3(1+w)}, \quad (4.3.2)$$

i.e. exactly like in standard cosmology, cf. Eq. (1.1.8). In particular, $\rho^{(4)} = \text{const}$ for $w = -1$, in accordance with the interpretation as a 4D cosmological constant.

The system of Friedmann equations (4.2.20) can now be integrated forward in time, given appropriate initial conditions. Denoting evaluation at initial time by a subscript i , those can be taken, for instance, as ρ_i, a_i, c_i and H_{ai} , while H_{ci} is then already determined by the constraint (4.2.20a). Without loss of generality,¹⁵ we can set $a_i = c_i = 1$ as well as $t_i = 0$. The time evolution of a and c is then uniquely determined by the initial conditions H_{ai} and $\bar{\rho} := \rho_i/M_6^4$, as well as the model parameter $r_c := M_5^3/(2M_6^4)$.

We will first discuss pure dust ($w = 0$) and pure CC ($w = -1$) solutions, and finally a general mixture of both fluid components, which will be fit to supernova data.

Pure dust

For $p = 0$ we are (since we are also considering $p_\phi = 0$ here) in a special case of the more general class $p = p_\phi$. In this class, there are exact solutions of the Friedmann equations (4.2.20) for which the scale factors $a(t)$ and $c(t)$ are equal. This is clear because in this case of equal energy momentum components in x - and ϕ -direction it is possible also to demand the corresponding symmetry of the metric components. Hence, the setup is locally indistinguishable from a 5D/6D ‘‘DGP’’ model, i.e. a five-dimensional, homogeneous codimension-one brane; only one of the spatial dimensions is trivially compactified, but this has no geometrical impact because it induces no curvature. Accordingly, the two Friedmann equations (4.2.20) become equivalent and read

$$H_a = \frac{1}{8M_6^4} (\rho - 6M_5^3 H_a^2), \quad (4.3.3)$$

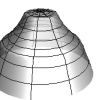
which is readily recognized as the generalization of the corresponding DGP equation (1.4.20) to a 5D/6D setup. Returning to the case $p = p_\phi = 0$, and using the above definitions, this becomes

$$H_a = \frac{\bar{\rho}}{8a^4} - \frac{3r_c}{2} H_a^2, \quad (4.3.4)$$

¹⁴For a general linear EOS $p_\phi = w_\phi \rho$, energy conservation (4.2.11) yields $\rho \propto e^{-3(1+w)a - (1+w_\phi)c}$.

Hence, the choice $p_\phi = 0$ is somewhat special in that it is the only choice which implies the standard scaling (4.3.2) for $\rho^{(4)}$, apart from the stabilized scenario $c = \text{const}$, discussed below.

¹⁵The general solutions are obtained from those by simply rescaling a and c .



where the scaling of ρ is that of dust in four spatial dimensions, but looks like radiation from a 4D point of view. This already suggests that this solution will not give rise to a viable 4D phenomenology: instead of heaving a 4D limit for $M_6 \rightarrow 0$, the model instead approaches a 5D behavior. This will indeed be confirmed below.

Note that, as discussed below Eq. (4.2.21), for this solution the wave components of the Weyl tensor vanish, and so the brane is embedded in a Minkowski bulk. The reason is that setting $a = c$ restored planar symmetry of the setup making Taub's theorem applicable again, cf. Sec. 1.4.2.

These ‘‘plane symmetric’’ solutions with $a(t) = c(t)$ are only realized for initial conditions satisfying $H_{ai} = H_{ci}$. Generically, if this condition is violated, the solutions will be different; in particular, they will not be embedded in a Minkowski bulk, but will emit plane gravitational waves into the bulk. However, it turns out that these generic solutions always rapidly approach the $a = c$ solution. This is shown in Fig. 4.2a, where the numerically obtained solutions for different initial conditions H_{ai} (but fixed $\bar{\rho}$ and r_c) are plotted, together with the plane symmetric $a = c$ solution. In other words, this solution is an attractor for the most general solutions with $p = p_\phi = 0$. While the attractor is approached, gravitational waves are emitted into the bulk, tending to zero at late times, see Fig. 4.3a.

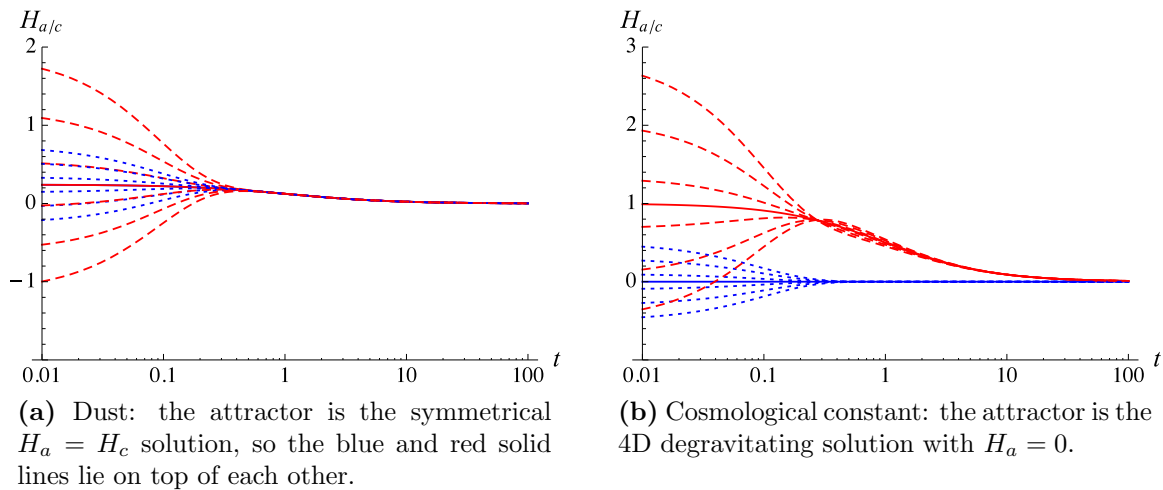


Figure 4.2: The Hubble parameters H_a (blue, dotted) and H_c (red, dashed) for different initial conditions generically approach the attractor solutions (solid lines). Time and the Hubble parameters are measured in the same fixed but arbitrary units, and the parameters were set to $\bar{\rho} = 2$ and $r_c = 0.1$, but the qualitative attractor behavior is the same for other choices.

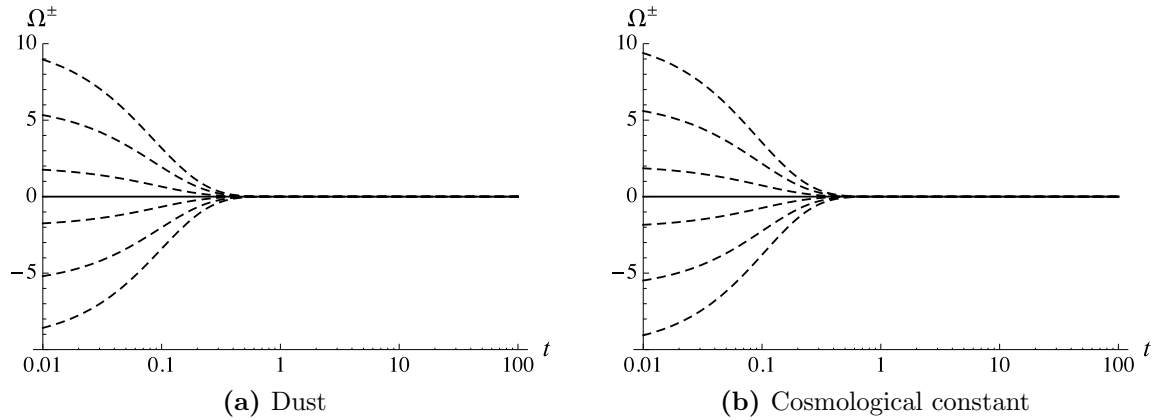


Figure 4.3: The Weyl component (4.2.21), measuring the emission of gravitational waves into the bulk, for the same solutions as those shown in Fig. 4.2. The solid lines correspond to the attractor solutions, for which the Weyl tensor vanishes.

Pure cosmological constant

For $p = -\rho$ (and still $p_\phi = 0$), corresponding to a 4D CC, one can easily check that the Friedmann equations (4.2.20) allow for the exact solutions

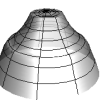
$$a(t) = 1, \quad c(t) = 1 + \frac{\bar{\rho}}{2} t. \quad (4.3.5)$$

Since $\dot{a}(t) = 0$, the Weyl components (4.2.21) are again zero, leaving us with a flat bulk spacetime.

Again, these are not the generic solutions—they only correspond to the subclass for which $H_{ai} = 0$. But as in the case of pure dust, it turns out that they represent attractor solutions, which are again rapidly approached for general initial conditions, see Fig. 4.2b, thereby emitting gravitational bulk waves, cf. Fig. 4.3b.

This solution is conceptually interesting in that it represents an explicit realization of the *degravitation mechanism* (see Sec. 1.3): The 4D CC—which in standard cosmology inevitably results in a nonvanishing Hubble parameter—is completely absorbed into extra-dimensional curvature, embodied by the expansion rate H_c of the compact dimension, whereas the four large brane-dimensions are completely flat. (Note that, unlike in GR, where the CC leads to a constant Hubble parameter, here H_c is not constant but falls off like $\sim 1/(\bar{\rho} t)$ asymptotically.) Moreover, the attractor behavior shows that this solution is dynamically approached, meaning that there is no need for fine-tuning. This dynamical adjustment is achieved by the possibility to emit gravitational waves into the bulk.

Just to be clear, this mechanism represents no degravitation from the 5D brane point of view: the spacetime curvature that is caused by the 4D CC is given by the expansion in ϕ -direction, so the 5D brane geometry is not flat. Only when restricted to the four non-compact brane dimensions does it reduce to Minkowski spacetime. Thus, the CC is not completely transformed into extrinsic curvature, but also intrinsic brane-



curvature. This is to be contrasted with the situation in two codimensions (which will be studied in Chap. 5), where there are degravitating solutions for which all curvature is completely extrinsic, in the form of a conical deficit. This seems much more promising with respect to the CC problem, because then an observer has no means of detecting the impact of the CC by local on-brane observations. Here, instead, the expansion¹⁶ of the compact dimension would at some point cause it to be large enough to become observable even at low energies. One could try to arrange this to happen late enough not to cause immediate phenomenological problems, but this would likely reintroduce another fine-tuning.

Furthermore, so far it is not clear whether the assumption $p_\phi = 0$ —which was imposed here by hand—could be realized in some UV model in a natural way, or if it would also correspond to an implicit fine-tuning. But apart from these potential pitfalls, the model is in any case only phenomenologically viable if it allows for a 4D regime in order not to spoil the success of standard GR. We will now show that this is not the case, by fitting the model (with a fluid containing both dust and a cosmological constant) to supernova (SN) data.

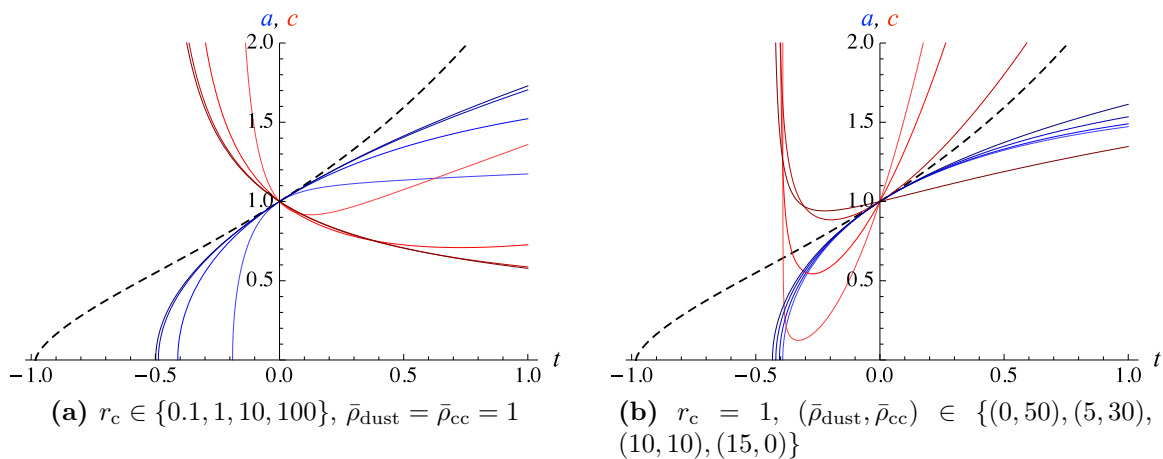


Figure 4.4: Plots of the scale factors a (blue) and c (red) for various choices of parameters; the dashed black lines correspond to a standard Λ CDM cosmology with $\Omega_\Lambda = 0.72$. The lightest curves correspond to the first parameter in each list. All dimensionful quantities are measured in units of H_{ai} .

¹⁶One might have expected that one could avoid this problem by demanding the compact dimension to collapse, instead of expand, by reversing the sign of H_c . However, this is not allowed, because the sign of H_c is the same as that of ρ , which we assume to be positive. This is due to the fact that time-reversal symmetry is broken in the Friedmann equations (4.2.20) by demanding to have only outgoing bulk waves. Of course, one could argue that these are absent if one chooses to be exactly on the attractor solution, but this would reintroduce another fine-tuning.

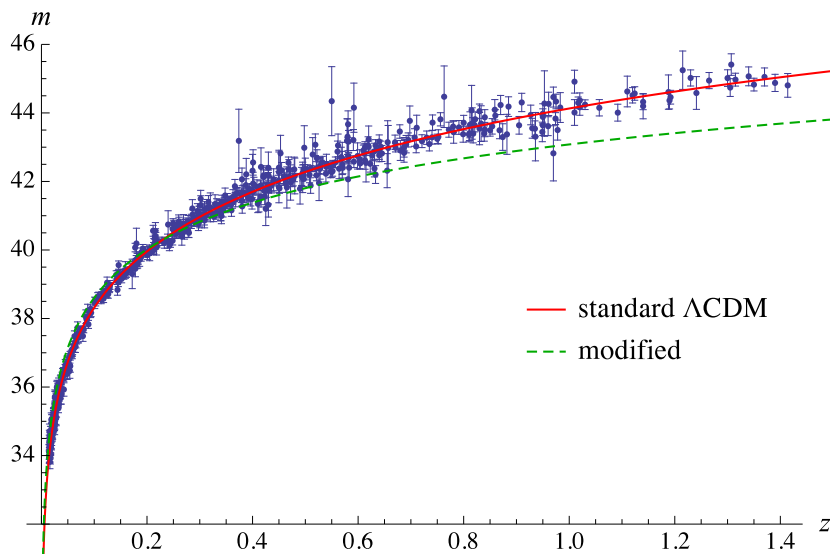


Figure 4.5: Magnitudes of the Union 2.1 SNe as function of redshift, together with the Λ CDM best fit ($\Omega_\Lambda = 0.72$). The dashed green line is the best fit obtained for the modified Friedmann equations (4.2.20) with $p_\phi = 0$ and two fluid components ($w = 0$ and $w = -1$).

Dust and cosmological constant

The solutions for a general mixture of dust ($w = 0$) and a CC ($w = -1$) can easily be obtained by numerically integrating the system of ODEs (4.2.20). At late times, since the dust component dilutes faster, they approach the CC attractor (4.3.5), possibly with an intermediate dust attractor regime, depending on the parameters. Some exemplary solutions for certain parameter choices are shown in Fig. 4.4, and compared to the evolution of the scale factor in standard Λ CDM with $\Omega_\Lambda = 0.72$, the best fit value from the SN data. Clearly, the evolution of the 3D scale factor a (blue curves) is always far away from the successful Λ CDM. This is also seen from a corresponding fit to the SN magnitudes m taken from the Union 2.1 data set [P⁺12], which is performed as explained in Sec. 1.1.2. The result¹⁷ is shown in Fig. 4.5, which clearly rules out the $p_\phi = 0$ model.

Physically, the reason for this failure lies in the fact that the compact extra dimension always has a nontrivial dynamics which is comparable to, or even dominant over, that of the three large dimensions. Indeed, in the attractor solutions, either $H_c = H_a$ for dust, or even $H_c \neq 0$ and $H_a = 0$ for a CC. This suggests that stabilizing the compact extra dimension could help avoiding this problem. We will see in the next section that this is indeed the case.

¹⁷The fit does not yield a finite best-fit value for r_c but tends towards $r_c \rightarrow \infty$, thereby becoming insensitive to $\bar{\rho}_{\text{dust}}$ and $\bar{\rho}_{\text{cc}}$, and approaching the dashed curve shown in Fig. 4.5.



4.3.2 Stabilized fifth dimension

We now turn to case (ii) mentioned at the beginning of Sec. 4.3: The azimuthal pressure p_ϕ is assumed to be such that the compact dimension is stabilized, i.e. that $c = \text{const}$. We do not have a specific UV model at hand that would automatically achieve this in a consistent way, but we can still check a posteriori whether p_ϕ is physically reasonable in the sense that it satisfies the null energy condition (NEC). This does not yield a sufficient, but at least a necessary criterion for the existence of an actual stabilization mechanism in terms of healthy high energy degrees of freedom.

First of all, setting $H_c = 0$ in the energy conservation equation (4.2.11) again implies the standard scaling (4.3.2) for the energy density. Next, the first modified Friedmann equation (4.2.20a) simplifies to

$$3H_a = \frac{1}{2M_6^4} (\rho - 3M_5^3 H_a^2). \quad (4.3.6)$$

After dimensionally reducing the energy density and Planck masses according to

$$\rho \rightarrow \frac{\rho^{(4)}}{2\pi c}, \quad M_5^3 \rightarrow \frac{M_4^2}{2\pi c}, \quad M_6^4 \rightarrow \frac{M_5^3}{2\pi c}, \quad (4.3.7)$$

where $2\pi c$ is the (constant) physical circumference of the compact extra dimension, this is exactly the DGP Friedmann equation (1.4.20) (for $\mathcal{C} = 0$, which is consistent with having set the Newton-like Weyl components to zero). To be more precise, it corresponds to the normal branch of the DGP cosmology. The self-accelerating branch would have been obtained for the choice $\sigma = +\text{sgn}(y)$ in (4.2.17), corresponding to *incoming* wave components. However, for $\dot{c} = 0$ the wave components (4.2.21) are in fact zero, so there are neither incoming nor outgoing waves, and the brane is instead embedded in a Minkowski bulk. Thus, we could also allow for the other branch here, because it (trivially) also fulfills the outgoing wave condition. But it is interesting to note that as soon as c were not stabilized perfectly, but allowed to fluctuate (like in a realistic UV model where the radion has a finite mass), the self-accelerating branch has to be dismissed by means of the wave criterion.

One can easily check that the corresponding bulk solution has not only $c(t) \equiv e^{C_0} = \text{const}$, but even $C(t, y) = \text{const}$. In other words, the 6D model differs from the DGP model only in the addition of a trivial compact dimension, which does not take part in the geometrodynamics at all. Therefore, it is not surprising that we exactly recover the DGP cosmology.

On the one hand, this is good news, because the DGP model does indeed allow for a 4D regime, as was intended by the stabilization requirement. On the other hand, it seems like the model is not very interesting because it is indistinguishable from DGP—at least at the level of (homogeneous and isotropic) cosmology. However, this is not necessarily the case: As already mentioned, we need some specific form of p_ϕ which stabilizes the compact extra dimension. It can be read off from Eq. (4.2.20b), leading

to an effective EOS parameter

$$w_\phi := \frac{p_\phi}{\rho} = \frac{3w - 1}{2} - \frac{1 + w}{2\sqrt{1 + \chi}} + \frac{4}{3\chi} \left(\sqrt{1 + \chi} - 1 \right), \quad (4.3.8)$$

where $\chi := \rho M_5^3 / 3M_6^8 > 0$. (Note that w_ϕ is generically time dependent, due to the BIG terms.) For dust ($w = 0$) or radiation ($w = 1/3$), w_ϕ is bounded from below by -1 and $-2/3$, respectively. Thus, the NEC is always satisfied for these sources. For a CC ($w = -1$), however, one finds $w_\phi \leq -4/3$, thus violating the NEC. This implies that a CC-source could *not* be stabilized by healthy degrees of freedom in an actual UV model and, on the other hand, suggests that a stabilization *is* possible for dust or radiation.

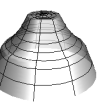
This makes the model potentially interesting, because at early times, when the cosmological fluid is dominated by radiation or dust, it should behave like the DGP model, thus allowing for a 4D regime when $H_a \gg r_c \equiv M_4^2 / M_5^3$. At late times, one expects two kinds of modifications: First, there is the usual DGP-like transition to a 5D regime; but second, there should also be another transition when the CC starts to dominate and the stabilization mechanism breaks down. This would lead to a time-evolution of the compactification size c , which would generically have observable consequences for the evolution of the scale factor a . But in order to quantify these consequences, we would need an actual UV model that describes how exactly the stabilization breaks down and thus how the time evolution of c would look like. This is beyond the scope of the present work and requires further study.

4.4 Summary and outlook

In this chapter, we derived the modified Friedmann equations of the “cosmic ring” setup, which generalizes the DGP model by adding a compact spatial dimension (of size $2\pi c$) to the spacetime. The brane thus becomes a five-dimensional object of codimension one, and all brane matter was assumed to be distributed homogeneously over the fifth, compact dimension.

This additional dimension has the important consequence that a brane with cosmological symmetries (i.e. 3D homogeneity and isotropy) can emit gravitational waves into the bulk. The reason is that the fifth dimension breaks the planar symmetry which protects the DGP scenario against bulk waves via Taub’s theorem. Regarding the Friedmann equations, this implies that a closed system of on-brane equations can only be obtained after imposing further restrictions upon the bulk geometry. For a source-free bulk, the physically necessary assumption is the exclusion of incoming waves.

It was shown here that this can successfully be done by means of the standard decomposition of the Weyl tensor which—as discussed in Chap. 2—correctly disentangles left- and right-moving plane gravitational waves. In addition, this method allowed to set the Newton-like gravitational bulk fields to zero, thereby arriving at a minimal



extension of the $\mathcal{C} = 0$ DGP cosmology, in which the bulk spacetime only differs from Minkowski in the presence of purely outgoing gravitational waves.

In order to explicitly solve the modified Friedmann equations, it was necessary to specify an EOS for the pressure p_ϕ in direction of the compact extra dimension. We considered two scenarios:

- (i) $p_\phi = 0$: Interestingly, this choice yields degravitating solutions, for which the effect of a 4D CC is completely absorbed by H_c , i.e. the expansion rate of the compact dimension, leaving the 4D on-brane geometry flat. Moreover, these solutions were found to be attractors, thus constituting a dynamical adjustment mechanism to $H_a = 0$ even for $H_{ai} \neq 0$, which is realized via the emission of gravitational bulk waves. The model hence provides an explicit dynamical degravitation mechanism (at the full nonlinear level!), which sounds very promising for addressing the CC problem. But unfortunately, we found that this is only achieved at the expense of losing a 4D regime, making the model phenomenologically unviable, as was shown by performing a corresponding SN fit.

But there is still an important lesson to be learned here: As reviewed in Sec. 1.2.1, Weinberg's powerful no-go theorem [Wei89] tells us that there cannot be any dynamical adjustment mechanism (without fine-tuning) in terms of a 4D theory with any (finite) number of additional fields. Even though it is formulated in 4D, it also applies to theories with compact extra dimensions, since they can (at low energies) be understood in terms of a 4D EFT with a finite number of Kaluza-Klein fields (with masses below the cutoff). But the situation is quite different for *infinite* extra dimensions [DGS03]: In that case, integrating out the bulk leads to a nonlocal 4D EFT (or, equivalently, a continuum of Kaluza-Klein modes), to which the no-go theorem is not applicable. To see how this manifests itself in our model, note that dropping the sixth (infinite) dimension can formally be achieved by simply taking $M_6 \rightarrow 0$. But in this limit, the first Friedmann equation (4.2.20a) shows that $\rho \neq 0$ inevitably requires $H_a \neq 0$, and so degravitation becomes impossible. This shows the crucial importance of the infinite dimension for the dynamical adjustment mechanism,¹⁸ as expected from EFT reasoning and Weinberg's argument.

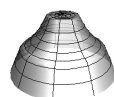
- (ii) $\dot{c} = 0$, determining p_ϕ implicitly: In this case one exactly recovers DGP cosmology. This is not surprising, after realizing that the compact extra dimension has turned into a mere spectator, taking part in neither the brane nor the bulk dynamics. However, the stabilizing pressure violates the NEC when the CC starts to dominate. Therefore, even though this model has nothing to say with respect to the CC problem, it predicts a breakdown of the stabilization and thus a potentially interesting late-time modification of 4D cosmology (on top of the DGP-like

¹⁸Note, however, that it is not clear whether the choice $p_\phi = 0$ corresponds to another implicit fine-tuning, or if it could be achieved in a technically natural way. This would need to be further studied in the case the model could be improved to become phenomenologically viable.

modification). But quantitative statements can only be made in an actual UV model which dynamically resolves the stabilization mechanism.

The most promising route for future research therefore consists in modeling such a mechanism. One way would be to build an actual UV model, e.g. using a scalar field that wraps around the compact dimension, as was for instance done (at the static background level) in [KK07]. Another possibility would be to parametrize our ignorance of the actual stabilization mechanism by imposing $c(t)$ to have some explicit form controlled by few parameters, and trying to learn something about “good” mechanisms by fitting these parameters to observational data.

Alternatively, one could leave the realm of the homogeneous background evolution and study perturbations, in order to get a grasp on CMB predictions, which might already make the model distinguishable from standard DGP.



APPENDIX TO CHAPTER 4

Note: This appendix is to large extend a verbatim reproduction of the one in [NS15a].

4.A Full bulk solution

We will now show that under the assumption of vanishing Newton terms, the full bulk solution can be derived explicitly. To this end, it is useful to choose new coordinates¹⁹ in which the metric takes the form

$$ds^2 = e^{2(\eta-3\alpha)} (-dt^2 + dy^2) + e^{2\alpha} \delta_{ij} dx^i dx^j + e^{-6\alpha} W^2 d\phi^2, \quad (4.A.1)$$

where η, α and W are functions of (t, y) . This is the generalization of the 4D cylindrical coordinates (2.5.1), with the three x -directions taking the role of z and y substituting the radial coordinate r . However, here we will not require W to vanish at some point, since there is no symmetry axis in the manifold under investigation; instead, we assume the brane to be again located at $y = 0$, and require the metric functions to be invariant under reflections $y \mapsto -y$ according to Z_2 symmetry, cf. Fig. 4.1. The numerical factors in (4.A.1) were adapted such that the (modified) Einstein field equations, as in 4D, cf. (2.5.4), take a rather simple form:

$$\frac{W''}{W} - \frac{\ddot{W}}{W} = \mathcal{T}_t^t + \mathcal{T}_y^y, \quad (4.A.2a)$$

$$\alpha'' - \ddot{\alpha} + \frac{W'}{W} \alpha' - \frac{\dot{W}}{W} \dot{\alpha} = \frac{1}{4} \left(\mathcal{T}_t^t + \mathcal{T}_y^y - \mathcal{T}_x^x + \mathcal{T}_\phi^\phi \right), \quad (4.A.2b)$$

$$6 \left(\alpha'^2 + \dot{\alpha}^2 \right) - \frac{W'}{W} \eta' - \frac{\dot{W}}{W} \dot{\eta} + \frac{\ddot{W}}{W} = -\mathcal{T}_y^y, \quad (4.A.2c)$$

$$6 \left(\alpha'^2 - \dot{\alpha}^2 \right) + \eta'' - \ddot{\eta} = \mathcal{T}_\phi^\phi, \quad (4.A.2d)$$

$$12\alpha'\dot{\alpha} - \frac{W'}{W} \dot{\eta} - \frac{\dot{W}}{W} \eta' + \frac{\dot{W}'}{W} = \mathcal{T}_y^t. \quad (4.A.2e)$$

¹⁹For the sake of notation we will still denote them by $x^A = (t, y, x^i, \phi)$.



Here, for convenience, we defined

$$\mathcal{T}^M_N := e^{2(\eta-3\alpha)} \tilde{T}^M_N, \quad (4.A.3)$$

with \tilde{T}^M_N denoting the effective 6D energy momentum tensor, including the brane induced gravity terms,²⁰

$$\tilde{T}^M_N = \frac{1}{M_6^4} (T^m_n - M_5^3 G^{(5)m}_n) \frac{\delta(y)}{e^{\eta-3\alpha}} \delta^M_m \delta^n_N \quad (4.A.4a)$$

$$\equiv \text{diag}(-\tilde{\rho}, 0, \tilde{p}, \tilde{p}, \tilde{p}, \tilde{p}_\phi) \frac{\delta(y)}{e^{\eta-3\alpha}}, \quad (4.A.4b)$$

where the effective fluid components in the last line are the ones defined in (4.2.8).

The Newton terms (for $y \neq 0$) in these coordinates, after some simplifications using (4.A.2), become

$$\Phi^{(x)} = e^{2(3\alpha-\eta)} \frac{1}{2} \left[\alpha'' - \ddot{\alpha} + \alpha'^2 - \dot{\alpha}^2 \right], \quad (4.A.5a)$$

$$\Phi^{(\phi)} = e^{2(3\alpha-\eta)} \frac{3}{2} \left[\alpha'' - \ddot{\alpha} + 3 \left(\alpha'^2 - \dot{\alpha}^2 \right) \right], \quad (4.A.5b)$$

and so setting them equal to zero is equivalent to

$$\alpha'^2 = \dot{\alpha}^2 \quad \Leftrightarrow \quad \alpha' = \pm \dot{\alpha}. \quad (4.A.6)$$

The bulk ($y \neq 0$) Einstein equations (4.A.2) then reduce to

$$W' = \pm \dot{W}, \quad (4.A.7a)$$

$$\eta'' - \ddot{\eta} = 0, \quad (4.A.7b)$$

$$12\dot{\alpha}^2 + \frac{\ddot{W}}{W} - \frac{\dot{W}}{W} (\dot{\eta} \pm \eta') = 0, \quad (4.A.7c)$$

where the choice of signs in (4.A.7a) and (4.A.7c) has to be the same as for α in (4.A.6). So α and W are both functions of $(t \pm y)$, i.e. they are both either *left-moving 1D waves*, or both *right-moving 1D waves*. η can in general be a superposition of left- and right-moving 1D waves. In order to create the δ -sources on the right hand side of (4.A.2), the following junction conditions have to be fulfilled:

$$[\alpha'] = -\frac{e^{\eta_0-3\alpha_0}}{4} (\tilde{\rho} + \tilde{p} - \tilde{p}_\phi), \quad (4.A.8a)$$

$$\frac{[W']}{W_0} = -e^{\eta_0-3\alpha_0} \tilde{p}, \quad (4.A.8b)$$

$$[\eta'] = e^{\eta_0-3\alpha_0} \tilde{p}_\phi. \quad (4.A.8c)$$

²⁰Since the brane is located at a constant coordinate position, and its surrounding is covered by a single coordinate patch, we can again use δ -functions to effectively implement Israel's junction conditions.

Now the only way to satisfy these, in the nontrivial case of nonvanishing right hand sides, is to choose α (and thus also W) to be of opposite wave character (left-/right-moving) on the left and right side of the brane at $y = 0$. Since we do not want waves propagating towards the brane, we take them to be right-moving on the right, and left-moving on the left; so we choose the plus sign for $y < 0$, and the minus sign for $y > 0$. Requiring α and W to be continuous then yields:

$$\alpha(t, y) = \alpha_0(t - |y|), \quad (4.A.9a)$$

$$W(t, y) = W_0(t - |y|), \quad (4.A.9b)$$

$$\eta(t, y) = \begin{cases} \eta_{L<}(t + y) + \eta_{R<}(t - y) & (y < 0) \\ \eta_{L>}(t + y) + \eta_{R>}(t - y) & (y > 0). \end{cases} \quad (4.A.9c)$$

The only remaining Einstein equation (4.A.7c) (for $\dot{\alpha}_0 \neq 0$), as well as continuity of η further imply²¹

$$\eta_{L<} = \eta_{R>} + c_1, \quad \eta_{L>} = \eta_{R<} + c_1, \quad (4.A.10)$$

with some constant c_1 , allowing to eliminate two of the four functions appearing in (4.A.9c), say $\eta_{L<}$ and $\eta_{L>}$. The jumps of the first derivatives of the metric functions can now be expressed directly in terms of on-brane functions, which—together with equation (4.A.7c)—yields

$$[\alpha'] = -2\dot{\alpha}_0, \quad (4.A.11a)$$

$$[W'] = -2\dot{W}_0, \quad (4.A.11b)$$

$$[\eta'] = -2(\dot{\eta}_{R>} - \dot{\eta}_{R<}), \quad (4.A.11c)$$

$$12\dot{\alpha}_0^2 + \frac{\ddot{W}_0}{W_0} - 2\frac{\dot{W}_0}{W_0}\dot{\eta}_{R>} = 0. \quad (4.A.11d)$$

Since the three jumps can be expressed in terms of the on-brane sources using the junction conditions (4.A.8), this constitutes a system of four ODEs for the five unknown functions²² $\alpha_0(t)$, $W_0(t)$, $\eta_{R>}(t)$, $\eta_{R<}(t)$ and $\rho(t)$. But there is still a residual gauge freedom which allows us to require

$$\eta_0(t) = 3\alpha_0(t) \quad (4.A.12)$$

by an appropriate redefinition of the t and y coordinates (see Appendix 4.B), so that the five dimensional induced metric becomes

$$ds_{(5)}^2 = -dt^2 + e^{2\alpha_0} \delta_{ij} dx^i dx^j + e^{-6\alpha_0} w_0^2 d\phi^2. \quad (4.A.13)$$

²¹Incidentally, now all the metric functions have a reflection symmetry around $y = 0$ —which we didn't assume in this derivation. We thus found the curious result that this symmetry follows from setting the Newton-like field components to zero (and assuming nonzero $\tilde{\rho}, \tilde{p}$).

²²Note that η_0 can be written as $\eta_0(t) = \eta_{R<}(t) + \eta_{R>}(t) + c_1$, and we assume some equations of state to be given for the both pressure components p and p_ϕ .



This allows us to eliminate, say $\eta_{R<}$, thus leading to a closed system, which can be brought into the form:

$$2\dot{\alpha}_0 + [\alpha'] = 0, \quad (4.A.14a)$$

$$2\dot{W}_0 + [W'] = 0, \quad (4.A.14b)$$

$$[\dot{W}'] + 12W_0\dot{\alpha}_0 [\alpha'] - \dot{W}_0 (3[\alpha'] + [\eta']) = 0, \quad (4.A.14c)$$

$$4\dot{\eta}_{R>} + 3[\alpha'] + [\eta'] = 0. \quad (4.A.14d)$$

The gauge (4.A.12) is particularly useful, because it renders the induced 5D metric independent of η_0 . Therefore, the brane induced gravity terms contributing to $[\alpha']$, $[W']$ and $[\eta']$ also become independent of η_0 , and so the first three equations of (4.A.14) form a closed system for the three functions $\alpha_0(t)$, $W_0(t)$ and $\rho(t)$. After identifying the scale factors

$$a = e^{\alpha_0}, \quad c = W_0 e^{-3\alpha_0}, \quad (4.A.15)$$

from the induced metric (4.A.13), one can easily verify that they reproduce the modified Friedmann equations (4.2.20) (and the energy conservation equation) derived earlier.

The time evolution of $\eta_{R>}(t)$ decouples, and it is obtained by simply integrating the last equation (4.A.14d). The full function $\eta(t, y)$ can then be written as

$$\eta(t, y) = 3\alpha_0(t + |y|) - \eta_{R>}(t + |y|) + \eta_{R>}(t - |y|). \quad (4.A.16)$$

This completes the derivation of the complete bulk geometry, which will be known explicitly once the on-brane system (4.A.14), or equivalently (4.2.20), is solved for specific equations of state for the on-brane matter content.

Now that we know the whole bulk geometry, its interpretation becomes quite obvious: All the metric functions are purely 1D waves. In principle, these could be mere coordinate artifacts, like the time dependence of the DGP bulk solution, cf. Sec. 1.4.2; but here the wave components of the Weyl tensor are:

$$\Omega^+(t, y) = \begin{cases} 0 & (y < 0) \\ 2[\ddot{\alpha}_0(t - y) + 7\dot{\alpha}_0(t - y)^2 - 2\dot{\alpha}_0(t - y)\dot{\eta}_{\text{out}>}(t - y)] & (y > 0), \end{cases} \quad (4.A.17a)$$

$$\Omega^-(t, y) = \begin{cases} 2[\ddot{\alpha}_0(t + y) + 7\dot{\alpha}_0(t + y)^2 - 2\dot{\alpha}_0(t + y)\dot{\eta}_{\text{out}>}(t + y)] & (y < 0) \\ 0 & (y > 0). \end{cases} \quad (4.A.17b)$$

These are generally nonzero, showing that there are in fact real physical waves: a bulk observer would see test particles accelerated as described in Sec. 2.3. Moreover, they are indeed propagating away from the brane on both sides, as was intended by the choice (4.A.9a), (4.A.9b)—despite the fact that the solution (4.A.16) for η is a superposition of incoming and outgoing waves, so this part of the metric indeed *is* a pure coordinate artifact.

4.B Fixing the residual gauge

In this section we show that the gauge choice (4.A.12) is always possible. To this end, note that the form of the metric (4.A.1) is unchanged under a redefinition of the t and y coordinates of the form

$$\begin{pmatrix} t \\ y \end{pmatrix} \mapsto \begin{pmatrix} \bar{t} \\ \bar{y} \end{pmatrix} = \begin{pmatrix} f(t, y) \\ g(t, y) \end{pmatrix}, \quad (4.B.1)$$

with

$$\begin{pmatrix} \dot{f} \\ f' \end{pmatrix} = \pm \begin{pmatrix} \dot{g}' \\ \dot{g} \end{pmatrix} \quad \text{and} \quad g'^2 \neq \dot{g}^2. \quad (4.B.2)$$

After this transformation, the metric functions will take the form

$$\bar{\alpha} = \alpha, \quad \bar{W} = W, \quad e^{-2\bar{\eta}} = e^{-2\eta} (g'^2 - \dot{g}^2). \quad (4.B.3)$$

If we now define the function

$$h(t) := \int^t e^{\eta_0(t') - 3\alpha_0(t')} dt', \quad (4.B.4)$$

then a transformation of the form (4.B.1) with

$$f(t, y) = \frac{1}{2} [h(t+y) + h(t-y)] \quad \text{and} \quad g(t, r) = \frac{1}{2} [h(t+y) - h(t-y)] \quad (4.B.5)$$

will lead to $\bar{\eta}_0 = 3\bar{\alpha}_0$.



CHAPTER 5

THE UNIVERSE AS A COSMIC STRING

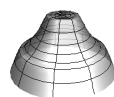
Let us now turn to another straightforward generalization of the DGP model: instead of adding a compact dimension to the brane (and bulk) as in the previous chapter, now *only the bulk* is augmented by another *infinite* dimension. This corresponds to the BIG model in two codimensions.

As already discussed in Sec. 1.3, this setup is particularly interesting with respect to the CC problem for the following reason: according to (higher dimensional) GR, a codimension-two brane equipped with a 4D CC (and no other sources) leads to a geometry in which only extra space gets curved, in the form of an angular deficit in the bulk, while the four brane dimensions remain completely flat,¹ see Sec. 5.1. It thus provides an explicit example of the degravitation mechanism. This degravitating solution is the straightforward generalization of a usual cosmic string in standard 4D GR. Employing this analogy, we will refer to the model as the “cosmic string” setup; similarly, for the 4D vacuum energy density the term “brane tension” will be used interchangeably.

Furthermore, the BIG terms furnish the model with the possibility of a 4D regime, which is crucial in order not to spoil the success of GR on the scales where it has been tested, while still allowing for the degravitating solution (because the BIG terms vanish for a flat brane). Therefore, codimension-two BIG seems like the ideal candidate for solving the CC problem.

In fact, the idea that higher codimensional BIG could solve the CC problem was already pointed out in [DG01, DGS02]. But this proposal suffered a major setback as it was found to contain a ghost (i.e. a mode whose kinetic term comes with the wrong sign, see Sec. 5.4) when linearized around a Minkowski background [DR03, HHvS11], thus rendering the theory unstable. There has, however, recently been the claim [BHN12] that these results were overhasty, and that the alleged ghost mode would in fact be no dynamical (but a constrained) quantity, thereby not threatening the stability of the theory. This appeared to reopen the window of opportunity for BIG

¹Note that this is only true for sub-critical values of the CC ($\lambda < 2\pi M_6^4$) for which the deficit angle is less than 2π , cf. Sec. 5.1. Super-critical cosmic strings will be studied in Chap. 6.



in two codimensions.

Further reasons for the rather slow progress towards a more detailed understanding of the codimension two setup, like the derivation of its modified Friedmann equations,² are more of a technical nature: First, for more realistic, non-static geometries, the bulk curvature generically diverges at the position of the brane. This requires regularizing the infinitely thin brane idealization before quantitative predictions can be made. Second, the possibility of gravitational bulk waves even for 3D homogeneous and isotropic sources makes it impossible to derive a closed set of on-brane Friedmann equations without excluding incoming waves, just like in the cosmic ring model of Chap. 4.

Several things will be done in this chapter: First, in Sec. 5.3, we tackle the problem of obtaining the fully consistent, dynamical cosmological evolution of the codimension-two brane with induced gravity terms for an arbitrary (but sub-critical) homogeneous and isotropic fluid—not just a pure tension which allows for the well known static solution. To deal with the aforementioned technical difficulties, we first introduce a very convenient regularization in Sec. 5.2, in which the infinitely thin (codimension-two) brane is blown up to a small (codimension-one) ring of finite circumference [KK07, BHdRT09]. Then, in Sec. 5.3 we solve the complete (nonlinear) system of coupled bulk and brane field equations in its full glory, which can only be done numerically. Incoming bulk waves are simply excluded by choosing trivial initial data in the bulk, and extending the domain of integration to sufficiently large radii.³ The result will be that the parameter space of the theory is divided into two regions:

- (i) A degravitating regime, in which the Hubble parameter dynamically approaches zero despite a nonvanishing on-brane energy density. This shows that the model is indeed capable of providing an automatic adjustment mechanism that dynamically degravitates a CC at the full nonlinear level.
- (ii) A super-accelerating regime, where the Hubble parameter grows unbounded. Since this growth is not caused by any matter source, it points towards some pathological degree of freedom in the (modified) gravitational sector. Furthermore, the effective energy density $\hat{\rho}$ which “sources”⁴ bulk gravity, becomes negative for these solutions. In analogy to the DGP case (cf. Sec. 1.4.2), this indicates the presence of a ghost mode. In summary, this class of solutions seems to be plagued by some instability.

Let us emphasize that, although these behaviors are inferred numerically, it turns out that an exact expression determining the boundary between regions (i) and (ii) can be

²A modified Friedmann equation on a codimension-two brane (without BIG) was derived in [NS05] by making several simplifying assumptions. However, we think that not all of them are justified; moreover, we found that after including the BIG terms, this equation led to complex solutions, questioning its validity.

³The outgoing wave boundary condition derived in Chap. 3 unfortunately turns out not to be very helpful in this particular setup, as will be discussed below.

⁴As already discussed below Eq. (1.4.8), the BIG terms are really a kinetic modification, and not a mere source-modification, which is why we use the quotation marks here.

derived analytically.

The (numerical) detection of an instability, which in particular exists for a vanishing energy density on the brane, i.e. around Minkowski, casts some doubt on the validity of the results of Ref. [BHN12] claiming that the theory would be stable at linear order on a flat background. Clarifying this issue presents the second major objective of this chapter: In Sec. 5.4 we investigate the ghost issue very carefully, extending the analysis to nonzero values of the brane tension. The calculation is performed by linearizing around the nontrivial deficit angle solution, which allows for an analytic treatment and thus provides a completely independent, nontrivial cross-check of the numerical (albeit nonlinear) stability analysis. We will find that the two complementary approaches give results which are in perfect agreement: The linear calculation reveals a tachyonic ghost mode in a region of parameter space exactly matching the one derived in the previous (nonlinear) analysis in the limit of vanishing Hubble parameter on the brane.⁵ Therefore, the pathological, super-accelerating behavior of the nonlinear cosmological solutions is indeed a manifestation of this ghost instability, yielding an overall consistent picture.

In the case of a vanishing brane tension, we find that the ghost is present for all phenomenologically interesting values of the induced Planck scale. This agrees with the older results in the literature [DR03, HHvS11], but is in clear contradiction to the claims of Ref. [BHN12]. We were able to resolve this tension by explicitly tracking down the (very subtle) errors made in [BHN12]. The interested reader is referred to the appendix of our publication [ENS15].

However, the motivation of [BHN12] for questioning the ghost result in the first place was based on a very physical EFT argument: If the BIG model can be thought of as arising as the low energy EFT of a healthy, more fundamental theory, how can it contain a ghost? The third central aim of this chapter is to resolve this EFT paradox. To describe the problem in more detail, imagine we start with a purely six-dimensional theory which allows for the spontaneous formation of a stable codimension-two, string-like object, with some localized degrees of freedom. In this full theory with 6D GR, there should be no instability. Then, we can ask what the corresponding EFT looks like if we restrict ourselves to energies well below the scale at which the transverse width of the defect, or the microscopic degrees of freedom that gave rise to it, can be resolved. Following the usual EFT reasoning, we write down all operators compatible with the required symmetries (i.e. bulk and brane diffeomorphism invariance) and arrive at the following action (cf. [DGS03]),

$$\mathcal{S} = \underbrace{\int d^6 X \sqrt{-g^{(6)}} \left(\frac{M_6^4}{2} \mathcal{R}^{(6)} \right)}_{\mathcal{S}_B} + \underbrace{\int d^4 x \sqrt{-g} \left(\frac{M_4^2}{2} \mathcal{R} - \lambda + \mathcal{L}_m \right)}_{\mathcal{S}_b}. \quad (5.0.1)$$

The first term \mathcal{S}_B is the bulk Einstein-Hilbert action,⁶ i.e. the Ricci scalar of the 6D

⁵Since the background geometry in the linear analysis is static, the Hubble dependence of the stability bound corresponds to higher order corrections, which are not captured at the linear level.

⁶Note that we fine-tuned the bulk CC to zero, but it turns out that relaxing this simplifying assump-



metric $\mathbf{g}^{(6)}$, with corresponding fundamental Planck scale M_6 . The second, brane part \mathcal{S}_b consists of: the BIG action, i.e. the 4D Ricci scalar constructed from the 4D induced metric \mathbf{g} , controlled by the induced Planck mass M_4 ; the brane tension λ (or 4D vacuum energy, equivalently), related to the brane CC Λ via $\lambda \equiv M_4^2 \Lambda$; and finally \mathcal{L}_m , encoding all brane-localized degrees of freedom which are dynamically resolved (i.e. have masses below the cutoff) and are minimally coupled to \mathbf{g} . Note that \mathcal{L}_m does not contain any vacuum energy contribution, since it is by definition completely contained in λ . In order to be of phenomenological relevance, M_4 should be identified with the usual 4D Planck mass M_{Pl} , and \mathcal{L}_m should ultimately contain all Standard Model fields.

Now, the crucial point is that both M_4 and λ should be included in any natural EFT, since they are generically generated via quantum loops of the brane-localized degrees of freedom. But all the previous ghost calculations in the literature were done around the Minkowski background, for which the tension λ is tuned to zero, while M_4 was taken to be large (in order to have an appropriate 4D regime). Since our analysis also probes the parameter space at $\lambda > 0$, we are able to resolve the aforementioned EFT paradox in the following way: As soon as λ is large enough, the theory enters the stable, ghost-free regime (or the super-critical regime, for which a stability analysis is still lacking). In other words, *the ghost pathology is only present if λ is tuned unnaturally small while the induced gravity scale M_4 is chosen large*. In particular, it is sufficient to choose M_4 and Λ in a natural way, i.e. of the same order, to be on the safe side. This will be discussed in more detail in Sec. 5.5.1.

Having resolved all these puzzles, the final pressing question remains: Is the model phenomenologically viable, and can it thereby solve the CC problem? After all, the fact that the theory is unstable around a Minkowski background is not per se problematic, because the necessary background curvature for $\lambda > 0$ is still purely extrinsic, i.e. the 4D background *is* in fact still Minkowski. This question will be answered in Sec. 5.5.2.

5.1 Static deficit angle solution

After choosing bulk coordinates y in which the brane is located at $y^m = (0, 0)$, the brane part of the action (5.0.1) can be augmented to a 6D integral over the coordinates $X^M = (x^\mu, y^m)$ by inserting⁷ $1 = \int d^2y \delta^{(2)}(y)$. The gravitational equations of motion are then obtained by varying the full action with respect to the metric $g_{MN}^{(6)}$, and read⁸

$$M_6^4 G_{MN}^{(6)} = \frac{\delta^{(2)}(y)}{\sqrt{g^{(2)}}} \delta_M^\mu \delta_N^\nu (T_{\mu\nu} - M_4^2 G_{\mu\nu}), \quad (5.1.1)$$

tion is not necessary for the point we want to make here. Furthermore, a vanishing value could be obtained naturally by assuming unbroken bulk SUSY.

⁷Note that in our conventions the 2D delta function transforms like a density, so there is no metric determinant factor in its normalization condition.

⁸Here we assumed the metric $\mathbf{g}^{(6)}$ to be block-diagonal, otherwise the determinant factor on the right-hand side would read $\sqrt{-g^{(4)}}/\sqrt{-g^{(6)}}$.

the 4D energy momentum tensor \mathbf{T} contains both the vacuum energy λ and the contributions from \mathcal{L}_m .

Before turning to the ambitious task of finding the dynamical cosmological solutions to these equations, let us first review the static solution for the case of a pure tension brane, which is the main motivation for studying the codimension-two model in the first place. The corresponding 4D energy momentum tensor has the form

$$T^\mu{}_\nu = -\lambda\delta^\mu{}_\nu. \quad (5.1.2)$$

This source is maximally symmetric in the brane directions, and so the induced metric is either Minkowski or (anti-) de Sitter spacetime. We make the (educated) guess and assume it to be Minkowski. (This could, of course, turn out to be too strong an assumption, but in that case the equations of motion would tell us so.) Furthermore, we take the brane to be embedded in the bulk in a straight way (like a straight, infinitely long string), allowing to require $O(2)$ symmetry in the y -directions. It is therefore convenient to introduce polar coordinates (r, ϕ) in extra space, and so the corresponding metric ansatz can be written (in Gaussian normal coordinates) as

$$ds^2 = f(r)^2 \eta_{\mu\nu} dx^\mu dx^\nu + dr^2 + c(r)^2 d\phi^2. \quad (5.1.3)$$

We assume the axis (i.e. the brane) to be located at $r = 0$, so $c(0)$ should vanish, and the coordinates r and ϕ have the standard ranges $[0, \infty)$ and $[0, 2\pi)$, respectively. A straightforward calculation of the 6D Einstein tensor's $(\phi\phi)$ component gives

$$G^{(6)\phi}{}_\phi = 4\frac{f''}{f} + 6\frac{f'^2}{f^2}, \quad (5.1.4)$$

which, by means of the corresponding component of the field equations (5.1.1), implies⁹ $f = \text{const}$, and we can set $f \equiv 1$ without loss of generality. Incidentally, this also already solves the (rr) -component of (5.1.1), and so only the $(\mu\nu)$ -components remain, containing just one independent equation. Since the induced metric is flat, the 4D induced Einstein tensor $G_{\mu\nu}$ vanishes, and this remaining equation explicitly reads

$$\frac{c''}{c} = -\frac{\delta(r)}{2\pi c} \frac{\lambda}{M_6^4}, \quad \text{implying} \quad c(r) = \left(1 - \frac{\lambda}{\lambda_{\text{crit}}}\right) r, \quad (5.1.5)$$

where we introduced the *critical tension*

$$\lambda_{\text{crit}} := 2\pi M_6^4. \quad (5.1.6)$$

Hence, the full solution is

$$ds^2 = \eta_{\mu\nu} dx^\mu dx^\nu + dr^2 + \left(1 - \frac{\delta}{2\pi}\right)^2 r^2 d\phi^2, \quad (5.1.7)$$

⁹There is also the nontrivial solution $f \propto (r + r_*)^{2/5}$, cf. Sec. 5.2 below, but this would not allow for an axis.

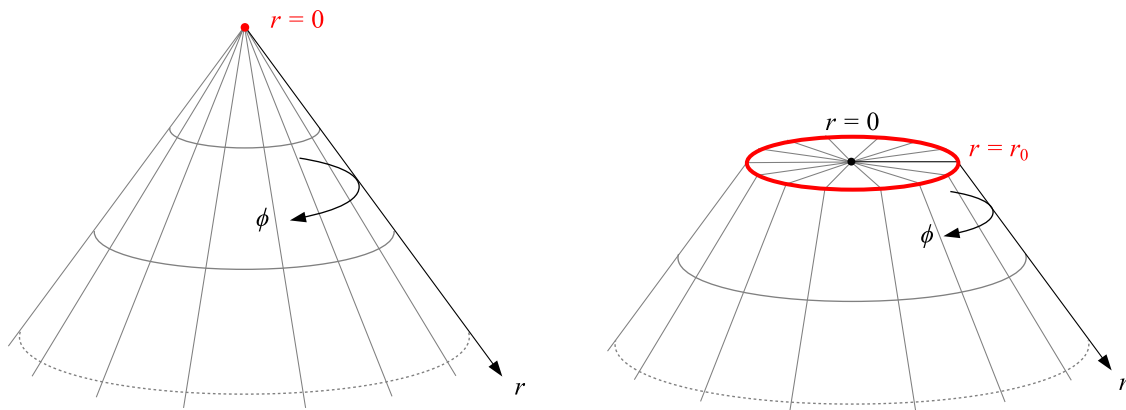


and is readily recognized as locally flat spacetime, with a wedge of angle

$$\delta := \frac{\lambda}{M_6^4} \quad (5.1.8)$$

removed from extra space. This solution is the trivial generalization of the well-known cosmic string solution in standard 4D GR [Vil81, His85] to a “string” with a three-dimensional axis, corresponding to the spatial brane dimensions [Sun99, CLP00]. Thus, the assumption of 4D flatness was justified, and the only effect of the 4D vacuum energy λ is to curve the extra dimensions into a conical shape of deficit angle δ , with the brane residing at the tip of the cone, cf. Fig. 5.1a. As promised, the degravitation mechanism is fully at work.

Of course, we do not know a priori whether this solution is stable (i.e. an attractor solution) if the 3D Hubble parameter is allowed to have a nonvanishing value. In other words, we can at this stage not tell if this setup provides an adjustment mechanism which dynamically cancels a CC. In Sec. 5.3 we will find that it indeed does, at least in some region of parameter space.



(a) Without regularization, the brane is a genuine codimension-two object and sits at the tip of the cone, corresponding to a conical singularity.

(b) In our regularization, the brane is blown up to a ring and thus becomes a codimension-one object. The conical singularity is replaced by a flat cap.

Figure 5.1: Visualization of the static deficit angle solution, without and with regularization. Only the two extra dimensions are depicted, embedded into a fictitious three-dimensional space. The brane is drawn in red, and is located at $r = 0$ and $r = r_0$, respectively. Locally, spacetime is Riemann flat everywhere, apart from the extrinsic curvature localized at the brane position.

5.2 Regularization

The static pure tension solution is very special in that the bulk geometry is locally flat arbitrarily close to the brane, and all curvature is localized on an ultra-local, purely

conical singularity. Generically, the situation is very different: For more general matter sources, or for dynamical perturbations of the pure tension solution, the bulk spacetime away from the brane gets curved as well. As a consequence, the gravitational field typically diverges (logarithmically) as $r \rightarrow 0$, just like the electric field of a charged string. But $r = 0$ is the brane position, and this is exactly the place where we want to evaluate the metric in order to infer the on-brane geometry. Therefore, it is necessary for our purposes to introduce some kind of regularization.

In electrostatics, it is clear that the divergence is an artifact of the idealization in which the line-charge is treated as infinitely thin. The same holds here, and so a natural way of regularizing is to give the brane a finite thickness. In a more fundamental theory, which dynamically resolves the degrees of freedom that give rise to the topologically defect, this would be implemented automatically, like for instance in the case of a Nielsen-Olesen vortex [NO73]. Instead of invoking such an elaborate mechanism, we will instead make use of the powerful EFT paradigm, saying that: as long as we are asking low energy questions, the microscopic details of the string are irrelevant. That is, at energies well below the inverse brane width—which is in particular relevant when studying late time cosmology—physical predictions should not depend on the concrete details of the regularization, or of an actual UV model. Thus, we can make our lives easier by choosing a regularization which is technically simple. To be concrete, we will promote the codimension-two point in extra space to a ring of finite (proper) circumference $2\pi R$. On the level of the action, this amounts to replacing the brane part by¹⁰

$$\mathcal{S}_b \longrightarrow \int d^5x \sqrt{-g^{(5)}} \left(\frac{M_5^3}{2} \mathcal{R}^{(5)} - \lambda^{(5)} + \mathcal{L}_m^{(5)} \right). \quad (5.2.1)$$

Furthermore, we assume all brane matter to be distributed homogeneously across the compact ϕ direction, so that the regularization respects the $O(2)$ symmetry. Indeed, any ϕ dependent configurations would correspond to higher Kaluza-Klein modes, which can only be excited at energies of order $1/R$ and are thus beyond the realm of our low energy EFT. This implies that the most general 5D induced metric can be written as

$$ds_{(5)}^2 \equiv g_{\alpha\beta}^{(5)} dx^\alpha dx^\beta = g_{\mu\nu} dx^\mu dx^\nu + R^2 d\phi^2, \quad (5.2.2)$$

with all metric components being independent of ϕ . In general, however, R can be a function of the 4D coordinates x^μ (just like the $g_{\mu\nu}$). From a 4D low energy EFT point of view, this corresponds to an additional field, usually called *radion*,¹¹ which physically measures the regularized brane circumference $2\pi R$. The properties of this degree of freedom would again ultimately be dictated by the concrete UV model; in

¹⁰Note that the action is now formally identical to the action (4.1.1) of the cosmic ring model. But, as already remarked there, we will here assume to have a (regular) axis in the interior of the ring, and so the two models are topologically different, cf. Fig. 4.1.

¹¹More precisely, “radion” refers to the fluctuations of R around some background value, as in Sec. 5.4.2 (where the radion is denoted by φ).



our EFT regularization, we are instead free to impose them by hand. In most¹² of our studies, we will demand the brane width to be *stabilized*, i.e. R to be constant. The (physically justified) assumption behind this choice is that there be some UV model which would lead to a defect of stable size, the fluctuations of which are controlled by some UV model parameter, corresponding to the radion mass in the EFT picture. Setting $R = \text{const}$ is thus equivalent to working in the limit where this mass is above the cutoff. Technically, this is achieved by appropriately dialing the $(\phi\phi)$ -component of the 5D energy momentum tensor, $p_\phi^{(5)} \equiv T^{(5)\phi}_\phi$, as was already done in Chap. 4. To probe whether this component is physically reasonable, we will again check a posteriori if it satisfies the NEC.

The ϕ -symmetric form of the metric (5.2.2) allows us, by comparing the brane actions (5.2.1) and (5.0.1), to identify

$$M_5^3 = \frac{M_4^2}{2\pi R} \quad \text{and} \quad \lambda^{(5)} = \frac{\lambda}{2\pi R}. \quad (5.2.3)$$

Hence, the stabilization requirement also implies that the 4D Planck mass and tension are constant.¹³

As a first simple example, let us verify that the proposed regularization is able to correctly reproduce the static deficit angle solution. To this end, we consider the source

$$T^{(5)\alpha}_\beta = -\lambda^{(5)}\delta_\mu^\alpha\delta_\beta^\mu + p_\phi^{(5)}\delta_\phi^\alpha\delta_\beta^\phi. \quad (5.2.4)$$

Without stabilization, $p_\phi^{(5)}$ would also equal $-\lambda^{(5)}$ for a pure 5D tension brane. But we will instead insist on radial stability and read off the required $p_\phi^{(5)}$ from the field equations. Since we are looking for a static solution, we can again make the ansatz (5.1.3), and demand the brane to be located at the constant coordinate position $r = r_0$. Hence, the proper radius is $R = r_0$, and the field equations can be written with delta functions as

$$M_6^4 G_{MN}^{(6)} = \delta(r - r_0) \delta_M^\alpha \delta_N^\beta \left(T_{\alpha\beta}^{(5)} - M_5^3 G_{\alpha\beta}^{(5)} \right). \quad (5.2.5)$$

The stabilization $R \equiv \text{const}$ (and 4D flatness of the ansatz) implies that the induced Einstein tensor $\mathbf{G}^{(5)}$ vanishes, and the Einstein equations explicitly read

$$\frac{c''}{c} + 3 \left(\frac{f''}{f} + \frac{f'^2}{f^2} + \frac{f'c'}{fc} \right) = -\delta(r - r_0) \lambda^{(5)}, \quad (5.2.6a)$$

$$6 \frac{f'^2}{f^2} + 4 \frac{f'c'}{fc} = 0, \quad (5.2.6b)$$

$$4 \frac{f''}{f} + 6 \frac{f'^2}{f^2} = \delta(r - r_0) p_\phi^{(5)}. \quad (5.2.6c)$$

¹²The non-stabilized case will only be investigated to prove that our main conclusions are largely insensitive to this assumption.

¹³Furthermore, it makes no difference whether we choose to work in the Einstein- or Jordan-frame, a technical subtlety (without physical consequences, though) which arises for a nonzero radion.

The general solution of the last equation for $r \neq r_0$ is either $f \propto (r + r_*)^{2/5}$ with some constant r_* , or $f \equiv \text{const}$. In the former case (5.2.6b) implies $c \propto (r + r_*)^{-3/5}$ [which also solves (5.2.6a)], and in the latter case (5.2.6a) yields $c \propto r$ [while (5.2.6b) is already fulfilled].

In the interior ($r < r_0$) we must take $f_{<}(r) = \text{const}$ (which we can again set = 1) and $c_{<}(r) = r$ in order to have a regular axis. But in the exterior, we can still choose between the two branches.

(i) $f \neq \text{const}$:¹⁴

In this case continuity of the metric across the brane implies that the exterior ($r > r_0$) solution is

$$f_{>}(r) = \left(\frac{r + r_*}{r_0 + r_*} \right)^{2/5}, \quad c_{>}(r) = r_0 \left(\frac{r_0 + r_*}{r + r_*} \right)^{3/5}. \quad (5.2.7)$$

The constant r_* and the stabilizing pressure p_ϕ are then obtained by performing the delta-matching of Eqs. (5.2.6a) and (5.2.6c), just like in Sec. 4.2, which yields

$$\frac{r_*}{r_0} = \frac{3}{5(1 - \lambda/\lambda_{\text{crit}})} - 1, \quad \frac{p_\phi^{(5)}}{M_6^4} = \frac{8}{3r_0} \left(1 - \frac{\lambda}{\lambda_{\text{crit}}} \right). \quad (5.2.8)$$

Evidently, this solution has the peculiar property that the pressure which is required to stabilize the pure tension brane is nonzero even for $\lambda = 0$, i.e. if there is no tension at all. For this reason, we discard this branch as unphysical, and move on to the other alternative:

(ii) $f = \text{const}$:

In this case $f \equiv 1$ everywhere, and the full solution for the metric is

$$ds^2 = \eta_{\mu\nu} dx^\mu dx^\nu + dr^2 + c(r)^2 d\phi^2, \quad (5.2.9a)$$

$$c(r) = \begin{cases} r & (r < r_0) \\ r_0 + \left(1 - \frac{\delta}{2\pi}\right) (r - r_0) & (r > r_0), \end{cases} \quad (5.2.9b)$$

with δ defined as before (5.1.8), and the pressure is simply

$$p_\phi^{(5)} = 0. \quad (5.2.10)$$

In other words, a pure 5D tension brane has to be supplemented by an additional $(\phi\phi)$ -component of the energy-momentum tensor which cancels $\lambda^{(5)}$.¹⁵ This pressure component trivially satisfies the NEC, and in particular vanishes for $\lambda = 0$.

¹⁴The first case was excluded in the unregularized calculation above, because it does not allow $c(0) = 0$, as required to have an axis there; furthermore, we now see that it requires a nonvanishing p_ϕ component. In the cosmic string literature, the corresponding solution is sometimes called the ‘‘Melvin’’ or ‘‘Kasner’’ branch [LG89, CLV99].

¹⁵In Ref. [KK07], for instance, this was achieved explicitly by wrapping an additional scalar field around the compact dimension.



Therefore, this represents the physically reasonable solution we were looking for. The spacetime is Minkowski in the interior, and locally flat space with a deficit angle δ in the exterior region. Thus, it is indeed the regularized version of the cosmic string solution discussed above, which is recovered in the limit $R (= r_0) \rightarrow 0$. The conical singularity is replaced by a flat disk, leading to a capped cone embedding geometry, see Fig. 5.1b.

Note that, if the tension equals the critical value $\lambda_{\text{crit}} \equiv 2\pi M_6^4$, the deficit angle becomes 2π and the embedding geometry degenerates to a cylinder. For even larger values, the exterior space compactifies, closing up in a conical singularity. This *super-critical* regime will be the subject of Chap. 6. In the present chapter, we restrict ourselves to sub-critical values of the tension, $\lambda < \lambda_{\text{crit}}$.

After this warm up exercise, it is time to deal with the time dependent, cosmological setup.

5.3 Cosmology

Note: The results presented in this section (and in the corresponding appendices below) arose in collaboration with Stefan Hofmann, Justin Khoury and Florian Niedermann and were published in [NSHK15].

We now consider a 3D homogeneously and isotropically sourced brane in a vacuum bulk. Ultimately, we are only interested in the evolution of the on-brane geometry, i.e. of the 3D scale factor (or Hubble parameter). To derive its modified Friedmann equation, we could again try to proceed like in the DGP model in Sec. 1.4.2, and extract all local information from the bulk field equations. However, this procedure is bound to fail, because the field equations in the present regularized setup are locally identical¹⁶ to those of the cosmic ring model of Chap. 4, where we showed that it is impossible to arrive at a closed system of on-brane equations without additional assumptions about the bulk geometry. A physically necessary requirement for an empty bulk is the absence of incoming gravitational waves. In the ring model it was possible to implement this condition using the Weyl decomposition discussed in Chap. 2, because there one was dealing with plane waves. But now, due to the different topology of the model, we will encounter radial (or “cylindrical”) gravitational bulk waves, which is exactly the case in which the Weyl decomposition was proven to fail in Chap. 2.

Furthermore, Chap. 3 showed that an outgoing wave condition for cylindrical waves is necessarily nonlocal (in time), already in the case of a scalar field on Minkowski space. Thus, one cannot expect to be able to find a local criterion in the case of gravitational waves. In fact, by introducing (generalized) Einstein-Rosen coordinates, as we will do

¹⁶The model is still topologically distinct, cf. Fig. 4.1, and will thus also have a physically different behavior. However, this can only be seen if the bulk geometry is taken into account, as will be done below.

below, the gravitational case can exactly be mapped onto the simple case of a scalar field on flat spacetime, because in those coordinates the only dynamical degree of freedom satisfies exactly the same wave equation. We can therefore already conclude that *the modified Friedmann equations of codimension-two BIG are necessarily nonlocal*.

The only way to circumvent this nonlocality would be to also exclude outgoing waves by embedding the brane in Minkowski spacetime¹⁷ like in the DGP model. Below, we shall however see that this is too strong an assumption, not allowing for any nontrivial cosmology on a codimension-two brane. In other words, bulk waves are not only possible (due to the absence of Taub’s/Birkhoff’s theorem in a cylindrically symmetric setup), but in fact *necessary* for a cosmologically evolving codimension-two brane.

5.3.1 Coordinates and field equations

Bulk geometry

Since we have to take into account the full bulk geometry, it is reasonable to choose coordinates in which the bulk field equations are as simple as possible—instead of using the Gaussian normal coordinates (like in the DGP case or the cosmic ring model) which are engineered to bring the junction conditions into their simplest form.

The FRW symmetries in the spatial brane directions (3D homogeneity and isotropy) and the radial $O(2)$ symmetry in the perpendicular bulk directions imply that the setup is the 6D version of what Throne [Tho65] calls “whole cylinder symmetry”. Hence, we can adapt the corresponding most general metric ansatz (2.5.1) to the case of a three-dimensional axis,¹⁸

$$ds^2 = e^{2(\eta^* - 3\alpha^*)} (-dt^{*2} + dr^{*2}) + e^{2\alpha^*} \delta_{ij} dx^i dx^j + e^{-6\alpha^*} W^2 d\phi^2. \quad (5.3.1)$$

Here, η^* , α^* and W are all functions of the temporal and radial coordinates (t^*, r^*) , covering the whole manifold. The factors of 3—as compared to (2.5.1)—in the first and last term, counting the dimensionality of the axis, were included to make the field equations as simple as in the 4D case.

These coordinates were also used to derive the full bulk solution in the cosmic ring scenario, see Appendix 4.A. This was possible because the two models are locally indistinguishable. However, they are topologically different, cf. Fig. 4.1. The correct radial topology can now be implemented by requiring to have a (regular) axis in the interior of the ring. In particular, this implies that W vanishes at the axis and that its gradient $\nabla W \equiv (\partial_{t^*} W, \partial_{r^*} W)$ is spacelike and outward pointing (assuming that the radial coordinate r^* is defined such that it gets larger as one moves away from the

¹⁷More generally, one could also allow a nonzero but static bulk curvature, parametrized by some mass parameter, like in the DGP setup. But this would, in particular, allow for a Minkowski bulk by setting this parameter to zero.

¹⁸Note that we are restricting ourselves to 3D spatial flat geometries for simplicity; the case with spatial curvature could trivially be achieved by using the appropriate spatial part of the line element (1.1.4) instead.



axis), at least in a neighborhood of the axis. However, as will be discussed in Chap. 6, Appendix 6.A, this character of ∇W cannot change in a vacuum region, so it is true in the whole interior. Furthermore, since we restrict ourselves to sub-critical brane energy densities in this chapter, the character does not change across the brane (cf. Sec. 6.3.2), and ∇W is also spatial and outward pointing in the exterior.

This requirement already excludes the cosmic ring solution derived in Sec. 4.A [because there W was a function of $(t - |y|)$, i.e. its gradient was lightlike]. Moreover, it allows a further simplification of the metric (5.3.1). To see how this works [Tho65], note that (5.3.1) is invariant under the residual coordinate transformations

$$(t^*, r^*) \mapsto (t, r), \quad (5.3.2a)$$

$$e^{2\eta^*} \mapsto e^{2\eta} = e^{2\eta^*} [(\partial_{r^*} r)^2 - (\partial_{t^*} r)^2]^{-1}, \quad (5.3.2b)$$

with t and r being some functions of (t^*, r^*) such that $(\partial_{t^*} r)^2 - (\partial_{r^*} r)^2 \neq 0$ and

$$\begin{pmatrix} \partial_{t^*} r \\ \partial_{r^*} r \end{pmatrix} = \pm \begin{pmatrix} \partial_{r^*} t \\ \partial_{t^*} t \end{pmatrix}. \quad (5.3.3)$$

In particular, this implies the following integrability condition for the function r ,

$$-\partial_{t^*}^2 r + \partial_{r^*}^2 r = 0. \quad (5.3.4)$$

Now, in *vacuum*, the sum of the (t^*) - and (r^*) -Einstein equations yield

$$-\partial_{t^*}^2 W + \partial_{r^*}^2 W = 0, \quad (5.3.5)$$

and so we can use W as the new radial coordinate,

$$r = W(t^*, r^*), \quad (5.3.6)$$

[and a new t coordinate implicitly defined by (5.3.3)] without changing the remaining form of the metric. Note that if ∇W had been timelike, the sign of $e^{2\eta^*}$ would have changed according to (5.3.2b), and so r would have been a temporal coordinate; for a lightlike gradient the coordinate transformation would have been singular. Furthermore, if ∇W had been spatial but *inward*-pointing (as will be the case in the exterior region of a super-critical brane, see Sec. 6.3.2), then the new radial coordinate r would have *decreased* as one moves away from the axis. But in the present case, ∇W is spatial and outward-pointing everywhere, and so r behaves like a usual radial coordinate. The line element then simplifies to

$$ds^2 = e^{2(\eta-3\alpha)} (-dt^2 + dr^2) + e^{2\alpha} \delta_{ij} dx^i dx^j + e^{-6\alpha} r^2 d\phi^2, \quad (5.3.7)$$

and the vacuum field equations read

$$\ddot{\alpha} = \alpha'' + \frac{1}{r} \alpha', \quad (5.3.8a)$$

$$\eta' = 6r \left(\dot{\alpha}^2 + \alpha'^2 \right), \quad \dot{\eta} = 12r \dot{\alpha} \alpha', \quad (5.3.8b)$$

where again dot and prime denote ∂_t and ∂_r , respectively. We have thus obtained the 6D generalization of the 4D Einstein-Rosen (ER) wave geometry discussed in Sec. 2.5.2. The remarkable fact that the full dynamics in the vacuum region is again completely captured by the single function α , obeying the linear, standard cylindrical wave equation (5.3.8a), makes this choice of coordinates particularly convenient for a numerical implementation. (Below we will see, however, that the junction conditions also involve η , making the coupled bulk-brane system nonlinear again.) In addition, it confirms the aforementioned fact that the outgoing wave condition for cylindrical gravitational bulk waves is exactly the one discussed in Chap. 3.

The only subtlety with this choice of coordinates is that Eq. (5.3.5) is only true in vacuum; otherwise, the right hand side is proportional to $T^{t^*}_{t^*} + T^{r^*}_{r^*}$, which is non-vanishing at the brane position. As a consequence, the integrability condition (5.3.4) is violated for the choice (5.3.6) at the brane, and so the ER coordinates (5.3.7) can only be used on *separate patches* in the interior and exterior, but are not continuously connected across the brane. This is the price we have to pay for having the simple vacuum field equations (5.3.8). In order to distinguish the interior from the exterior coordinate patches, we will put tildes on all interior quantities in what follows.

At this point, we can also verify the claim made above, that it is not possible to embed the brane in a Minkowski bulk (as could be done in the DGP model), if it is required to have a nontrivial cosmological evolution: Setting the $(ijij)$ - and $(i\phi i\phi)$ -components of the Riemann tensor to zero turns out to be equivalent to

$$\alpha'^2 = \dot{\alpha}^2 \quad \text{and} \quad \alpha' = 0, \quad (5.3.9)$$

and therefore $\alpha \equiv \text{const}$ in a Minkowski bulk. But the on-brane scale factor is given by $\exp\{\alpha[t, r_0(t)]\}$, see Eq. (5.3.12) below, and would thus be constant as well. Hence, the codimension-two bulk is necessarily curved for a cosmologically evolving brane.¹⁹ Furthermore, this curvature must be time-dependent—otherwise it would be characterized by some constant parameters, which could in particular be set to zero, leading back to a Riemann-flat bulk. In other words, *a cosmological codimension-two brane necessarily emits gravitational bulk waves.*

Brane geometry and sources

Since we are not using Gaussian normal coordinates, the brane does not sit at a constant radial bulk coordinate anymore. Instead, it follows a trajectory $r_0(t)$ in the exterior, and $\tilde{r}_0(\tilde{t})$ in the interior coordinates. Its form will be determined by the junction conditions below, and thus in particular depends on the choice of $p_\phi^{(5)}$, which in turn

¹⁹Note that in this derivation we assumed that we can choose the ER coordinates (5.3.7), which is only allowed if the gradient of W is spacelike, as discussed above. This is no additional restriction, because otherwise the geometry would not really be of codimension two. But if this assumption is dropped, it is indeed possible to have a Minkowski bulk, as was explicitly found in the cosmic ring setup in Chap. 4.



is defined by the stabilization requirement $R = \text{const.}$ ²⁰ Therefore, the 5D induced metric on the brane is

$$ds_{(5)}^2 = -\frac{e^{-6\alpha_0}}{\gamma^2} dt^2 + e^{2\alpha_0} \delta_{ij} dx^i dx^j + e^{-6\alpha_0} r_0^2 d\phi^2 \quad (5.3.10a)$$

$$= -\frac{e^{-6\tilde{\alpha}_0}}{\tilde{\gamma}^2} d\tilde{t}^2 + e^{2\tilde{\alpha}_0} \delta_{ij} dx^i dx^j + e^{-6\tilde{\alpha}_0} \tilde{r}_0^2 d\phi^2, \quad (5.3.10b)$$

where the subscript “0” denotes evaluation at the brane, e.g. $\alpha_0(t) := \alpha(t, r_0(t))$, and the functions $\gamma, \tilde{\gamma}$ are defined as

$$\gamma := \frac{e^{-\eta_0}}{\sqrt{1 - \dot{r}_0^2}}, \quad \tilde{\gamma} := \frac{e^{-\tilde{\eta}_0}}{\sqrt{1 - \dot{\tilde{r}}_0^2}}. \quad (5.3.11)$$

Note that a dot now means ∂_t when acting on an exterior function, but $\partial_{\tilde{t}}$ on interior ones. From (5.3.10) we can read off the brane’s scale factor and proper circumference $2\pi R$,

$$a \equiv e^{\alpha_0} = e^{\tilde{\alpha}_0}, \quad R \equiv r_0 e^{-3\alpha_0} = \tilde{r}_0 e^{-3\tilde{\alpha}_0}. \quad (5.3.12)$$

After introducing the proper time τ via

$$d\tau := \frac{e^{-3\alpha_0}}{\gamma} dt = \frac{e^{-3\tilde{\alpha}_0}}{\tilde{\gamma}} d\tilde{t}, \quad (5.3.13)$$

the induced metric (5.3.10) becomes

$$ds_{(5)}^2 \equiv g_{\alpha\beta}^{(5)} dx^\alpha dx^\beta = -d\tau^2 + a^2 \delta_{ij} dx^i dx^j + R^2 d\phi^2. \quad (5.3.14)$$

Hence, the 3D Hubble parameter is recognized as²¹

$$H \equiv \frac{\dot{\circ} a}{a}, \quad (5.3.15)$$

where the circle \circ was introduced as shorthand for $d/d\tau$.

The symmetries of our system allow for a fluid ansatz of the localized 5D surface energy-momentum tensor

$$T^{(5)\alpha}_{\beta} = \text{diag}(-\rho^{(5)}, p^{(5)}, p^{(5)}, p^{(5)}, p_{\phi}^{(5)}) \quad (5.3.16)$$

$$\equiv \frac{1}{2\pi R} \text{diag}(-\rho, p, p, p, p_{\phi}), \quad (5.3.17)$$

²⁰The general, non-stabilized case is discussed in Appendix 5.A.1.

²¹If R is not required to be constant, there is also a similar “Hubble” parameter for R , measuring the expansion rate of the circumference, see Appendix 5.A.1.

which is covariantly conserved ($\nabla_\alpha^{(5)} T^{(5)\alpha}_\beta = 0$) with respect to the induced metric $g_{\alpha\beta}^{(5)}$. The only nontrivial component of those is the zero component, yielding the 5D energy conservation equation

$$\dot{\rho}^{(5)} + 3H(\rho^{(5)} + p^{(5)}) = 0. \quad (5.3.18)$$

Here we already used $R = \text{const}$, implying that the 4D energy density ρ and pressure p satisfy the standard conservation equation as in 4D GR. For a general linear equation of state $p = w\rho$, the energy density will thus have the usual scaling

$$\rho \propto a^{-3(1+w)}. \quad (5.3.19)$$

For convenience, the BIG terms can again be absorbed into an effective energy-momentum tensor²²

$$\hat{\mathbf{T}}^{(5)} := \mathbf{T}^{(5)} - M_5^3 \mathbf{G}^{(5)}. \quad (5.3.20)$$

Due to the 5D Bianchi identities, it is also covariantly conserved and thus represents a legitimate “source” for the 6D Einstein equations. In the stabilized case, the corresponding 4D components are explicitly given by

$$\hat{\rho} = \rho - 3M_4^2 H^2, \quad \hat{p} = p + M_4^2 (2\dot{H} + 3H^2), \quad \hat{p}_\phi = p_\phi + 3M_4^2 (\dot{H} + 2H^2). \quad (5.3.21)$$

Junction conditions

Using different coordinate patches in the interior and exterior forbids a formulation of the equations of motion in terms of delta functions as in Gaussian normal coordinates. Thus, instead of performing a delta-matching, we have to use the covariant version of the junction conditions, which was worked out by Israel [Isr66, Isr67]. First, one requires the line element to be continuous across the shell, which was already implemented in Eqs. (5.3.12) and (5.3.13). Note that they imply $\alpha_0(t) = \tilde{\alpha}_0(\tilde{t})$ and $r_0(t) = \tilde{r}_0(\tilde{t})$, but $\eta_0(t) \neq \tilde{\eta}_0(\tilde{t})$ in general. Second, the surface energy momentum tensor is related to the discontinuity of the extrinsic curvature via

$$[K]g_{\alpha\beta}^{(5)} - [K_{\alpha\beta}] = \frac{1}{M_6^4} \hat{T}_{\alpha\beta}^{(5)}. \quad (5.3.22)$$

Here, $[X] := X - \tilde{X}$, and K is the trace of $K_{\alpha\beta}$, which is the pullback of the extrinsic curvature tensor

$$K_{MN}^{(6)} = h_{MP} \nabla^P n_N, \quad (5.3.23)$$

where $h_{MN} \equiv g_{MN} - n_M n_N$ is the 6D induced metric and n^M is the outward-pointing²³ normal vector, which for the exterior and interior is given by

$$n^M = \gamma e^{3\alpha_0} (\dot{r}_0, 1, 0, 0, 0, 0) \quad \text{and} \quad \tilde{n}^M = \tilde{\gamma} e^{3\tilde{\alpha}_0} (\dot{\tilde{r}}_0, 1, 0, 0, 0, 0), \quad (5.3.24)$$

²²Note that here $\hat{\mathbf{T}}$ is defined without the factor $1/M_6^4$, unlike $\hat{\mathbf{T}}$ in previous chapters.

²³By “outward” we mean away from the axis (not away from the brane), which, as discussed above, corresponds to the direction of increasing r or \tilde{r} in the sub-critical case, justifying the choice of signs in (5.3.24).



respectively. Here the ordering of coordinates is the same as in (5.3.7).

The straightforward calculation of $K_{\alpha\beta}$ yields the following nontrivial components

$$K^0_0 = \frac{\gamma}{R} \frac{r_0 \ddot{r}_0}{1 - \dot{r}_0^2} + n^M \partial_M (\eta - 3\alpha)|_0, \quad (5.3.25a)$$

$$K^i_j = n^M \partial_M \alpha|_0 \delta^i_j, \quad (5.3.25b)$$

$$K^\phi_\phi = \frac{\gamma}{R} - 3n^M \partial_M \alpha|_0. \quad (5.3.25c)$$

The components of $\tilde{K}_{\alpha\beta}$ have the same form, but with tildes on all quantities. Before plugging these into the junction conditions, it is useful to express everything in terms of a minimal (but complete) set of on-brane quantities. Those can be taken to be H and R , completely characterizing the intrinsic geometry, as well as η_0 and $\xi := r_0 \alpha'|_0$ (plus their interior counterparts $\tilde{\eta}_0$, $\tilde{\xi} := \tilde{r}_0 \tilde{\alpha}'|_0$), which are sufficient to uniquely infer the extrinsic embedding of the brane in the bulk. To verify this statement, note that all terms appearing in (5.3.25) can be expressed in terms of these functions as

$$\gamma = \sqrt{e^{-2\eta_0} + 9H^2 R^2}, \quad \dot{r}_0 = \frac{3HR}{\gamma}, \quad \frac{r_0 \ddot{r}_0}{1 - \dot{r}_0^2} = \frac{3R^2}{\gamma^2} \left(\dot{H} + H \dot{\eta}_0 \right), \quad (5.3.26a)$$

$$n^M \partial_M \alpha|_0 = \frac{\gamma}{R} (\xi + \dot{r}_0 \psi), \quad n^M \partial_M \eta|_0 = \frac{6\gamma}{R} (\xi^2 + \psi^2 + 2\dot{r}_0 \xi \psi), \quad (5.3.26b)$$

with

$$\psi := r_0 \dot{\alpha}|_0 = \frac{HR}{\gamma} (1 - 3\xi), \quad (5.3.26c)$$

and similarly for the interior quantities (by adding tildes everywhere). These relations can readily be derived by using the Einstein equations (5.3.8b) in the limit $r \rightarrow r_0$, Eqs. (5.3.12) and (5.3.13), and the stability condition $R = \text{const.}$ ²⁴

Plugging all this into the (0) - and (j) -components of the junction conditions (5.3.22) finally yields the modified Friedmann equations

$$H^2 = \frac{\rho}{3M_4^2} + \frac{1}{r_c^2} (\gamma - \tilde{\gamma}), \quad (5.3.27a)$$

$$\dot{H} = -\frac{3}{2f} \left[\frac{p}{3M_4^2} + H^2 - \frac{1}{r_c^2} \left(\gamma g_1(\xi, \chi) - \tilde{\gamma} g_1(\tilde{\xi}, \tilde{\chi}) \right) \right], \quad (5.3.27b)$$

where we defined

$$f := 1 - \frac{9R^2}{2r_c^2} \left(\frac{1}{\gamma} - \frac{1}{\tilde{\gamma}} \right), \quad (5.3.28)$$

²⁴For the non-stabilized case, see Appendix 5.A.1.

and

$$g_1(\xi, \chi) := 1 + 2(9\chi - 1)[3\chi + \xi(3\xi - 2)(9\chi - 1)], \quad \chi := \frac{H^2 R^2}{\gamma^2}. \quad (5.3.29)$$

Furthermore, in analogy to the DGP model, we introduced the *crossover scale*

$$r_c^2 := \frac{3M_4^2}{2\pi M_6^4} \equiv \frac{3RM_5^3}{M_6^4}. \quad (5.3.30)$$

Note, however, that r_c is not yet the physically relevant crossover scale, which will be derived in Sec. 5.5.2.

The function f will play a crucial role in the qualitative behavior of the model. Equation (5.3.27b) already shows that the time evolution becomes singular as $f \rightarrow 0$.²⁵ Later, we will furthermore see that the sign of f decides on the stability of the theory.

As a consistency check, one can explicitly verify that—like in standard GR—the second modified Friedmann equation (5.3.27b) already follows from (5.3.27a) and energy conservation (5.3.18), as is guaranteed by the Gauss-Codazzi relations (and the 4D Bianchi identities). In other words, Eq. (5.3.27b) is redundant and one only needs to keep the stronger (constraint) equation (5.3.27a). Alternatively, one can use the dynamical equation (5.3.27b) to calculate the time evolution and only impose the constraint at the initial time. This procedure is better suited for our numerical implementation below; at later times, the constraint can then be used as an important consistency check for the solver.

It remains to consider the (ϕ) -component of the junction conditions, which determines the stabilizing pressure p_ϕ . Simplifying as before, we find

$$\frac{p_\phi}{3M_4^2} = -\dot{H} \left[1 - \frac{3R^2}{r_c^2} \left(\frac{1}{\gamma} - \frac{1}{\tilde{\gamma}} \right) \right] - 2H^2 + \frac{6}{r_c^2} \left(\gamma g_2(\xi, \chi) - \tilde{\gamma} g_2(\tilde{\xi}, \tilde{\chi}) \right), \quad (5.3.31)$$

with

$$g_2(\xi, \chi) := \chi + [3\chi - \xi(9\chi - 1)]^2. \quad (5.3.32)$$

This can later be used to check whether p_ϕ fulfills the NEC.²⁶

The general form of the modified Friedmann equations (5.3.27) is similar to those in the DGP model, cf. Sec. 1.4.2: They are just the standard 4D Friedmann equations, modified by terms whose sizes are controlled by the crossover r_c . In particular, the standard 4D result is recovered in the limit $r_c \rightarrow \infty$, as it should be. We can thus expect to have the required 4D regime whenever $Hr_c \gg 1$ (as long as $\gamma - \tilde{\gamma}$ does not get large).

²⁵A singularity could in principle be avoided if the numerator also vanishes if $f = 0$, but this is generically not the case, because the pressure p can be chosen independently from f . Moreover, we will see below that this singularity is indeed approached dynamically, in a small regime in parameter space close to $f = 0$.

²⁶Without stabilization, this equation would instead provide a dynamical equation of motion for $R(\tau)$, for some given p_ϕ , see Appendix 5.A.1.



But there is also a crucial difference: In the DGP model, the dynamics of the modification term was solely encoded in *intrinsic* brane quantities [Hubble and the scale factor, cf. Eq. (1.4.20)], whereas here it inevitably depends on the *extrinsic* brane dynamics via $\eta_0, \tilde{\eta}_0$. In other words, we once again are struck by the fact that there is no closed set of Friedmann equations on a codimension-two brane, if the bulk is not taken into account. Of course, we already knew this from our preceding investigations, and we also understand the physical origin of this failure (the presence of gravitational bulk waves), so we did not expect the choice of ER coordinates to change anything about this fact.

Instead, the main motivation for introducing these coordinates, was to reduce the dynamical vacuum equation to the simple linear cylindrical wave equation (5.3.8a). Therefore, we know from Chap. 3 what the required outgoing wave condition looks like. Can we now make use of this, and at least derive a closed on-brane system that is only nonlocal in time? Unfortunately, the answer is “no”. On the one hand, the ER coordinates simplified the bulk equations, but on the other hand they complicated the brane embedding in the sense that in these coordinates (in which we know how to implement the wave condition) the brane follows some nontrivial trajectory $r_0(t)$. But the kernel integral in the boundary condition (3.4.11) runs over t at fixed r_0 , so the integral would *not* be a convolution over the on-brane time τ , cf. Fig. 5.2. This means that in order to implement the outgoing wave boundary condition, it is not enough to determine α on the brane, one also needs to solve for its bulk profile. (In addition, one would also need to implement a “regular axis” boundary condition in the interior, entailing the same problems.) Conversely, if we used Gaussian normal coordinates to bring the brane back to a fixed bulk coordinate, the field equations would change and we would lose knowledge of the outgoing wave condition.

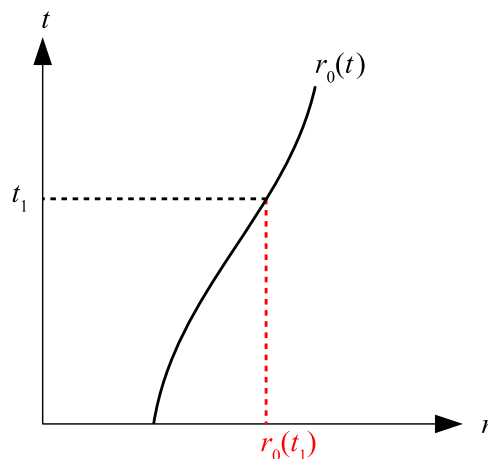


Figure 5.2: A moving boundary makes the outgoing wave boundary condition (3.4.11) also nonlocal in space: To evaluate the required convolution at some time t_1 , one needs the past values of α along $r = r_0(t_1)$ (red dashed line), which are different from the on-brane values $\alpha_0(t) \equiv \alpha[t, r_0(t)]$ (solid curve).

In other words, the Friedmann equations (5.3.27) are, from the 4D point of view, nonlocal both in space *and* time. But now that we have come so far, we will not let us stop by this final obstacle. Instead, we will make use of the bulk equations' simplicity and accept the challenge to solve the complete nonlinear, coupled brane-bulk system numerically.

5.3.2 Generalized static solution

Before approaching the full dynamical solutions, let us first reconsider the case of a static solution, but now not sourced by a pure tension, but by FRW-symmetric brane matter with an arbitrary (linear) EOS $p = w\rho$. One might expect no static solution to exist in this case, like in standard cosmology; let us now show that this is not true. To this end, we assume the metric functions and the brane position r_0, \tilde{r}_0 to be time independent. Consequently, the Hubble parameter H vanishes, and the intrinsic brane geometry is Riemann flat, as in the pure tension case.

In the interior, the only regular solution is $\tilde{\alpha}(\tilde{r}) \equiv \text{const}$ and $\tilde{\eta}(\tilde{r}) \equiv 0$, i.e. Minkowski space. In the exterior, the general solution of (5.3.8) is

$$\alpha(r) = \alpha_1 \ln\left(\frac{r}{r_0}\right) + \alpha_0 \quad \text{and} \quad \eta(r) = 6\alpha_1^2 \ln\left(\frac{r}{r_0}\right) + \eta_0, \quad (5.3.33)$$

with α_0, α_1 and η_0 being constants of integration. α_0 can be set to zero by a rigid rescaling of t, r and x^i , while the remaining two are determined by the junction conditions (5.3.27), yielding

$$\eta_0 = -\ln\left(1 - \frac{\rho}{\rho_{\text{crit}}}\right), \quad (5.3.34a)$$

$$\alpha_1 = \frac{1}{3} \left(1 - \sqrt{\frac{2\rho_{\text{crit}} + (1+3w)\rho}{2(\rho_{\text{crit}} - \rho)}}\right), \quad (5.3.34b)$$

where the *critical energy density* $\rho_{\text{crit}} := 2\pi M_6^4$ is the same as the critical tension λ_{crit} . Note that the solution is ill-defined for $\rho = \rho_{\text{crit}}$, and we will again restrict ourselves to sub-critical energy densities $\rho < \rho_{\text{crit}}$ throughout this chapter. The remaining junction condition (5.3.31) gives the effective EOS parameter for the stabilizing angular pressure

$$w_\phi := \frac{p_\phi}{\rho} = 6\alpha_1^2 \left(\frac{\rho_{\text{crit}}}{\rho} - 1\right) \geq 0 \quad (\text{for } 0 < \rho < \rho_{\text{crit}}), \quad (5.3.35)$$

satisfying the NEC. We have thus indeed obtained a consistent static solution for an



arbitrary 4D perfect fluid, with line element²⁷

$$ds^2 = e^{2\eta_0} \left(\frac{r}{r_0}\right)^{6\alpha_1(2\alpha_1-1)} (-dt^2 + dr^2) + \left(\frac{r}{r_0}\right)^{2\alpha_1} \delta_{ij} dx^i dx^j + \left(\frac{r}{r_0}\right)^{-6\alpha_1} r^2 d\phi^2. \quad (5.3.36)$$

For the pure tension case, Eq. (5.3.34b) implies $\alpha_1 = 0$, and we reproduce the Riemann flat deficit angle solution of Sec. 5.1.²⁸ For a general EOS, however, $\alpha_1 \neq 1$ and the bulk is curved—while the brane stays completely flat. In other words, *the degravitation mechanism also applies to a general cosmological fluid, not only to a CC.* The impact of the matter source is again completely absorbed by extrinsic curvature, with the only difference that the corresponding static bulk geometry is not locally flat anymore. The only assumption was that there would be some underlying UV model which stabilizes the brane width. The healthy EOS parameter (5.3.35) suggests that this can be achieved by healthy degrees of freedom. The fact that this also stabilizes the axial direction is rather surprising.

The fact that *all* FRW matter can be degravitated already casts some doubt on a phenomenological success of the theory. But a priori, we do not know whether this solution is stable. In fact, the analogy to the Einstein static universe suggests that it is not. Furthermore, even if it is, the model is still designed to allow for a 4D regime at early times. Whether the late-time modifications could make the model competitive with (or even superior to) Λ CDM can only be decided once the dynamical solutions are known.

We will therefore continue our quest for the general cosmological solutions. In the end, we will find that (i) this generalized degravitating solution indeed *is* stable, in some region of parameter space; (ii) the 4D mechanism would only work in the complementary region, but (iii) the latter case is plagued by a ghost instability.

5.3.3 Boundary and initial conditions

Before the full bulk field equations can be integrated forward in time, one needs to specify appropriate boundary and initial conditions. The boundary condition at the axis ($\tilde{r} = 0$) is dictated by demanding a smooth axis—otherwise we would not have a proper regularization. The absence of both a curvature and a conical singularity implies

$$\tilde{\alpha}'|_{\tilde{r}=0}(\tilde{t}) = 0, \quad (5.3.37a)$$

$$\tilde{\eta}|_{\tilde{r}=0}(\tilde{t}) = 0, \quad (5.3.37b)$$

²⁷This is the 6D generalization of the 4D static cylindrical solution discussed in Sec. 2.5.1. There, the continuous coordinate patch analogous to (5.3.1) was used by leaving the metric function W nontrivial, whereas here, the gauge $W = r$ leaves us with two discontinuously connected coordinate patches inside and outside the brane ($0 = \tilde{\eta}_0 \neq \eta_0$).

²⁸This can be checked explicitly by transforming back to continuous coordinates via $t^* = e^{\eta_0} t$, $r^* = e^{\eta_0}(r - r_0) + r_0$.

respectively. For an actual infinite bulk the other boundary condition should be implemented at radial infinity ($r \rightarrow \infty$), and one would impose (local) asymptotic flatness there. But solving the system numerically forces us to cut off the bulk at some finite radius r_{\max} , and we have to impose boundary conditions there. The appropriate one is clearly the outgoing wave condition derived in Chap. 3. However, this criterion is nonlocal and would require performing the convolution integral (3.4.11) at each time step. To avoid this complication, we will instead use the following trick: Below, we will choose trivial initial data at $t = t_i \equiv 0$ in the bulk (apart from a small region $\delta r \sim \sigma$ very close to the brane, as is required by continuity), and so the first gravitational wave crest will only reach r_{\max} after the time $t = r_{\max} - \sigma$. [Note that radial gravitational waves propagate at speed 1 in ER coordinates (5.3.7).] Therefore, by making the exterior bulk domain large enough,²⁹ i.e. choosing $r_{\max} = t_{\max} + \sigma$, we can make sure that no wave excitation has reached the numerical boundary at the final time t_{\max} of integration, and we can simply use the trivial fixed boundary condition

$$\alpha|_{r=r_{\max}}(t) = \text{const.} \quad (5.3.38)$$

Let us now turn to the initial conditions, i.e. the Cauchy data that needs to be prescribed at the initial time τ_i, \tilde{t}_i, t_i of the numerical integration. By a global rescaling of coordinates, we can initially set the on-brane scale factor to unity,

$$\tilde{\alpha}_0|_i = \alpha_0|_i = 0, \quad (5.3.39)$$

where the subscript i denotes evaluation at initial time. This implies that the brane's initial coordinate position is

$$\tilde{r}_0|_i = r_0|_i = R, \quad (5.3.40)$$

where R is a free parameter, just like the initial values H_i and ρ_i .

In the bulk, we need to specify the radial profiles

$$\tilde{\alpha}_i(\tilde{r}), \quad \dot{\tilde{\alpha}}_i|_i(\tilde{r}), \quad (\tilde{r} < R), \quad (5.3.41a)$$

$$\alpha_i(r), \quad \dot{\alpha}_i|_i(r), \quad (r > R), \quad (5.3.41b)$$

which must be compatible with the boundary conditions (5.3.37) and (5.3.38).

In order not to prepare any unnecessary bulk waves, we will always choose the profile of the static solution discussed in Sec. 5.3.2,

$$\tilde{\alpha}_i(\tilde{r}) = 0, \quad \alpha_i(r) = \alpha_1 \ln\left(\frac{r}{R}\right), \quad (5.3.42)$$

where the constant α_1 , for a given EOS parameter w and initial energy density ρ_i , is obtained from (5.3.34b). In particular, for a CC ($w = -1$), we get $\alpha_1 = 0$ and thus $\alpha_i(r) = 0$.

²⁹Of course, this makes the exterior domain of integration (and thus the numerical cost) quadratically sensitive to the time t_{\max} we want to simulate. But we will never need so large t_{\max} that this becomes a problem; otherwise, it might have been worthwhile to use the nonlocal outgoing wave condition.



If we also chose trivial initial velocity profiles, the solutions would always remain static. Instead, we demand a nonzero initial Hubble parameter H_i ; continuity at the brane then implies

$$\dot{\alpha}_0|_i = \frac{H_i}{\tilde{\gamma}_i}, \quad \dot{\alpha}_0|_i = \frac{H_i}{\gamma_i}(1 - 3\alpha_1). \quad (5.3.43)$$

The initial time derivatives can thus be parametrized as

$$\dot{\alpha}|_i(\tilde{r}) = \frac{H_i}{\tilde{\gamma}_i} \tilde{F}(\tilde{r}), \quad \dot{\alpha}|_i(r) = \frac{H_i}{\gamma_i}(1 - 3\alpha_1)F(r), \quad (5.3.44)$$

with some profile functions F, \tilde{F} satisfying the boundary conditions

$$\tilde{F}'(0) = 0, \quad \tilde{F}(R) = 1 = F(R), \quad F(r_{\max}) = 0. \quad (5.3.45)$$

For definiteness, we will choose³⁰

$$\tilde{F}(\tilde{r}) = 1, \quad F(r) = \exp\left[-\frac{(r-R)^2}{\sigma^2}\right]. \quad (5.3.46)$$

The flat profile inside is motivated by the observation that for R small enough, the regularity condition at the axis implies that $\tilde{\alpha}' \approx 0$. In the exterior region, we choose a sharply localized Gaussian profile ($\sigma \ll R$), in order not to put too much kinetic energy into the gravitational field, which could have a large impact on the on-brane evolution for long times. With those choices, we expect the on-brane evolution to become insensitive to the initial conditions for late times.

The initial data is now completely specified, since $\tilde{\eta}_{0i}$ and η_{0i} are determined³¹ by the regularity condition (5.3.37b) together with the constraints (5.3.8b) and the junction condition (5.3.27a) across the brane. Specifically, we find

$$\tilde{\eta}_{0i} = 6 \int_0^R d\tilde{r} \tilde{r} \left(\tilde{\alpha}'^2 + \dot{\alpha}|_i^2 \right) = \frac{6H_i^2}{\gamma_i^2} \int_0^R d\tilde{r} \tilde{r} \tilde{F}^2 = \frac{3H_i^2 R^2}{e^{-2\tilde{\eta}_{0i}} + 9H_i^2 R^2}, \quad (5.3.47)$$

an implicit equation for $\tilde{\eta}_{0i}$ which can be solved numerically, see Fig. 5.9. The first expression suggests that $\tilde{\eta}_{0i}$ is the gravitational energy stored inside the cylinder initially; and indeed, it is (up to a constant factor) nothing but the Thorne's C-energy (cf. Sec. 2.7), generalized to 6 dimensions.

The exterior η_{0i} is then obtained from (5.3.27a), which can be rewritten as

$$\frac{\rho_i}{\rho_{\text{crit}}} = r_c^2 H_i^2 + \sqrt{e^{-2\tilde{\eta}_{0i}} + 9H_i^2 R^2} - \sqrt{e^{-2\eta_{0i}} + 9H_i^2 R^2}. \quad (5.3.48)$$

³⁰Strictly speaking, this choice of F does not exactly fulfill $F(r_{\max}) = 0$. But for $\sigma \ll R$ (as will be chosen in our numerics), the deviation from 0 is below the numerical resolution and hence consistent for our purposes.

³¹In fact, the full radial profiles of $\tilde{\eta}, \eta$ can be calculated from (5.3.8b), but are not needed for the evolution of α . Only $\tilde{\eta}_0, \eta_0$ enter in the junction conditions, which can be obtained by using (5.3.8b) evaluated at the brane, see Eq. (5.3.54).

However, this equation does not always have a (real) solution for η_{0i} and thereby places an upper bound on the energy density (not only initially, because the constraint is valid at all times):

$$\boxed{\frac{\rho}{\rho_{\text{crit}}} < r_c^2 H^2 + \sqrt{e^{-2\tilde{\eta}_0} + 9H^2 R^2} - 3|H|R.} \quad (5.3.49)$$

Clearly, this *criticality bound* is the generalization of the static one ($\rho < \rho_{\text{crit}}$) to the dynamical case of an expanding (or collapsing) brane. The modifications can be understood as follows: if $\tilde{\eta}_0 > 0$, there is gravitational energy inside the ring, which contributes to the total energy thus strengthening the bound, i.e. the system becomes super-critical already for smaller ρ ; likewise, the expansion rate contributes to the energy density on the ring and therefore also makes the bound stronger. On the other hand, the BIG term $\propto r_c^2$ corresponds to intrinsic curvature which absorbs some of the energy density, thereby weakening the bound. Geometrically, the reason for the bound is again that its violation would imply a different (compact) exterior topology, cf. Appendix 6.A. In this chapter, we restrict ourselves to the sub-critical regime, in which the extra-space is topologically \mathbb{R}^2 ; this choice was already made by introducing standard ER coordinates, as discussed in Sec. 5.3.1. In Chap. 6, these coordinates will be adapted to the super-critical case.

In summary, for given model parameters R , r_c and w , as well as initial conditions parametrized by H_i , ρ_i and σ , the system can be integrated forward in time. In fact, the three quantities H_i , R and r_c only enter the equations of motion via two independent dimensionless combinations, which can for instance be chosen as $H_i r_c$ and $H_i R$.

5.3.4 Numerical algorithm

Note: Parts of this section are verbatim reproductions of Appendix B of the publication [NSHK15].

Since the dynamical bulk equation (5.3.8a) is the same as the linear wave equation discussed in Chap. 3, we can use the same discretization scheme (cf. Sec. 3.5.1) here: In the interior and exterior we replace the continuous coordinates (\tilde{t}, \tilde{r}) and (t, r) by equidistant lattices of spacing

$$\Delta\tilde{t} = \Delta\tilde{r} =: \tilde{\epsilon} \quad \text{and} \quad \Delta t = \Delta r =: \epsilon, \quad (5.3.50)$$

respectively. (Note that $\tilde{\epsilon}$ and ϵ can be chosen differently.) Inside the domains of integration, the bulk initial data is then evolved forward in time as discussed in Sec. 3.5.1, i.e. using

$$\alpha_{(n)}^{(i+1)} = -\alpha_{(n)}^{(i-1)} + \alpha_{(n+1)}^{(i)} + \alpha_{(n-1)}^{(i)} + \frac{\epsilon}{2r_{(n)}} \left(\alpha_{(n-1)}^{(i)} - \alpha_{(n+1)}^{(i)} \right), \quad (5.3.51)$$

(and similarly for $\tilde{\alpha}$), where the discrete indices i and n label the lattice coordinates $t^{(i)}$ and $r_{(n)}$, respectively. At $\tilde{r} = 0$ ($\Leftrightarrow \tilde{n} = 0$) and $r = r_{\text{max}}$ ($\Leftrightarrow n = N$), the appropriate



boundary conditions (5.3.37a) and (5.3.38) translate to

$$\tilde{\alpha}_{(0)}^{(i)} = \tilde{\alpha}_{(1)}^{(i)} \quad \text{and} \quad \alpha_{(N)}^{(i)} = \alpha_{(N)}^{(i-1)}, \quad (5.3.52)$$

respectively.

The only nontrivial part is how the interior and exterior regions are glued together. The value at the brane, $\tilde{\alpha}_0(\tilde{t}) = \alpha_0(t)$ is determined by the dynamical junction condition (5.3.27b). (More precisely, this equation yields the Hubble parameter H at time $t^{(i)}$, which is in turn used to calculate α_0 at $t^{(i+1)}$, and similarly for the interior.) However, there is a slight complication because the time steps Δt and $\Delta \tilde{t}$ do not correspond to the same physical time steps: the discretized version of equation (5.3.13) is

$$\frac{\Delta t}{\gamma} = \frac{\Delta \tilde{t}}{\tilde{\gamma}}, \quad (5.3.53)$$

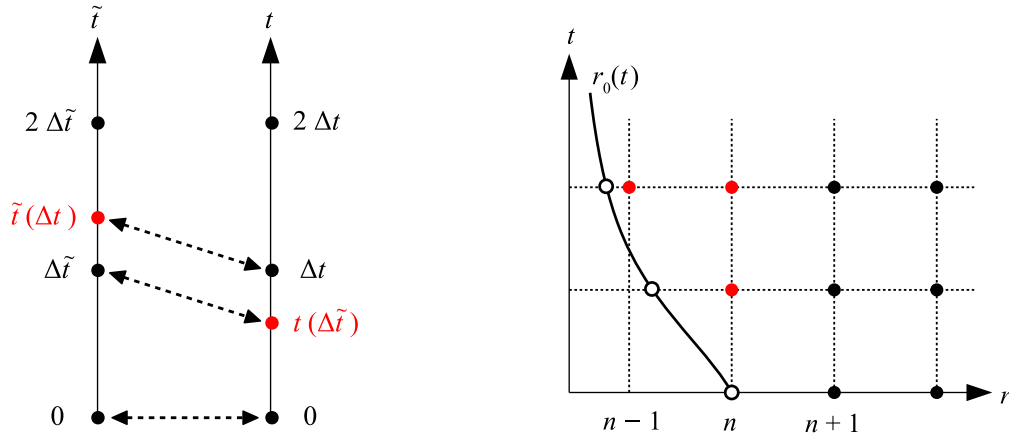
and $\gamma \neq \tilde{\gamma}$ whenever there is a modification to the 4D evolution, cf. (5.3.27a). Now suppose we are given all relevant initial data at time \tilde{t}_i, t_i (which we can assume to correspond to the same physical time, and set equal to zero, without loss of generality). Then we use (5.3.27b) to determine $\tilde{\alpha}_0$ and α_0 at the next time step, i.e. $\tilde{\alpha}_0(\Delta \tilde{t})$ and $\alpha_0(\Delta t)$. Those we use as the appropriate boundary conditions to solve the bulk equation (5.3.51), which in turn allows to calculate $\tilde{\eta}_0(\Delta \tilde{t})$ and $\eta_0(\Delta t)$ with the discretized version of

$$\frac{d\eta_0}{dt} = \dot{\eta}_0 + \dot{r}_0 \eta' |_0 \quad (5.3.54a)$$

$$= 6r_0 \left[2\dot{\alpha}_0 \alpha' |_0 + \dot{r}_0 \left(\dot{\alpha}_0^2 + \alpha' |_0^2 \right) \right], \quad (5.3.54b)$$

(and similarly for $\tilde{\eta}_0$) where we used (5.3.8b) in the limit $r \rightarrow r_0^+$ (or $\tilde{r} \rightarrow \tilde{r}_0^-$). We now want to iterate this process, but to use (5.3.27b) again, we need $\tilde{\eta}_0$ and η_0 at the same physical time (i.e. both at $\Delta \tilde{t}$, or both at Δt). Assume that for instance Δt is “ahead in time”, i.e. $\tilde{t}(\Delta t) > \Delta \tilde{t}$, cf. Fig. 5.3a. We then estimate $\eta_0[t(\Delta \tilde{t})]$ by linearly interpolating between $\eta_0(0)$ and $\eta_0(\Delta t)$. With this we can repeat the procedure to obtain $\tilde{\eta}_0(2\Delta \tilde{t})$, from which we get $\tilde{\eta}_0[\tilde{t}(\Delta t)]$ —again by linear interpolation. Then we can calculate $\eta_0(2\Delta t)$ and continue the iteration.

A second complication stems from the fact that even though the physical brane circumference $2\pi R$ is kept fixed, the brane’s coordinate position $\tilde{r}_0 = r_0$ will be time-dependent for any nontrivial evolution of α , because $R = r_0 e^{-3\alpha_0} = \tilde{r}_0 e^{-3\tilde{\alpha}_0}$. But since we use a fixed spatial grid, and the brane moves with a (coordinate) speed less than 1, this implies that the brane position almost always lies in between two grid points. We again solve this problem by linear interpolation: Suppose the brane (say, in the exterior coordinate patch) is initially located at some grid point n , cf. Fig. 5.3b. Equation (5.3.27b) (with the appropriate initial data) gives the new value of α_0 at the new brane position (which is also determined by α_0). Assume that the brane moved to smaller r , as in Fig. 5.3b. Then the new value of α at n cannot be obtained using (5.3.51), because it would require initial data at the point $n-1$, which lies outside



(a) Using two different coordinate patches for the interior and exterior geometry implies that the temporal grid points do not correspond to the same physical time at the position of the brane. The values of $\tilde{\eta}_0$ and η_0 at the red points, which are needed in (5.3.27b), are found by linearly interpolating between the neighboring black points.

(b) Sketch of the spacetime grid. The white points indicate the brane position, which in general does not lie on a grid point, but on which the boundary data for α is given. Black points are calculated using the wave equation (5.3.51). For the red points, this is not possible because of the lack of initial data, so they are obtained by linearly interpolating between the neighboring black and white points.

Figure 5.3: Visualization of the interpolations that occur in the numerical algorithm.

the domain of integration. In those cases, we estimate the new value of $\alpha_{(n)}$ by linearly interpolating between the brane value and the new value at the point $n+1$ [which can be obtained from (5.3.51)]. Whenever the brane crosses one spatial grid point, then there are two³² values of α which cannot be calculated from (5.3.51), in which case we determine both of them by linear interpolation.

Finally, we checked that the numerically results are practically unchanged if instead of linear interpolations we use quadratic interpolations everywhere. This shows that the numerical errors are mainly not due to the interpolation, but to the discretization. But those errors are very well under control, as will be discussed in Appendix 5.B.

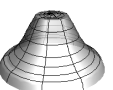
5.3.5 Numerical solutions

The numerical solutions that we found can be classified into two categories, according to their qualitative behavior:

(i) Degravitating solutions:

In this class, the geometry dynamically approaches the general static solution

³²More than two interpolations are never necessary at one time step, because the brane's coordinate speed is less than 1.



discussed in Sec. 5.3.2, while emitting ER waves into the bulk. In particular, the Hubble parameter on the brane approaches zero at late times, in agreement with the degravitation idea. This happens for any EOS parameter w , i.e. *all* matter is degravitated, not just a CC.

(ii) *Super-accelerating solutions:*

Here, the Hubble parameter grows unbounded (in fact, it even accelerates), and the bulk geometry expands accordingly. From the bulk perspective the reason for this pathological, unstable behavior is the effective energy density $\hat{\rho}$ turning negative.

The delineating surface in parameter space between these two cases is found to coincide with the surface $f = 0$, where f is the function defined in (5.3.28).³³

Let us now present an exemplary solution from each class, before discussing the corresponding regions of parameter space in Sec. 5.3.6. Let us emphasize that, while we will only explicitly present the numerical results for a pure tension source ($w = -1$), all results apply in complete analogy to other choices. [Explicitly, we checked the cases of pure dust ($w = 0$), pure radiation ($w = 1/3$), and a mixture of dust and CC.]

Degravitating example

First, we consider the parameters

$$H_i r_c = 0.1, \quad H_i R = 0.05, \quad \rho = 0.8\rho_{\text{crit}}. \quad (5.3.55)$$

(Furthermore, we choose $\sigma = 0.02R$ and $\tilde{\epsilon} = 10^{-3}R$, $\epsilon = 2 \times 10^{-4}R$.) The numerical results are plotted in Fig. 5.4. Initially, the metric functions $\tilde{\alpha}, \alpha$ increase around the brane, according to the initial velocities (5.3.44), (5.3.46). Subsequently, they settle back to the static configuration by emitting ER waves into the bulk. Accordingly, the Hubble parameter on the brane starts at the nonzero value H_i and dynamically relaxes to zero. This shows that the general static solution with FRW symmetries, presented in Sec. 5.3.2, is stable,³⁴ and thus represents an explicit example of a *dynamically degravitation mechanism at the full nonlinear level*. This is one of the main results of this analysis.

Since our investigation relies on the assumption of having a constant brane circumference, stabilized by an angular pressure p_ϕ , it is worthwhile checking if the required p_ϕ satisfies the NEC. This is indeed the case, as can be seen from Fig. 5.4c, suggesting that the stabilization could be achieved via healthy DOF in some UV model. Furthermore, at late times p_ϕ approaches 0, i.e. the value predicted by (5.3.35).

³³To be precise, there is a third class of solutions, which run into a singularity at $f = 0$ in finite proper time. They all live in a very small vicinity of the $f = 0$ surface in parameter space, cf. Sec. 5.3.6.

³⁴Here, stability is only verified for perturbations respecting the FRW symmetries; in Sec. 5.4.2, stability of the static pure tension will be shown for arbitrary (linear) perturbations. It is plausible that the same also holds for the general static solution.

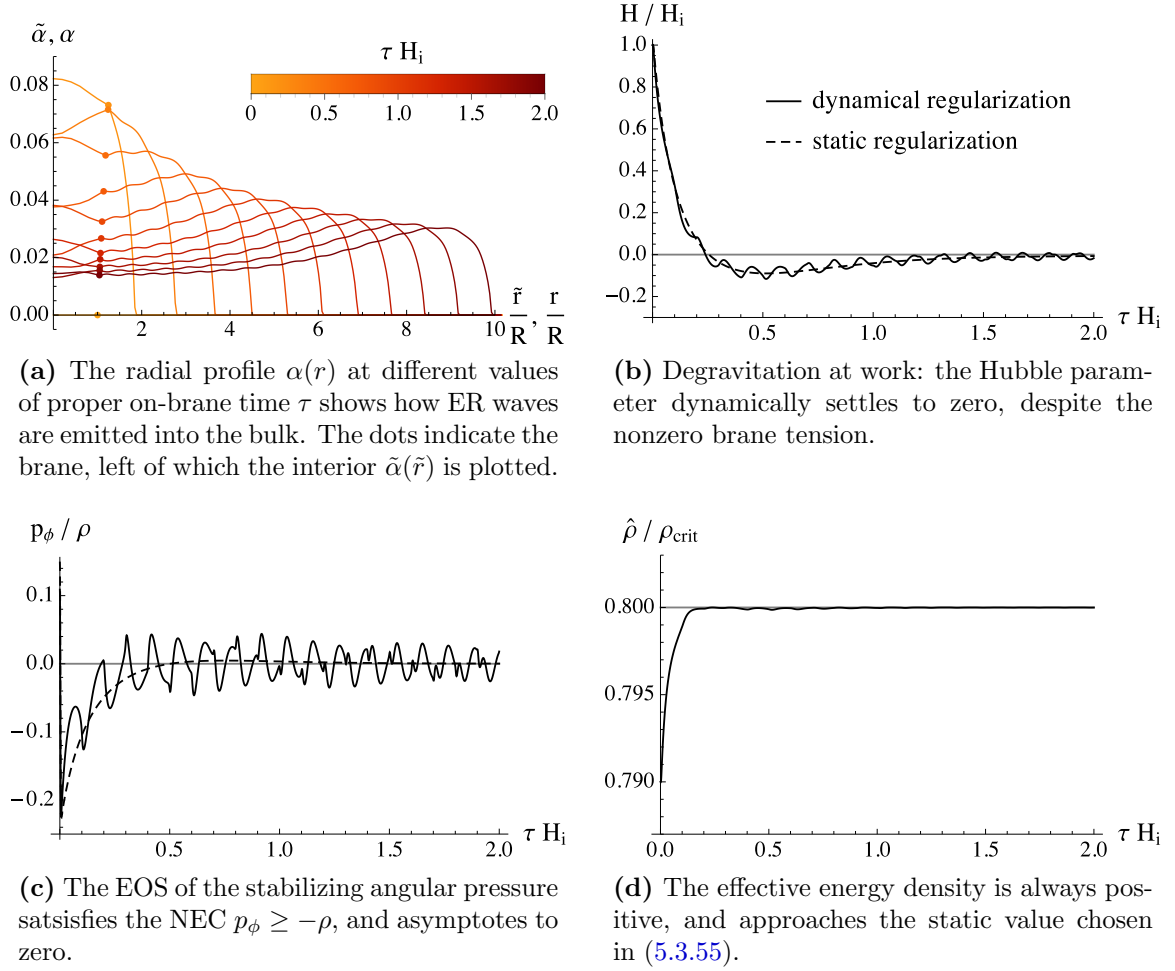
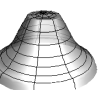


Figure 5.4: The degravitating solution for the parameters (5.3.55). The numerical error bars, discussed in Appendix 5.B, are smaller than the line widths.

Finally, Fig. 5.4d shows the effective energy density $\hat{\rho}$, as defined in (5.3.21). It is always positive and thus corresponds to a healthy effective source from the bulk point of view. A 4D regime would be characterized by $\hat{\rho} \approx 0$, and so we are always deep in the 6D regime, as expected from the choice $H_i r_c = 0.1$. At late times, since $H \rightarrow 0$, $\hat{\rho} \rightarrow \rho = 0.8\rho_{\text{crit}}$.

The small wiggles in $\tilde{\alpha}$, α , and the corresponding small oscillations of H , p_ϕ and $\hat{\rho}$, are caused by gravitational waves which are moving back and forth in the interior between the axis and the brane, where they are partially transmitted into the bulk, leading to a decrease in the amplitude of the fluctuations. This is in line with the observation that their wavelength is of order R . They are thus sensitive to the microscopic details of our specific regularization, and are clearly an artifact of the specific form of initial data that we chose. Therefore, we do not consider them as physically relevant; the generic, trustworthy, and (presumably) regularization independent predictions are the smooth functions that are obtained by coarse-graining over these small oscillations.



An efficient way of testing this regularization independence is by modifying Israel’s junction conditions by hand, such that no waves can propagate into the interior. This can be achieved by replacing the extrinsic curvature inside the brane by its static value, leading to what was called the “static regularization” in [NSHK15]. Intuitively, this can be thought of as gluing a perfectly reflecting boundary onto the inside of the brane. Thereby, the brane- and exterior bulk evolution decouple from the interior, and so the spacetime inside the ring can be discarded altogether. Of course, this is an ad hoc assumption and not justified by the Einstein equations, or an actual physical model of the reflecting boundary. One might even worry that it could correspond to some additional, unwanted matter on the brane. Furthermore, since the interior spacetime is lost, one can not ensure a regular axis, and so it is a priori not clear whether the topology could be altered by this procedure. Therefore, the “static regularization” should only not be viewed as an actual, consistent regularization, but rather as a test of the robustness of our findings against the microscopic details of our specific (“dynamical”) regularization. And this test is astonishingly successful: The corresponding evolution of the Hubble parameter is shown as a dashed line in Fig. 5.4b, and perfectly follows the smoothed version of the oscillating one in the “dynamical” regularization.³⁵ This is a very nice (and important) demonstration of the regularization independence of our results.

Super-accelerating example

Next, we choose a slightly larger value for the crossover, but keep all other parameters unchanged. Explicitly, we take

$$H_i r_c = 0.25, \quad H_i R = 0.05, \quad \rho = 0.8 \rho_{\text{crit}}, \quad (5.3.56)$$

(and set $\sigma = 0.02R$ and $\tilde{\epsilon} = 10^{-3}R$, $\epsilon = 5 \times 10^{-4}R$). We still expect to be far away from a 4D regime; but this time, the dynamics is completely different, as can be seen from Fig. 5.5: The bulk geometry does not settle back to the static configuration, but the initial expansion continues, and even accelerates. Accordingly, the Hubble parameter does not approach zero, but instead even increases (at increasing rate!), see Fig. 5.5b.³⁶ This pathological, *super-accelerating* behavior is accompanied by a subsequent violation of the NEC, by both the stabilizing pressure p_ϕ , and the effective energy density $\hat{\rho}$. (Note that both start out positively.) In summary, the static solution is no attractor for this choice of parameters, and the model instead behaves completely unstable.

A priori, this instability could be caused by the pathological EOS for p_ϕ which we encountered, and thus ultimately by the requirement to have a fixed brane circumference.

³⁵A similar statement holds for α , but this is not depicted here; the interested reader is referred to [NSHK15].

³⁶Again, this qualitative behavior is the same in the “static regularization”, shown as a dashed line. The rise is a bit faster, because the parameters are in that case closer to the (slightly modified) stability bound, see the discussion in [NSHK15].

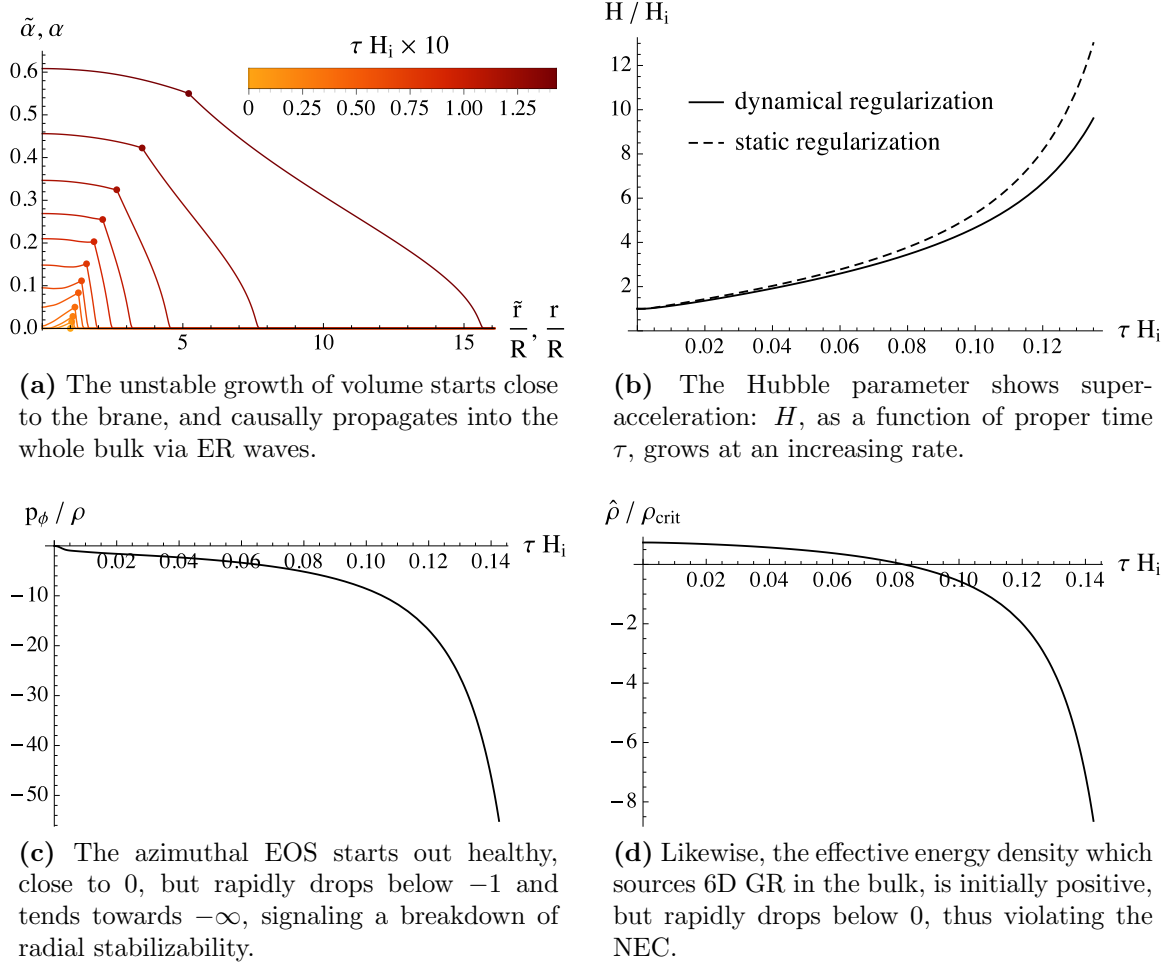


Figure 5.5: The super-accelerating solution for the parameters (5.3.56). The numerical error bars are again smaller than the line widths.

It would, of course, be rather surprising if a stabilization condition in the end leads to an instability; moreover, the EOS is initially larger than -1 , and only later violates the NEC. But this signals the breakdown of stabilizability of the radial direction, and one can still wonder if relaxing this assumption would cure the pathology. In order to definitely rule out this possibility, it is shown in Appendix 5.A.1 that the instability still persists if the assumption $R = \text{const}$ is replaced by the (physically clearly admissible) choice $p_\phi = 0$. In other words, the pathological behavior is *not* caused by the stabilization requirement; rather, p_ϕ 's violation of the NEC is caused by the unstable behavior, the origin of which must lie somewhere else.

The fact that the solution for the parameters (5.3.55) was stable, and became unstable by *only* increasing the crossover r_c , implies that *the instability is caused by the BIG terms*. From the bulk perspective, they correspond to an additional on-brane source, resulting in the total effective energy density $\hat{\rho} \equiv \rho - 3M_4^2 H^2$. For large enough H , this becomes negative, leading to a NEC-violating effective brane source. Since H grows



unbounded, this happens necessarily at some point, as is also confirmed explicitly by Fig. 5.5d. However, $\hat{\rho}$ starts out *positively*, and only turns negative at some later point, when the super-acceleration has already begun. Therefore, the negative $\hat{\rho}$, even though it is a clear manifestation of a pathology, can not be viewed as its cause. In other words, the question whether a solution will belong to the degravitating or super-accelerating regime, is not decided by the (initial) sign of $\hat{\rho}$. It is then natural to ask if there is some other function of the model parameters (and possibly also of the initial conditions), from which the question of stability of the corresponding solution can already be answered initially, without having to run the numerics. We will show in Sec. 5.3.6 that such a function does indeed exist.

Volume stabilization

But before doing so, let us subject our regularization to yet another consistency check, concerning the 2D extra space volume inside the regularized brane: By stabilizing R , we ensure a fixed proper circumference $2\pi R$ of the thick brane, but a priori this says nothing about its proper radius, which can be different from R in a curved space. It is hence worthwhile to check if this radius is also sufficiently stabilized in our scheme, and in particular if it vanishes in the limit $R \rightarrow 0$. If this were not the case, it would be unclear if the spacetime geometry which we found actually corresponds to a properly regularized codimension-two brane.

To this end, we can consider the interior 2D volume V_{int} in the ER time slicing, as a function of proper on-brane time τ ,

$$V_{\text{int}}(\tau) = 2\pi \int_0^{\tilde{r}_0(\tau)} d\tilde{r} \tilde{r} e^{\tilde{\eta}-6\tilde{\alpha}}, \quad (5.3.57)$$

which can easily be computed by numerical integration. The relative change of this volume is depicted as the dashed lines in Fig. 5.6, for both the degravitating and super-accelerating examples presented above. In order to quantify its change, we compare it to the relative change of the 3D brane volume $V_b \propto e^{3\alpha_0}$ (solid lines). We see that the time evolution of the latter is clearly dominant; in this sense, the interior volume is sufficiently stabilized. Furthermore, the small oscillations in V_{int} with frequencies of order R^{-1} are again caused by the bouncing waves in the interior region, and are thus an artifact of the specific initial conditions. If these small fluctuations are ignored, V_{int} basically stays at the flat-space value πR^2 , which is drawn as the gray line in Fig. 5.6a. This confirms that the interior volume would indeed vanish in the limit $R \rightarrow 0$, as required. Finally, note that the super-accelerating case in Fig. 5.6b in particular shows that the interior space does not collapse in radial direction, which might otherwise have been a potential source of the accelerated expansion in x -direction. (This is also confirmed by the “static regularization” [NSHK15], in which the brane-evolution is completely decoupled from the interior, but still super-accelerates, see Fig. 5.5b.)

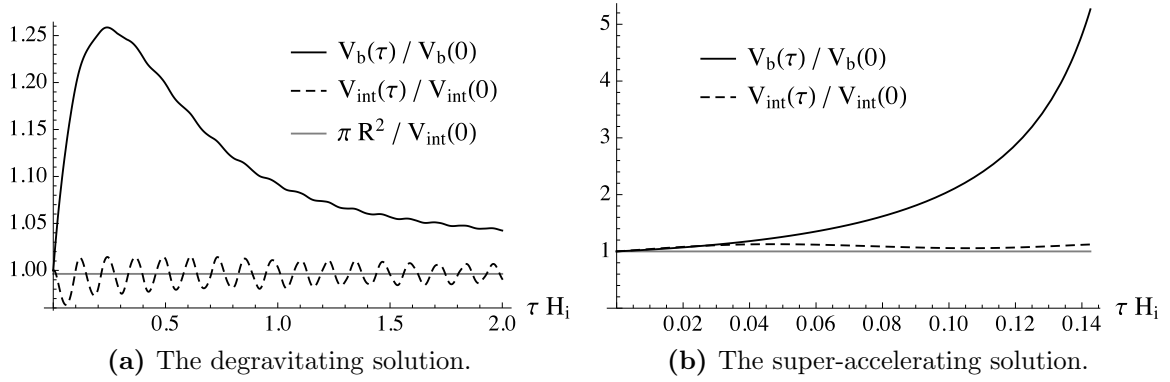


Figure 5.6: The 2D extra space volume inside the regularized brane V_{int} (5.3.57) is approximately constant as compared to the 3D brane volume $V_b \propto e^{3\alpha_0}$, confirming a successful stabilization also of the transverse brane width in our regularization.

5.3.6 Scanning parameter space

From the second (dynamical) modified Friedmann equation (5.3.27b), we already know that the time evolution becomes singular for $f = 0$, where f is defined in (5.3.28). Furthermore, it turns out that in the degravitating and super-accelerating examples presented above, f is negative and positive, respectively. This suggests that the stability of the model might be decided upon by sign of f . To test this hypothesis, we performed a numerical scan over the parameter space.

The result is shown in Fig. 5.7a. Each dot in this diagram corresponds to a run of the numerics for different r_c and ρ_i , while $RH_i = 0.05$ was kept fixed. A green dot (1) means that the solution was found to degravitate, i.e. settle down to the static solution. A red dot (2) is used for solutions which showed the super-accelerating behavior, with $\hat{\rho}$ eventually turning negative. The gray region (3) corresponds to super-critical energy densities for which the bound (5.3.49)—drawn as a dashed line—is violated, and is thus not covered by our current analysis.³⁷ The solid line is not a fit to the numerically obtained boundary, but a plot of the analytic condition $f = 0$. The perfect agreement leaves no doubt that it is indeed the sign of f which determines the stability of the model. We can thus conclude that, at least for FRW symmetries,³⁸ *BIG in two codimensions is stable if and only if the function f is negative*. Using f 's definition (5.3.28) and the constraint (5.3.27a), we can write the corresponding *stability bound* as

$$\boxed{\frac{\rho}{\rho_{\text{crit}}} > r_c^2 \left(H^2 + \frac{2\tilde{\gamma}^2}{9R^2 + 2r_c^2\tilde{\gamma}} \right)}. \quad (5.3.58)$$

Even though the stability of each particular solution was only inferred from the numerical late time behavior, we have thus obtained a completely analytic criterion. In

³⁷The super-critical regime will be investigated in Chap. 6.

³⁸This restriction will be dropped in Sec. 5.4.2.



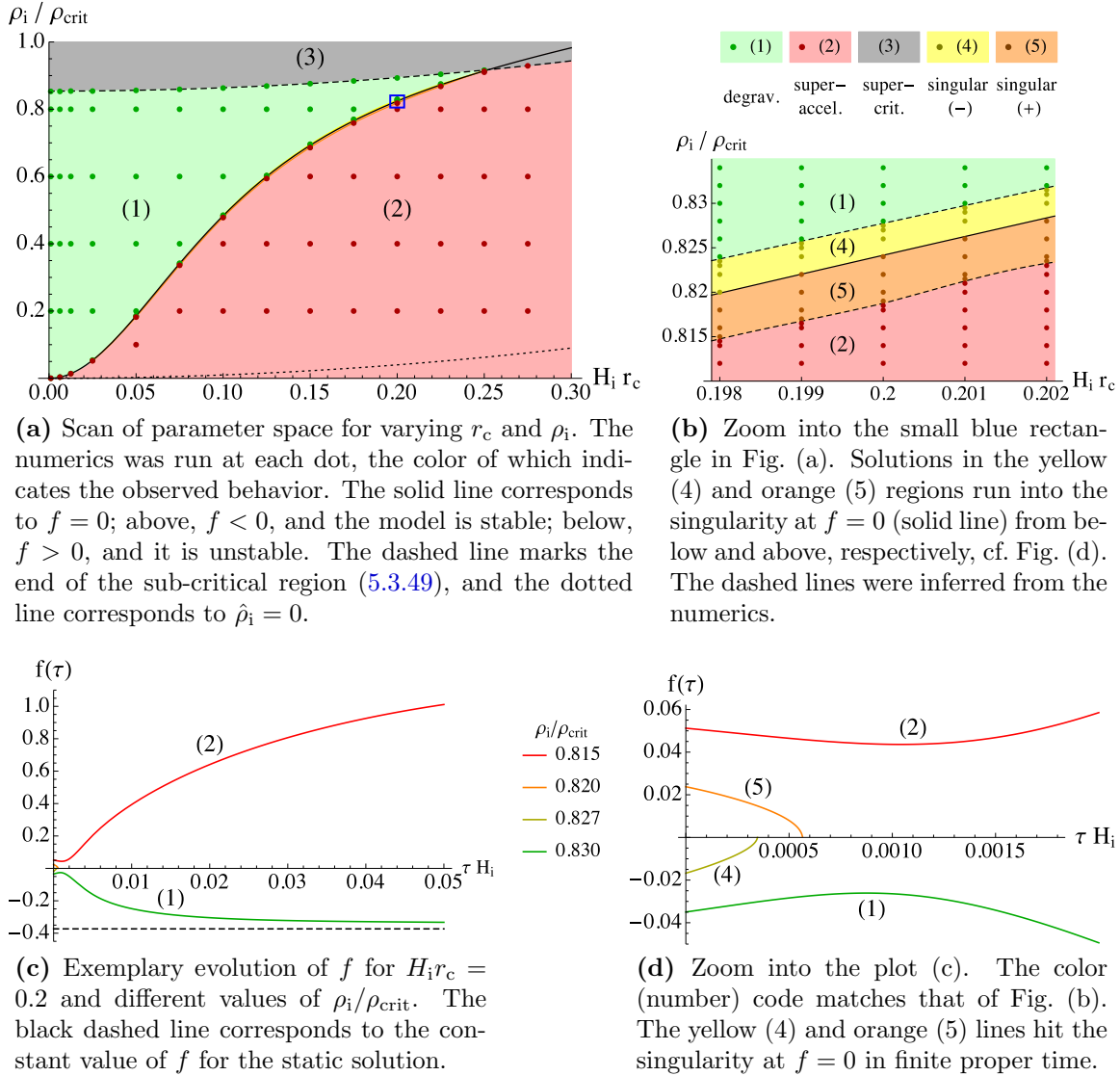


Figure 5.7: Results of the nonlinear, numerical stability analysis of the model. The parameters that are held fixed are $w = -1$, $H_i R = 0.05$ and $\sigma = 0.02R$.

Sec. 5.4.2 we will show how the stability can also be inferred analytically at the linear level.

If the initial value of f is close to 0, the time evolution dynamically approaches the singularity at $f = 0$, where H diverges. (The divergence is clear from the dynamical junction condition (5.3.27b), but was also observed numerically.) This is depicted for some representative solutions in Figs. 5.7c and 5.7d. If the initial distance of f from 0 is large enough, the singularity is avoided, and f either approaches the value predicted by the static solution (in the stable regime), or keeps growing (in the unstable regime). This means that the stable and unstable regions are separated by a physical singularity, making it impossible to dynamically evolve from one to the other.

A similar scan over $H_i r_c$ - ρ_i -space was performed for a different brane circumference ($RH_i = 0.025$), and for different matter sources—dust ($w = 0$) and radiation ($w = 1/3$)—with the same outcome: For $f < 0$, the solutions dynamically approach the general static solution of Sec. 5.3.2, while for $f > 0$ they super-accelerate.

Bulk dependence

Since we now have analytic expressions for both the criticality bound (5.3.49) as well as the stability bound (5.3.58), we can discuss the shape of the stable region in parameter space. The discussion of the phenomenological implications will be deferred to Sec. 5.5.2.

The two bounds depend on the three intrinsic brane quantities ρ/ρ_{crit} , Hr_c and HR , but also on the (interior) bulk geometry via the extrinsic curvature ingredient $\tilde{\gamma}$. To find the physical interpretation of this parameter, recall that according to (5.3.26a) $\tilde{\gamma}$ can be written as $\sqrt{e^{-2\tilde{\eta}_0} + 9H^2R^2}$, and can therefore in principle take values in the range

$$3|H|R < \tilde{\gamma} < \sqrt{1 + 9H^2R^2}. \quad (5.3.59)$$

The resulting parameter plots for the two limiting cases and one intermediate value (for fixed HR) are shown in the upper row of Fig. 5.8. The actual value of $\tilde{\gamma}$ is determined by $\tilde{\eta}_0$, which is (proportional to) the C-energy inside the regularized brane, see the discussion below Eq. (5.3.47). If $\tilde{\eta}_0 = 0$, corresponding to the upper limit in (5.3.59), there is no gravitational energy inside the ring; in this case the stable region is maximal. As $\tilde{\eta}_0$ increases, the criticality bound is pushed down due to the extra C-energy. Finally, the lower limit in (5.3.59) corresponds to $\tilde{\eta}_0 \rightarrow \infty$, i.e. an infinite amount of interior C-energy, where the green region completely disappears. This could only be achieved by allowing $\tilde{\alpha}$ to oscillate radially at arbitrarily short wavelengths, which is certainly not the situation we are interested in: we would take our effective regularization serious at length scales much below R , thus exceeding the range of validity of the EFT. We can only hope to make regularization independent statements if such effects are ignored. Therefore, the radial profile of $\tilde{\alpha}$ should be taken as smooth as possible, leading to a value of $\tilde{\eta}_0$ close to zero.

More quantitatively, if the radial variation of $\tilde{\alpha}$ is negligible, we can use (5.3.47) to relate $\tilde{\eta}_0$ to HR , as we already did for the initial conditions. This dependence is



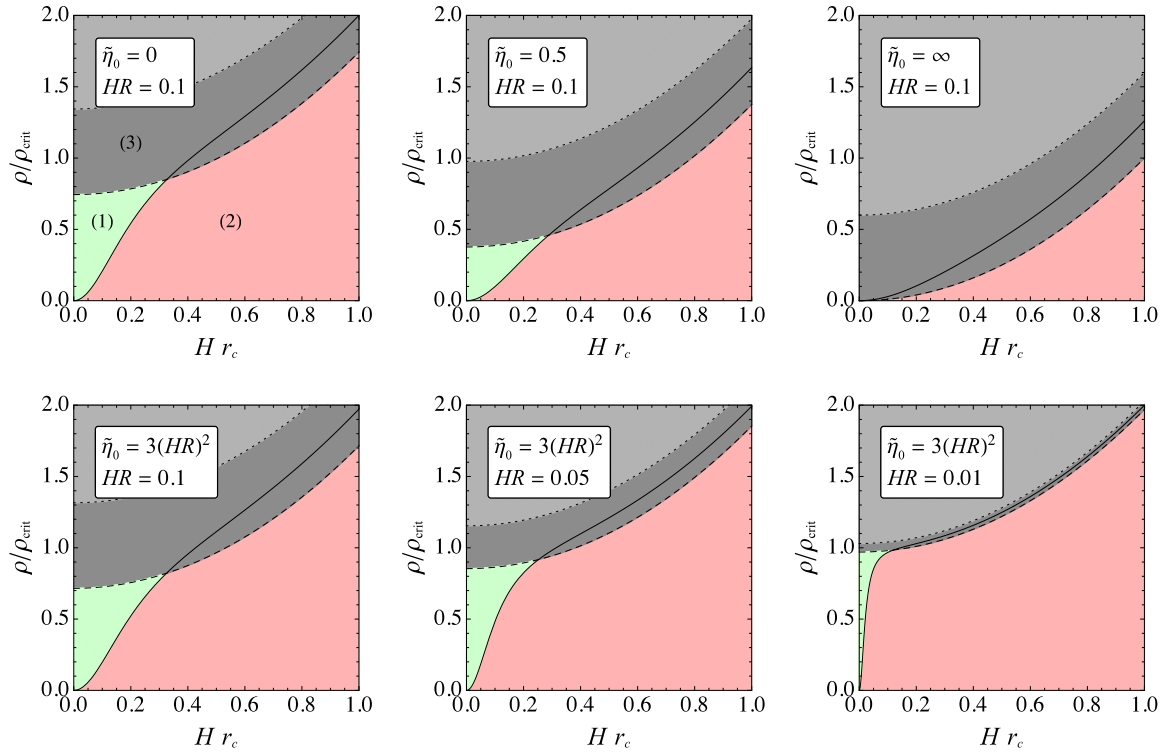


Figure 5.8: Stability portrait in full parameter space, with the same color coding as in Fig. 5.7a. The solid curves are the stability bound (5.3.58), the dashed curves show the criticality bound (5.3.49). In the upper row, the increasing C-energy $\propto \tilde{\eta}_0$ inside the brane pushes the critical line down; the lower row shows that decreasing R pushes the stability bound to the left, only leaving a very narrow stable window close to $Hr_c = 0$ as $HR \rightarrow 0$. [The dotted curves mark the beginning of the *super-critical* region, investigated in Chap. 6; the *critical* region between the dashed and dotted curves is not studied in this thesis.]

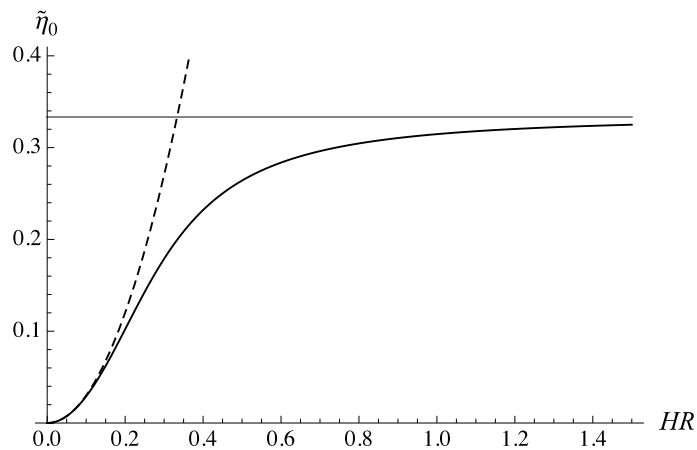


Figure 5.9: The value of $\tilde{\eta}_0$ for a flat radial profile of $\tilde{\alpha}$ is obtained by numerically solving (5.3.47). At small HR it goes like $3H^2R^2$ (dashed line), and at large HR it approaches $1/3$ (gray line).

plotted in Fig. 5.9; the maximum value of $\tilde{\eta}_0$ has thus been reduced from ∞ to $1/3$. Furthermore, the criticality and stability bounds are now independent of the fourth parameter $\tilde{\gamma}$. It still knows something about the interior geometry, but only via the well-justified assumption of having a smooth radial profile of $\tilde{\alpha}$.

In the physically relevant situation, in which the Hubble radius $1/H$ is much larger than the regularization scale R , we are close to the origin in Fig. 5.9, where

$$\tilde{\eta}_0 \sim 3(HR)^2 \quad (HR \rightarrow 0). \quad (5.3.60)$$

In this limit we are completely insensitive to any radial dependence of $\tilde{\alpha}$, apart from assuming a regular axis, Eq. (5.3.37). This assumption should clearly hold in any other regularization as well, and so we can be confident that our corresponding results should be regularization independent.

The corresponding parameter plots, for different values of HR , are shown in the lower row of Fig. 5.8. As HR decreases, the green region approaches $\rho = \rho_{\text{crit}}$ from below, and gets squeezed towards the $HR_c = 0$ axis from the right. This already looks worrisome regarding phenomenology; the final verdict will be decided in Sec. 5.5.2.

Comparison to DGP

The stability portrait of parameter space, as discussed above, has some interesting similarities with the DGP model. To see this, let us write the DGP Friedmann equation (1.4.29) as

$$\frac{\rho}{\rho_{\text{crit}}^{\text{DGP}}} = (r_c^{\text{DGP}} H)^2 - \sigma r_c^{\text{DGP}} |H|, \quad (5.3.61)$$

where the DGP crossover scale r_c^{DGP} is the one defined in (1.4.2), and the DGP ‘‘critical density’’ is³⁹

$$\rho_{\text{crit}}^{\text{DGP}} := \frac{12M_5^6}{M_4^2}. \quad (5.3.62)$$

The corresponding parameter plot is depicted in Fig. 5.10. This time, the parameter space is only one-dimensional, because the value of $\rho/\rho_{\text{crit}}^{\text{DGP}}$ is already uniquely determined for a given HR_c^{DGP} —up to the choice of sign σ . Thus, the parameter plot only consists of two separate curves, corresponding to the normal ($\sigma = -1$) and self-accelerating ($\sigma = +1$) branch. The effective energy density here simplifies to $\hat{\rho} = -\sigma r_c^{\text{DGP}} |H|$, and is thus positive (negative) on the normal (self-accelerating) branch. Furthermore, as reviewed in Sec. 1.4.2, the normal DGP branch is stable, while the self-accelerated branch suffers from a ghost instability.

In these respects, our findings generalize the DGP behavior to two codimensions, with the following alterations:

³⁹There is some ambiguity in defining the analogue of the 6D critical density $\rho_{\text{crit}} \equiv 2\pi M_6^4$: instead of using M_4 to get the right dimensionality, one could for instance use H , as was done in [NSHK15]; the qualitative discussion is, however, not affected by this.



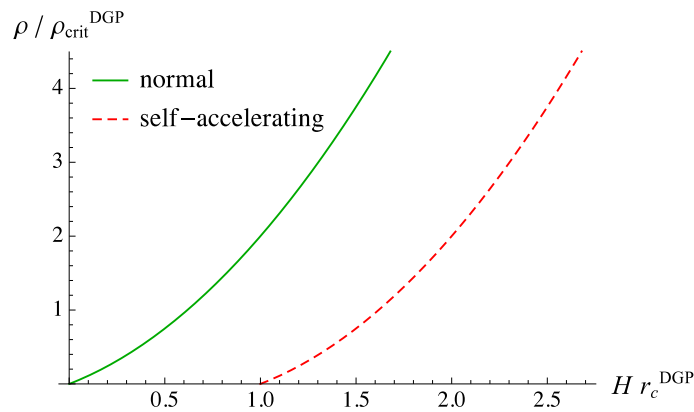


Figure 5.10: The analogue of the contour plots in Fig. 5.8 for the DGP model: Parameter space consists of two separate curves, corresponding to the (stable) normal, and the (unstable) self-accelerated branch. There is no criticality bound on ρ here, and thus no analogue of the gray regions in Fig. 5.8.

- There is an additional free parameter (corresponding to the choice of deficit angle), which makes the parameter plot two-dimensional.
- The stable and unstable regimes thereby become connected in parameter space, but are now separated by a physical singularity.
- The effective energy density $\hat{\rho}$ can initially be chosen positive in the unstable regime, and only dynamically turns negative at some later time.
- Here, the unstable behavior is present already at the (nonlinear) background level (indicated by a super-accelerating scale factor), whereas in the DGP case it is only revealed at the level of (linear) perturbations (while the background evolution is “only” self-accelerating⁴⁰).
- There is the criticality bound (5.3.49) on ρ , which is absent in DGP.

5.4 Ghost or no ghost? Resolving the tension

Note: The results presented in this section (and in the corresponding appendix below) arose in collaboration with Ludwig Eglseer and Florian Niedermann and were published in [ENS15].

The preceding section revealed an unstable behavior of codimension-two BIG at the nonlinear level. While it was possible to obtain an analytic criterion for (in)stability, the

⁴⁰This acceleration without an energy source could of course already be used as an argument against the physical relevance of the self-accelerating branch, even more so in combination with a negative $\hat{\rho}$.

actual statement that the model is (un)stable in the corresponding regions in parameter space was only inferred numerically. In this section, we will perform a linear stability analysis of the model, by studying small metric fluctuations around the static deficit angle solution discussed in Sec. 5.2.⁴¹ A priori, the instability could be intrinsically nonlinear, and thus be invisible at the linear level.⁴² But we shall see that this is not the case, and the instability already shows up linearly. Such instabilities are typically associated with ghost and/or tachyon modes, as will be briefly reviewed in Sec. 5.4.1. Then, in Sec. 5.4.2, we will use the vacuum persistence amplitude $\langle 0|0\rangle_T$ in the presence of an external source T as a technical tool to test for tachyon- and ghost modes around the deficit angle background in codimension-two BIG.

This analysis will serve several purposes: First, by truncating the field equations at linear order, it is possible to solve them analytically, and so the nonlinear but numerical detection of the instability above is complemented by a linear but *analytical* calculation. In particular, this allows us to confirm the linearized version of the stability bound (5.3.58). Furthermore, we will allow arbitrary fluctuations, and so the assumption of FRW symmetries is relaxed. Finally, we can pin down the physical origin of the instability: it is caused by a tachyonic ghost mode which exists in the corresponding region of parameter space. This is the same ghost that was already found around a Minkowski background in the literature [DR03, HHvS11]. We were able to track down the errors⁴³ made in [BHN12] which led to the wrong conclusion that the model would be linearly stable around Minkowski, thereby resolving the tension that existed in the literature. But the main new insight of our investigations is that, around the nontrivial deficit angle background, *the ghost disappears if the brane tension is not tuned unnaturally small*. This reconciles the codimension-two BIG model with the expectations from a natural EFT point of view, as will be discussed in more detail in Sec. 5.5.1.

It should be emphasized that the background geometry which is required to exorcise the ghost is only curved in the extra dimensions, while the four brane-dimensions are still completely flat. This means that in the stable region of parameter space, *the model allows for stable 4D Minkowski vacua which dynamically degravitate a CC*. It is thus a priori still a good candidate for addressing the CC problem. Section 5.5.2 is devoted to the final pressing question whether this can be achieved in a phenomenologically viable way. Unfortunately, it will be answered in the negative. The reason is that a 4D regime, which is a vital property of BIG with regard to observations, can only be achieved in the unstable region. Ultimately, *this rules out the theory for sub-critical energy densities*.

⁴¹ It should be mentioned that such a linear analysis was also performed in [KK07]. However, the ghost/tachyon issue was not addressed, and the analysis differed from ours in that the brane width was not assumed to be stabilized at the level of fluctuations. But we will find full agreement whenever this difference is irrelevant.

⁴² This was indeed the conclusion in [NSHK15], drawn under the (false) assumption that the claim of [BHN12] was correct.

⁴³ This analysis is not presented here. The interested reader is referred to [ENS15].



5.4.1 The problem with ghosts and tachyons

Let us first briefly recall the definitions of—as well as the problems associated with—tachyon and ghost instabilities. For more detailed discussions, we refer to the literature, e.g. [CHT03, Woo07, Sbi15].

A *tachyon* is a field whose *mass term* has the wrong sign. For example, consider a scalar field ϕ in 4D Minkowski with the action

$$\mathcal{L}_{\text{tach}} = -\frac{1}{2}(\partial_\mu\phi)^2 + \frac{m^2}{2}\phi^2, \quad (5.4.1)$$

corresponding to an inverted harmonic oscillator. Instead of oscillatory, this would yield exponentially growing solutions, constituting the instability. However, such a theory need not be pathological at a fundamental level. Indeed, it can easily be cured by simply adding higher order potential terms like $\propto -\phi^4$ to the Lagrangian, which would make the Hamiltonian bounded from below. In this case, the tachyon would merely be caused by expanding the theory around the unstable vacuum $\phi = 0$; the true vacuum at some $\phi_0 > 0$ would be stable, and the corresponding fluctuations would have positive mass squared, just like in the Higgs model.

On the other hand, a *ghost* instability is due to a wrong sign *kinetic term*, such as

$$\mathcal{L}_{\text{gh}} = \frac{1}{2}(\partial_\mu\phi)^2 + \frac{m^2}{2}\phi^2. \quad (5.4.2)$$

Note that here the mass term still has the wrong absolute sign, but therefore the correct (healthy) relative sign with respect to the kinetic term. Otherwise, there would again be exponentially growing solutions, and the field would be a *tachyonic ghost*. But either way, a theory with a ghost is unacceptable. This is not yet clear from the free theory (5.4.2), because the overall sign is in fact irrelevant and could be absorbed by a field redefinition. But as soon as it interacts with healthy degrees of freedom, like in the toy model

$$\mathcal{L}_{\text{gh,int}} = \frac{1}{2}(\partial_\mu\phi)^2 + \frac{m^2}{2}\phi^2 - \frac{1}{2}(\partial_\mu\psi)^2 - \frac{M^2}{2}\psi^2 - c\phi^2\psi^2, \quad (5.4.3)$$

an instability emerges, because now more and more energy can (and will) be stored in both fields without violating energy conservation. Classically, this would lead to diverging field amplitudes, which quantum-mechanically corresponds to a catastrophic production of ghost particles. This problem cannot be overcome as for a tachyon. Adding higher order terms like $(\partial_\mu\phi)^4$ would not render the Hamiltonian positive definite; alternatively, if one tried to make the prefactor of the kinetic term field dependent such that it changes sign for large enough field values, the theory would hit a strong coupling (or a classical singularity) when this term reaches zero. (This behavior was exactly encountered in the cosmological solutions close to the stability bound, studied in Sec. 5.3.) Therefore, a ghost is much more severe than a tachyon, and cannot be tolerated.

Let us finally point out a slight subtlety regarding the quantization of ghost modes: Canonical quantization of (5.4.2) leads to a Hamiltonian (neglecting vacuum energy)

$$H_{\text{gh}} = \int \frac{d^3p}{(2\pi)^3} (-\omega) a_{\mathbf{p}}^\dagger a_{\mathbf{p}}, \quad (5.4.4)$$

where $\omega := \sqrt{\mathbf{p}^2 + m^2}$. The negative sign is caused by the ghost and correctly reflects the unboundedness of H_{gh} . It might now seem like a clever idea to define $b^\dagger := a$ as the actual creation operator, because then—even though the operator (5.4.4) would keep its negative sign—the corresponding n -particle states would carry positive energy (with respect to the vacuum). Note that, in the path integral formulation, this would correspond to choosing the standard Feynman $i\epsilon$ prescription for the ghost field ϕ , while the above quantization would require the opposite, $-i\epsilon$ prescription.

But, not too surprisingly, this trick does not help at all: It results in a theory which possesses no normalizable ground state (defined by $b|0\rangle = 0$), and which contains negative norm states. In other words, this quantum theory is completely ill-defined. When testing a theory for ghost modes, it does not matter which quantization procedure is used—either an unbounded Hamiltonian, or an inconsistent quantum theory would indicate the presence of a ghost. Below, we will use the standard Feynman prescription and hence test for consistency via the vacuum persistence amplitude. The identification of a tachyon is more straightforward, as it simply amounts to the wrong relative sign of the kinetic and the effective mass term, resulting in imaginary poles of the corresponding propagator, irrespective of the quantization procedure.

5.4.2 Linear stability analysis

Note: This section is to large extent a verbatim reproduction of the corresponding section in [ENS15].

We will now consider small metric perturbations around the pure tension deficit angle background (5.2.9),

$$g_{AB} = \gamma_{AB} + h_{AB}, \quad (5.4.5)$$

with

$$\gamma_{AB} = \text{diag} [-1, 1, 1, 1, 1, c(r)^2], \quad (5.4.6)$$

where $c(r)$ is given in (5.2.9b). Note that we work in polar coordinates $X^A = (x^\mu, r, \phi)$, and the brane is located at $r = r_0 \equiv R$. All indices on first order quantities will be lowered and raised with the background metric γ_{AB} and its inverse γ^{AB} .

The question we want to answer is whether h_{AB} contains—at the linear level—unstable modes (tachyons or ghosts, or both), which can be sourced by an additional (small) on-brane source U^α_β , i.e.

$$T^{(5)\alpha}_\beta = {}^0T^{(5)\alpha}_\beta + {}^1T^{(5)\alpha}_\beta, \quad (5.4.7a)$$



with

$${}^0T^{(5)\alpha}{}_{\beta} = -\frac{\lambda}{2\pi R}\delta^{\alpha}{}_{\mu}\delta^{\mu}{}_{\beta} \quad \text{and} \quad {}^1T^{(5)\alpha}{}_{\beta} =: -\frac{1}{2}U^{\alpha}{}_{\beta}. \quad (5.4.7b)$$

Since the source is distributed in a ϕ -symmetric way, it is sufficient to consider metric perturbations that also respect this symmetry, because only those are sourced. This means that the h_{AB} are ϕ -independent functions, and that $h_{\phi\mu} = h_{\phi r} = 0$. Furthermore, we can keep the brane at the fixed coordinate position $r_0 = \text{const}$ ($= R$) without loss of generality, because a proper motion in radial direction (which is not ruled out by stabilizing the ϕ -direction), as well as a dependence of the physical brane radius on the spatial brane coordinates, can still be accomplished by allowing for nonzero $h_{\mu r}$ components. The metric perturbations therefore take the form

$$h_{AB} = \begin{pmatrix} h_{\mu\nu} & h_{\mu r} & 0 \\ h_{r\nu} & h_{rr} & 0 \\ 0 & 0 & h_{\phi\phi} \end{pmatrix} =: \begin{pmatrix} -N & h_{0j} & l' & 0 \\ h_{i0} & h_{ij} & h_{ir} & 0 \\ l' & h_{rj} & h_{rr} & 0 \\ 0 & 0 & 0 & h_{\phi\phi} \end{pmatrix}. \quad (5.4.8)$$

A prime is again shorthand for ∂_r . It is convenient to decompose the 3D spatial components of h_{AB} as

$$h_{0i} = N_i + \partial_i L, \quad (5.4.9a)$$

$$h_{ij} = D_{ij} + \partial_{(i}V_{j)} + \partial_i\partial_j B + \delta_{ij}S, \quad (5.4.9b)$$

$$h_{ir} = G'_i + \partial_i F', \quad (5.4.9c)$$

where—from a 3D point of view— D_{ij} is a transverse traceless tensor, and N_i, V_i, G_i are transverse vectors, i.e.

$$D^i{}_i = \partial_i D^i{}_j = 0, \quad (5.4.10a)$$

$$\partial_i N^i = \partial_i V^i = \partial_i G^i = 0, \quad (5.4.10b)$$

while N, l, L, B, S, F are scalars. Even though this decomposition is not manifestly Lorentz-covariant like the approach in [BHN12], it has the great advantage that it is invertible on the space of bounded functions, and so it does not introduce any “split ambiguity” (see Appendix A of [ENS15]). The reason is of course that the Laplace operator Δ_3 has no nontrivial bounded solutions, unlike the d’Alembert operator \square_4 . This makes the identification of dynamical degrees of freedom much more straightforward.

The analogous decomposition of the (ab) -components is⁴⁴

$$h_{ab} = \nabla_a \nabla_b b + \gamma_{ab} s, \quad (5.4.11)$$

⁴⁴Note that in codimension two there is no tensor part, and the vector part is absent due to ϕ -symmetry.

with ∇_a denoting the covariant derivative with respect to the background metric γ_{ab} . Explicitly, this gives

$$h^r_r = b'' + s, \quad h^\phi_\phi = \frac{c'}{c} b' + s. \quad (5.4.12)$$

Again, the relation (5.4.11) is invertible, because the Laplace operator Δ_2 has an empty kernel.

Gauge-invariant variables

The linearized bulk theory is invariant under the gauge transformations

$$\delta h_{AB} = \nabla_{(A} \xi_{B)}. \quad (5.4.13)$$

In order not to spoil the ϕ -symmetry, the ξ_A are subject to

$$\xi_\phi = 0, \quad \partial_\phi \xi_\mu = \partial_\phi \xi_r = 0. \quad (5.4.14)$$

Instead of choosing a particular gauge, we will work with a complete set of gauge-invariant variables, which can be chosen to be⁴⁵

$$D_{ij}, \quad s, \quad (5.4.15a)$$

$$J := 3S + s, \quad O := B + b - 2F, \quad (5.4.15b)$$

$$P := \dot{B} - \dot{b} - 2(L - l), \quad Q := \ddot{B} - N - 2\dot{L}, \quad (5.4.15c)$$

$$C_i := N_i - \dot{G}_i, \quad W_i := 2G_i - V_i, \quad (5.4.15d)$$

where the dot is still shorthand for ∂_t .

Since we use coordinates in which the brane is located at a fixed coordinate position ($r = r_0$), there is a further on-brane restriction on the gauge transformations,

$$\xi_r|_0 = 0, \quad (5.4.16)$$

where the subscript “0” denotes evaluation at the brane. This implies that on the brane, there exists an additional gauge invariant function, namely

$$\varphi := h^\phi_\phi|_0, \quad (5.4.17)$$

which will also appear explicitly in the junction conditions below. Physically, it corresponds to the radion field, measuring fluctuations in the size-modulus of the regularized brane.

⁴⁵One might worry that, since the definitions of P, Q and C_i involve time derivatives of some metric functions, one could be turning actual dynamical quantities into constrained ones “by hand”. However, this is not the case, as can explicitly be seen by choosing the gauge $B = b = L = G_i = 0$ (in the bulk), which is always possible.



Bulk equations of motion

The bulk vacuum Einstein equations at linear order in h_{AB} read

$$\square_6 h_{AB} + \nabla_A \nabla_B h^C_C - 2\nabla_C \nabla_{(A} h^C_{B)} + \gamma_{AB} (\nabla^C \nabla^D h_{CD} - \square_6 h^C_C) = 0, \quad (5.4.18)$$

where $\square_6 := \nabla^A \nabla_A$. These can now be projected onto the tensor, vector and scalar components, according to the decomposition of the metric perturbations (5.4.9). Let us emphasize that this projection only requires to divide by Laplace operators, which does not introduce any homogeneous functions in the resulting equations. This is in contrast to the 4D covariant split adopted in [BHN12], where one has to divide by d'Alembert operators, making the analysis much more subtle and complicated (see Appendix A of [ENS15]).

In the following, we omit all equations which are redundant due to the Bianchi identities. However, since we are particularly interested in distinguishing dynamical from constrained quantities, we only omit those components of (5.4.18) which appear in the Bianchi identities without time-derivatives. In other words, we always keep the stronger equations. Explicitly, we drop the $(ij)^{(V)}$, $(0i)^{(L)}$, $(ir)^{(F)}$ and (rr) equations, where the superscripts refer to the projections according to (5.4.9).

The resulting complete set of bulk equations of motion, expressed in terms of the gauge invariant variables (5.4.15) is:

- Tensor:

$$\boxed{\square_6 D_{ij} = 0} \quad (5.4.19)$$

This is simply the (ij) -component of (5.4.18), projected onto the tensor part. It shows that D_{ij} is dynamical, carrying two independent DOF.

- Vector:

$$\boxed{\Delta_3 W_i + 2\dot{C}_i = 0} \quad (5.4.20a)$$

$$\boxed{\square_6 C_i = 0} \quad (5.4.20b)$$

The first one is the vector-projected (ir) -bulk equation, showing that W_i is constrained. The second one is the vector-projection of the $(0i)$ -bulk equation, with W_i eliminated by means of the constraint. Thus, C_i is dynamical, carrying two DOF.

- Scalar:

$$\boxed{(2\Delta_3 + 3\Delta_2) J + 4\Delta_3 s + 3\Delta_2 \Delta_3 O = 0} \quad (5.4.21a)$$

$$\boxed{2\dot{J} + \Delta_3 (\dot{O} + P) = 0} \quad (5.4.21b)$$

$$\boxed{J - s - Q + \Delta_3 O + \dot{P} = 0} \quad (5.4.21c)$$

$$\boxed{\square_6 J = 0, \quad \square_6 s = 0} \quad (5.4.21d)$$

The first equation is the (00) -component of (5.4.18), the second one is its $(0r)$ -component (already integrated once in r , requiring fall-off conditions in the bulk)

and the third one is the difference of the $(\phi\phi)$ - and the (rr) -equations (also integrated in r). These three are constraint equations that can—for instance—be solved for O, P and Q . Plugging these solutions into the two scalar-projected (ij) -components of (5.4.18), and taking suitable linear combinations, yields the two dynamical equations (5.4.21d) for J and s .

In summary, there are 6 dynamical DOF (2 vector, 2 tensor and 2 scalar), all of which satisfy the 6D wave equation in the bulk. This is the correct number of propagating DOF in six-dimensional GR with azimuthal symmetry. (Without this symmetry, there would be 3 additional DOF.) Below, we will also see that all of these 6 DOF can indeed be sourced.⁴⁶

Junction conditions

It remains to derive the linearized junction conditions (5.3.22). To this end, it is useful to perform a 3D tensor-vector-scalar decomposition of the (perturbation of the) energy-momentum tensor, analogous to (5.4.9):

$$U_{0i} = U_i^{(N)} + \partial_i U^{(L)}, \quad (5.4.22a)$$

$$U_{ij} = U_{ij}^{(D)} + \partial_{(i} U_{j)}^{(V)} + \partial_i \partial_j U^{(B)} + \delta_{ij} U^{(S)}. \quad (5.4.22b)$$

Linearized energy conservation then decomposes into

$$-\dot{U}_{00} + \Delta_3 U^{(L)} = -\frac{\lambda}{2\pi R} \dot{\varphi}, \quad (5.4.23a)$$

$$-\dot{U}^{(L)} + \Delta_3 U^{(B)} + U^{(S)} = -\frac{\lambda}{2\pi R} \varphi, \quad (5.4.23b)$$

$$-2\dot{U}_i^{(N)} + \Delta_3 U_i^{(V)} = 0, \quad (5.4.23c)$$

while $U_{ij}^{(D)}$ and $U_{\phi\phi}$ are unconstrained.

A straightforward calculation gives the following nonvanishing components of the extrinsic curvature tensor K^α_β at linear order around the deficit angle background (5.4.6):

$${}^1 K^\mu_\nu = \frac{1}{2} (\partial_r h^\mu_\nu - \partial^\mu h_{\nu r} - \partial_\nu h^\mu_r)|_0, \quad (5.4.24a)$$

$${}^1 K^\phi_\phi = \frac{1}{2} \left(\partial_r h^\phi_\phi - \frac{c'}{c} h^r_r \right) \Big|_0. \quad (5.4.24b)$$

Plugging this (and the linearized 5D Einstein tensor) into (5.3.22), projecting onto the desired components, and simplifying the BIG terms by means of the bulk equations in the limit $r \rightarrow r_0 (= R)$, yields the following junction conditions in the $(\mu\nu)$ -sector:

⁴⁶This contradicts the claim in [BHN12], where only 5 sourced DOF were found, allowing to argue that the ghost mode (here s , see below) would not be dynamical. This wrong conclusion was reached by employing a gauge transformation which is in fact not allowed by the requirement of SO(2) symmetry, see Appendix A in [ENS15].



- Tensor:

$$\boxed{M_6^4 [D'_{ij}] + M_5^3 \square_4 D_{ij}|_0 = U_{ij}^{(D)}} \quad (5.4.25)$$

- Vector:

$$\boxed{M_6^4 [C'_i] + M_5^3 \square_4 C_i|_0 = U_i^{(N)}} \quad (5.4.26)$$

- Scalar (recall that δ denotes the deficit angle):

$$M_6^4 \left([J'] + \frac{\delta}{2\pi R} \varphi \right) + M_5^3 \square_4 J|_0 = -U^\mu{}_\mu + 3U^{(S)} \quad (5.4.27a)$$

$$4M_6^4 \left([s'] + \frac{\delta}{2\pi R} \varphi \right) + M_5^3 \square_4 (s|_0 + 3\varphi) = -U^\mu{}_\mu + 3U^\phi{}_\phi \quad (5.4.27b)$$

These last two equations are not yet sufficient to solve for J and s , because they contain φ as a third unknown on-brane function. It is determined by the only remaining $(\phi\phi)$ -junction condition. After using the jump of the r -derivative of the bulk equation (5.4.21c), it takes the simple form

$$M_6^4 \square_4 [b'] + M_5^3 \square_4 s|_0 = U^\phi{}_\phi. \quad (5.4.28)$$

Furthermore, the second equation in (5.4.12) shows that continuity of $h^\phi{}_\phi$ implies

$$[b'] = \left[\frac{c}{c'} \right] (\varphi - s|_0) = \frac{R\delta}{2\pi - \delta} (\varphi - s|_0). \quad (5.4.29)$$

Using this in (5.4.28) yields the desired equation determining φ ,

$$\frac{R\delta}{2\pi - \delta} M_6^4 \square_4 (\varphi - s|_0) + M_5^3 \square_4 s|_0 = U^\phi{}_\phi, \quad (5.4.30)$$

thereby closing the system of equations of motion for all gauge invariant variables.

[For completeness, let us note that the jump in the r -derivative of the constrained scalar O is determined by the $(ij)^{(B)}$ component of Israel's junction conditions. After using again the bulk equations, as well as (5.4.29) and the fact that $[H'] = 0$ (due to continuity of the metric), it simplifies to

$$M_6^4 \left\{ [O'] + \frac{R\delta}{2\pi - \delta} (s|_0 - \varphi) \right\} + M_5^3 \left(\frac{J - s}{3} - Q + \varphi \right) \Big|_0 = U^{(B)}, \quad (5.4.31)$$

where an overall Δ_3 was dropped. The jumps in the r -derivative of all the remaining constrained gauge-invariant quantities (W_i, P and Q) can readily be obtained from the r -derivatives of the corresponding bulk equations.]

As a consistency check, we explicitly verified that all the junction conditions, together with the bulk equations, imply the energy conservation equations (5.4.23), as is guaranteed by the Gauss-Codazzi equations.

As discussed in Sec. 5.2, we will now require the proper circumference of the regularized brane to be constant, implying

$$\varphi = 0. \quad (5.4.32)$$

(The case without stabilization is considered in Appendix 5.A.) The appropriate U_ϕ^ϕ which is needed to achieve this stabilization is then determined by Eq. (5.4.30), which now simplifies to

$$U_\phi^\phi = (M_5^3 - \beta R M_6^4) \square_4 s|_0, \quad \beta := \frac{\delta}{2\pi - \delta}. \quad (5.4.33)$$

The junction conditions for the two dynamical scalars then become

$$M_6^4 [J'] + M_5^3 \square_4 J|_0 = -U_\mu^\mu + 3U^{(S)}, \quad (5.4.34a)$$

$$4M_6^4 [s'] - 2f_0 M_5^3 \square_4 s|_0 = -U_\mu^\mu, \quad (5.4.34b)$$

where we defined the dimensionless constants

$$f_0 := 1 - \frac{3\beta}{4\alpha}, \quad \alpha := \frac{M_5^3}{2R M_6^4} \equiv \frac{r_c^2}{6R^2}. \quad (5.4.35)$$

All the junction conditions, viz. (5.4.25), (5.4.26) and (5.4.34), now share the same, DGP-like structure. The only (but crucial) difference is that the BIG term in the junction condition for s comes with a negative sign if $f_0 > 0$. Note that this f_0 is nothing but the static (i.e. background) limit of the function f we found in the nonlinear cosmology analysis in Sec. 5.3. Therefore, one might already suspect that the scalar mode s will be a ghost in that parameter regime. We will now show that this is indeed the case.

Tachyonic ghost

We will use the vacuum to vacuum transition probability (in presence of an external source) as a diagnostic tool to probe for ghost modes. For the linear theory, it is given by

$$|\langle 0|0\rangle_T|^2 = \exp[-\text{Im}(\mathcal{A})], \quad (5.4.36)$$

with

$$\mathcal{A} := R \int d^4x d\phi \, {}^1T_{\alpha\beta}^{(5)} h^{\alpha\beta}|_0. \quad (5.4.37)$$

Here, $h^{\alpha\beta}|_0$ should be evaluated at the classical solution in the presence of $T_{\alpha\beta}$, and poles in the propagators should be treated with the standard Feynman prescription. If the probability (5.4.36) is larger than one (or, equivalently, the imaginary part of \mathcal{A} is negative) then unitarity is violated,⁴⁷ implying the existence of a ghost mode.

⁴⁷As discussed in Sec. 5.4.1, this unitarity violation does not mean that the theory cannot be consistently quantized. Unitarity can indeed be restored by choosing a non-standard $i\epsilon$ prescription for



Since the ghost lies within the scalar sector, we can limit ourselves to a source with vanishing tensor- and vector components. Using the bulk equations to eliminate all constrained quantities, the source coupling term can—using integration by parts and energy conservation (5.4.23)—then be brought into the form

$$\mathcal{A} = \frac{\pi R}{3} \int d^4x \left[2 (U^\mu{}_\mu - 3U^{(S)}) J|_0 + U^\mu{}_\mu s|_0 \right]. \quad (5.4.38)$$

Furthermore, it will be sufficient to consider a source satisfying $U^\mu{}_\mu = 3U^{(S)}$, for which only s gets excited (i.e. J can consistently be set to zero) and the coupling term (5.4.37) simply reads

$$\mathcal{A}^{(s)} = \frac{\pi R}{3} \int d^4x U^\mu{}_\mu s|_0. \quad (5.4.39)$$

In the following, it will be convenient to work in 4D Fourier space, i.e. we introduce

$$\hat{s}(p, r) := \int d^4x e^{-ip \cdot x} s(x, r) \quad (p \cdot x := p_\mu x^\mu). \quad (5.4.40)$$

The bulk equation (5.4.21d) then becomes

$$(-p^2 + \Delta_2) \hat{s} = 0 \quad (p^2 := p_\mu p^\mu), \quad (5.4.41)$$

where the covariant 2D Laplace operator with respect to the deficit angle background geometry (5.4.6) reads (for ϕ -symmetric fields, as we are considering)

$$\Delta_2 = \partial_r^2 + \frac{c'}{c} \partial_r = \begin{cases} \partial_r^2 + \frac{1}{r} \partial_r & (r < r_0) \\ \partial_r^2 + \frac{1}{r + \beta r_0} \partial_r & (r > r_0). \end{cases} \quad (5.4.42)$$

The most general solution of (5.4.41), which is continuous across the brane, regular at the origin, and falls off at radial infinity,⁴⁸ is given by

$$\hat{s}(p, r) = \begin{cases} \frac{I_0(r\sqrt{p^2})}{I_0(r_0\sqrt{p^2})} \hat{s}|_0 & (r < r_0) \\ \frac{K_0(\bar{r}\sqrt{p^2})}{K_0(\bar{r}_0\sqrt{p^2})} \hat{s}|_0 & (r > r_0), \end{cases} \quad (5.4.43)$$

the ghost mode, reversing the sign of the ghost-residue in the propagator. However, this leads to a Hamiltonian which is not bounded from below, which—as soon as interactions are included—causes a catastrophic instability. This instability is already present at the classical level, and has nothing to do with quantizing the theory. In any case, a ghost shows that the theory is pathological and thus useless.

⁴⁸Furthermore, for $p^2 < 0$, i.e. for modes which correspond to waves propagating in the bulk, one can check that the solution (5.4.43) corresponds to solely *outgoing* radial waves, if the retarded prescription $\text{Im}(\omega) = +\epsilon$ is used, as would be appropriate for a classical calculation. This is an important consistency requirement as the brane is the only source of gravitational waves in the bulk. Note, however, that below we will use the Feynman prescription $\text{Im}(\omega^2) = +\epsilon$, since we are calculating the vacuum amplitude in the quantum theory.

where I_n and K_n are the modified Bessel functions of the first and second kind, respectively, and $\bar{r} := r + \beta r_0$. A priori, the solution is only defined for $p^2 > 0$. We find its analytic continuation by choosing the branch cut of the square root in the standard way, i.e. along the negative real axis.

Plugging (5.4.43) into the junction condition (5.4.34b) yields

$$\frac{4M_6^4}{R} Z(p) \hat{s}|_0 = -\hat{U}^\mu{}_\mu, \quad (5.4.44)$$

with the inverse s -propagator

$$Z(p) := \alpha f_0 z^2 - zY(z), \quad (5.4.45a)$$

$$Y(z) := \frac{I_1(z)}{I_0(z)} + \frac{K_1[(1+\beta)z]}{K_0[(1+\beta)z]}, \quad (5.4.45b)$$

where we introduced the dimensionless variable

$$z := R\sqrt{p^2} \equiv R\sqrt{\mathbf{p}^2 - \omega^2}. \quad (5.4.46)$$

The source coupling term (5.4.39) finally becomes

$$\mathcal{A}^{(s)} = -\frac{R^2}{24M_6^4} \int \frac{d^4p}{(2\pi)^3} \left| \hat{U}^\mu{}_\mu(p) \right|^2 \frac{1}{Z(p)}, \quad (5.4.47)$$

where the branch cuts and poles in the ω -integration are surrounded according to the Feynman prescription, i.e. $\text{Im}(\omega^2) = +\epsilon$ along the integration contour. The analytic structure of Z^{-1} , for some fixed value $|\mathbf{p}| \neq 0$ is shown in Fig. 5.11a. The branch cuts along the real axis can be interpreted as a continuum of gapless Kaluza Klein modes, like in the DGP model [DHK07]. They are also present in pure 6D GR with a cylindrical source, and are thus not expected to cause any problems. Below, we will confirm this expectation.

For $f_0 > 0$, however, there are additional isolated poles at

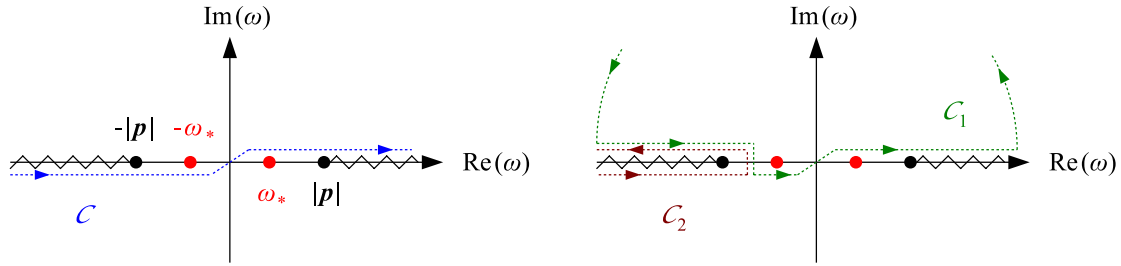
$$\omega = \pm \sqrt{\mathbf{p}^2 - m_*^2} =: \pm \omega_*, \quad (5.4.48)$$

where m_* is given by $m_* = z_*/R > 0$, with z_* being the solution of

$$\alpha f_0 z_* = \frac{I_1(z_*)}{I_0(z_*)} + \frac{K_1[(1+\beta)z_*]}{K_0[(1+\beta)z_*]}. \quad (5.4.49)$$

The right hand side of this equation, i.e. the function $Y(z)$ is plotted in Fig. 5.12, and shows that there is indeed a solution $z_* > 0$ if and only if $f_0 > 0$ (irrespective of the value of β). The negative sign of the mass term in the dispersion relation (5.4.48) shows that this pole in the propagator of the scalar mode s is a tachyon, implying the existence of exponentially growing solutions for $s|_0(t)$. Below, we will show that it is also a ghost, in agreement with the Minkowski result in [DR03, HHvS11], but





(a) The contour \mathcal{C} (dotted blue line) indicates the Feynman-contour of integration.

(b) Decomposition of \mathcal{C} into a closed path around one of the poles (\mathcal{C}_1) and a branch cut contribution (\mathcal{C}_2). The half circle, which closes the contour at infinity, does not contribute to $\mathcal{A}^{(s)}$.

Figure 5.11: Analytic structure of the $\omega \equiv p^0$ dependence of the s -propagator $1/Z(p)$, see Eq. (5.4.45), for some fixed value $|\mathbf{p}| \neq 0$ and $f_0 > 0$. The poles at $\pm\omega_*$ correspond to the tachyonic ghost. For $|\mathbf{p}| > m_*$ they lie on the real axis, between the origin and the branch cuts starting at the poles at $\pm|\mathbf{p}|$; for $|\mathbf{p}| < m_*$ they lie on the imaginary axis. For $f_0 < 0$ these poles are absent.

generalizing it to a background with nonzero deficit angle in the parameter regime where $f_0 > 0$.

Even though (5.4.49) cannot be solved analytically, one can obtain the asymptotic formula for m_* in the physically relevant limit $\alpha \rightarrow \infty$ (i.e. $R \ll M_5^3/M_6^4$) by expanding the Bessel function for small arguments, yielding

$$m_*^2 \sim \frac{1 - \delta/2\pi}{R^2 f_0 \alpha \ln(\alpha)} \quad (\alpha \rightarrow \infty). \quad (5.4.50)$$

Note that for $\delta = 0$ (and neglecting the small logarithmic correction) this agrees with the tachyon mass derived in [DR03, HHvS11], viz. $m_* \sim M_6^2/M_4$. However, the non-trivial deficit angle background gives rise to an important modification: as δ increases, f_0 approaches zero and Fig. 5.12 shows that the tachyon then becomes infinitely heavy, as the intersection moves to larger values of z . When the threshold $f_0 = 0$ is crossed, the pole finally disappears completely.

To disentangle the tachyon and branch cut contribution to $\mathcal{A}^{(s)}$, we consider two independent integration contours in the complex ω -plane: a closed path \mathcal{C}_1 encircling one of the poles, and another open path \mathcal{C}_2 running along both sides of the branch cut in opposite directions, see Fig. 5.11b. It can be shown that the half circle in \mathcal{C}_1 does not contribute to the amplitude.⁴⁹ It thus follows that the original integration along \mathcal{C} can be decomposed into the sum of \mathcal{C}_1 and \mathcal{C}_2 .

⁴⁹In Fig. 5.11b we only show the case when the contour has to be closed in the upper half-plane, in which the pole and branch cut on the negative real axis contribute. But one can easily check that the other case gives exactly the same result.

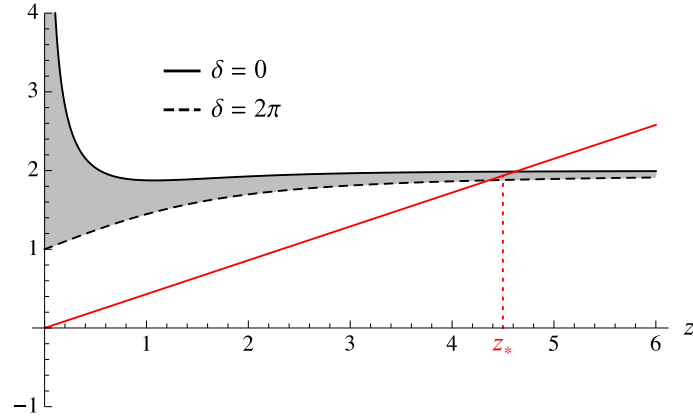


Figure 5.12: Graph of the right-hand side of Eq. (5.4.49), which determines the ghost mass $m_* \equiv z_*/R$. For values of the deficit angle δ between 0 and 2π , the curve lies in the shaded region. It always goes to 2 as $z \rightarrow \infty$. The red line corresponds to the left-hand side of the equation, for some positive value of f_0 . For $f_0 < 0$ its slope is negative and there is no solution z_* .

As for the branch cut contour \mathcal{C}_2 , we checked numerically that—at least for an ω -independent source—its contribution to the imaginary part of $\mathcal{A}^{(s)}$ is positive, see Fig. 5.13. Hence, the branch cut contains no ghost modes.

The contribution of \mathcal{C}_1 to the amplitude is proportional to the sum of the residues of all enclosed poles. Therefore, to show that the tachyon—in the parameter region where it exists—is also a ghost, let us investigate the residue of this pole for the case $|\mathbf{p}| > m_*$, i.e. when the poles lie on the real axis (as in Fig. 5.11a). [For momenta $|\mathbf{p}| < m_*$, the pole lies on the imaginary axis and only contributes to the real part of $\mathcal{A}^{(s)}$, which does not affect the vacuum transition probability (5.4.36). Physically speaking, the ghost can only be excited for momenta larger than its mass.] A straightforward calculation gives

$$\text{Res} \left(\frac{1}{Z(p)}, \omega = \pm \omega_* \right) = \mp \frac{1}{\omega_* R^2} \left[2\alpha f_0 + \beta + \left(\frac{I_1}{I_0} \right)^2 - (1 + \beta) \left(\frac{K_1}{K_0} \right)^2 \right]^{-1}. \quad (5.4.51)$$

Here, the arguments of the Bessel I and K functions are z_* and $(1 + \beta)z_*$, respectively. It turns out that the expression in square brackets, when evaluated numerically, is always positive. However, we did not succeed in extracting this information analytically, and therefore Fig. 5.14 shows the contour plot of the residue—leaving out the overall factor $\mp 1/\omega_* R^2$ —as a function of the two independent model parameters $\delta/2\pi \equiv \beta/(1 + \beta)$ and $f_0 \equiv 1 - 3\beta/4\alpha$. For a non-negative, sub-critical tension we have $\delta \in [0, 2\pi)$ and $f_0 \leq 1$. Furthermore, as already discussed, the ghost pole only exists for $f_0 > 0$. Thus, the plot in Fig. 5.14 covers the whole relevant parameter space, and one can see that the expression in square brackets is indeed always positive.



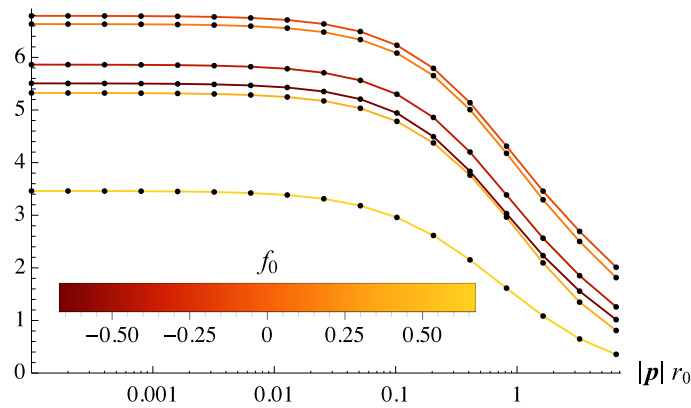


Figure 5.13: Numerical evaluation of the branch-cut contribution, viz. $-\text{Im} \left[R \int_{C_2} d\omega Z^{-1}(\omega, \mathbf{p}) \right]$. The positive values imply that there are no ghost modes, irrespective of the sign of f_0 . Here, the deficit angle was chosen as $\delta = \pi$, but other values do not change this result.

One can easily check that this result leads to a negative⁵⁰ imaginary part of $\mathcal{A}^{(s)}$, corresponding to a ghost. This ghost mode can be excited for 3-momenta $|\mathbf{p}|$ larger than the ghost mass m_* . However, since the ghost is also a tachyon, which can be excited with arbitrarily low momenta, the linearized theory is completely unstable (for all momenta), if $f_0 > 0$.

If, on the other hand, $f_0 < 0$, the pole (and thus the tachyonic ghost) is absent and the model is stable. The stable and unstable regimes are visualized in a parameter plot in Fig. 5.15. It also shows that the tachyon mass diverges as the borderline $f_0 = 0$ is approached. Thus, the tachyonic instability is more severe close to the stability bound.

5.5 Discussion

The main result of the two preceding sections can be summarized as follows: The (radially stabilized, sub-critical) codimension-two BIG model is stable if and only if the function

$$f \equiv 1 - \frac{9R^2}{2r_c^2} \left(\frac{1}{\gamma} - \frac{1}{\tilde{\gamma}} \right)$$

is negative. In this case, the model dynamically degravitates all FRW matter and approaches the general static solution presented in Sec. 5.3.2 via the emission of ER waves into the bulk. If f is positive, the theory is unstable, leading to a pathological super-acceleration with negative effective energy on the brane. The instability is caused

⁵⁰The sign from the overall factor in (5.4.51) is compensated by the one from the negative/positive orientation when encircling the pole at $\pm\omega_*$, cf. Fig. 5.11b. Then, there is one more minus sign from the explicit overall factor in (5.4.47).

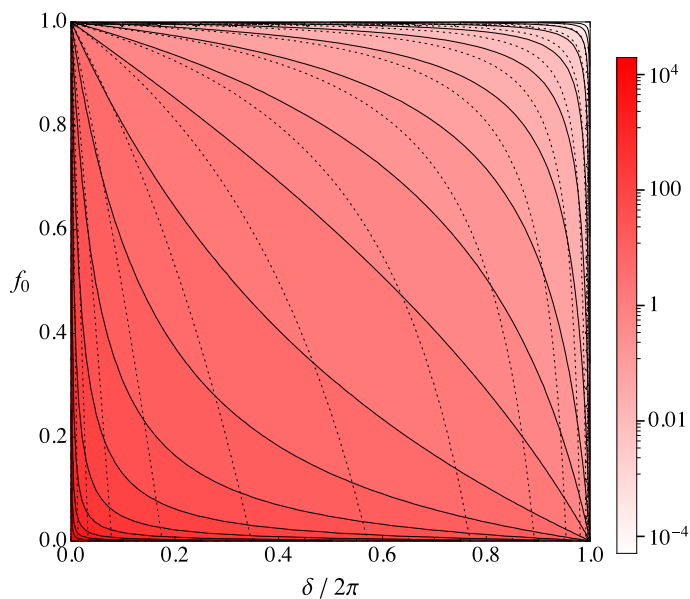


Figure 5.14: Contour plot of the ghost residue (5.4.51) times $\mp \omega_* R^2$, as a function of the deficit angle δ and f_0 as defined in (5.4.35), showing that it is indeed positive in the whole parameter space (in which the pole at ω_* exists, i.e. for $f_0 > 0$). The dotted lines are lines of constant α , which $\rightarrow 0$ on the left and $\rightarrow \infty$ on the right.

by a tachyonic ghost mode, which only exists for $f > 0$.⁵¹

Let us now discuss the physical implications of these findings. First, in Sec. 5.5.1, we will discuss how our results reconcile codimension-two BIG with the expectation of a healthy theory based on natural EFT arguments. Then, Sec. 5.5.2 finally answers the question whether the model can pass phenomenological tests in the ghost-free regime and thus offer a potential solution to the CC problem.

5.5.1 EFT perspective

As already discussed in the introduction to this chapter, the appearance of a ghost instability is at first unexpected, because the model can be thought of as the low energy EFT of some healthy underlying UV theory. Indeed, this was the main physical argument in [BHN12] for questioning the existence of the ghost altogether. The argument is that the BIG terms should always be included from a natural EFT point of view; so how can a healthy microscopic theory be pathological, only because it is reduced to an EFT at low energies?

⁵¹Strictly speaking, the ghost analysis was only performed at the linear level around the static deficit angle solution, where f reduces to $f_0 \equiv 1 - 3\beta/(4\alpha)$. The difference to f corresponds to higher order corrections $\propto H$, which cannot be seen linearly. But there is no reason to doubt that the numerically observed pathology for $H \neq 0$, and for other matter sources than a pure CC, is due to the same ghost pathology.



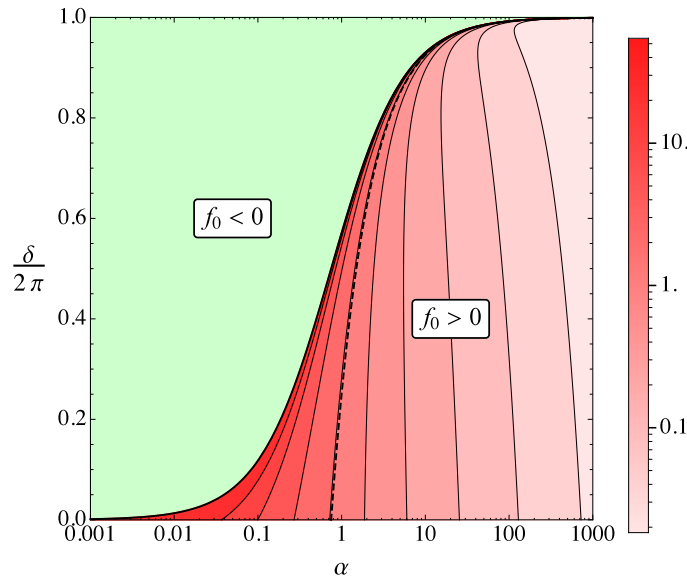


Figure 5.15: Stability of the linearized theory is determined by the two model parameters $\alpha \equiv M_5^3/(2M_6^4 R)$ and deficit angle δ . The tachyonic ghost only exists in the red region ($f > 0$), where the contours indicate its mass (in units of $1/R$). The dashed line corresponds to the stability bound in the alternative regularization of [NSHK15].

Now we saw that the conclusion of [BHN12] was erroneous, and that the ghost *is* present around a Minkowski background: f_0 is always positive for $\delta = 0$ ($\Leftrightarrow \lambda = 0$), cf. Fig. 5.15. But since we extended the ghost analysis to nontrivial background geometries ($\delta \neq 0$), we are now able to present the resolution of the EFT puzzle: Generically, for a truly natural EFT, not only the BIG terms should be included, but also the brane tension λ , cf. Eq. (5.0.1). But if λ is large enough, the stability bound is eventually crossed and the model is in the healthy regime, as can be seen from Fig. 5.15. In other words, all previous ghost analyses on Minkowski worked under the unnatural assumption that, while the induced gravity scale M_4 was allowed to be large, the tension λ was fine-tuned exactly to zero.

To be more quantitative, let us express the (linearized) stability bound $f_0 < 0$ in terms of the parameters M_6, R, M_4, λ , which define the EFT action (5.0.1):

$$\boxed{\frac{1}{\lambda} < \frac{3R^2}{2M_4^2} + \frac{1}{2\pi M_6^4}}. \quad (5.5.1)$$

In this form, it is obvious that the model is always stable if the emergent quantities R, M_4, λ are all of the same order, as could be expected in a natural EFT. Note that this statement holds for any value of the fundamental scale M_6 . No fine-tuning is required to arrive at a healthy low energy theory. On the contrary, if the tension λ is tuned towards zero, but M_4 is kept constant, the bound gets violated, reproducing the Minkowski ghost result.

It should be noted that the same also holds for the brane radius R : if solely R is

decreased, the bound also gets violated at some point, because $\lambda < 2\pi M_6^4$ in the sub-critical regime. But again, naturally one would expect R not to be much smaller than $\lambda^{-1/4}$, because the zero-point fluctuations of the brane thickness (radion) should give a contribution $\sim R^{-4}$ to the tension (or brane vacuum energy), driving the EFT back into the stable region.

5.5.2 Phenomenology

Having completed the ghost exorcism in great detail, we can now turn to the crucial question whether the model, in the ghost-free regime, can survive phenomenological tests.

The key question is if the BIG mechanism can successfully be used to achieve an approximate 4D regime, like in the DGP model. For instance, we can ask what the (linearized) gravitational field of a point mass on the brane would look like. In this case, the only nonvanishing energy momentum component is

$${}^1T_{00}^{(5)} = \frac{m}{2\pi R} \delta^{(3)}(\mathbf{x}), \quad (5.5.2)$$

with the factor $2\pi R$ included such that m is the 4D mass of the point source. This source only excites static scalar modes,⁵² and gives rise to the on-brane Newtonian potential

$$\Phi \equiv -\frac{1}{2}h_{00}|_0 \equiv \frac{1}{2}N|_0 = -\frac{1}{6}(2J + s)|_0, \quad (5.5.3)$$

where we used the (static) field equations (5.4.21) (in the on-brane limit). The solution for J can be obtained just like the one for s before, ultimately yielding ($x := |\mathbf{x}|$)

$$\Phi(x) = -\frac{m}{8\pi M_4^2 x} \times \mu(x). \quad (5.5.4)$$

The first factor is the standard 4D GR result scaling like $\propto 1/x$, and the modification is encoded in the (dimensionless) function

$$\mu(x) := \frac{2}{3\pi} \int_0^\infty dz \sin\left(z \frac{x}{R}\right) \left[\frac{4}{z + Y(z)/2\alpha} - \frac{1}{f_0 z - Y(z)/\alpha} \right], \quad (5.5.5)$$

with $Y(z)$ as defined in (5.4.45b), and still $f_0 \equiv 1 - 3\beta/4\alpha$.

As a first consistency check, we notice that for $\beta = \text{const}$ and $\alpha \rightarrow \infty$ (i.e. $M_4 \gg RM_6$) $\mu \rightarrow 1$, and so we recover the correct 4D result. However, we already know from the ghost analysis that in this limit one *always* ends up in the pathological regime, cf. Fig. 5.15. But this is not yet the end of the story. To be compatible with current experimental bounds, it is sufficient for the deviations from the 4D force law only to kick in at large enough distances, such that the theory passes high precision solar system measurements, like Lunar Laser Ranging (LLR) [AGK09, and references therein].

⁵²Note that we are hereby effectively fixing a gauge, implying that N becomes observable.



Therefore, in order to decide on the success of the theory we should determine the length scale at which the deviations from the $1/x$ scaling first occur. The ultimate question is whether this distance scale, for given model parameters, can be sufficiently large within the stable region in parameter space.

To determine the physical crossover scale, note that for small (large) x , the integrand in (5.5.5) mainly contributes at large (small) z . Using the asymptotic expansion of the integrand in the relevant regime, and performing the integral⁵³ then yields

$$\mu(x) \sim \frac{\beta - \alpha}{3\beta/4 - \alpha} \quad (x \rightarrow 0), \quad (5.5.6a)$$

$$\mu(x) \sim 3\alpha(1 + \beta) \left(\frac{R}{x}\right)^2 \quad (x \rightarrow \infty). \quad (5.5.6b)$$

Thus, we indeed find a 4D Newtonian potential $\propto 1/x$ at small length scales,⁵⁴ and a 6D scaling $\propto 1/x^3$ at large scales. There can also be an intermediate regime, where

$$\mu(x) \sim \frac{n\alpha}{3\pi} \left(\frac{R}{x}\right), \quad n \in \{1, 2, 8, 9, 16\}, \quad (5.5.7)$$

corresponding to a 5D scaling $\propto 1/x^2$ of Φ . The concrete value of n depends on the parameters α, β , but it only takes values in the range 1 to 16.⁵⁵ Physically, this 5D regime can be caused by two different effects: One is due to our regularization, where from a 6D perspective we are considering not a point, but a ring source of radius R . From far away, it looks like a point, but from close enough it eventually becomes a one-dimensional line source. This only happens for $x \lesssim R$, meaning that we become sensitive to the (regularization-dependent) microscopic details, which we do not trust anyway. Therefore, these cases are not relevant for our purposes. The other one is realized for $\beta \rightarrow \infty$, and is due to the fact that in this limit the deficit angle approaches 2π , and so one of the exterior bulk dimensions effectively compactifies. (This was also observed in [KK07].) Put differently, the field lines of the point source can not spread into the sixth dimension, thus leading to a 5D scaling of the Newtonian force. At large enough distances, this effect becomes less important, and eventually (for finite β) there

⁵³Apart from the 4D case, these integrals are typically UV divergent; e.g. the 6D limit involves $\int_0^\infty dy \sin(y)y \ln y$. This is only a technical problem caused by working in Fourier space and using an infinitely small point source. (It occurs as well when deriving the Green's function of the Laplace operator in more than three dimensions in this way.) Technically, it can easily be solved by regularizing the integrals like $\lim_{\epsilon \rightarrow 0} \int dy (\dots) \exp(-\epsilon y)$. This is equivalent to the physically justified method of smearing the source over a region of size ϵ , and taking $\epsilon \rightarrow 0$ in the end for the point source limit.

⁵⁴The constant $\neq 1$ can be absorbed into a redefinition of the observed 4D Planck mass. However, this will spoil the correct 4D limit of the (ij) -components of the metric, implying a vDVZ discontinuity, cf. Footnote 56.

⁵⁵There are six different cases, which can be obtained analytically by first taking the limit $\alpha \rightarrow 0$ or $\rightarrow \alpha_{\text{stab}} \equiv 3\beta/4$, then the limit $\beta \rightarrow 0$, $\beta = \text{const}$ or $\beta \rightarrow \infty$, and finally expanding the integrand for large z . The corresponding values for n are 9, 8, 16 and 9, 1, 2, respectively.

is always the transition to the 6D scaling (5.5.6b). This intermediate 5D regime can also occur at distances $x \gg R$, and is hence potentially relevant. The corresponding values of n are 2 (for $\alpha \rightarrow \alpha_{\text{stab}} \equiv 3\beta/4$) and 16 (for $\alpha \ll \beta$).

These asymptotic formulas can also be verified numerically, by computing the integral (5.5.5) for given α, β . Some examples (for which the deviations from the 4D scaling occur at $x \gg R$) are shown in Fig. 5.16, confirming our analytic discussion.

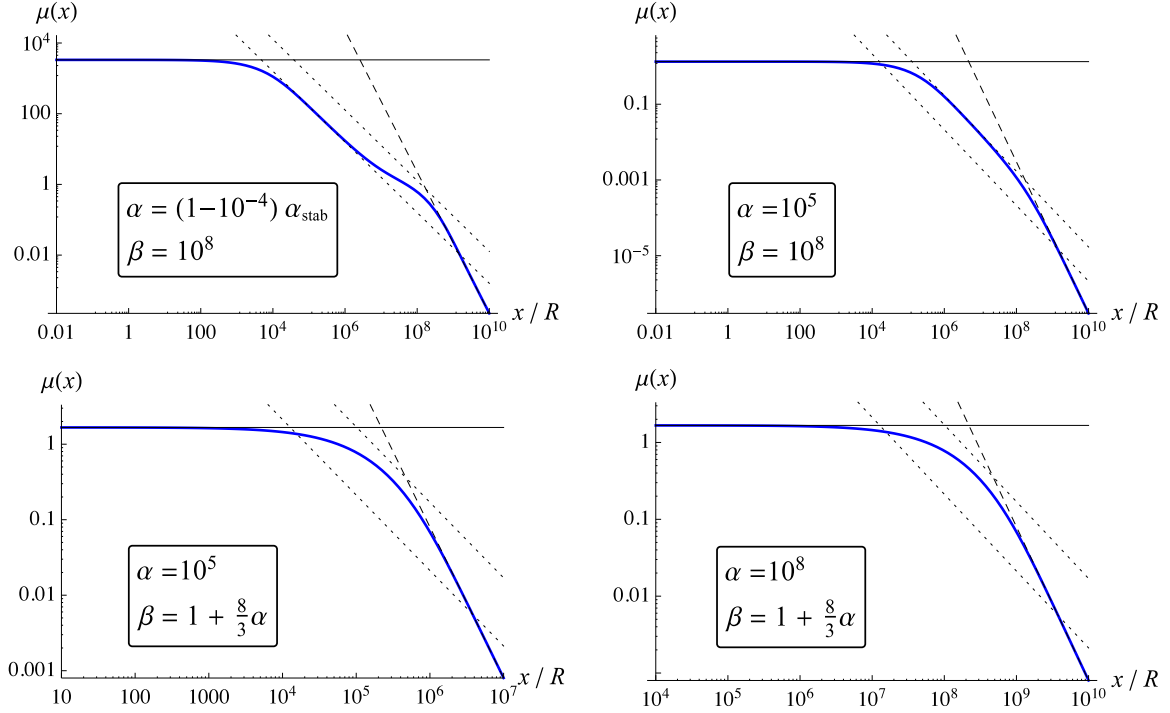


Figure 5.16: Modification of the 4D Newtonian potential of a point source, obtained by numerically evaluating the integral (5.5.5) (blue curves). At small x , μ approaches the asymptotic form (5.5.6a) (solid lines), corresponding to a 4D scaling, and at large x the 6D scaling (5.5.6b) (dashed lines). The upper row shows examples for $\alpha \rightarrow \alpha_{\text{stab}}$ and $\alpha \ll \beta$, realizing the intermediate 5D regimes (5.5.7) with $n = 2$ and $n = 16$, respectively (dotted lines). In the lower row, β takes the value that corresponds to a deficit angle δ in the middle of its allowed range within the healthy region, i.e. in the (vertical) center of the green region in Fig. 5.15. In this case, the 5D window is too small to be realized. The crossover always occurs at the value predicted by (5.5.8), corresponding to the intersection of the solid and dotted lines.

We can now give an analytic expression for the *physical crossover length* x_c , i.e. the length scale at which the deviations from the 4D scaling law first kick in. Since the transition to the 5D scaling always occurs before the one to the 6D scaling, we have to compare (5.5.6a) and (5.5.7), yielding

$$x_c = \frac{n}{12\pi} \left(\frac{3\beta - 4\alpha}{\beta - \alpha} \right) \alpha R. \quad (5.5.8)$$



In the stable region of parameter space, the factor in brackets takes values within the range $(0, 3)$, with its maximum approached in the limit $\beta \rightarrow \infty$ (at constant α), and its minimum at the border to the unstable region. Therefore, in order for the physical crossover x_c to be much larger than the brane width R (as is clearly necessary for a viable theory), we see that α has to be much larger than one. The stability bound $3\beta > 4\alpha$ then also requires $\beta \gg 1$. In the parameter plot Fig. 5.15, this corresponds to the narrow green stripe in the upper right corner, corresponding to the near critical regime $\delta \rightarrow 2\pi$ [recall that the deficit angle $\delta \equiv \beta/(1 + \beta)$]. This near-critical window was also observed in [KK07].

Since $n \leq 16$, we can derive the following upper bound from (5.5.8),

$$x_c < \frac{4}{\pi} \alpha R \equiv \frac{2}{3\pi} \left(\frac{r_c}{R} \right) r_c, \quad (5.5.9)$$

which is saturated for $\alpha \ll \beta \rightarrow \infty$. In the second form (where we used $\alpha \equiv r_c^2/6R^2$), we see that the actual physical crossover x_c is enhanced relative to the naive crossover r_c by a factor of r_c/R , which is $\gg 1$ for potentially interesting parameter choices ($\alpha \gg 1$).

This analysis shows that by choosing α large enough, the physical crossover can in principle be made arbitrarily large, meaning that the theory could always pass solar system tests like LLR.⁵⁶ But this is where cosmology enters the stage: So far, the discussion only applied to the case $H = 0$, corresponding to a 4D Minkowski background. But the nonlinear analysis in Sec. 5.3 revealed that the stability bound gets modified for $H \neq 0$. (Note that this Hubble-dependence cannot be seen at the linear level around the deficit angle background, and was therefore not obtained in [KK07].) This is visualized in Fig. 5.17, showing that the green (stable) region gets smaller as HR_c is increased. In fact, there is an absolute maximum value $HR_c|_{\max} \approx 0.39$, beyond which there is *no* stable point in parameter space anymore.

In other words, a healthy theory is incompatible with HR_c being larger than unity. But this is not necessarily a problem yet, since the linear analysis above showed that the physical crossover x_c can be much larger than r_c . However, the stability and criticality bounds (5.3.58) and (5.3.49) imply that stable sub-critical solutions only exist if

$$(HR_c)^2 < \frac{3}{2} HR \left(1 - \frac{3HR}{\sqrt{1 + 9H^2 R^2}} \right) < \frac{3}{2} HR, \quad (5.5.10)$$

with the second inequality asymptotically saturated in the physically relevant limit $HR \ll 1$. Together with (5.5.9), this implies

$$Hx_c < \frac{1}{\pi}, \quad (5.5.11)$$

⁵⁶There is, however, a vDVZ discontinuity [vDV70, Zak70], which can be seen by calculating also the (ij) -components of the linearized metric, leading to light bending predictions incompatible with observations. (It would only be absent in the limit $\beta \rightarrow 0$ or $\alpha \rightarrow \infty$, which is always in the ghost regime.) However, this could well be an artifact of the first order approximation, and might disappear nonlinearly close enough to the source. This ‘‘Vainshtein mechanism’’ [Vai72], first proposed for massive gravity, was also demonstrated to be at work in the DGP model [DDGV02]. However, this question would here only become relevant if the theory would pass cosmological tests.

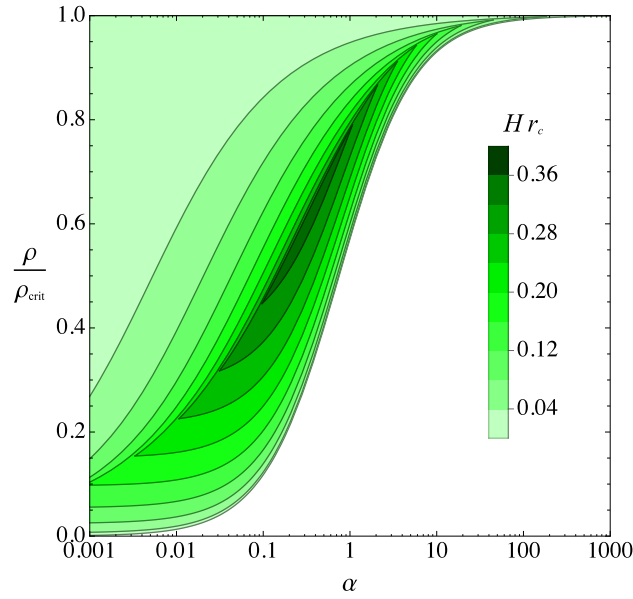


Figure 5.17: The green areas depict the stable, sub-critical regions, for different values of the Hubble parameter on the brane. They are delimited by the stability bound (5.3.58) from below, and by the criticality bound (5.3.49) from above. For $H = 0$, Fig. 5.15 is reproduced (with $\rho \mapsto \lambda$). For $H > 0$, the stable region gets deformed: the lower bound rises and the upper bound decreases; eventually, for $Hr_c > 0.387\dots$, there is no green region left. [Here, the most optimistic case $\tilde{\eta}_0 = 0$ was chosen, corresponding to the lower bound in (5.3.59) and a vanishing C-energy inside the brane. For larger values, the green region would disappear even faster.]

and so Hx_c is also always smaller than one, meaning that *there is no 4D regime in the cosmology of the healthy, sub-critical theory*.⁵⁷ Of course, this only follows from (5.5.11) if x_c is also the correct crossover in the cosmological context.⁵⁸ But this presumption is compatible with the numerical analysis, because in the healthy region the solutions were always found to immediately degravitate all matter, i.e. approach the static $H = 0$ solution without any resemblance of a 4D behavior. Furthermore, if instead r_c were the correct cosmological crossover scale (as was assumed in [NSHK15], and as would also be compatible with the numerical observations), then things get even worse, because Eq. (5.5.10) then implies $Hr_c \ll 1$ for $HR \ll 1$.

In summary, neither Hr_c nor Hx_c can be larger than one in the sub-critical ghost-free region, suggesting that the 6D BIG cosmology should never allow for a 4D regime, and this is exactly what is found by our extensive, dynamical, nonlinear investigation of the

⁵⁷Note that even a maximum value Hx_c somewhat larger than one would not be sufficient: To have a 4D behavior for the whole cosmic history down to early times, the theory would need to allow for $Hx_c \gg 1$.

⁵⁸One might have hoped that the correct cosmological crossover could be read off from the modified Friedmann equations (5.3.27), as in the DGP model. But here in 6D, this is complicated by the fact that the modification terms all depend on the a priori unknown bulk geometry.



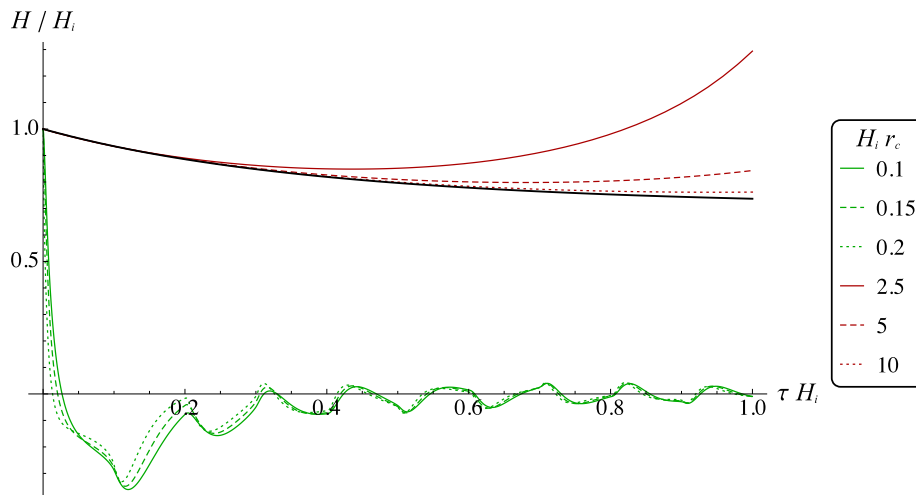


Figure 5.18: Comparison of the 6D BIG cosmology with initial fluid components (5.5.12) to standard Λ CDM (black curve), starting at matter-CC equality, i.e. $\Omega_\Lambda = \Omega_m = 0.5$ at $\tau = 0$. The degravitating solutions (green curves) are always far away from the 4D evolution. For $H_i r_c \gg 1$, the BIG mechanism is at work, and the 4D cosmology is traced (red curves). However, all these solutions eventually enter the pathological super-acceleration, caused by the ghost instability. [Here, $R = 0.05/H_i$ is kept constant, which for (5.5.12) puts the stability bound to $H_i r_c \approx 0.21$. The overall picture is the same for other choices of R .]

full brane bulk system. This is visualized by the green curves in Fig. 5.18, where the resulting Hubble evolution is compared to standard Λ CDM (black curve), for different values of $H_i r_c$ (and fixed $R = 0.05/H_i$). The cosmological fluid here consists of dust and a CC, with

$$\rho_i^{\text{dust}} = \rho_i^{\text{CC}} = [0.8 + (H_i r_c)^2] \frac{\rho_{\text{crit}}}{2}. \quad (5.5.12)$$

For these parameters, the stability bound implies $H_i r_c \lesssim 0.21$. Evidently, these stable solutions are always far away from the 4D evolution. Unfortunately, this failure already rules out the theory as a phenomenologically viable modification of GR. In other words, the healthy near-critical window that remained as potentially viable in the linear analysis, closes once the (nonlinear) cosmological brane evolution is taken into account.

Alternatively (but equivalently), one can phrase the problem as follows: If we *require* the theory to exhibit a 4D regime, then we must choose $H x_c$ (or $H r_c$) larger than one. In principle, this mechanism indeed works, as can be seen from the red curves in Fig. 5.18, which—unlike the degravitating solutions—do trace the standard Λ CDM evolution. But the problem is that in these cases, we are always deep inside the unstable region of parameter space. Accordingly, the deviations from 4D do not correspond to a healthy transition to a 6D regime,⁵⁹ which should be attended by degravitation;

⁵⁹Therefore, this analysis can also not help identifying the actual cosmological crossover scale; indeed, both $H r_c$ and $H x_c$ are always still larger than 1 when the deviations from 4D occur.

instead, they indicate the onset of the ghost instability, leading to super-acceleration.

Either way, the message is that the (sub-critical) ghost-free and phenomenologically viable regions are mutually incompatible. The remaining window of opportunity for the model lies within the super-critical regime, which was excluded so far. This will be the subject of the next chapter; in particular, we will find that super-critical energy densities necessarily lead to a compact extra space (thereby generalizing the static result to dynamical geometries). Therefore, the system is qualitatively different from the original BIG setup with two infinite extra-dimensions, and should thus be regarded as a different theory. The main result of this chapter can therefore briefly be summarized as follows: *BIG with two infinite codimensions, albeit being a healthy theory for natural EFT parameters, is phenomenologically not viable and therefore ruled out.*



APPENDIX TO CHAPTER 5

5.A Non-stabilized circumference

In this appendix, we investigate the case when the brane circumference $2\pi R$ is not kept constant. The main motivation is to show that the instability of the model is not an artifact of this assumption. Without the stabilization requirement, the $(\phi\phi)$ -component of the brane energy-momentum tensor is not fixed anymore, and can a priori be chosen arbitrarily. For definiteness, and to make sure that it corresponds to a physically admissible source, we will choose $T^\phi_\phi = 0$.

5.A.1 Nonlinear cosmology

First, let us consider the cosmological setup, and replace the requirement $R = \text{const}$ by $p_\phi = 0$. The extrinsic curvature is still given by (5.3.25), but now the relations (5.3.26a) read

$$\gamma = \sqrt{e^{-2\eta_0} + H_r^2 R^2}, \quad \dot{r}_0 = \frac{H_r R}{\gamma}, \quad \frac{r_0 \ddot{r}_0}{1 - \dot{r}_0^2} = \frac{R^2}{\gamma^2} \left[\dot{H}_r + H_r (H_R + \dot{\eta}_0) \right], \quad (5.A.1)$$

whereas (5.3.26b) still hold, but with

$$\psi \equiv r_0 \dot{\alpha}|_0 = \frac{R}{\gamma} (H - \xi H_r). \quad (5.A.2)$$

(Recall that $\xi \equiv r_0 \alpha'|_0$; furthermore, all interior relations are again obtained by putting tildes on all quantities.) Here we introduced the azimuthal ‘‘Hubble’’ parameter

$$H_R := \frac{\dot{R}}{R}, \quad \text{and (for notational convenience)} \quad H_r := \frac{\dot{r}_0}{r_0} \equiv 3H + H_R. \quad (5.A.3)$$

Accordingly, the 5D BIG terms also receive contributions $\propto H_R$. Explicitly, we find

$$\hat{\rho}^{(5)} = \rho^{(5)} - M_5^3 3 (H^2 + H H_R), \quad (5.A.4a)$$

$$\hat{p}^{(5)} = p^{(5)} + M_5^3 \left(2\dot{H} + \dot{H}_R + 3H^2 + H_R^2 + 2H H_R \right), \quad (5.A.4b)$$

$$\hat{p}_\phi^{(5)} = M_5^3 3 \left(\dot{H} + 2H^2 \right), \quad (5.A.4c)$$



where we already used $p_\phi^{(5)} = 0$ in the last term. As a consistency check, one can easily verify that all expressions given here reduce to the ones in the main text for $H_R \rightarrow 0$. Energy conservation now reads

$$\dot{\rho}^{(5)} + 3H(\rho^{(5)} + p^{(5)}) + H_R \rho^{(5)} = 0, \quad (5.A.5)$$

which for an EOS $p^{(5)} = w\rho^{(5)}$ implies

$$\rho^{(5)} \propto \frac{a^{-3(1+w)}}{R}. \quad (5.A.6)$$

As a consequence, the dimensionally reduced 4D quantity $\rho \equiv 2\pi R \rho^{(5)}$ scales exactly as before. We can still formally introduce the four dimensional Planck-scale and the crossover-scale as in (5.2.3) and (5.3.30) respectively, but one has to keep in mind that they are now functions of time as well. Specifically, they scale with R as $M_4(\tau), r_c(\tau) \propto \sqrt{R(\tau)}$.

After some algebra, the junction conditions (5.3.22) finally become

$$H^2 + HH_R = \frac{\rho}{3M_4^2} + \frac{1}{r_c^2}(\gamma - \tilde{\gamma}), \quad (5.A.7a)$$

$$\dot{H} = \frac{\mathbf{a} + \mathbf{b}}{1 - 4\mathbf{c}}, \quad \dot{H}_R = \frac{\mathbf{a}(1 - 3\mathbf{c}) + \mathbf{b}}{1 - 4\mathbf{c}}, \quad (5.A.7b)$$

with the following definitions:

$$\mathbf{a} := -\frac{w\rho}{M_4^2} - H_R(2H + H_R) + 3H^2 + \frac{3}{r_c^2} \left\{ \gamma [1 - 4(\xi + \dot{r}_0\psi)] - \text{“tilde”} \right\}, \quad (5.A.8a)$$

$$\mathbf{b} := \mathbf{c}H_R(3H + H_R) - 2H^2 + \frac{6}{r_c^2} \left\{ \gamma [4\dot{r}_0\xi\psi + (1 + \dot{r}_0^2)(\xi^2 + \psi^2)] - \text{“tilde”} \right\}, \quad (5.A.8b)$$

$$\mathbf{c} := \frac{R^2}{r_c^2} \left(\frac{1}{\gamma} - \frac{1}{\tilde{\gamma}} \right). \quad (5.A.8c)$$

This time there are two dynamical equations of motion, Eqs. (5.A.7b), which will be used to numerically determine H and H_R . The constraint (5.A.7a) again serves as a nontrivial consistency check for the numerics.

The initial data will be chosen as before, but now we also have to specify an initial value for H_R , which we will (for simplicity) set to zero:

$$H_R|_i = 0. \quad (5.A.9)$$

Furthermore, the constant values for R and r_c which were chosen in the case $H_R = 0$, will here be used as the initial values $R|_i$ and $r_c|_i$ when comparing the corresponding solutions.

The numerical algorithm is completely analogous to the stabilized case discussed in the main text, and we can now reconsider the super-accelerating example of Sec. 5.3.5,

but for the non-stabilized case with $p_\phi = 0$. To this end, we choose the parameters (5.3.56) (but with grid-spacings $\tilde{\epsilon} = 10^{-3} \times R_i$ and $\epsilon = 2 \times 10^{-3} R_i$).

The results are shown in Fig. 5.A.1. The two Hubble parameters H and H_R both increase, implying a super-accelerated expansion. Fig. 5.A.1b shows the effective energy density from a 6D perspective, which for $H_R \neq 0$ is given by

$$\hat{\rho} \equiv \rho - 3M_4^2 (H^2 + HH_R). \quad (5.A.10)$$

Again, it becomes negative and tends towards $-\infty$. This shows that the instability is not due to the unphysical pressure p_ϕ encountered in the $H_R = 0$ scenario. On the contrary, the unphysical behavior of p_ϕ is a *consequence* of the instability, and the requirement of stabilizing the brane width R despite this instability. This can also be understood from Fig. 5.A.1a, which shows that without any stabilization the super-acceleration is dominantly in ϕ -direction (H_R grows faster than H).

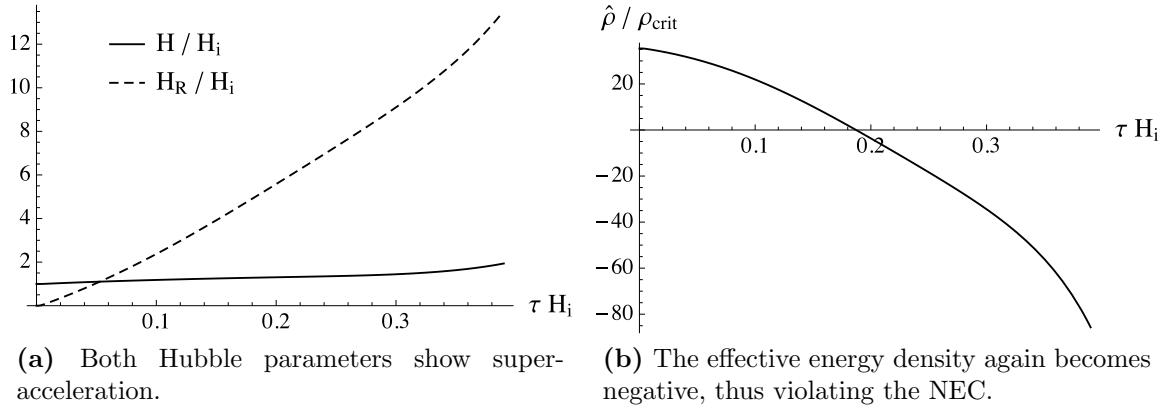


Figure 5.A.1: Plots of the numerical results for the super-accelerating solution in the case $p_\phi = 0$. The unstable behavior encountered in the case $H_R = 0$ is not cured by setting $p_\phi = 0$. The estimated numerical error-bars are again smaller than the line widths.

5.A.2 Linear ghost analysis

Note: This section is to large extent a verbatim reproduction of the corresponding appendix in [ENS15].

We will now show that the instability is still due to the ghost mode if the brane circumference is not stabilized. At the linear level, this means that the radion φ is not set to zero, and U_ϕ^ϕ is a priori arbitrary. For simplicity, we will again only consider the case

$$U_\phi^\phi = 0. \quad (5.A.11)$$



The two junction conditions (5.4.27b) and (5.4.30) can still be used to derive a closed equation⁶⁰ for s ,

$$M_6^4[s'] + M_5^3 \left[\left(1 - \frac{3\alpha}{2\beta}\right) \square_4 + \frac{\beta - 2\alpha}{2\alpha(1 + \beta)R^2} \right] s|_0 = -\frac{1}{4}U^\mu{}_\mu. \quad (5.A.12)$$

After performing a 4D Fourier transform and using the general bulk solution (5.4.43) for \hat{s} , we arrive at

$$\frac{4M_6^4}{R} \tilde{Z}(p) \hat{s}|_0 = -\hat{U}^\mu{}_\mu, \quad (5.A.13)$$

where now the inverse s -propagator is given by (in terms of $z := r_0\sqrt{p^2}$)

$$\tilde{Z}(p) := \alpha f_1 z^2 + f_2 - z \left(\frac{I_1(z)}{I_0(z)} + \frac{K_1((1 + \beta)z)}{K_0((1 + \beta)z)} \right), \quad (5.A.14)$$

with

$$f_1 := 2 \left(\frac{3\alpha}{2\beta} - 1 \right), \quad f_2 := \frac{\beta - 2\alpha}{1 + \beta}. \quad (5.A.15)$$

This is very similar to the inverse s -propagator in the stabilized case, Eq. (5.4.45). The only difference is that the coefficient f is slightly modified into f_1 and—more importantly, as we will see below—there is an additional constant (i.e. p -independent) term f_2 .

As before, we can restrict ourselves to sources for which only the scalar mode s is excited. This can be achieved by setting all tensor- and vector source terms to zero, and requiring

$$3\hat{U}^{(S)} = \left(1 - \frac{f_2}{4\tilde{Z}}\right) \hat{U}^\mu{}_\mu. \quad (5.A.16)$$

In this case, the scalar mode J can again be set to zero, and the full source vertex (5.4.37) takes the same form as before (5.4.47), with the replacement $Z \rightarrow \tilde{Z}$. Therefore, the stability analysis is completely analogous.

It can now easily be checked that the propagator \tilde{Z}^{-1} has a tachyonic pole ($\Leftrightarrow \tilde{Z}$ is zero for some $z_* > 0$) if and only if $f_1 > 0$ or $f_2 > 0$. The corresponding regions in parameter space are depicted in Fig. 5.A.2. They are disjoint, and separated by a narrow (but finite) stripe in which the tachyon is absent and the model is thus linearly stable.

⁶⁰Note that when comparing this equation to the one derived in Ref. [KK07], viz. Eq. (5.41) therein (the corresponding scalar mode is called X in [KK07], and is related to ours via $s = -3X$), one has to take into account that the energy momentum tensor $\tau^\mu{}_\nu$ in [KK07] differs from our $U^\mu{}_\nu$: $\tau^\mu{}_\nu$ is defined in the Einstein frame and thus satisfies standard energy conservation ($\partial_\mu \tau^\mu{}_\nu = 0$), whereas $U^\mu{}_\nu$ is defined in the Jordan frame, for which, on the deficit angle background, additional terms $\propto \lambda$ have to be included, cf. our Eq. (5.4.23). We thank Nemanja Kaloper for clarifying this point.

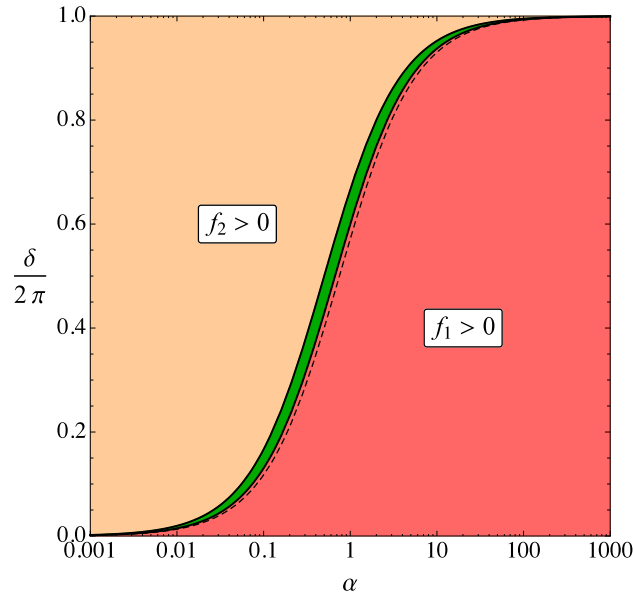


Figure 5.A.2: Without stabilization (and $U_\phi^\phi = 0$), there are three regions in parameter space: in the lower right region, where $f_1 > 0$, there is a tachyonic ghost; the delimiting line is almost the same as in the non-stabilized case, shown as a dashed line. In the dark green region in the middle $f_1, f_2 < 0$, and the model is linearly stable. In the upper left region $f_2 > 0$ and there is a tachyon which is not a ghost. It shows that the static deficit angle background is not stable if U_ϕ^ϕ is not used to fix the brane circumference, as expected.

The case $f_1 > 0$ is very similar to the condition $f > 0$ in the stabilized case. Indeed, the delimiting line $f = 0$ in parameter space, shown as a dashed line in Fig. 5.A.2, only gets shifted by a small amount.

The case $f_2 > 0$, however, implies that there is also a tachyon in the upper left region in parameter space. At first, it might be surprising that this region is also unstable, because it also includes the case $\alpha = 0$, which is just pure 6D GR without any induced terms and should be a healthy theory. The resolution to this puzzle is rather simple: Evaluating the residue of \tilde{Z}^{-1} at the tachyon pole as we did in Sec. 5.4.2, we find that, while it is again negative for $f_1 > 0$, it is *positive* for $f_2 > 0$. In other words, the tachyon is only a ghost in the lower right region. In the upper left region, the tachyon is not a pathology, but merely a reflection of the fact that, *without fixing the brane circumference, the static deficit angle background is not stable*. Instead, the brane wants to expand (or collapse) in radial direction, as should be expected.

To summarize, the ghost-criterion is basically independent of whether the circumference is stabilized or not. In particular, the naturalness discussion from Sec. 5.5.1 still applies to the case of free radial expansion. On the other hand, the static deficit angle solution is then not stable under angular size fluctuations. To overcome this problem, we have to make additional assumptions about the underlying microscopic model. In fact, from a fundamental perspective, the existence of some sort of stabilization mechanism has to be expected as there are known stable vortex configurations in



two codimensions [NO73]. Fixing the proper circumference with a suitable azimuthal pressure turned out to be a convenient way of realizing such a mechanism in an effective low energy description.

5.B Numerical errors and consistency checks

In this appendix, we present the numerical error estimates, as well as the consistency checks which were used to test the trustability of our numerical solver.

One way to estimate the numerical uncertainties is to check how much the calculated quantities change when the grid-spacing decreases. For instance, one can define an error estimate δA for some quantity A calculated with grid-spacing ϵ as

$$\delta A(\epsilon) := A(2\epsilon) - A(\epsilon). \quad (5.B.1)$$

If $A(\epsilon)$ converged to its true value linearly in ϵ as $\epsilon \rightarrow 0$, this would give exactly the correct error, for a faster convergence the true error would even be smaller. The plots in Fig. 5.B.1 show the corresponding error of the Hubble parameter for the degravitating and pathological solutions presented in Sec. 5.3.5. In the Hubble plots, Figs. 5.4b and 5.5b, the corresponding error-bars would not exceed the line thickness. The dashed curves depict the error estimates when the grid spacing is doubled; the scaling of the errors is compatible with an (approximately linear) convergence as $\epsilon \rightarrow 0$.

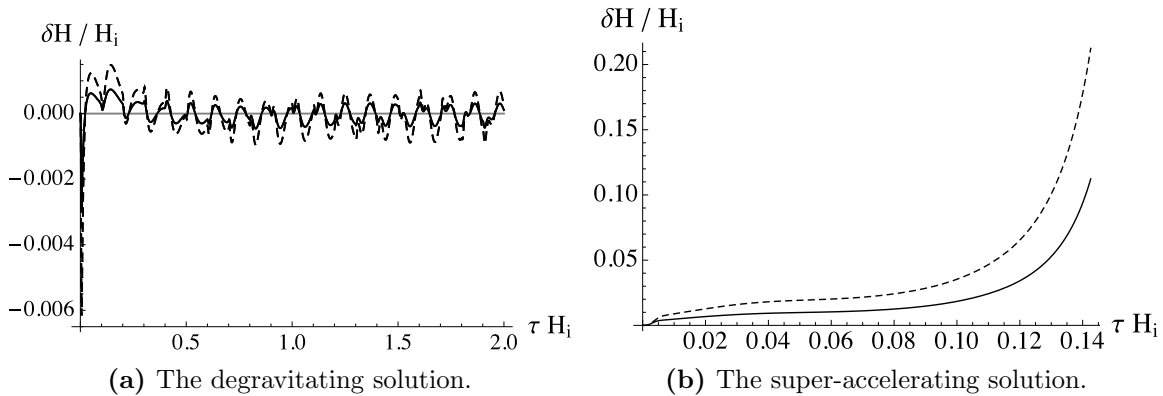


Figure 5.B.1: Numerical error estimates, as defined in (5.B.1), of the Hubble parameter for the solutions presented in Sec. 5.3.5. The dashed lines correspond to the doubled lattice spacing, showing that the numerically obtained Hubble evolution converges (approximately linearly) as $\epsilon \rightarrow 0$.

There are several nontrivial consistency checks that can be performed. The most important one is the constraint (5.3.27a), which is only imposed at the initial time, and should be automatically fulfilled at all later times. Its violation,

$$\delta C := H^2 - \frac{\rho}{3M_4^2} - \frac{1}{r_c^2} (\gamma - \tilde{\gamma}), \quad (5.B.2)$$

measured in units of H_i^2 , is plotted in Fig. 5.B.2; it is indeed compatible with being zero within the numerical uncertainties. Another test comes from the fact that some quantities (like Hubble) which should be continuous across the brane can be calculated independently in the interior or exterior coordinate patch in our numerical scheme. The difference between them (measured in units of H_i) is shown as the dotted line in the same plots, and it is again compatible with zero.

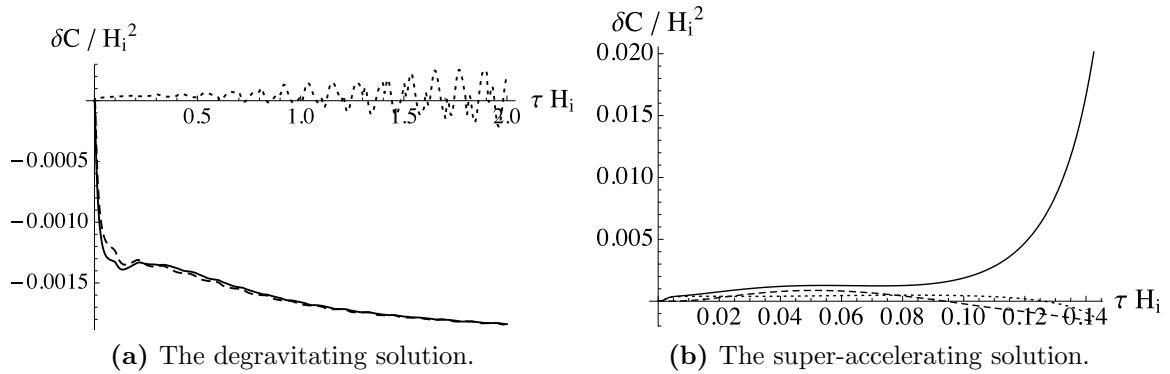


Figure 5.B.2: Numerical consistency checks for the solutions presented in Sec. 5.3.5. The solid and dashed curves show the constraint violation (5.B.2) in the interior and exterior, respectively. The dotted line is the difference between H in the interior and exterior. All violations are compatible with being zero within the numerical uncertainties.



CHAPTER 6

SUPER-CRITICAL COSMIC STRINGS

Note: This chapter is to large extent a verbatim reproduction of the publication [NS15b], which arose in collaboration with Florian Niedermann.

The preceding results motivate an investigation of the codimension-two BIG setup also for super-critical 4D energy densities on the brane. Indeed, the parameter plots in Fig. 5.8 suggest that—if the stability bound can be extended above the lower criticality bound—the theory should *always* be stable in the super-critical regime (the light gray regions in Fig. 5.8), irrespective of the value of r_c . In particular, it would thus be possible to make r_c (or x_c) large enough to achieve the required 4D regime, the failure of which was the crux that ruined the sub-critical model.

Since super-critical cosmic strings have not been very well studied even within standard GR, we will first focus on the pure 4D setup. This already enables us to understand the crucial physics of the system. The straightforward generalization to 6D BIG will be discussed at the end in Sec. 6.9.

6.1 Summary

In General Relativity, local cosmic strings are well known to produce a static, locally flat spacetime with a wedge removed. If the tension exceeds a critical value, the deficit angle becomes larger than 2π , leading to a compact exterior that ends in a conical singularity. In this chapter, we investigate dynamical solutions for cosmic strings with super-critical tensions. To this end, we model the string as a cylindrical shell of finite and stabilized transverse width (like in Chap. 5) and show that there is a marginally super-critical regime in which the stabilization can be achieved by physically reasonable matter.

We show numerically that the static deficit angle solution is unstable for super-critical string tensions. Instead, the geometry starts expanding in axial direction at an asymptotically constant rate, and a horizon is formed in the exterior spacetime, which has the shape of a growing cigar. We are able to find the analytic form of the attractor



solution describing the interior of the cosmic string. In particular, this enables us to analytically derive the relation between the string tension and the axial expansion rate. Furthermore, we show that the exterior conical singularity can be avoided for dynamical solutions. The fact that the exterior space closes up and becomes compact, however, is unavoidable and still persists in the time-dependent case.

Since our main motivations comes from codimension-two braneworld models, we finally derive the corresponding 4D Friedmann equation, relating the on-brane Hubble parameter to the brane CC.

6.2 Introduction and outline

Local cosmic strings were first derived as topologically nontrivial solutions of the Abelian Higgs Model by Nielsen and Olesen [NO73]. In GR, they give rise to a static geometry which sufficiently far away from the string is locally flat and can be characterized by a deficit angle δ corresponding to a wedge that has been removed from spacetime. The value of δ is linearly related to the string tension λ (mass per unit length): $\delta = \lambda/M_{\text{Pl}}^2$, with the reduced Planck mass $M_{\text{Pl}}^2 \equiv 1/(8\pi G_{\text{N}})$. This spacetime was first studied in [Vil81, Got85, His85].

Once the tension reaches the critical value $2\pi M_{\text{Pl}}^2$, the deficit angle becomes 2π , thus implying the exterior topology of an infinite cylinder [Lin90]. Introducing the dimensionless parameter $\bar{\lambda} := \lambda/(2\pi M_{\text{Pl}}^2)$, this critical value corresponds to $\bar{\lambda} = 1$. For even higher values of the string tension, the angular defect exceeds 2π ; thus, the exterior spacetime of the static solution closes up and ends in a conical singularity¹ [Ort91]. However, the status of these so-called “super-critical” or “super-massive” solutions remained unclear due to the occurrence of the singular axis away from the string. One way to give a physical meaning to the singularity is to replace it with another (sub-critical) tension string [BPRSU14].

In this chapter, we further explore the geometry of super-critical cosmic strings. Instead of introducing additional strings, *we relax the assumption of having a static geometry*. A first purely numerical attempt in that direction was made in [Cho98] by considering a super-critical Nielsen-Olesen (NO) string. There it was found that once the tension $\bar{\lambda}$ exceeds ~ 1.6 , *both* the transverse and axial string directions begin to expand at a comparable rate. In this work we will be able to analytically confirm this bound. In contrast to [Cho98], we will be mostly interested in describing the remaining parameter space: $1 < \bar{\lambda} \lesssim 1.6$. We show that within this “marginally super-critical” regime the transverse string dimensions can be stabilized, whereas the axial dimension expands at an asymptotically constant rate. This fact makes these solutions especially interesting for models with two extra-dimensions according to which the string is promoted to a braneworld describing our universe. Then, the constant axial

¹For both sub- and super-critical tensions, there is a second class of solutions, usually referred to as the “Melvin” or “Kasner” branch [LG89, CLV99], which has even a curvature singularity in the super-critical case. However, we discard this branch due to its unphysical properties, cf. Sec. 6.4.

expansion rate corresponds to a de Sitter on-brane geometry, and having a stabilized transverse dimension is a necessary requirement to obtain a 4D regime in those theories, cf. Chap. 5.

Furthermore, the analysis of [Cho98] lacks a detailed discussion of the geometry away from the string. In particular, it was not answered whether the second axis still bears a *conical* singularity (which does not lead to asymptotically diverging curvature invariants) as it is the case for the static solution. Our approach allows us to get a complete understanding of both the geometry and the underlying dynamics of the system in the marginally super-critical regime. For example, we show that the exterior conical singularity can be completely avoided for a dynamical solution and should thus be regarded as an artifact caused by assuming a static geometry. In addition, we find (numerically) that a horizon emerges, which can (but need not) lie between the string and the second (regular) axis.

In order to technically simplify the problem, we again use the ring regularization like in Chap. 5, i.e. the string is modeled as cylindrical shell of fixed circumference $2\pi R$. Again, this simplified description should capture all essential physics as long as we are interested in low energy questions which do not require to resolve the inner structure of the defect. Since the only scale determining the dynamics of the system is the axial expansion rate H , this condition should clearly be satisfied as long as $HR \ll 1$.²

In Sec. 6.3, we present the metric ansatz and field equations, and discuss the classification of sub- and super-critical strings, as well as the geometrical implications. As a first consistency check of our description, we reproduce the well-known static deficit angle solution in Sec. 6.4, which—in the super-critical case—leads to a second singular axis in the exterior vacuum region. In order to see whether these are stable solutions, we numerically study the time evolution of the system in Sec. 6.5. To that end, we choose initial data close to the static configuration but include cylindrical symmetric gravitational waves in the interior and exterior region close to the shell to provide the system with a nonvanishing initial kinetic energy. We find that the sub-critical string, after emitting the cylindrical waves, settles back to the static deficit angle solution. The super-critical system, however, starts to approach a non-static solution instead. *This result proves that the static super-critical solution is not stable under perturbations.* Moreover, the numerical results allow to infer several properties of the new dynamical attractor solution in the marginally super-critical regime defined by $1 < \bar{\lambda} \lesssim 1.6$:

- The geometry expands in axial direction at a constant rate.
- There is a horizon in the exterior region.
- The exterior space is cigar-shaped and expands, whereas the interior space is nearly flat and can be stabilized.

Let us emphasize that for $\bar{\lambda}$ close to 1, the observed expansion rate satisfies $HR \ll 1$. Therefore, in that regime we expect all the results to be completely insensitive to the

²We find a posteriori that this condition is indeed satisfied for the attractor solutions in the marginal super-critical regime.



microscopic inner structure of the string. They should thus equally hold for other regularizations like a full cylinder for which the tension would be smeared out over the interior region, or the original UV model described in [NO73].

For even larger values of the tension, $\bar{\lambda} \gtrsim 1.6$, we find that the azimuthal pressure required to stabilize the shell's circumference violates the Null Energy Condition (NEC). Hence, in this regime a stabilization cannot be achieved by physical degrees of freedom. Since at this point HR is already close to one, it is a priori not clear whether this result would still hold for a more realistic NO-like string. However, it turns out that our NEC-bound is in nice agreement with the one derived in [Cho98], where the full radial profile was resolved. This is a strong indication that our simplified model can in fact be successfully used in the *whole* stabilizable (i.e. marginally super-critical) regime to capture the essential physics—instead of the more complicated microscopic NO-system. This result is also in agreement with the idea of “topological inflation” [Vil94, Lin96, LL94]. In that context, it is argued that once $HR \sim 1$, the interior space of the defect starts to inflate in *both* axial and radial direction at the same rate, or in other words, there is a de Sitter phase inside the cosmic string. This is plausible because at this point its boundary lies outside the corresponding horizon and thus the interior is causally disconnected from the exterior, which makes it locally equivalent to a pure de Sitter universe.

We derive the analytic form of the attractor solution in the interior of the shell in Sec. 6.6 by making an appropriate scaling ansatz for the metric. This in turn enables us to derive the relation between the string tension λ and H analytically. In the marginally super-critical regime, we find up to small corrections of order $(HR)^2$:

$$HR \approx \bar{\lambda} - 1 . \tag{6.2.1}$$

The analytic result for the interior geometry can be mapped by a coordinate transformation, described in Appendix 6.B, to a solution discussed earlier by Witten [Wit82] and Gregory [Gre03]. To our knowledge, this is the first time that this solution is matched to a specific matter model.

Furthermore, we are able to show that the conical singularity in the exterior is an artifact caused by assuming a static geometry. More precisely, in Sec. 6.7 we demonstrate that the singularity can be completely avoided by choosing the initial conditions appropriately. In that case the exterior space ends radially in a smooth axis.³ Moreover, we argue that the value of H is completely independent of the choice of initial conditions and solely depends on the string parameters R and λ , as expected for an attractor solution. A corresponding parameter plot, summarizing our results, is discussed in Sec. 6.8.

For a cosmic string formed during a phase transition in the early universe, say at the GUT scale, we would generically expect a sub-critical tension of order $\bar{\lambda} \sim 10^{-6}$. However, in [Ort91] it was argued that super-critical cosmic strings could also arise at this scale when the coupling between scalar and gauge fields is very weak (in a

³The existence of a singularity-free inflating solution was already anticipated in [Vil94, KK07].

NO-framework). In order to further clarify their phenomenological status for standard cosmology, we review arguments previously given by Thorne [AT92]. In this context, it is shown in Appendix 6.A that an open cylindrical geometry cannot evolve classically into a closed one. This result implies that the formation of super-critical strings cannot be described within classical GR. So far, it is not clear whether their formation through a quantum-mechanical tunneling process would lead to phenomenologically relevant effects.

However, these solutions might be interesting in the context of codimension-two braneworld models, where the string is promoted to a 3-brane representing our universe. A corresponding generalization of Eq. (6.2.1) can be understood as a modified Friedmann equation. The axial expansion rate H then plays the role of the ordinary Hubble parameter describing the spatial expansion of our universe. In that context, the regime $HR \ll 1$, corresponding to a marginally super-critical tension, is the most interesting one as it is enforced by a huge separation between the cosmological length scale H^{-1} and the microscopic scale R given by the thickness of the string. The six-dimensional setup in the case of a pure tension brane is discussed in Sec. 6.9. We draw our conclusions in Sec. 6.10.

Finally, in Appendix 6.C we show that the super-critical cosmic strings covered by our analysis can indeed be described consistently within classical GR, as long as the transverse string size R is much larger than the Planck length, since this ensures a sub-Planckian 4D energy density.

6.3 Coordinates and geometry

Since the setup is the 4D analogue of the one discussed in Chap. 5, we can follow Sec. 5.3.1 and make the general metric ansatz

$$ds^2 = e^{2(\eta^* - \alpha^*)} (-dt^{*2} + dr^{*2}) + e^{2\alpha^*} dz^2 + e^{-2\alpha^*} W^2 d\phi^2, \quad (6.3.1)$$

now with a one-dimensional axis, which is the original form used by Thorne [Tho65]. Here, $\phi \in [0, 2\pi)$ and $z \in (-\infty, \infty)$ are coordinates in angular and axial direction, respectively, and the functions α^* , η^* , W only depend on the temporal and radial coordinates (t^*, r^*) . One virtue of this ansatz is that radial light-rays correspond to $dt^* = \pm dr^*$, thus making the causal structure evident in t^* - r^* -diagrams, a fact which we will often use in our analysis.

As in Sec. 5.3.1, we can fix the residual gauge freedom of the metric (6.3.1) by choosing the new radial coordinate⁴

$$r = W(t^*, r^*) \quad (6.3.2)$$

in vacuum. Again, this choice is not admissible across the shell, and so the interior and exterior coordinate patches are not continuously connected. To distinguish them,

⁴By using r as a spatial coordinate, we implicitly assume that the gradient of W is spacelike. We will come back to this important subtlety in Sec. 6.3.2.



we again put tildes on the interior coordinates and metric functions. The metric then takes the standard Einstein-Rosen [ER37] form

$$d\tilde{s}^2 = e^{2(\tilde{\eta}-\tilde{\alpha})} (-d\tilde{t}^2 + d\tilde{r}^2) + e^{2\tilde{\alpha}} dz^2 + e^{-2\tilde{\alpha}} \tilde{r}^2 d\phi^2, \quad (6.3.3a)$$

$$ds^2 = e^{2(\eta-\alpha)} (-dt^2 + dr^2) + e^{2\alpha} dz^2 + e^{-2\alpha} r^2 d\phi^2, \quad (6.3.3b)$$

in the interior and exterior, respectively. The corresponding vacuum equations in 4D become

$$\ddot{\alpha} = \alpha'' + \frac{1}{r}\alpha', \quad (6.3.4a)$$

$$\eta' = r \left(\dot{\alpha}^2 + \alpha'^2 \right), \quad (6.3.4b)$$

$$\dot{\eta} = 2r\dot{\alpha}\alpha', \quad (6.3.4c)$$

and similarly for the interior (with tildes on all quantities).

The symmetry axis is located in the interior coordinate patch at $\tilde{r} = 0$. Regularity at this axis and elementary flatness, i.e. absence of a conical singularity, requires

$$\tilde{\alpha}'|_{\tilde{r}=0}(\tilde{t}) = 0 \quad \text{and} \quad (6.3.5a)$$

$$\tilde{\eta}|_{\tilde{r}=0}(\tilde{t}) = 0, \quad (6.3.5b)$$

respectively.

6.3.1 Induced geometry

The induced metric on the cylindrical shell is

$$ds_{(\text{ind})}^2 = -d\tau^2 + e^{2\alpha_0} dz^2 + R^2 d\phi^2, \quad (6.3.6)$$

where here and henceforth the subscript “0” denotes evaluation at the position of the shell. The proper time τ on the surface is related to the interior and exterior time coordinates via

$$d\tau = \frac{e^{-\alpha_0}}{\gamma} dt = \frac{e^{-\tilde{\alpha}_0}}{\tilde{\gamma}} d\tilde{t}, \quad (6.3.7)$$

where

$$\gamma := \frac{e^{-\eta_0}}{\sqrt{1 - \dot{r}_0^2}} \quad \text{and} \quad \tilde{\gamma} := \frac{e^{-\tilde{\eta}_0}}{\sqrt{1 - \dot{\tilde{r}}_0^2}}. \quad (6.3.8)$$

The functions $\tilde{r}_0(\tilde{t})$ and $r_0(t)$ describe the radial position of the shell in the two coordinate patches, and $\dot{r}_0 := dr_0/dt$, $\dot{\tilde{r}}_0 := d\tilde{r}_0/d\tilde{t}$.

In order to have a well defined regularization of the infinitely thin cosmic string, we again assume the proper circumference of the cylinder to be stabilized:

$$R := r_0 e^{-\alpha_0} = \tilde{r}_0 e^{-\tilde{\alpha}_0} = \text{const.} \quad (6.3.9)$$

As already mentioned, on a fundamental level this would be enforced by some underlying UV physics that gave rise to the cosmic string. Effectively, working well below this UV scale at which the inner structure of the string could be probed, it can be achieved by assuming a suitable azimuthal pressure component p_ϕ . We will check a posteriori whether this pressure is physically reasonable, i.e. whether it satisfies the NEC.

The surface energy momentum tensor on the shell is given by

$$T^m_n = \frac{1}{2\pi R} \text{diag}(-\lambda, -\lambda, p_\phi), \quad (6.3.10)$$

where the overall factor ensures that λ is the one-dimensional string tension. Throughout this chapter we will assume that $\lambda \geq 0$. Let us, for later convenience, also introduce the dimensionless quantities

$$\bar{\lambda} := \frac{\lambda}{2\pi M_{\text{Pl}}^2}, \quad \bar{p}_\phi := \frac{p_\phi}{2\pi M_{\text{Pl}}^2}. \quad (6.3.11)$$

Fixing R implies that the 3D energy conservation equation for this source simply becomes $\lambda = \text{constant}$. The pressure p_ϕ will in general be time-dependent, and its value will be inferred from one of the junction conditions, see below. Furthermore, the entire dynamics of the induced metric (6.3.6) is now encoded in the single function $H := d\alpha_0/d\tau = d\tilde{\alpha}_0/d\tau$, measuring the expansion rate of the string in axial direction.

For future reference, note that the stabilization condition implies

$$\dot{r}_0 = \frac{HR}{\gamma}, \quad \dot{\tilde{r}}_0 = \frac{HR}{\tilde{\gamma}}, \quad (6.3.12)$$

which allows us to rewrite (6.3.8) as

$$\gamma = \sqrt{e^{-2\eta_0} + H^2 R^2}, \quad \tilde{\gamma} = \sqrt{e^{-2\tilde{\eta}_0} + H^2 R^2}. \quad (6.3.13)$$

6.3.2 Super-criticality

The interpretation of r and \tilde{r} as radial coordinates implicitly assumes that the gradient $\nabla W := (\partial_{t^*} W, \partial_{r^*} W)$ of the function W in the original metric (6.3.1) was spacelike. If it had been timelike, the coordinate r defined by (6.3.2) would in fact be a temporal coordinate, cf. the discussion in Sec. 5.3.1.

In order to have a smooth symmetry axis in the interior, and hence a well defined regularization of the cosmic string, we have to assume that ∇W was spacelike in the interior region. Furthermore, since \tilde{r} should take positive values, ∇W had to be outward pointing. As discussed in more detail in Appendix 6.A, the character of ∇W in the exterior is then fixed by the amount of string tension λ that is localized on the cylindrical shell. There are three cases:⁵

⁵The corresponding 6D bounds are obtained by replacing $HR \mapsto 3HR$, and the BIG terms can be included via $\bar{\lambda} \rightarrow \bar{\lambda} - r_c^2 H^2$. This agrees with the criticality bound (5.3.49), and those shown in Fig. 5.8.



(i) For λ small enough, viz.

$$\bar{\lambda} < \tilde{\gamma} - |H| R, \quad (6.3.14)$$

the exterior gradient $\nabla W^{(\text{ext})}$ is also spacelike and outward pointing, leading to a conical, but infinite exterior geometry with $r \in (r_0, \infty)$.

(ii) In the intermediate regime

$$\tilde{\gamma} - |H| R \leq \bar{\lambda} \leq \tilde{\gamma} + |H| R, \quad (6.3.15)$$

$\nabla W^{(\text{ext})}$ is timelike⁶ and r is thus a temporal coordinate. We exclude this “critical” case from our current analysis.

(iii) If the tension is large enough,

$$\bar{\lambda} > \tilde{\gamma} + |H| R, \quad (6.3.16)$$

then $\nabla W^{(\text{ext})}$ is again spacelike but *inward* pointing. Thus, r is again a spatial coordinate; but now it decreases as one moves away from the cylinder surface. In principle, there could be some $r_{\min} > 0$, at which r starts increasing again. However, this would imply that ∇W changed character from inward to outward pointing at r_{\min} , and one can show that this is not possible in vacuum, see Appendix 6.A. Thus, r has the finite range $r \in (r_0, 0)$ and at the point $r = 0$ there will be a second axis, which can generically be singular.

We will refer to the first and third case as “sub-” and “super-critical”, respectively. In the static case $H \rightarrow 0$ and $\tilde{\gamma} \rightarrow 1$, and so the conditions take the form (i) $\bar{\lambda} < 1$ and (iii) $\bar{\lambda} > 1$, while the “critical” range (ii) degenerates to $\bar{\lambda} = 1$, cf. Sec. 6.4. In the present chapter, we are mainly interested in the super-critical regime (iii).

6.3.3 Junction conditions

The vacuum Einstein field equations (6.3.4) have to be supplemented by Israel’s junction conditions [Isr66, Isr67], linking the interior and exterior geometries across the cylinder surface:

$$T^m_n = M_{\text{Pl}}^2 ([K^p_p] \delta^m_n - [K^m_n]). \quad (6.3.17)$$

Here, $[X] := X - \tilde{X}$, and K_{mn} is the (pullback of the) extrinsic curvature tensor. The outward-pointing normal vectors in the interior and exterior are given by

$$\tilde{n}^\mu = \tilde{\gamma} e^{\tilde{\alpha}_0} (\dot{\tilde{r}}_0, 1, 0, 0) \quad \text{and} \quad n^\mu = \sigma \gamma e^{\alpha_0} (\dot{r}_0, 1, 0, 0), \quad (6.3.18)$$

respectively, with $\sigma = \pm 1$. In order for the normal vector n^μ to be outward-pointing, σ has to be +1 in the sub-critical case. But for super-critical tensions, the exterior radial

⁶Or light-like, if one of the bounds is saturated. In that case the coordinate transformation would be singular.

coordinate decreases as one moves away from the cylinder, so in that case one has to choose $\sigma = -1$.

Using these normal vectors, it is straightforward to show that the nonvanishing components of K^m_n are⁷

$$K^0_0 = \frac{\sigma\gamma}{R} \frac{r_0 \ddot{r}_0}{1 - \dot{r}_0^2} + n^\mu \partial_\mu (\eta_0 - \alpha_0), \quad (6.3.19a)$$

$$K^z_z = n^\mu \partial_\mu \alpha_0, \quad (6.3.19b)$$

$$K^\phi_\phi = \frac{\sigma\gamma}{R} - n^\mu \partial_\mu \alpha_0. \quad (6.3.19c)$$

The components of \tilde{K}^m_n have the same form, but with tildes on all quantities and $\sigma \rightarrow +1$. Plugging this and (6.3.10) into (6.3.17), the $(\bar{0})$ -component of the junction conditions becomes⁸

$$\bar{\lambda} = \tilde{\gamma} - \sigma\gamma. \quad (6.3.20)$$

The (\tilde{z}) -component, after eliminating $\bar{\lambda}$ using (6.3.20) as well as η by means of the vacuum equations (6.3.4) in the limit $r \rightarrow r_0$, and expressing everything in terms of the intrinsic cylinder quantities H and R , can be written as

$$\frac{dH}{d\tau} R^2 = - \left[\bar{\lambda} + \sigma\gamma f(\chi, \xi) - \tilde{\gamma} f(\tilde{\chi}, \tilde{\xi}) \right] \left(\frac{\sigma}{\gamma} - \frac{1}{\tilde{\gamma}} \right)^{-1}, \quad (6.3.21)$$

where

$$f(\chi, \xi) := \chi + (1 - \xi)^2 (1 - \chi)^2, \quad (6.3.22a)$$

$$\xi := r_0 \partial_r \alpha_0, \quad \chi := \left(\frac{HR}{\gamma} \right)^2. \quad (6.3.22b)$$

The complete set of equations of motion consists of the vacuum field equations (6.3.4) in the interior and exterior region, the dynamical (second order in time) junction condition (6.3.21), and energy conservation ($\lambda = \text{const.}$), supplemented by the boundary conditions (6.3.5) (as well as appropriate boundary conditions for the exterior domain which will be discussed later). Equation (6.3.20) is a constraint, i.e. it only contains first time derivatives, and only has to be imposed at the initial moment of time. Its conservation is guaranteed by the Gauss-Codazzi and vacuum field equations [Isr66, Isr67], and will later serve as an important consistency check for the numerical implementation.

Finally, the (ϕ) -junction condition determines the azimuthal pressure p_ϕ that is needed to keep the circumference of the cylinder constant. A similar calculation as before yields

$$\bar{p}_\phi = \sigma\gamma g(\chi, \xi) - \tilde{\gamma} g(\tilde{\chi}, \tilde{\xi}), \quad \text{with} \quad g(\chi, \xi) := 2(\chi - \chi\xi + \xi). \quad (6.3.23)$$

⁷In these formulas, evaluation at the surface should of course be performed *after* taking all occurring r -derivatives.

⁸Note that without choosing the correct sign $\sigma = -1$ in the super-critical case, this equation would imply $\bar{\lambda} < \tilde{\gamma}$, in contradiction to the condition (6.3.16).



6.4 Static solution

Before investigating dynamical solutions, let us first briefly review the much simpler and well-known case of static cosmic string geometries [Vil81, Got85, His85], i.e. the original 4D versions of the solution discussed in Sec. 5.3.2 for a pure tension source. After setting to zero all time-derivatives, the vacuum equations (6.3.4) can easily be integrated, yielding

$$\alpha(r) = \alpha_1 \ln \left(\frac{r}{r_0} \right), \quad \eta(r) = \alpha_1^2 \ln \left(\frac{r}{r_0} \right) + \eta_0, \quad (6.4.1)$$

where we already used a local rescaling of t and r to set $\alpha_0 = 0$. The same holds in the interior, but here the regularity conditions (6.3.5) imply $\tilde{\alpha}_1 = \tilde{\eta}_0 = 0$, so the geometry inside the cylinder is Minkowski. The two constants α_1, η_0 and the azimuthal pressure \bar{p}_ϕ are then determined by the junction conditions (6.3.20), (6.3.21) and (6.3.23):⁹

$$\eta_0 = -\ln |1 - \bar{\lambda}|, \quad \alpha_1 = 0 = \bar{p}_\phi. \quad (6.4.2)$$

Hence, the metric functions in the exterior are also constant, and so the spacetime around the string is locally flat as well. However, the nonzero value of η_0 corresponds to a nontrivial global geometrical effect. This can be seen explicitly after rescaling coordinates according to $(t^*, r^*) = (e^{\eta_0} t, \sigma e^{\eta_0} (r - r_0) + r_0)$. Here, the sign was chosen such that the new radial coordinate r^* is again *increasing* for super-critical tensions as well, and the shift makes the metric continuous across the shell. Hence, the spacetime is again covered by a single coordinate patch, in which the metric reads:

$$ds^2 = -dt^{*2} + dr^{*2} + dz^2 + W(r^*)^2 d\phi^2, \quad (6.4.3)$$

with

$$W(r^*) = \begin{cases} r^* & (r^* \leq r_0) \\ (1 - \bar{\lambda}) r^* + \bar{\lambda} r_0 & (r^* > r_0). \end{cases} \quad (6.4.4)$$

While the ratio of physical circumference to radius equals 2π inside, it is smaller outside, corresponding to a conical geometry with defect angle $2\pi\bar{\lambda} \equiv \lambda/M_{\text{Pl}}^2$.

For super-critical tensions $\bar{\lambda} > 1$, the physical circumference decreases as one moves away from the string and vanishes for some $r_1 > r_0$. This means that there is a second axis at this point in the exterior, and because the regularity condition (6.3.5b) is violated,¹⁰ there is a conical singularity at r_1 .

Even though these static solutions do exist in the super-critical case, it is not a priori clear whether they are stable (attractor) solutions. In order to answer this question, we next investigate general time-dependent solutions. As discussed above, the fact that the exterior space closes up in a second axis is unavoidable also in the dynamical case. However, as we will see, the conical singularity can (at least in some cases) be avoided.

⁹Equation (6.3.21) is a quadratic equation in α_1 , which has the second solution $\alpha_1 = 2$, usually referred to as the ‘‘Melvin’’ or ‘‘Kasner’’ branch [LG89, CLV99]. However, (6.3.23) would then imply $\bar{p}_\phi \neq 0$ for $\lambda = 0$, which is why we discard this branch.

¹⁰Unless $\bar{\lambda} = 2$; we discard this exceptional case in our discussion.

6.5 Numerical results

The dynamical solutions can again be obtained numerically, just like for the 6D case in Chap. 5, i.e. with the same discretization scheme and numerical algorithm as explained in Sec. 5.3.3. The only difference—apart from the absence of the BIG terms, and the slightly different 4D equations of motion—is that in the super-critical case the sign σ is -1 . In particular, this ensures that the constraint equation always has a real solution for η_0 , unlike in Chap. 5, where this led to the criticality bound. Furthermore, the exterior radial coordinate r decreases for super-critical tensions, ending in a second axis $r = 0$. The adequate boundary condition is then $\alpha'|_{r=0} = 0$ to avoid a curvature singularity, while $\eta|_{r=0}$ depends on the initial conditions; if it is nonzero, there is a conical singularity, as for the static solution above. The boundary condition at the interior axis remains unchanged, viz. $\tilde{\alpha}'|_{\tilde{r}=0} = \tilde{\eta}|_{\tilde{r}=0} = 0$, corresponding to a smooth axis.

Since our first main objective is to check whether the static solutions discussed in Sec. 6.4 are stable, we choose the corresponding flat profile as initial data,

$$\tilde{\alpha}_i(\tilde{r}) = 0 = \alpha_i(r), \quad (6.5.1)$$

where the subscript i denotes evaluation at the initial time $\tilde{t}_i = t_i = \tau_i = 0$ (without loss of generality). For vanishing initial velocity profiles $\dot{\tilde{\alpha}}_i(\tilde{r})$ and $\dot{\alpha}_i(r)$, the solution would remain static for all times. This is of course not what we are interested in, so we will choose some nonzero profile functions. As in Sec. 5.3.3, we can parametrize them as

$$\dot{\tilde{\alpha}}_i(\tilde{r}) = \frac{H_i}{\tilde{\gamma}_i} \tilde{F} \left(\frac{\tilde{r}}{R} \right), \quad \text{and} \quad \dot{\alpha}_i(r) = \frac{H_i}{\gamma_i} F \left(\frac{r}{R} \right), \quad (6.5.2)$$

with some profile functions \tilde{F} and F , satisfying the boundary conditions

$$\tilde{F}'(0) = 0, \quad \tilde{F}(1) = 1 = F(1). \quad (6.5.3)$$

Note that in the sub-critical case the domain of definition of F is $[1, \infty)$, but for super-critical string tensions it is the same as that of \tilde{F} , viz. $[0, 1]$, in which case it should also satisfy $F'(0) = 0$.

As discussed in Sec. 5.3.3, the initial data is now completely specified. It consists of the two parameters $\bar{\lambda}$, $H_i R$ and the two functions $\tilde{F}(x)$, $F(x)$, which are all dimensionless. Let us now present the numerical results.

6.5.1 Sub-critical tension

Before turning to the super-critical case in Sec. 6.5.2, let us first consider a dynamical solution for a sub-critical tension. This will help us gain confidence in the numerical solver and explicitly demonstrate that the deficit angle geometry reviewed in Sec. 6.4 is an attractor solution. As an example we choose the parameters

$$\bar{\lambda} = 0.5, \quad H_i R = 0.1, \quad (6.5.4)$$



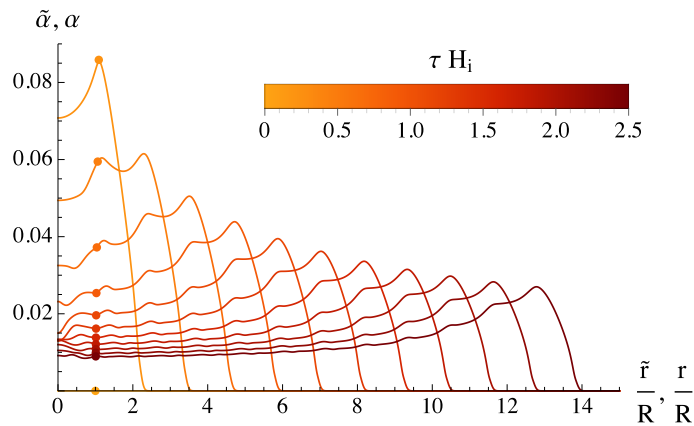


Figure 6.1: The radial profile of α at different values of τ for a sub-critical tension. The dots indicate the shell's position, left of which the plotted function is $\tilde{\alpha}(\tilde{r})$. After the initial perturbation is carried away in form of outgoing gravitational waves, the metric settles back to the static deficit angle geometry.

and the functions

$$\tilde{F}(x) = 1, \quad F(x) = \exp\left[-\frac{(x-1)^2}{\sigma^2}\right], \quad (6.5.5)$$

with $\sigma = 0.1$, i.e. the initial velocity is localized around the regularized string.

Fig. 6.1 shows the combined radial profile of the metric function $\tilde{\alpha}$ and α at various moments of time. The initial velocity profile leads to a rapid increase around the position of the cosmic string. Subsequently, it falls back down, thereby emitting cylindrically symmetric gravitational waves. Meanwhile, the coordinate position of the cylinder (indicated as dots in the plots) stays approximately constant. The small oscillations in the r -profile of α of frequency $\sim 1/R$ are due to waves in the interior of the cylinder which are reflected at the axis and partially reflected at the cylinder's surface. At late times, α asymptotically settles back to a constant profile, i.e. back to the static deficit angle solution we started with.

This can also be seen from Fig. 6.2a which shows the expansion rate $H \equiv d\alpha_0/d\tau$ as a function of time. After starting with a positive value, it becomes negative, turns around and asymptotically approaches zero. The oscillatory modulations are again due to the gravitational waves which are moving back and forth in the interior. Finally, Fig. 6.2b shows the effective EOS of the stabilizing pressure p_ϕ . Again, the oscillatory behavior is imprinted in the evolution; but more importantly, we see that it never becomes smaller than -1 , and therefore p_ϕ is physically reasonable in the sense that it satisfies the NEC. Furthermore, at late times it approaches zero, in agreement with the prediction (6.4.2).

We checked that the qualitatively same behavior is found for other values of $\bar{\lambda}$ and $H_i R$, as long as they satisfy the condition (6.3.14): the system always approaches the static conical defect geometry at late times. Hence, this solution is indeed an attractor

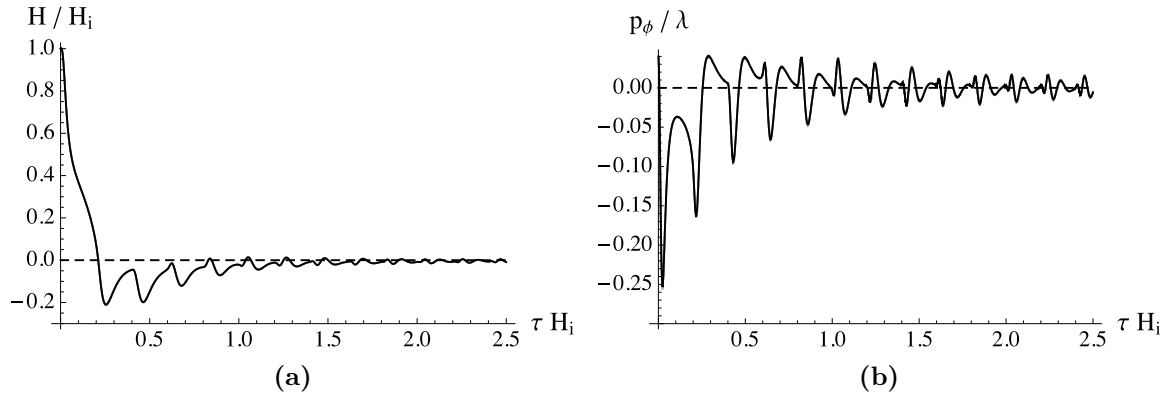


Figure 6.2: For sub-critical tensions, both the axial expansion rate H and azimuthal pressure p_ϕ oscillate and approach zero at late times, in accordance with the analytic predictions for the static solution. The numerical error estimates do not exceed the line thickness.

in the case of sub-critical string tensions.¹¹

6.5.2 Super-critical tension

Next, let us turn to the actual case of interest: super-critical string tensions. As an example, we consider the parameters

$$\bar{\lambda} = 1.5, \quad H_i R = 0.35, \quad (6.5.6)$$

and a flat initial velocity profile for both¹² $\tilde{\alpha}$ and α :

$$\tilde{F}(x) = 1, \quad F(x) = 1. \quad (6.5.7)$$

This time, the system shows a qualitatively completely different behavior. Figure 6.3a shows that the expansion rate H , instead of going to zero, approaches a constant nonzero value. This is one of the main results of the present chapter: *The static defect angle geometry is no stable solution in the case of super-critical string tensions. Instead, the attractor solutions are those in which the string expands in axial direction at a constant rate.*

The EOS of the azimuthal pressure is depicted in Fig. 6.3b. It also approaches a constant value at late times; but more importantly, it is again always larger than -1 and hence consistent with a radial stabilization by means of physically reasonable matter. However, the asymptotic value of p_ϕ/λ depends on the tension, as will be discussed in Sec. 6.6, which will ultimately lead to a break down of stabilizability.

¹¹These are of course just the 4D versions of the stable solutions found in Chap. 5 for vanishing BIG terms ($r_c = 0$).

¹²This choice can be justified a posteriori, because the attractor solutions at asymptotically late times approach roughly constant r -profiles. But we checked that the same attractor solutions are approached for other initial velocity profiles, like e.g. a Gaussian as before. Furthermore, they are still approached if $H_i R$ is made smaller, i.e. if the system is perturbed with less energy.



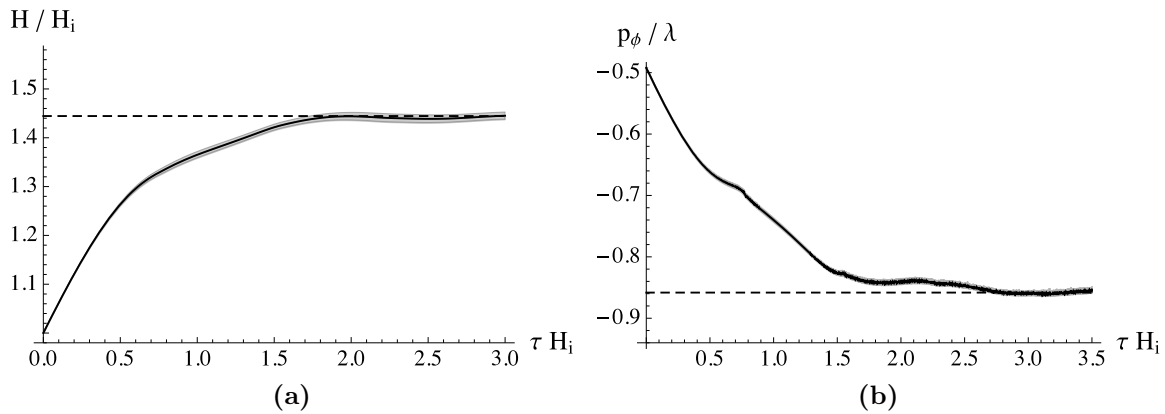


Figure 6.3: For super-critical tensions, the axial expansion rate H and azimuthal pressure p_ϕ both tend to constant, nonzero values at late times. This shows that the static solution is not an attractor anymore. The numerical error estimates are indicated by the gray bands. The dashed lines correspond to the analytic predictions derived in Sec. 6.6.

The radial coordinate position of the cylinder is now no longer approximately constant, but approaches a constant velocity, as can be seen in Fig. 6.4. Quite remarkably, it turns out that in the exterior coordinate patch, this asymptotic velocity is 1 (within the numerical uncertainties); this is just the speed of light, since in the coordinates (6.3.3) radial light rays correspond to $dr = \pm dt$. This means that no signal from beyond the dashed line in Fig. 6.4b can ever reach the string, drawn as a solid (green) line, or in other words: *A horizon is formed outside the super-critical cosmic string.* This is the second main result of our analysis.

On the other hand, the asymptotic velocity in the interior coordinate patch is less than 1, so no horizon is formed inside the regularized string. Note that, even though the exterior speed asymptotically approaches unity, it always stays below 1. Otherwise, there would also be contradictions because: (i) the shell represents a massive object, which can not travel exactly at the speed of light; (ii) moving at the speed of light is a coordinate invariant statement, so if it did hold in the exterior, it would also have to hold in the interior coordinate patch.

In the example we showed in Fig. 6.4, the conical singularity at $r = 0$, from the string's point of view, is hidden behind the horizon. However, this is no generic feature of the solutions, because the actual position of the horizon depends on the initial condition $H_i R$: smaller values move the dashed line in Fig. 6.4b to the left. By choosing $H_i R$ small enough, the horizon can be pushed so far that it crosses the axis, implying that the conical singularity is no longer hidden. But as will be shown in Sec. 6.7, for time dependent geometries the conical singularity can be avoided altogether.

6.5.3 Radial geometry

As already mentioned, the intrinsic geometry on the cylindrical shell is fully characterized by the axial expansion rate H , because after fixing R this expansion is the only

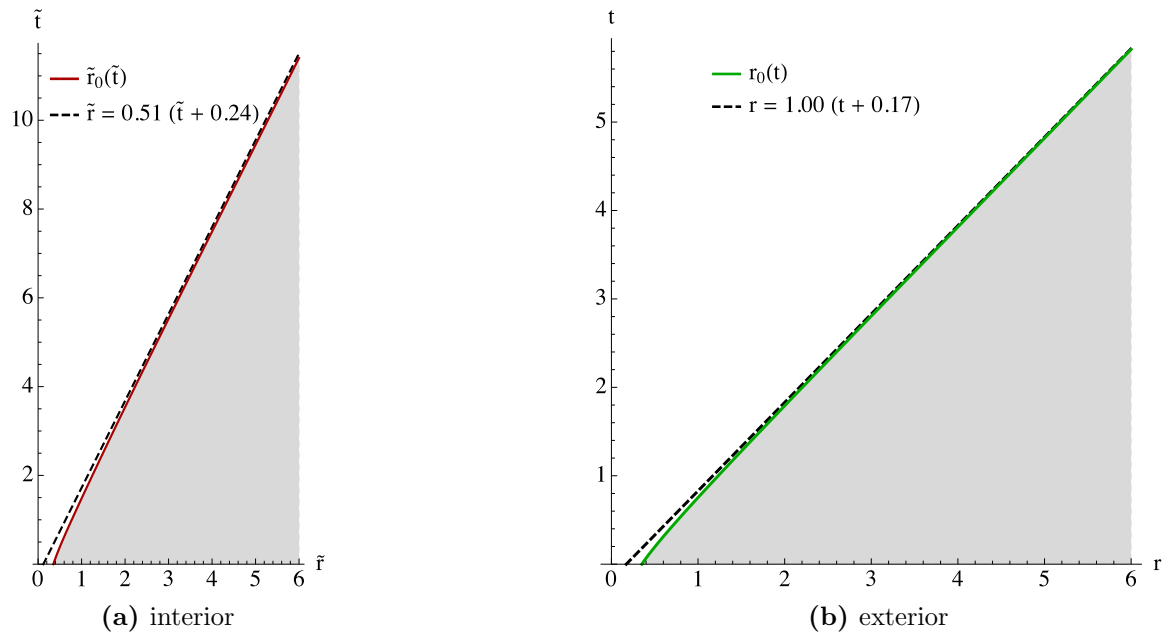


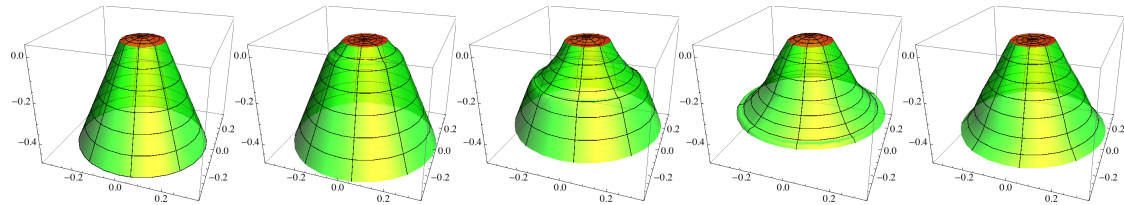
Figure 6.4: For super-critical string tensions, the shell’s position approaches a constant velocity in the interior and in the exterior coordinate patch. In the interior, this asymptotic velocity is < 1 and its actual value depends on $\bar{\lambda}$. In the exterior, it is generically $= 1$, implying a horizon. The coordinates in either patch only range from the axes to the shell, so the gray regions are not part of the spacetime.

nontrivial feature of the induced metric (6.3.6). However, the full metric (6.3.3) contains much more information, namely how space inside and outside the shell is curved in the radial direction, and how it evolves in time. The interior is of particular interest because we want to model a cosmic string with no strong dynamics inside, and so we would like the interior cross-sectional area to be approximately constant in order to have a successful regularization. Fixing R only keeps the shell’s circumference constant, but does not a priori say anything about the area. The constant velocity of the shell in the interior could even lead one to suspect that the area might actually be growing. However, the constancy of the velocity is of course a coordinate dependent statement, so one has to look at the invariant¹³ area. Furthermore, it would be nice to get some intuition about what the exterior geometry actually “looks like”.

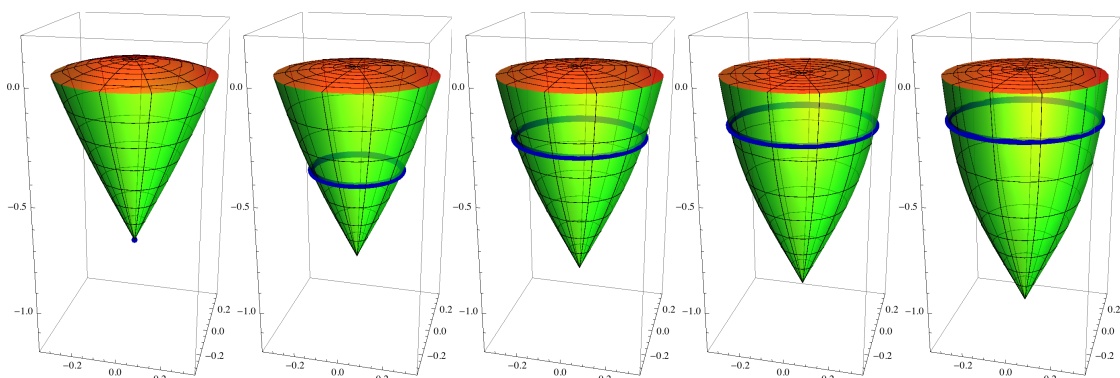
The radial warping of the full metric can be visualized by drawing embedding diagrams of the two-dimensional temporal and axial slices (i.e. $t, z = \text{const}$) in a fictitious three-dimensional space. These diagrams are shown in Fig. 6.5, where the interior is drawn red and the exterior green. The series of diagrams in each row corresponds to snapshots taken at equidistant times τ , starting at $\tau = 0$ on the left and increasing to the right.

¹³It is still slicing dependent, but this does not affect the question whether the area is asymptotically constant or growing.

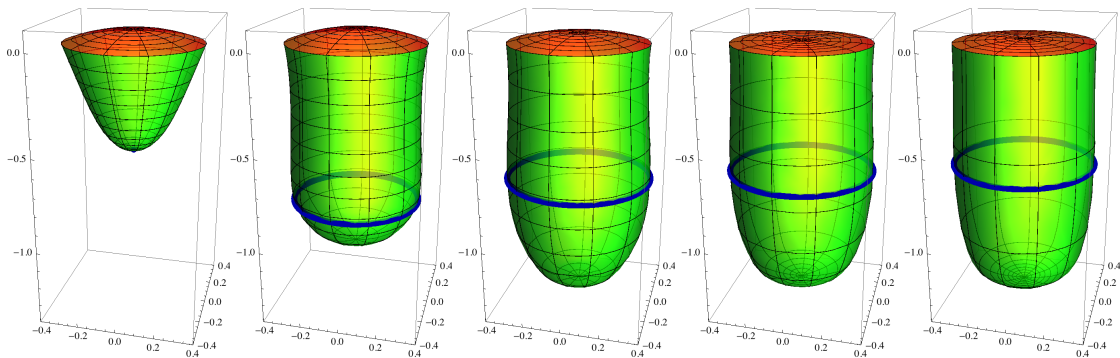




(a) Sub-critical ($\bar{\lambda} = 0.5$): After the Einstein-Rosen waves have been emitted, the geometry asymptotically settles to the static defect angle solution. An animation is included in this thesis as a flip-book in the bottom right corner.



(b) Super-critical ($\bar{\lambda} = 1.5$): The interior initially oscillates and settles to a constant profile at late times. The exterior keeps growing, and the light ray stays at a finite distance away from the shell, due to the horizon.



(c) Super-critical ($\bar{\lambda} = 1.5$), without a conical singularity. The qualitative behavior is the same as before.

Figure 6.5: Embedding diagrams of the radial geometry at equidistant time steps $\Delta\tau$. The interior of the regularized string is drawn red, the exterior green. In the super-critical cases, a light ray emitted from the exterior axis towards the shell is drawn as a solid blue line, visualizing the formation of a horizon.

Fig. 6.5a corresponds to the sub-critical case $\bar{\lambda} = 0.5$. The exterior space is cut off at some finite radius in the pictures, but actually extends to infinity. One can clearly see how the shell creates a deficit angle, making the exterior space conical. As time evolves, the disturbance induced by the initial conditions moves outwards in the form of a cylindrical gravitational wave, and the geometry asymptotically settles to the static defect angle solution.¹⁴

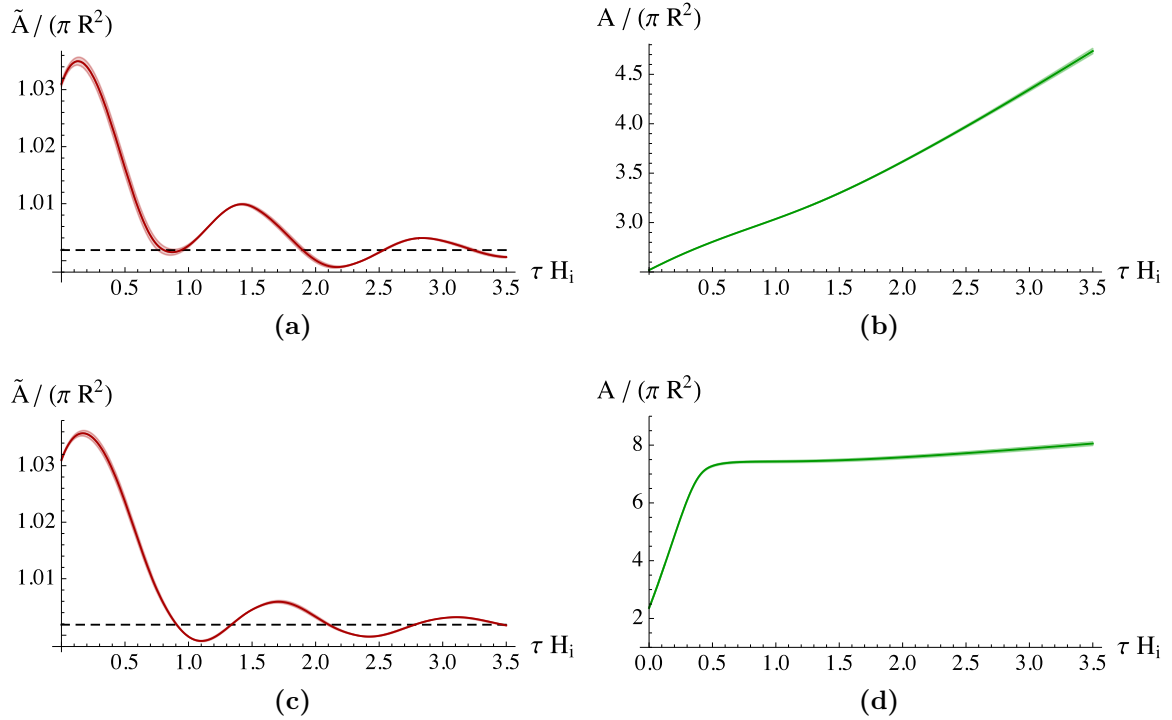


Figure 6.6: Interior (left column) and exterior (right column) area of the super-critical cosmic string geometry with (upper row) and without (lower row) conical singularity at the exterior axis. The interior area approaches a constant value in accordance with the analytic prediction (6.6.10) (dashed lines), confirming a successful stabilization, whereas the exterior area keeps growing.

The super-critical case $\bar{\lambda} = 1.5$ is shown in Fig. 6.5b. Here, the exterior space closes up and ends in a conical singularity, making the space compact. The causal structure is visualized by adding a radial light ray that is initially emitted from the exterior axis (solid blue lines). Asymptotically, it stays at a finite distance away from the shell, in accordance with the formation of a horizon. Furthermore, one can already see from these diagrams that the interior area indeed stays approximately constant, in accordance with a successful stabilization, whereas the exterior area increases. To make these statements more quantitative, Fig. 6.6a shows the interior cross-sectional

¹⁴The initial defect angle is slightly larger than the final one, because the initial kinetic energy gives an additional contribution.



2D area

$$\tilde{A}(\tau) := 2\pi \int_0^{\tilde{r}_0(\tau)} \tilde{r} e^{\tilde{\eta}-2\tilde{\alpha}} d\tilde{r}. \quad (6.5.8)$$

The gravitational waves moving back and forth inside the shell give rise to very small oscillations of this area, but at late times it indeed approaches a constant value. In Sec. 6.6 we will derive an analytic prediction for its value, which is shown as a dashed line. Hence, our numerical solution can indeed be viewed as a successful regularization of a stabilized cosmic string. On the other hand, the exterior area $A(\tau)$, plotted in Fig. 6.6b, gets larger at an asymptotically constant rate.

Finally, Fig. 6.5c shows the embedding geometry for the same super-critical tension $\bar{\lambda} = 1.5$, but with initial conditions which remove the conical singularity, as discussed in Sec. 6.7. These nontrivial initial conditions lead to a much more rapid increase in the exterior area for the first time steps. But apart from that, the qualitative behavior is the same as in the case with conical singularity. In particular, the interior area again approaches the constant value and the exterior size keeps growing, see Figs. 6.6c and 6.6d. However, the asymptotic growth rate is smaller than in the conical case, showing that the speed at which the exterior space gets larger is not only set by the string tension, but also influenced by the amount of C-energy that is needed to smooth out the conical singularity.

6.6 Analytic results

From the numerical investigations we learned that for super-critical string tensions, the system asymptotically approaches a constant axial expansion rate H at late times. In this section, we will derive the analytic relation between the tension $\bar{\lambda}$ and HR . To this end, we first of all make use of the fact that the numerical results reveal another quite generic behavior: For different choices of initial conditions the shell generically approaches a constant (coordinate) velocity

$$\dot{\tilde{r}}_0(\tilde{t}) \rightarrow \tilde{v} < 1 \quad \text{and} \quad \dot{r}_0(t) \rightarrow 1. \quad (6.6.1)$$

Plugging this into (6.3.12), we conclude that $\tilde{\gamma}$ and γ also approach constants:¹⁵

$$\tilde{\gamma} \rightarrow \frac{HR}{\tilde{v}}, \quad \gamma \rightarrow HR. \quad (6.6.2)$$

Substituting this into the junction condition (6.3.20), we obtain

$$\boxed{\bar{\lambda} = HR \left(1 + \frac{1}{\tilde{v}} \right)}. \quad (6.6.3)$$

¹⁵Using (6.6.2) to eliminate γ in (6.3.20) shows that the solution asymptotically approaches the critical bound (6.3.15) from above.

This is not yet the relation we are looking for, because it still contains the additional unknown parameter \tilde{v} . But the numerics show that the value of \tilde{v} only depends on $\bar{\lambda}$ (and not on the initial conditions). Hence, there should be a second relation between the parameters lifting the degeneracy of (6.6.3). However, in order to derive this relation analytically, one needs to know the complete interior geometry of the attractor solution. Fortunately, it turns out that this solution can indeed be found.

We look for a solution $\tilde{\alpha}$ which leads to a shell coordinate which is changing at a constant rate \tilde{v} , i.e. $\tilde{r}_0 = \tilde{v}\tilde{t}$.¹⁶ Together with (6.3.9), this condition fixes the time dependence of $\tilde{\alpha}_0$:

$$\tilde{\alpha}_0 = \ln \left(\frac{\tilde{v}\tilde{t}}{R} \right), \quad (6.6.4)$$

In order to extend this function into the interior space of the shell, we look for scaling solutions of (6.3.4a) which depend on \tilde{r} only through the ratio $x := \tilde{r}/\tilde{t}$. The only solution of this type, which is also compatible with (6.6.4), is¹⁷

$$\tilde{\alpha}(\tilde{t}, \tilde{r}) = \ln \left[\frac{\tilde{t}}{\Omega} \left(1 + \sqrt{1 - x^2} \right) \right] \quad \text{with} \quad \Omega := \frac{R}{\tilde{v}} \left(1 + \sqrt{1 - \tilde{v}^2} \right). \quad (6.6.5)$$

Integrating (6.3.4b) and (6.3.4c) then yields

$$\tilde{\eta}(\tilde{t}, \tilde{r}) = 2 \ln \left(\frac{1 + \sqrt{1 - x^2}}{2\sqrt{1 - x^2}} \right), \quad (6.6.6)$$

where the elementary flatness condition $\tilde{\eta}|_{\tilde{r}=0} = 0$ was implemented. The complete scaling solution for the interior region now reads

$$d\tilde{s}^2 = \left(1 + \sqrt{1 - x^2} \right)^2 \left[\frac{\Omega^2}{4} \left(\frac{-d\tilde{t}^2 + d\tilde{r}^2}{\tilde{t}^2 - \tilde{r}^2} \right) + \frac{\tilde{t}^2}{\Omega^2} dz^2 \right] + \left(\frac{\Omega x}{1 + \sqrt{1 - x^2}} \right)^2 d\phi^2, \quad (6.6.7)$$

which is an exact vacuum solution of the Einstein equations.

We can now evaluate (6.6.6) at the shell, use (6.3.13) and (6.6.2) to finally obtain

$$HR = \frac{4\tilde{v}\sqrt{1 - \tilde{v}^2}}{(1 + \sqrt{1 - \tilde{v}^2})^2}. \quad (6.6.8)$$

This is the second relation we were looking for.¹⁸ The two equations (6.6.3) and (6.6.8), which allow to determine the parameter combination HR as a function of the tension $\bar{\lambda}$, are the main analytical result of our work. For small velocities $\tilde{v} \ll 1$ we find a linear dependence

$$HR \approx \bar{\lambda} - 1. \quad (6.6.9)$$



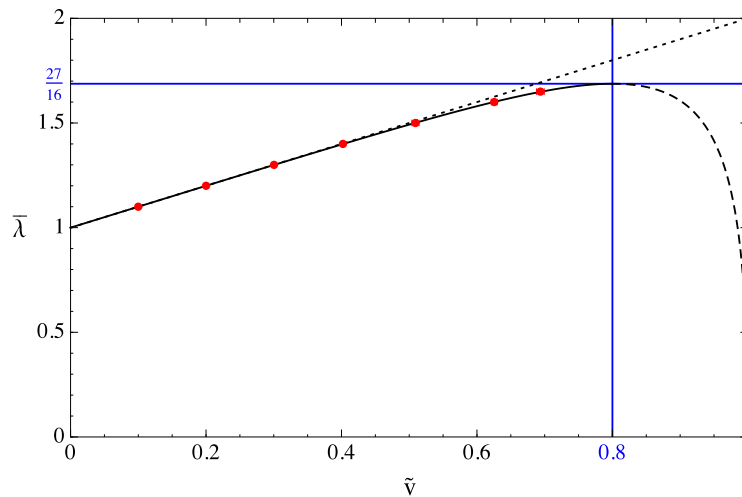


Figure 6.7: There are scaling solutions only for $\bar{\lambda} < 27/16 \approx 1.69$. Above that value the system (6.6.3) and (6.6.8) has no real solution. Below, there are two branches, one corresponding to $\tilde{v} < 4/5$ and the other to $\tilde{v} > 4/5$. The red dots, showing the numerical results, single out the former branch as being the attractor solution and thus physically interesting.

The exact system does not possess solutions for arbitrarily large tensions. In fact, there is the rather stringent bound $\bar{\lambda} < 27/16 \approx 1.69$ corresponding to a velocity $\tilde{v} = 4/5$. Below that value there are two branches of solutions corresponding to $\tilde{v} < 4/5$ and $\tilde{v} > 4/5$. Only the former branch turns out to be an attractor. These results are summarized in Figs. 6.7 and 6.8. The solid curves depict the analytical result for the attractor branch, whereas the dashed curves show the other branch. Each dot corresponds to one run of the numerics for different values of $\bar{\lambda}$. The number of time step was chosen such that the convergence of H and \tilde{v} was sufficiently accurate. The corresponding error bars, usually not exceeding the size of the dots, are also shown. The dots lie almost perfectly on the solid line, confirming our analytical predictions. Moreover, Fig. 6.8 nicely illustrates that the linear dependence of HR on $\bar{\lambda}$ in (6.6.9), drawn as a dotted line, is a very good approximation for almost the whole regime.

At first sight, the physical origin of the bound $\bar{\lambda} < 27/16$ is unclear because it looks as if the system cannot be solved for larger tensions. This puzzle can be resolved by calculating the pressure in ϕ -direction, which we implemented to stabilize the physical circumference of the shell. This can be done by evaluating (6.3.23) for the scaling solutions described above. The resulting relation between p_ϕ and $\bar{\lambda}$ is shown in Fig. 6.9. We see that for $\bar{\lambda} < 128/81 \approx 1.58$, the EOS of p_ϕ satisfies the NEC, i.e. it is greater

¹⁶For simplicity, we assume that initially $\tilde{r}_0 = 0$. The general case with an initial offset, which has to be used when comparing to the numerical solutions, is simply obtained by letting $\tilde{t} \mapsto \tilde{t} + \text{const}$.

¹⁷This solution was also obtained in [Ech93].

¹⁸Note that, even though it relates local shell parameters, it implicitly depends on the entire interior geometry through the use of (6.6.6); for instance, it knows about the regularity at the axis.

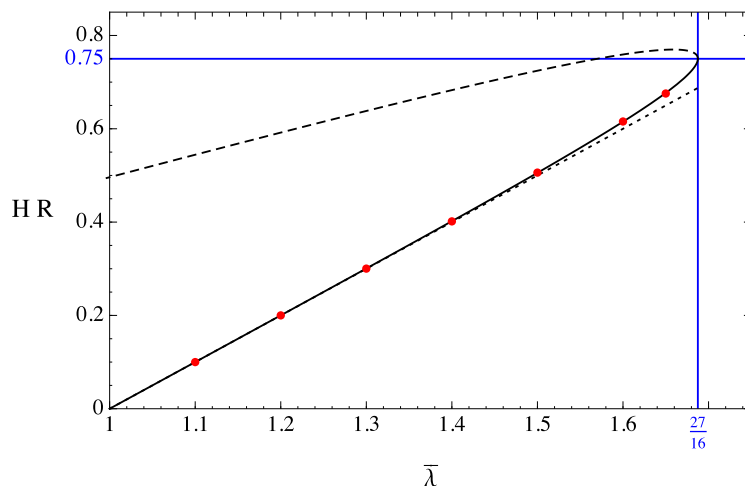


Figure 6.8: The axial expansion rate of the super-critical string as a function of the tension $\bar{\lambda}$. The linear relation (6.6.9) corresponds to a good approximation.

than -1 . This means that the shell can be stabilized by means of physically reasonable matter. However, for $\bar{\lambda} > 128/81$ —which happens *before* the maximum value $27/16$ is reached—the EOS drops below -1 , indicating that the shell can no longer be stabilized. Consequently, we should not trust the scaling solutions in this regime because their derivation relied explicitly on that assumption. In this regime a different approach that allows for an angular expansion of the shell is needed. This would require to go beyond the effective shell description of the transverse sector and could for instance be achieved by studying the full Nielsen-Olesen (NO) setup, as done numerically in [Cho98]. This work also allows for a nontrivial cross-check of our effective description: In [Cho98] it was found that a string with unit winding number starts expanding in transverse directions once $\bar{\lambda} > 1.57 \pm 0.06$.¹⁹ This is in perfect agreement with our result. Note that at this point HR is already close to one, and we are therefore no longer insensitive to the microscopic details of the string. The perfect numerical agreement between both approaches thus seems to be an accident, and indeed, for higher winding numbers, the stability bound derived in the NO setup is slightly below the one derived in our setup. This demonstrates that quantitative predictions get sensitive to the underlying UV model once HR is of order one.

We also checked explicitly that the numerically determined radial profiles of $\tilde{\alpha}$ and $\tilde{\eta}$ approach the analytic solutions (6.6.5) and (6.6.6), respectively. Within the numerical error bars, we found perfect agreement after the system was evolved sufficiently far in time.

Another consistency check of our analysis concerns the cross-sectional area of the interior space. As argued before, the area should be constant for the regularization to

¹⁹The translation to our variables is achieved via the identification $\bar{\lambda} = 8\pi|n|\eta^2/m_p^2$, which holds in the Bogomol'nyi limit.



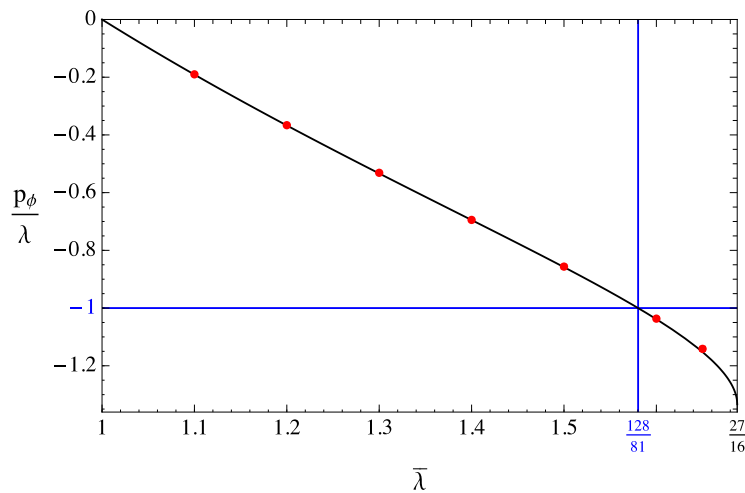


Figure 6.9: The string can be radially stabilized by physical matter as long as $\bar{\lambda} < 128/81 \approx 1.58$. For larger values of the tension the required azimuthal pressure violates the NEC, indicating a breakdown of stabilizability.

work properly. After substituting the scaling solution in (6.5.8), we find

$$\tilde{A} = \pi R^2 \frac{(1 + \sqrt{1 - \tilde{v}^2})^2}{4\tilde{v}^2} |\ln(1 - \tilde{v}^2)|, \quad (6.6.10)$$

which reduces to the flat space result in the limit $\tilde{v} \rightarrow 0$, as expected. Most importantly, this expression is time independent (and finite for $\tilde{v} < 1$) showing that our regularization scheme is stable. The analytical value is depicted in Figure 6.6a as a dashed line. It is approached by the numerical solution consistently.

The fact that the area inside the shell is exactly constant for the scaling solution suggests that the radial movement of the shell is just a coordinate relict. Indeed, as shown in Appendix 6.B, one can introduce new coordinates for which the shell sits at a constant coordinate position and the whole time dependence of the metric is related to the expansion in axial direction. Moreover, it will be show that the scaling solution is equivalent to a solution discussed by Witten [Wit82] and Gregory [Gre03], describing a “cigar” shaped universe. In both works the vacuum solution was discussed but without matching it to an actual matter model. To our knowledge this has been achieved for the first time within our super-critical string setup.

One might wonder whether the analytic scaling solution discussed above could also describe the asymptotic form of the exterior spacetime by simply replacing \tilde{v} by $v = 1$. However, this cannot work because Eq. (6.6.8) could then also be derived from the exterior²⁰ and would thus give the contradictory result $HR = 0$. Thus, the actual exterior solution cannot converge to the $v = 1$ scaling solution, at least not everywhere. This can also be understood by realizing that in the scaling solution the shell moves

²⁰It would only differ by the finite and constant overall factor $\exp(-\eta|_{r=0})$ corresponding to the conical singularity at the exterior axis.

at constant (coordinate) velocity; hence, for $v = 1$ it would always move exactly with the speed of light, which is impossible for a massive shell (and would also contradict $\tilde{v} < 1$, as already mentioned earlier). In other words, the actual attractor solution in the exterior would have to be one in which the shell's speed is not constant but only approaches 1 at late times, and can thus not be the simple scaling solution.

Nevertheless, we found that the numerical solution does indeed approach the $v = 1$ scaling solution for most r including the axis, but starts to deviate from it close to the shell. Moreover, the concrete form of these deviations remains sensitive to the initial conditions for all times, so it seems impossible to make any further generic statements about the full exterior attractor solution.

The convergence towards the scaling solution sufficiently far away from the string can also be seen qualitatively in the embedding diagrams in Figs. 6.5b and 6.5c, which nicely agree with the cigar shape of the scaling solution. The cigar keeps growing and presumably becomes infinitely long as $\tau \rightarrow \infty$, cf. Figs. 6.6b and 6.6d.

Our results are also relevant for 6D braneworld models. In this case the string is replaced by a 3-brane corresponding to our universe. A generalized version of Eq. (6.6.9) then plays the role of a modified Friedmann equation. This higher dimensional picture is discussed in Sec. 6.9.

Finally, let us emphasize that the relation we derived here relates the expansion rate to the tension of the (regularized) *super-critical* string. The conical singularity at the exterior axis can be interpreted as another (unregularized) *sub-critical* string. This point of view was for instance taken in Ref. [Gre03], where only the sub-critical brane was identified (in a 6D context). However, the corresponding deficit angle—and thus the tension of this sub-critical string—is not generically related to the expansion rate. Instead, it can be chosen independently, and in particular even be set to zero, as we will show in the next section (see also Fig. 6.5c). What was missed in [Gre03] is the second, super-critical brane, which is actually responsible for the inflationary behavior. In summary, *a sub-critical string only creates a deficit angle and does not inflate, whereas a super-critical string inflates in axial direction at the rate determined by the system (6.6.3) and (6.6.8).*

6.7 Removing the conical singularity

In Sec. 6.4, we saw that for super-critical string tensions, the static solution necessarily has a conical singularity at the exterior axis. This means that the vacuum Einstein equations are actually not satisfied there; instead, there is a second (unregularized, sub-critical) string sitting at the axis, the tension of which must be suitably dialed according to the tension of the original (regularized, super-critical) string. This is of course rather unsatisfactory, because we wanted to model a single super-critical cosmic string. Physically, there is no reason why the second string should be necessary.

This suggests that the second string—or equivalently, exterior conical singularity—is an artifact caused by the too strong assumption of having a static geometry. And indeed, for time dependent solutions, this need not be the case. The absence of a



conical singularity is equivalent to $\eta|_{r=0} = 0$. Using the vacuum field equation (6.3.4b), we can rewrite this as

$$\eta|_{r=0} = \eta_0 - \int_0^{r_0} r [(\partial_t \alpha)^2 + (\partial_r \alpha)^2] dr \stackrel{!}{=} 0. \quad (6.7.1)$$

For (regular) static solutions, α is constant and so $\eta|_{r=0} = \eta_0$, which is nonzero. But for time dependent solutions, the integral in (6.7.1) is positive. Hence, if $\eta_0 > 0$, one can always choose initial conditions for α , such that (6.7.1) is fulfilled at the initial time. But then it will in fact be fulfilled for all times, since the constraint (6.3.4c) implies that $\partial_t \eta|_{r=0} = 0$ (if α is regular, which we assume). Whether η_0 is positive, again depends on the string tension and the initial conditions for $\tilde{\alpha}$. Specifically, using the junction condition (6.3.20), one can show that (for super-critical tensions) $\eta_0 > 0$ is equivalent to

$$\bar{\lambda} < \tilde{\gamma} + \sqrt{1 + H^2 R^2}. \quad (6.7.2)$$

Thus, if $\bar{\lambda}$ lies inside the non-empty interval

$$\tilde{\gamma} + |H|R < \bar{\lambda} < \tilde{\gamma} + \sqrt{1 + H^2 R^2}, \quad (6.7.3)$$

the conical singularity at the exterior axis can always be removed by a suitable choice of initial data for α .

In the numerical examples that we studied, condition (6.7.2) was always satisfied. Indeed, for the flat profile function $F(x) = 1$, the initial constraint (6.3.4b) implies that the bound (6.7.2) is well above the bound $\bar{\lambda} < 27/16$, beyond which the solutions discussed above are no attractors anyway, see Fig. 6.10.

However, the rather arbitrary choice of initial profiles (6.5.7) does not automatically lead to a smooth axis. But we checked that the late time asymptotic behavior, as well as the relation between string tension and expansion rate, still persist if the initial data for α is deformed such that (6.7.1) is satisfied and the exterior geometry is perfectly smooth.

In other words, the deficit angle at the exterior axis corresponds to a sub-critical string that is put there in addition to the actual super-critical string of interest. Its tension is a parameter that is completely controlled by the initial data; in particular, it can be set to zero whenever (6.7.3) is satisfied. Furthermore, the asymptotic expansion rate H of the attractor solutions is completely insensitive to this sub-critical string and is instead set by the tension of the super-critical string. This can also be understood from the formation of the horizon: an observer co-moving with the cylindrical shell cannot even see the axis (at least for certain initial conditions), and hence cannot tell whether there is a conical singularity or not. Therefore, intrinsic quantities like H cannot depend on the exterior defect angle either.

The fact that the conical singularity can be removed in the dynamical case, while being physically satisfactory, raises another question: How does the system know which side of the shell is the interior and which the exterior? After all, both regions are described by the same metric ansatz and share the same boundary conditions at the axes. Still, the numerical results show that the shell's velocity approaches unity only

in the exterior, implying that the two regions do in fact evolve differently. Clearly, this difference must already be incorporated in the initial conditions. If those were completely symmetric as well, no difference between “inside” and “outside” could ever emerge.

And indeed there is such a difference: the difference between $\tilde{\eta}_{0i}$ and η_{0i} , measuring the gravitational C-energy²¹ in the interior and exterior, respectively. In the case in which the exterior conical defect was removed, this difference was caused by choosing a nontrivial initial profile for α only in the exterior. In the case with conical singularity, both initial profiles were chosen identically, but the localized energy-density corresponding to the conical defect also adds to the exterior C-energy, while there is no such contribution in the interior. Thus, in both cases η_{0i} was larger than $\tilde{\eta}_{0i}$, or in other words, there was more C-energy in the exterior than in the interior.

The symmetry of the setup then implies that the opposite also holds: If we interchange initial conditions, such that there is more C-energy in the “interior”, then the velocity will approach 1 there, and a constant < 1 in the “exterior”. But in this situation, we would simply interchange the names “interior” and “exterior”, because there should not be a horizon in the interior if we want to view it as a regularization of a thin cosmic string. Hence, the initial conditions should always be chosen such that there is less C-energy in the interior; or equivalently, the side with less C-energy should be identified as the actual interior. Note that, in particular, this qualification of inside and outside does not depend on whether there is a conical singularity at either axis.

As already remarked, in the completely symmetric case $\tilde{\eta}_{0i} = \eta_{0i}$ there can be no difference between inside and outside. In fact, we found that there is a finite region²² $\tilde{\eta}_{0i} \approx \eta_{0i}$ for which no difference emerges. In these cases *both* velocities approach unity, and so one cannot identify an interior, and can thus not speak of a regularized cosmic string. We therefore did not further investigate these cases.

6.8 Parameter plot

Our findings can nicely be summarized in the parameter plot shown in Fig. 6.10. It assumes a trivial radial profile of $\tilde{\alpha}$, which we chose as initial data for the numerics. (If the radial profile is nontrivial, $\tilde{\eta}_0$ is not rigidly related to HR , and so the parameter space becomes three-dimensional. Hence, this plot is only valid at initial time.)

In the bottom region (purple), the string is sub-critical and the static defect angle solution is an attractor. In the intermediate region between the solid purple and orange curves, the system is critical; this region is not covered in the present work. Above the orange curve, the string is super-critical, and in the shaded region (orange) it approaches the axially expanding scaling solutions discussed in this chapter. The upper bound of this region is $\bar{\lambda} = 27/16 \approx 1.69$, beyond which there is no solution for $\tilde{v}(\bar{\lambda})$ anymore and hence the geometry cannot approach the scaling solutions, cf. Sec. 6.6.

²¹Cf. Secs. 2.7 and 5.3.3.

²²We did not investigate this more quantitatively.



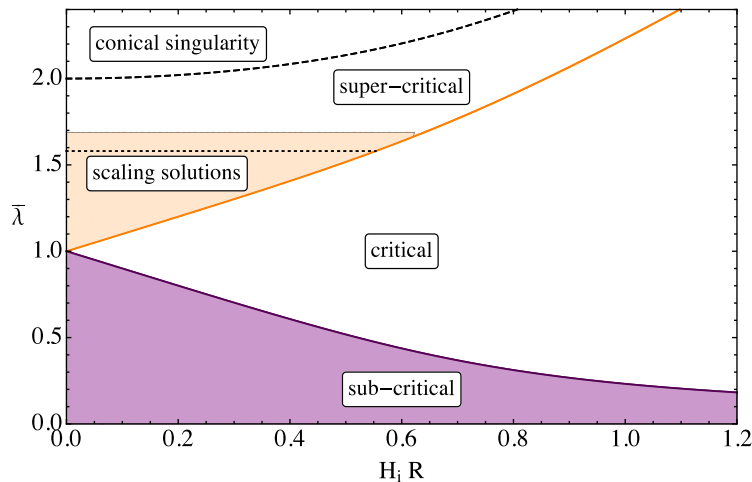


Figure 6.10: Region plot of parameter space at the initial time, when $\tilde{\alpha}(\tilde{r}) = 0$. The purple and orange curves are the borders between the sub-, critical, and super-critical regimes. In the purple region the static solutions are stable, whereas in the orange region the inflating scaling solutions are approached. Above the dotted line the radial stabilization breaks down; above the dashed curve the conical singularity at the exterior axis would become unavoidable.

However, before this bound is reached, the required azimuthal pressure p_ϕ violates the NEC for $\bar{\lambda} = 128/81 \approx 1.58$ (dotted black line), which should be interpreted as the statement that the string thickness cannot be stabilized anymore, in accordance with [Cho98]. Therefore, we did not further investigate the upper white region. Finally, the dashed black curve corresponds to the bound (6.7.2), beyond which the conical singularity at the exterior axis cannot be removed. It is well above the orange region, implying that in the cases we studied, which dynamically approach the analytic scaling solutions of Sec. 6.6, the conical singularity can always be removed.

6.9 Braneworld in 6D

The above results can easily be generalized to the case of a six-dimensional braneworld model, in which the string is promoted to a 3-brane describing our universe. The corresponding metric and field equations are those of Sec. 5.3, with the BIG terms set to zero (they will be included again below). The system can then be solved numerically in a similar fashion, and the results that we found are also analogous.²³ The axial expansion rate H , which in this case corresponds to the ordinary Hubble parameter, approaches again a constant, nonzero value. Furthermore, the coordinate velocity of the

²³After the publication of [NS15b], we also found a different class of attractor solutions in 6D, for which both asymptotic coordinate velocities are less than 1, and both the interior as well as the exterior metric is of the scaling form (6.9.3) at late times. These solutions will be discussed in more detail elsewhere.

brane exhibits the same asymptotic behavior (6.6.1) as in the 4D case, thus implying

$$\tilde{\gamma} \rightarrow \frac{3HR}{\tilde{v}}, \quad \gamma \rightarrow 3HR. \quad (6.9.1)$$

Using the 6D version of (6.3.20), we find

$$\bar{\lambda} = 3HR \left(1 + \frac{1}{\tilde{v}} \right), \quad (6.9.2)$$

where now $\bar{\lambda} := \lambda / (2\pi M_6^4)$, with M_6 denoting the six-dimensional Planck mass and λ the energy per 3D string volume, corresponding to a 4D vacuum energy. The analytic solutions in the interior can be derived in the same way as before, resulting in

$$\tilde{\alpha}(\tilde{t}, \tilde{r}) = \frac{1}{3} \ln \left[\frac{\tilde{t}}{\Omega} \left(1 + \sqrt{1 - x^2} \right) \right], \quad \tilde{\eta}(\tilde{t}, \tilde{r}) = \frac{4}{3} \ln \left(\frac{1 + \sqrt{1 - x^2}}{2\sqrt{1 - x^2}} \right), \quad (6.9.3)$$

still with $x \equiv \tilde{r}/\tilde{t}$ and Ω as defined in (6.6.5). This enables us to generalize (6.6.8) to

$$3HR = \tilde{v} (1 - \tilde{v}^2)^{\frac{1}{6}} \left(\frac{2}{1 + \sqrt{1 - \tilde{v}^2}} \right)^{\frac{4}{3}}. \quad (6.9.4)$$

As before, in the physically relevant regime where $HR \ll 1$, we can analytically eliminate \tilde{v} from the system (6.9.2) and (6.9.4), yielding a modified Friedmann equation

$$3HR \approx \bar{\lambda} - 1. \quad (6.9.5)$$

It should be noted that for a realistic value of the regularization scale, say $R \sim \text{TeV}^{-1}$, this equation would again require a tremendous amount of fine tuning between the two terms on the right hand side in order to describe the observed accelerated expansion of the universe. For generic values of the 4D vacuum energy $\bar{\lambda} \gtrsim \mathcal{O}(1)$, Eq. 6.9.5 predicts $H \sim R^{-1}$. Thus, these super-critical solutions within pure six dimensional GR cannot help with the cosmological constant problem.

The inclusion of the BIG terms can be accomplished by simply replacing $\bar{\lambda}$ by $\bar{\lambda} - 3r_c^2 H^2$. In the limit $HR \rightarrow 0$, this leads to the corresponding modified Friedmann equation

$$3M_{\text{Pl}}^2 H^2 \approx \lambda - \lambda_{\text{crit}}. \quad (6.9.6)$$

This is the standard 4D equation, with the vacuum energy shifted by an amount $\lambda_{\text{crit}} \equiv 2\pi M_6^4$. Since $M_6 \sim 10^{-3} \text{eV}$ (for a crossover of order of today's Hubble radius), this can again clearly not help with the CC problem. Moreover, since λ_{crit} is constant—i.e. fixed by the model parameter M_6 —it cannot readjust if λ changes (as during a phase transition), and so this presents no dynamical degravitation mechanism, but rather a small trivial shift in the 4D CC. This is in contrast to the sub-critical cosmology setup discussed in Chap. 5, where the brane tension was absorbed by the deficit angle, which *can* adjust dynamically.



Furthermore, it is a priori not clear whether the super-critical region in 6D BIG is ghost-free. Even though this is suggested by extrapolating the stability line found in the sub-critical region in Chap. 5 above the criticality bound, this issue would have to be investigated more rigorously. However, we did not further ascertain this matter, since the model does not seem very promising anyway.

But it should be noted that since the extra space is necessarily compact for a super-critical brane tension, we are not dealing with infinite extra dimensions anymore; accordingly, one expects to find a 4D behavior of gravity at length scales well above the corresponding Kaluza-Klein scale, i.e. the transverse bulk size, as in other related models like [AHDD98, ABPQ04]. Therefore, the BIG terms are not necessary anymore to recover 4D GR, and could even be discarded altogether.

Even if this model cannot solve the CC problem, it might still provide an interesting (and consistent!) late time modification of cosmology. Of course, so far we only discussed the simplest case of a pure tension brane. If one were to model a more realistic cosmological setup, the brane would also be equipped with other fluid components like dust or radiation. However, a preliminary numerical analysis revealed that the corresponding solutions are generically not stable; instead, the geometry undergoes a gravitational collapse. In fact, this is not too surprising, since we are here dealing with a compact bulk geometry, but did not include any stabilization of the extra dimensions. But there might still be a stable window for small enough dust components; otherwise, one could try to add some sort of bulk stabilization mechanism.²⁴ All of these issues are beyond the scope of this thesis, and are left for future research.

6.10 Conclusion and outlook

In this chapter, we studied the geometry of a single super-critical cosmic string. In a marginally super-critical regime, $1 < \bar{\lambda} \lesssim 1.6$, the string can consistently be modeled as a cylindrical shell of fixed circumference $2\pi R$. Within this parameter region, there are well known static solutions for which the geometry is compact and closes in a second singular axis away from the string. By numerically solving the full system of vacuum and shell matching equations, the instability of the static solution was demonstrated. It was shown that the system instead asymptotically approaches a time-dependent attractor solution with the following properties:

- The string expands in axial direction at a constant rate.
- A horizon is formed away from the string.
- The bulk geometry remains compact but becomes cigar-shaped and expands.
- The exterior conical singularity can always be avoided in these dynamical solutions.

²⁴A related 6D model, compactified and stabilized via flux quantization, but with sub-critical brane tensions, will be discussed in Chap. 7.

Moreover, an analytic relation between the tension λ , the string thickness R and the expansion rate H was derived.

Generalized to six-dimensional GR, these solutions correspond to a simple brane-world model with a single super-critical, pure tension brane. Since the extra dimensions are compact, the BIG terms are no longer a vital ingredient, and could even be dropped. The corresponding modified Friedmann equation is given by Eq. (6.9.5). Unfortunately, the parameters of the model have to be fine-tuned to be in accordance with the observed accelerated expansion of the universe. Whether it could still provide an interesting late time modification remains to be seen. One possible alternative idea would be to identify our universe not with the super-critical, but with the sub-critical brane which can sit at the opposite axis. This would have the advantage that the corresponding brane width is not related to R , and could be much smaller; in turn, $HR \lesssim 1$ would not necessarily be a problem. Furthermore, the new class of attractor solutions alluded to in Footnote 23 deserve further attention. In particular, it would be interesting to see whether there are stable solutions for nonvanishing dust-components. If so, these super-critical solutions might provide an interesting arena for a new spontaneous compactification mechanism, as well as consistent IR modifications of GR and cosmology.



APPENDIX TO CHAPTER 6

6.A Classification of exterior geometries

In this appendix, we give a complete classification of the character of a vacuum space-time described by the metric (6.3.1), depending on the gradient $\nabla W \equiv (\partial_{t^*} W, \partial_{r^*} W)$. Furthermore, we discuss which changes of character are admissible in vacuum, as well as across shells of matter and show how the change of character across such a shell depends on the surface energy density. Even though we concentrate on the case of 4D GR, the discussion applies similarly to 6D GR with the metric (5.3.1).

Character	Orientation of ∇W	W'_+	W'_-
D^+	spacelike outward	> 0	< 0
D^-	spacelike inward	< 0	> 0
D^\uparrow	timelike future	> 0	> 0
D^\downarrow	timelike past	< 0	< 0
$D^{+\uparrow}$	light-like outward-future	> 0	$= 0$
$D^{+\downarrow}$	light-like outward-past	$= 0$	< 0
$D^{-\uparrow}$	light-like inward-future	$= 0$	> 0
$D^{-\downarrow}$	light-like inward-past	< 0	$= 0$
D^\times	zero	$= 0$	$= 0$

Table 6.A.1: Definition of spacetime character, depending on the gradient of W .

Following Thorne [AT92, Appendix A], we define the “character” of spacetime depending on the orientation of ∇W as summarized in Table 6.A.1. Here and henceforth, “outward” (resp. “inward”) means in direction of increasing (decreasing) r^* , and “future” (“past”) refers to the direction of increasing (decreasing) t^* . In vacuum, W satisfies the (1+1)D wave equation $\partial_{t^*}^2 W = \partial_{r^*}^2 W$, the general solution of which can be written as

$$W(t^*, r^*) = W_+(t^* + r^*) + W_-(t^* - r^*). \quad (6.A.1)$$

It is easy to verify that each orientation of ∇W corresponds to a certain choice of signs for the derivatives²⁵ W'_+ and W'_- , as listed in Table 6.A.1.

²⁵Here and henceforth, the primes acting on W_\pm denote the derivative with respect to their argument



6.A.1 Changes of character in vacuum

Let us now discuss which changes of character are allowed in vacuum regions. The above discussion shows that a change of character is equivalent to a change of sign of W'_+ or W'_- . Thus, on the boundary between two spacetime regions of different character, we have $W'_+ = 0$ or $W'_- = 0$. But since these functions are constant along null-surfaces, it follows that *in vacuum, the character can only change across null-surfaces*.

Furthermore, since W'_+ is constant along an incoming light-ray ($dt^* + dr^* = 0$), the only possible changes along incoming rays are those in which W'_- changes sign, i.e. changes within the following sets:

$$\{D^+, D^\uparrow, D^{+\uparrow}\}, \quad \{D^-, D^\downarrow, D^{-\downarrow}\}, \quad \{D^{+\downarrow}, D^{-\uparrow}, D^\times\}.$$

Similarly, along outgoing null-rays ($dt^* - dr^* = 0$), the character can only change within

$$\{D^+, D^\downarrow, D^{+\downarrow}\}, \quad \{D^-, D^\uparrow, D^{-\uparrow}\}, \quad \{D^{+\uparrow}, D^{-\downarrow}, D^\times\}.$$

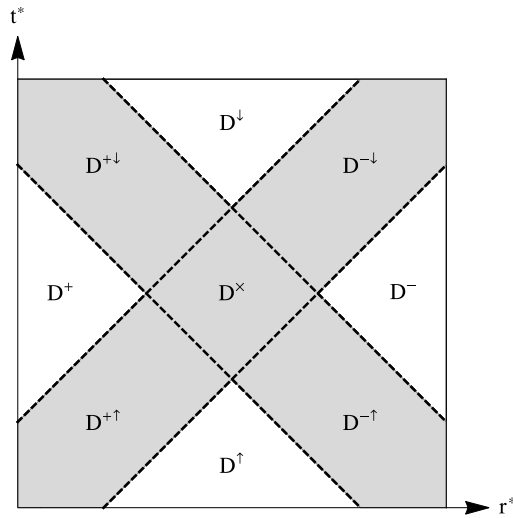
However, there is a further restriction on the directions of changes within all these sets, coming from the focusing theorem for null geodesics [AT92, MTW73]: It says that $d^2W/d\sigma^2 \leq 0$, where σ is the affine parameter along the null geodesic. Hence, the functions W'_+ and W'_- cannot get larger along any null rays. Thus, e.g. for the first set, the only admissible changes are

$$D^\uparrow \rightarrow D^{+\uparrow} \rightarrow D^+, \quad (6.A.2)$$

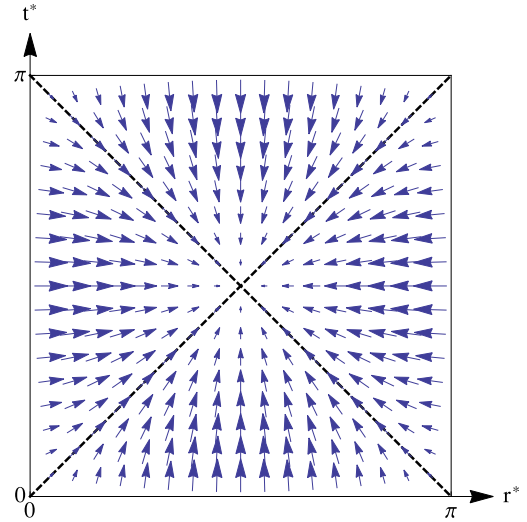
and similarly for the other sets. All changes that are finally possible, are summarized schematically in Fig. 6.A.1a: they are exactly those changes which are encountered along any incoming or outgoing null ray in this diagram. Note that in the gray shaded regions the Jacobian of the transformation (6.3.2) vanishes, and so these coordinates can only be adopted in any of the white regions separately. Furthermore, the new coordinate r which is set equal to W will be a spatial coordinate for D^+ and D^- , but a temporal coordinate for D^\uparrow and D^\downarrow . In a D^+ (resp. D^-) region, r decreases as one moves inward (outward); it cannot start increasing again, because this would require a change to D^- (D^+), which is not admissible. Hence, it decreases until eventually $r = 0$, implying an axis that delimits spacetime, as advertised in Sec. 6.3.2. (Similar statements hold in the temporal case, but there the “axes” correspond to physical, initial and final collapse singularities.)

There is actually a well-known example of a (vacuum) spacetime exhibiting all the different characters: the Gowdy universe [Gow71], in which $W = \sin(t^*) \sin(r^*)$. The corresponding vector plot of ∇W is shown in Fig. 6.A.1b. The spacetime character exactly matches that of Fig. 6.A.1a, with the gray regions degenerated to single lines. The two axes are located at $r^* \in \{0, \pi\}$, whereas $t^* \in \{0, \pi\}$ correspond to the Big

(not with respect to r^*), i.e. $W'_\pm(x) := dW_\pm(x)/dx$.



(a) All admissible changes of character in vacuum regions can be read off from this diagram, by following incoming or outgoing null rays.



(b) The gradient of W for the Gowdy universe, $W = \sin(t^*) \sin(r^*)$. The corresponding spacetime character matches that of Fig. 6.A.1a, with the gray regions degenerated to single lines.

Bang / Big Crunch singularities.²⁶

Coming back to our general discussion, we find another important result: *It is not possible for a vacuum region to dynamically evolve from D^+ to D^- or vice versa.* Therefore, a sub-critical cosmic string (for which the exterior geometry is D^+ , see below) can never evolve to a super-critical string (D^- exterior). In particular, super-critical strings cannot be formed by cylindrical collapse within classical GR.

6.A.2 Changes of character across the shell

Next, let us derive the relations given in Sec. 6.3.2, relating the spacetime character of the region outside the regularized cosmic string to its tension. In the interior, we assume the character to be D^+ , in order to have a well-defined regularization. Thus, we can safely adopt the Einstein-Rosen coordinates (6.3.3a) there. In the exterior, however, we keep the coordinates (6.3.1) because there we do not know the character yet. In these coordinates, the $(0)_0$ -component of the junction conditions (6.3.17) reads

$$\bar{\lambda} = \tilde{\gamma} - \gamma^* (\dot{r}_0^* \partial_{t^*} W + \partial_{r^*} W) |_0. \quad (6.A.3)$$

Here, γ^* is defined similarly to γ in (6.3.8), i.e. $\gamma^* := \exp(-\eta_0^*) / \sqrt{1 - \dot{r}_0^{*2}}$ and $\dot{r}_0^* := dr_0^*/dt^*$. Furthermore, continuity of the metric implies $W_0 = \tilde{r}_0$, which after differenti-

²⁶By extending the range of t^* to $(0, 2\pi)$, one could construct an example where forbidden changes like $D^\downarrow \rightarrow D^\uparrow$ were apparently allowed. However, they would be separated by the singularity at $t^* = \pi$, so they should be regarded as unphysical. More generally, the above argument using null geodesics implicitly assumes that no singularities are present.



ating with respect to τ yields

$$0 = \tilde{\gamma} \dot{\tilde{r}}_0 - \gamma^* (\partial_{t^*} W + \dot{\tilde{r}}_0^* \partial_{r^*} W) |_0. \quad (6.A.4)$$

Plugging the general solution (6.A.1) of W into (6.A.3) and (6.A.4), and solving for $W'_\pm|_0$, we find

$$W'_+|_0 = \frac{1}{2\gamma^*(1 + \dot{\tilde{r}}_0^*)} (\tilde{\gamma} + HR - \bar{\lambda}), \quad (6.A.5a)$$

$$W'_-|_0 = \frac{1}{2\gamma^*(1 - \dot{\tilde{r}}_0^*)} (\bar{\lambda} - \tilde{\gamma} + HR). \quad (6.A.5b)$$

Note that here we used the relation (6.3.12) to eliminate $\dot{\tilde{r}}_0$. Since the prefactors on the right hand side are manifestly positive, inspection of Table 6.A.1 immediately reveals that the spacetime character at the exterior boundary of the shell is:

$$D^+ \Leftrightarrow \bar{\lambda} < \tilde{\gamma} - |H| R, \quad (6.A.6a)$$

$$D^\uparrow \text{ or } D^\downarrow \Leftrightarrow \tilde{\gamma} - |H| R < \bar{\lambda} < \tilde{\gamma} + |H| R, \quad (6.A.6b)$$

$$D^- \Leftrightarrow \bar{\lambda} > \tilde{\gamma} + |H| R, \quad (6.A.6c)$$

thus verifying the result stated in Sec. 6.3.2. The orientation in the timelike case (6.A.6b) depends on the sign of H : it is D^\uparrow for $H > 0$ and D^\downarrow for $H < 0$. The light-like cases correspond to the saturation of one of the inequalities, e.g. $D^{+\uparrow} \Leftrightarrow \bar{\lambda} = \tilde{\gamma} - |H| R$ and $H > 0$, etc.

Since $\tilde{\gamma} = \sqrt{\exp(-2\tilde{\eta}_0) + H^2 R^2}$, the bounds on $\bar{\lambda}$, delineating the sub-, critical and super-critical regimes, depend on two parameters: $\tilde{\eta}_0$, which measures the gravitational C-energy inside the shell, and HR , i.e. the axial expansion rate measured in units of inverse circumference R^{-1} . For a flat profile $\partial_{\tilde{t}} \tilde{\alpha} = \text{const.}$ and $\partial_{\tilde{r}} \tilde{\alpha} = 0$ (as for the initial data in our numerics), $\tilde{\eta}_0$ and HR are rigidly related via the (integrated) constraint (6.3.4b), and so the bounds (6.A.6) can be plotted in a HR - $\bar{\lambda}$ -diagram. This is shown in Fig. 6.10, where the region below the lower solid (purple) curve corresponds to D^+ , the region in between the two solid lines is D^\uparrow (or D^\downarrow), and everything above the upper solid (orange) line is D^- .

6.B Co-moving coordinates

It is straightforward to check that after introducing new coordinates (\tilde{t}, \tilde{r}) according to

$$\tilde{t} = L \ln \left(\frac{L\tilde{t}}{r_+^2} \sqrt{1-x^2} \right), \quad \tilde{r} = \frac{r_+}{2} \left(1 + \frac{1}{\sqrt{1-x^2}} \right), \quad (6.B.1)$$

with $x \equiv \tilde{r}/\tilde{t}$, the scaling solution (6.6.7) takes the form

$$d\tilde{s}^2 = \frac{\tilde{r}^2}{L^2} \left(-d\tilde{t}^2 + e^{2\tilde{t}/L} dz^2 \right) + \left(1 - \frac{r_+}{\tilde{r}} \right)^{-1} d\tilde{r}^2 + 4r_+^2 \left(1 - \frac{r_+}{\tilde{r}} \right) d\phi^2. \quad (6.B.2)$$

Here, L is an arbitrary length scale which can be adjusted by rescaling (and shifting) \bar{t} . The constant r_+ denotes the position of the (regular) axis in the new coordinates, and the shell is now sitting at a constant coordinate position \bar{r}_0 . The two parameters r_+ and \bar{r}_0 , determining the range of \bar{r} , are related to R and \tilde{v} via

$$r_+ = R \frac{(1 + \sqrt{1 - \tilde{v}^2})}{2\tilde{v}}, \quad \bar{r}_0 = R \frac{(1 + \sqrt{1 - \tilde{v}^2})^2}{4\tilde{v}\sqrt{1 - \tilde{v}^2}}. \quad (6.B.3)$$

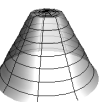
The metric (6.B.2) is exactly the 4D version of the one discussed by Witten in 5D [Wit82] and by Gregory for general dimensionality [Gre96]. The benefit of these coordinates lies in their simplicity which allows to read off the geometrical content directly from the metric. The entire dynamics consists in a de Sitter-like expansion in axial direction, whereas the radial profile—and hence in particular the interior area—is completely static. Note that the scaling solution is only a true attractor for the interior spacetime, i.e. the red surfaces in Figs. 6.5b and 6.5c. However, as discussed in the main text, the exterior geometry also approaches the scaling solution with $\tilde{v} \rightarrow 1$ sufficiently far away from the shell. Hence, we can use (6.B.2) also to picture the spacetime outside the string, if we neglect a small region close to it. Then the axis at r_+ corresponds to the south pole in Figs. 6.5b and 6.5c. The case with a conical singularity is simply obtained by appropriately adjusting the coefficient of $d\phi^2$ in (6.B.2). Moving away from the axis towards the string, $\bar{r} \rightarrow \infty$ (because in the limit $\tilde{v} \rightarrow 1$ Eq. (6.B.3) implies $\bar{r}_0 \rightarrow \infty$) and so the physical circumference approaches a constant value. The resulting embedding picture corresponds to a cigar-shaped geometry. In the interior, \tilde{v} is bounded by $3/5$ and so the ratio \bar{r}_0/r_+ is always smaller than $9/8$. At this point, one has not yet reached the vertical part of the cigar, and so the interior embedding geometry always corresponds to a nearly flat cap. These results nicely agree with what was found in Figs. 6.5b and 6.5c.

6.C Validity of EFT

General Relativity viewed as an EFT is valid up to the Planck scale M_P . Once the curvature scale exceeds this value, higher order operators become important and we can no longer trust its classical predictions. Generically, this happens once the 4D energy density becomes of order M_P^4 . For a cosmic string this depends on both the tension λ and the regularization scale R . A solid way to derive the regime of validity of the EFT consists in considering the extrinsic curvature of the string. To be specific, let us focus on the combination $\mathcal{K} := [K^c_c] - [K^0_0]$ which is determined by the $(^0_0)$ -component of the junction condition (6.3.17):

$$\frac{\mathcal{K}}{M_P} = \frac{\bar{\lambda}}{RM_P}. \quad (6.C.1)$$

Once \mathcal{K} exceeds M_P , we expect the EFT to break down, or equivalently, Quantum Gravity effects to become important. The super-critical solutions we described are



valid for $\bar{\lambda} \sim \mathcal{O}(1)$. Then (6.C.1) implies that classical GR is applicable if and only if R is much larger than the Planck length $L_P \equiv M_{\text{Pl}}^{-1}$. Alternatively, this result becomes obvious when we naively estimate the 4D energy density as the ratio λ/R^2 and require it to be smaller than M_{P}^4 . In other words, even though the energy per string length needs to be Planckian in order to enter the super-critical regime, the energy per string volume is sub-Planckian if the string's thickness is much larger than the Planck length. Also note that the marginally super-critical solutions only cover the range $HR < 3/4$, implying that the expansion energy $M_{\text{Pl}}^2 H^2$ is always smaller than M_{Pl}^2/R^2 and hence also sub-Planckian if $R \gg L_P$.

CHAPTER 7

THE UNIVERSE ON A RUGBY BALL

Note: The results presented in this chapter arose in collaboration with Florian Niedermann and were published in [NS16a] and [NS16b].

7.1 Introduction and summary

Chapter 5 showed that the BIG mechanism is not able to achieve the phenomenologically required 4D gravity regime on a codimension-two brane with infinite extra dimensions, without introducing ghost instabilities. But, as already discussed in Sec. 1.3, there is another well-known mechanism to recover a 4D gravity regime: compact extra dimensions. The compactness implies that the low energy spectrum contains a normalizable 4D graviton zero-mode which mediates the correct Newtonian $1/r^2$ force at distances much larger than the size of the extra dimensions. At shorter distances, the compact space becomes visible, resulting in a transition to the higher-dimensional scaling $1/r^{2+n}$. Current torsion-balance experiments [KCA⁺07] set an upper limit $\sim 50 \mu\text{m}$ on the size of the extra dimensions.

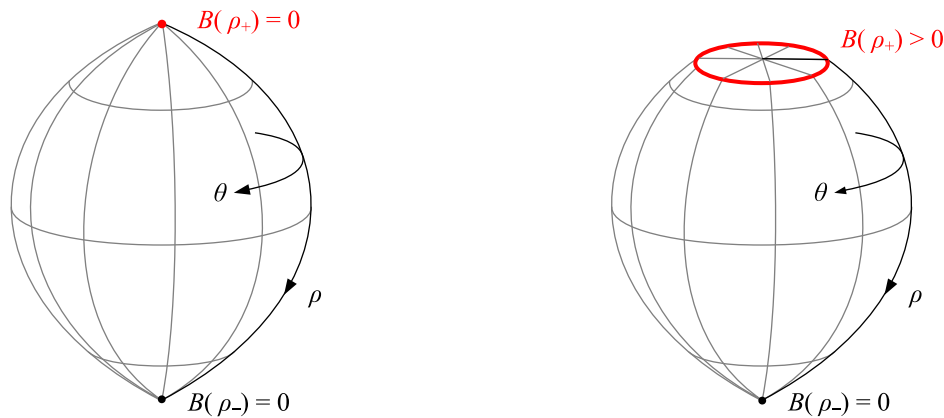
While the gravitationally accessible extra dimensions could be that large, collider experiments have currently tested non-gravitational physics up to the TeV scale. Hence, in the large extra dimension scenario all Standard Model matter must still be confined on a brane of size $\sim 1/\text{TeV}$. Originally, this setup was proposed as a framework for addressing the electroweak hierarchy problem [AHDD98], in which the huge difference between the Planck and electroweak scale is due to the enormous ratio between the bulk and brane size.¹ But in the case of two large compact extra dimensions, the deficit angle degravitation mechanism could work just like for two infinite extra dimensions, and so one can hope to find a solution to the CC problem in this way as well.

An immediate consequence of the compactness is the need for some stabilization mechanism that prevents the extra space from gravitational collapse. A concrete ex-

¹Of course, it remains to be checked whether this hierarchy could arise in some UV theory in a technically natural way.



ample [Sun99] uses a U(1) gauge field with nontrivial magnetic flux through the extra dimensions. A quantization condition fixes the total flux, so that the magnetic energy rises if the 2D volume shrinks, thus providing a counterforce to the gravitational attraction and allowing for stable configurations in which the two effects balance each other. This mechanism was used in [CG03]² to construct explicit solutions of the Einstein-Maxwell system with a bulk CC and two identical pure tension branes located at the opposite poles of the compact space with spherical topology. Indeed, the on-brane geometry is flat in these solutions, and the sole effect of the brane tensions is to introduce conical defects which deform the sphere into a rugby ball, see Fig. 7.1a. However, this does not solve the CC problem because flux quantization ultimately leads to a tuning relation between the brane tensions and the bulk CC. Violating this tuning would lead to a nonvanishing 4D curvature of just the same size that we would have obtained within standard GR, see [Nav03b, NPT04, GP04] (and [Bur13] for a recent review).³



(a) Without regularization, the brane is a genuine codimension-two object and sits at the tip of the rugby ball, corresponding to a conical singularity.

(b) In the regularization used in Sec. 7.3, the brane is again blown up to a codimension-one ring, replacing the conical singularity by a flat cap.

Figure 7.1: Embedding diagrams of the compact deficit angle—or “rugby ball”—geometry; (ρ, θ) are the polar and azimuthal coordinates, and B measures the azimuthal circumference, cf. Eq. (7.2.5a). The northern brane ($\rho = \rho_+$) corresponds to our universe. The second brane at the south pole ($\rho = \rho_-$) will be assumed only to carry a tension and thus requires no regularization.

In the next step [ABPQ04], the setup was supplemented with bulk supersymmetry (SUSY), resulting in the model of *supersymmetric large extra dimensions* (SLED), which will be the subject of this chapter. At the level of the classical equations of mo-

²See [CLP00, Nav03a] for similar approaches.

³Note that this failure is a crucial difference to the corresponding scenario with infinite extra dimensions: there, no stabilization and hence no tuning is required to obtain 4D flat solutions. If the brane tension changes, the bulk geometry would simply respond via adapting the deficit angle and sending Einstein-Rosen waves out to infinity.

tion, the only new ingredient is the dilaton ϕ —which renders the (classical) bulk theory *scale invariant* (SI)—while all other fields can consistently be set to zero. Furthermore, the bulk CC vanishes due to SUSY. The degravitating rugby ball solutions still exist in this setup, provided the brane tension does not couple to the dilaton. Moreover, the general 4D maximally symmetric solutions for two arbitrary (but dilaton-independent) brane tensions were found analytically [GGP04], and always have Minkowski branes. However, the situation with respect to the CC problem is not better than in the non-SUSY case, because flux quantization still requires the brane tensions to be fine-tuned against the flux quantum number. To overcome this problem, finally a *brane-localized flux* (BLF) was added to the theory [BvN11, BvN13]. If this term is also dilaton-independent (like the tension), it breaks the classical SI, which in turn allows the flux quantization condition to fix the dilaton integration constant instead of enforcing a tuning of model parameters. Since it was thought that, on the other hand, a dilaton-independent BLF still implies 4D flat solutions, this looked very promising with regard to the CC problem.

In the first part of this chapter, Sec. 7.2, we will show that the last proposal actually fails: 4D flatness is only ensured by a BLF which *does* couple to the dilaton, in precisely such a way that this term preserves SI. But in this case, the dilaton drops out of the flux quantization condition, which thus presents a tuning relation for the brane tensions as before. A subtlety of this derivation is that a nonvanishing BLF causes divergences at the (idealized) delta branes. In Sec. 7.2.3 we will show how those can be handled by adding an appropriate counter term to the action. This allows us to derive our main result in Sec. 7.2.6 without the need for regularizing the delta branes (or introducing a UV model as in [BDW15a, BDW15b]). We will find that *4D flatness is only guaranteed by SI brane couplings*. The resulting tuning issue, as well as its relation to Weinberg’s no-go theorem (cf. Sec. 1.2.1), will be discussed in Sec. 7.2.8. Finally, Sec. 7.2.9 responds to an objection [BDW16] to our derivation using delta branes.

In the second part, Sec. 7.3, we go one step further and ask how large the nonzero 4D curvature actually becomes for SI breaking dilaton-brane couplings, and a corresponding violation of the tuning relation. This question is still relevant, because if the answer were compatible with observational bounds, and the tuning violations would correspond to natural changes in the brane tension, the SLED program could still solve the CC problem. To avoid singularities (and potential ambiguities) which can occur for SI breaking brane couplings, we introduce a finite brane width in Sec. 7.3.1, using the same ring regularization as in previous chapters, cf. Fig. 7.1b. Again, a stabilizing angular pressure has to be added to allow for static solutions; in Sec. 7.3.2, we show that this gives rise to an additional contribution to the 4D Ricci $\hat{\mathcal{R}}$ as compared to the delta result. Since a realistic brane always comes with some finite thickness, this contribution—which is solely due to the brane width and independent of the form of the dilaton-brane couplings—should always be taken into account. For a relevant class of dilaton-brane couplings, we will derive a relation between the 4D curvature and the 2D extra space volume V in Sec. 7.3.3, and discuss its phenomenological implications in Sec. 7.3.4. Furthermore, in Sec. 7.3.5 the complete bulk-brane system will be solved numerically in a completely consistent way. This allows us to explicitly calculate the



relevant observables for a given set of model parameters, thus confirming the assumptions and approximations that went into the preceding analytic derivation. Moreover, it enables us to pin down the amount of tuning (imposed by flux quantization) that is needed to obtain sufficiently small values of $\hat{\mathcal{R}}$.

Our conclusion, as summarized in Sec. 7.4, is that unless the brane width is allowed to be much (~ 18 orders of magnitude) smaller than the bulk Planck length, the model is ruled out phenomenologically, because either $\hat{\mathcal{R}}$ or V are well above their observational bounds. But even if this were allowed, the SI breaking brane tension would lead to the same (actually worse) problem, unless some sort of fine-tuning is at work.

7.1.1 Conventions and notation

In this chapter, we use Weinberg’s sign conventions [Wei72], which are “+ − −” in the nomenclature of [MTW73], meaning that the metric is still mostly plus, but the Riemann and Einstein tensor have the opposite sign than for “+ + +” (which was used in all other parts of this thesis). Six-dimensional spacetime coordinates are denoted by X^M ($M = 0, \dots, 5$), 4D ones by x^μ ($\mu = 0, \dots, 3$), and the two extra space dimensions are labeled by y^m ($m = 1, 2$). Furthermore, ϵ^{mn} is a tensor (not a density), i.e. its components are $\pm 1/\sqrt{g_2}$. The delta function transforms as a density, so there is no metric determinant factor in its normalization condition $\int d^2y \delta^{(2)}(y) = 1$.

7.2 Delta branes with BLF

Note: This section is to large extent a verbatim reproduction of the corresponding sections in [NS16a].

The total action of the SLED model is given by [BvN11]

$$S = S_{\text{bulk}} + S_{\text{branes}}, \quad (7.2.1)$$

where the bulk part is

$$S_{\text{bulk}} = - \int d^6X \sqrt{-g} \left\{ \frac{1}{2\kappa^2} [\mathcal{R} + (\partial_M \phi)(\partial^M \phi)] + \frac{1}{4} e^{-\phi} F_{MN} F^{MN} + \frac{2e^2}{\kappa^4} e^\phi \right\}, \quad (7.2.2)$$

and the brane contributions are

$$S_{\text{branes}} = - \sum_b \int d^4x \sqrt{-g_4} \left\{ \mathcal{T}_b(\phi) - \frac{1}{2} \mathcal{A}_b(\phi) \epsilon_{mn} F^{mn} \right\}. \quad (7.2.3)$$

The field content consists of the 6D metric g_{MN} with corresponding Ricci scalar \mathcal{R} , a Maxwell field A_M with field strength $\mathbf{F} = d\mathbf{A}$, and the dilaton ϕ . κ and e denote

the gravitational and $U(1)$ ⁴ coupling constants, respectively. The sum in S_{branes} runs over $b \in \{+, -\}$, corresponding to the two 3-branes at the north and south pole of the compact extra space. One of them should ultimately be identified with our universe. The first term \mathcal{T}_b is the brane tension (or 4D vacuum energy density), and the second term corresponds to the *brane-localized flux* (BLF). At this stage, we allow both of them to have a priori arbitrary dilaton dependences. The central question we want to answer is how these must be chosen in order to obtain 4D flat solutions.

Under a (constant) rescaling $g_{MN} \mapsto \zeta g_{MN}$, $e^\phi \mapsto \zeta^{-1} e^\phi$, the bulk action transforms with a global scaling factor, $S_{\text{bulk}} \mapsto \zeta^2 S_{\text{bulk}}$. This implies that the classical bulk equations of motion are SI. This SI is respected by the branes if

$$\mathcal{T}_b(\phi) = \text{const} \quad \text{and} \quad \mathcal{A}_b(\phi) \propto e^{-\phi}, \quad (7.2.4)$$

and is broken otherwise.

7.2.1 Ansatz

We assume the geometry to be maximally symmetric in the four on-brane dimensions, as well as rotationally symmetric in extra space. This leads to the following most general ansatz,

$$ds^2 = W^2(\rho) \hat{g}_{\mu\nu} dx^\mu dx^\nu + d\rho^2 + B^2(\rho) d\theta^2, \quad (7.2.5a)$$

$$\mathbf{A} = A_\theta(\rho) \mathbf{d}\theta, \quad (7.2.5b)$$

$$\phi = \phi(\rho), \quad (7.2.5c)$$

where the 4D metric $\hat{g}_{\mu\nu}$ is maximally symmetric and thus completely characterized by the (constant) 4D Ricci scalar $\hat{\mathcal{R}}$. The extra space is labeled by the azimuth angle⁵ $\theta \in [0, 2\pi)$ and the polar angle $\rho \in [\rho_+, \rho_-]$, with $\rho_b = \rho_\pm$ denoting the brane positions at the north- and south pole, respectively, where $B|_{\rho=\rho_b} = 0$, cf. Fig. 7.1a.

7.2.2 Maxwell sector

After inserting the identity $1 = \int d^2y \delta^{(2)}(y)$ into the brane part (7.2.3), the total action (7.2.1) can be written as a single 6D integral $S = \int d^6X L$. The Maxwell part of the Lagrangian is

$$L_F = -\sqrt{-g} \frac{1}{4} e^{-\phi} \mathbf{F}^2 + \frac{1}{2} \sum_b \sqrt{-g_4} \mathcal{A}_b(\phi) \epsilon_{mn} F^{mn} \delta^{(2)}(y - y_b), \quad (7.2.6)$$

⁴This is not necessarily the $U(1)$ gauged by \mathbf{A} , which can in general have a different coupling [BvN11], which we will denote by \tilde{e} , and which appears in the flux quantization condition (7.2.9).

⁵Note that in this chapter, the azimuthal coordinate is denoted by θ , unlike in previous chapters, because ϕ is here reserved for the dilaton.



where $\mathbf{F}^2 \equiv F_{MN}F^{MN}$, and the corresponding field equations read

$$\partial_M \left[\sqrt{-g} e^{-\phi} F^{MN} - \sqrt{-g_4} \delta_m^M \delta_n^N \sum_b \mathcal{A}_b(\phi) \epsilon^{mn} \delta^{(2)}(y - y_b) \right] = 0. \quad (7.2.7)$$

With the ansatz (7.2.5), this gives the field strength⁶

$$F_{\rho\theta} = e^\phi \left[Q \frac{B}{W^4} + \frac{1}{2\pi} \sum_b \mathcal{A}_b(\phi) \delta(\rho - \rho_b) \right], \quad (7.2.8)$$

where Q is a constant of integration. However, this constant cannot be chosen freely, because it determines the total flux $\Phi_{\text{tot}} := \int d\rho d\theta F_{\rho\theta}$, which has to fulfill the flux quantization condition [RDSS83, BvN13]

$$\Phi_{\text{tot}} = 2\pi Q \int d\rho \frac{e^\phi B}{W^4} + \sum_b [\mathcal{A}_b(\phi) e^\phi]_{\rho=\rho_b} \stackrel{!}{=} \frac{2\pi n}{\tilde{c}} \quad (n \in \mathbb{N}). \quad (7.2.9)$$

We now encounter a peculiarity (which was missed in previous investigations [BvN11, BvN13, Bur13]): the presence of a localized delta-contribution to the field strength implies that the \mathbf{F}^2 term in the action, which also enters the Einstein and dilaton equations, contains a divergent part $\propto \delta(0)$. It is obviously caused by the BLF term, as it disappears for $\mathcal{A}_b = 0$, but is also definitely a relict of treating the branes as pointlike.

At this point, there are two routes one can follow: Either, one gives up the idealization of infinitely thin branes and tries to come up with a UV model which microscopically resolves the branes. A first step in this direction was currently taken in [BDW15a, BDW15b]. Alternatively, one can ask if the divergence can be somehow removed, rendering the delta description possible again. In this work, we pursue the latter option. Physically speaking, it is motivated by the EFT expectation that all physical predictions should be insensitive to the microscopic details of an underlying UV model, as long as we ask low energy questions. In the case at hand, the CC problem manifests itself in the IR, at energies well below a realistic (inverse) brane thickness. Indeed, if it were necessary to understand the full UV physics in order to solve the CC problem, it would actually not solve the problem in the realm in which it is posed in the first place—as an IR problem in a low energy EFT.

There are several observations which give us further confidence that our approach captures the correct physical picture:

- All divergences can be completely removed by adding a single counter term to the action.
- In the special case of vanishing dilaton, where the concrete UV model [BDW15a] applies, our results are in perfect agreement with [BDW15a], as will be discussed in Appendix 7.A.

⁶Note that in our conventions, and for the ansatz (7.2.5), $\epsilon^{\rho\theta} = 1/B$, and $\delta^{(2)}(y) = \delta(\rho)/(2\pi)$.

- In the end, it leads to the conclusion that $\hat{\mathcal{R}} = 0$ is ensured for SI brane couplings \mathcal{T}_b and \mathcal{A}_b , in line with Weinberg's general arguments [Wei89].

7.2.3 Counter term

Plugging the solution (7.2.8) back into the action yields

$$S_F|_{\text{sol}} = -\frac{1}{2} \int d^6 X \sqrt{-g} e^\phi \frac{Q^2}{W^8} + S_{\text{div}} , \quad (7.2.10)$$

where the last term is the divergent contribution

$$S_{\text{div}} = \frac{1}{2} \sum_b \int d^4 x \sqrt{-g_4} \frac{\delta^{(2)}(0)}{\sqrt{g_2}} e^\phi \mathcal{A}_b(\phi)^2 . \quad (7.2.11)$$

In order to obtain a finite action, it is *necessary* to introduce a counter term which cancels S_{div} , leading to the action

$$\tilde{S} := S - S_{\text{div}} . \quad (7.2.12)$$

Below, we will see that this subtraction is also *sufficient* in order to arrive at a consistent theory, because it removes all divergences from the Einstein and dilaton field equations. In other words, the theory defined by the action \tilde{S} provides an explicit realization of the SLED model with a BLF term, which still allows for consistently treating the branes as infinitely thin—unlike for the original action S .

Several further comments regarding the counter term S_{div} are in order:

- Since it does not contain \mathbf{A} , the Maxwell equations (7.2.7) and the corresponding solution (7.2.8) are not affected. (Otherwise, it could have been necessary to reiterate the process and introduce further counter terms.)
- It has the correct symmetries to qualify as a legitimate 4D brane action because the combination $\delta^{(2)}(y)/\sqrt{g_2}$ is a scalar.
- For later reference, note that the term preserves the SI of the theory for the choice $\mathcal{A}(\phi) \propto e^{-\phi}$.
- It cannot be viewed as a renormalization of the brane tension because of the factor $1/\sqrt{g_2}$. Due to this explicit dependence on the bulk metric, it will enter the Einstein equations differently than \mathcal{T}_b , see (7.2.18). But this factor is dictated both by general covariance, and the requirement to successfully cancel all divergences.
- The ill-defined quantity $\delta^{(2)}(0)$ should better be thought of as a large but finite constant, as would arise in some actual regularization, where the delta function



is replaced by some smeared function⁷ which has support in a small region of proper radius ϵ . In this case, $\delta^{(2)}(0)/\sqrt{g_2}$ would be replaced by $\sim 1/\epsilon^2$.

In the following, we present the dilaton and Einstein equations which are obtained from the action \tilde{S} .

7.2.4 Dilaton sector

The dilaton equation is

$$\begin{aligned} \frac{1}{\kappa^2} \square \phi + \frac{1}{4} e^{-\phi} \mathbf{F}^2 - \frac{2e^2}{\kappa^4} e^\phi \\ = \sum_b \frac{\delta_b^{(2)}}{\sqrt{g_2}} \left\{ \mathcal{T}'_b - \frac{1}{2} \mathcal{A}'_b \epsilon_{mn} F^{mn} + \frac{\delta^{(2)}(0)}{\sqrt{g_2}} e^\phi \mathcal{A}_b \left[\frac{1}{2} \mathcal{A}_b + \mathcal{A}'_b \right] \right\}, \end{aligned} \quad (7.2.13)$$

where the primes here denote $d/d\phi$, and $\delta_b^{(2)} \equiv \delta^{(2)}(y - y_b)$. The last term, proportional to $\delta^{(2)}(0)$, follows from the counter term in (7.2.12). Once we substitute the Maxwell solution (7.2.8), all divergent contributions exactly cancel as advertised, and the dilaton equation becomes, for the ansatz (7.2.5),

$$\frac{1}{\kappa^2} \Delta_2 \phi + \frac{1}{2} e^\phi \left(\frac{Q^2}{W^8} - \frac{4e^2}{\kappa^4} \right) = \sum_b \frac{\delta_b^{(2)}}{B} \left\{ \mathcal{T}'_b - \frac{Q}{W^4} e^\phi (\mathcal{A}'_b + \mathcal{A}_b) \right\}, \quad (7.2.14)$$

where the covariant 2D Laplace operator is⁸

$$\Delta_2 \phi = \frac{1}{BW^4} (BW^4 \phi')' = \phi'' + \left(\frac{B'}{B} + \frac{4W'}{W} \right) \phi'. \quad (7.2.15)$$

We now integrate this equation over a small ϵ -disc covering either the north or the south pole. By using Stokes' theorem and taking the limit $\epsilon \rightarrow 0$, we find the following boundary condition

$$[B\phi']_{\rho=\rho_b} = \frac{\kappa^2}{2\pi} \mathcal{C}_b, \quad (7.2.16)$$

with

$$\mathcal{C}_b := \left[\mathcal{T}'_b - \frac{Q}{W^4} e^\phi (\mathcal{A}'_b + \mathcal{A}_b) \right]_{\rho=\rho_b}. \quad (7.2.17)$$

In the SI case (7.2.4) \mathcal{C}_b is zero, which in turn allows for a regular dilaton profile with vanishing ρ -derivatives at the brane positions. On the other hand, if $\mathcal{C}_b \neq 0$ (as

⁷For concreteness, in our coordinates one could consider $\Theta(\epsilon - \rho)\rho/(\pi\epsilon^2)$. However, it is not quite clear how the BLF term could be modeled in such a regularization. A more consistent regularization was recently proposed in [BDW15a, BDW15b], which gives results in full agreement with our predictions, see Appendix 7.A.

⁸A prime denotes derivative with respect to the argument of the function: for a ρ -dependent function (like ϕ) the prime is $d/d\rho$, for the brane couplings (like \mathcal{T}_b) it still denotes $d/d\phi$.

expected in the non SI case), the ϕ profile becomes singular (thereby also implying a curvature singularity) since $B \rightarrow 0$ at the branes. A more explicit study of this case requires to regularize the setup, as will be done in Sec. 7.3, where the non SI case is investigated in a thick brane model.

7.2.5 Gravitational sector

The Einstein equations read

$$\begin{aligned} & \frac{1}{\kappa^2} \left[G^M{}_N + (\partial^M \phi) (\partial_N \phi) - \frac{1}{2} \delta_N^M (\partial \phi)^2 \right] + e^{-\phi} F^{MP} F_{NP} - \delta_N^M \left[\frac{1}{4} e^{-\phi} F^2 + \frac{2e^2}{\kappa^4} e^\phi \right] \\ &= \sum_b \frac{\delta_b^{(2)}}{\sqrt{g_2}} \left\{ \delta_\mu^M \delta_N^\mu \mathcal{T}_b + (\delta_m^M \delta_N^m - \delta_\mu^M \delta_N^\mu) \frac{\mathcal{A}_b}{2} \left[\epsilon_{mn} F^{mn} - e^\phi \mathcal{A}_b \frac{\delta^{(2)}(0)}{\sqrt{g_2}} \right] \right\}, \end{aligned} \quad (7.2.18)$$

where $(\partial \phi)^2 \equiv (\partial_M \phi) (\partial^M \phi)$. After plugging in the solution for the Maxwell field, again all the $\delta^{(2)}(0)$ -terms cancel. For the ansatz (7.2.5), there are three nontrivial Einstein equations—the (ν) , (ρ) and (θ) components—which explicitly read

$$\begin{aligned} -\frac{1}{\kappa^2} \left(\frac{\hat{\mathcal{R}}}{4W^2} + 3\frac{W''}{W} + \frac{B''}{B} + 3\frac{W'^2}{W^2} + 3\frac{W'B'}{WB} + \frac{1}{2}\phi'^2 \right) &= \frac{e^\phi}{2} \left(\frac{Q^2}{W^8} + \frac{4e^2}{\kappa^4} \right) \\ &+ \sum_b \frac{\delta_b^{(2)}}{B} \mathcal{T}_b, \end{aligned} \quad (7.2.19a)$$

$$\frac{1}{\kappa^2} \left(\frac{\hat{\mathcal{R}}}{2W^2} + 6\frac{W'^2}{W^2} + 4\frac{W'B'}{WB} - \frac{1}{2}\phi'^2 \right) = \frac{e^\phi}{2} \left(\frac{Q^2}{W^8} - \frac{4e^2}{\kappa^4} \right), \quad (7.2.19b)$$

$$\frac{1}{\kappa^2} \left(\frac{\hat{\mathcal{R}}}{2W^2} + 4\frac{W''}{W} + 6\frac{W'^2}{W^2} + \frac{1}{2}\phi'^2 \right) = \frac{e^\phi}{2} \left(\frac{Q^2}{W^8} - \frac{4e^2}{\kappa^4} \right), \quad (7.2.19c)$$

respectively. The difference of the (ρ) and (θ) equations is

$$\frac{W''}{W} - \frac{W'B'}{WB} + \frac{1}{4}\phi'^2 = 0, \quad (7.2.20)$$

which shows that a nontrivial dilaton profile necessarily implies a warped geometry. Thus, it was necessary to include the warping factor W in (7.2.5a) in order to allow for generic statements about the 4D maximally symmetric setup.

The boundary conditions for the metric functions can be obtained just like for the dilaton above, by integrating appropriate combinations of the Einstein equations over a small disc covering one brane. Explicitly, this yields

$$[B(W^4)']_{\rho=\rho_b} = 0, \quad (7.2.21a)$$

$$[B']_{\rho=\rho_b} = 1 - \frac{\kappa^2}{2\pi} [\mathcal{T}_b(\phi)]_{\rho=\rho_b}. \quad (7.2.21b)$$



7.2.6 Condition for 4D flatness

We now want to answer the question how the brane couplings $\mathcal{T}_b(\phi)$ and $\mathcal{A}_b(\phi)$ must be chosen in order to obtain 4D flat solutions. To this end, we consider the 2D trace of the Einstein equations, i.e. the sum of (7.2.19b) and (7.2.19c), which gives

$$\frac{1}{\kappa^2} \left(\frac{\hat{\mathcal{R}}}{W^2} + 4\Delta_2 \ln W \right) = e^\phi \left(\frac{Q^2}{W^8} - \frac{4e^2}{\kappa^4} \right), \quad (7.2.22)$$

with Δ_2 defined as in (7.2.15). Using the dilaton equation (7.2.13), we can rewrite this as

$$\frac{1}{2\kappa^2} \left[\frac{\hat{\mathcal{R}}}{W^2} + 2\Delta_2 (\phi + 2 \ln W) \right] = \sum_b \frac{\delta_b^{(2)}}{B} \mathcal{C}_b, \quad (7.2.23)$$

Following [GGP04], we multiply this equation with BW^4 and integrate over the whole extra space, yielding⁹

$$\boxed{\hat{\mathcal{R}} = \frac{2\kappa^2}{V} \sum_b W_b^4 \mathcal{C}_b}, \quad (7.2.24)$$

with the extra space volume

$$V := 2\pi \int d\rho BW^2 = \int d^2y \sqrt{g_2} W^2, \quad (7.2.25)$$

and the subscript b denoting evaluation at $\rho = \rho_b$. Equation (7.2.24) is the central result of the delta analysis, relating the on-brane curvature $\hat{\mathcal{R}}$ to the brane couplings encoded in \mathcal{C}_b via (7.2.17). The only assumption necessary for its derivation was to have a 4D maximally symmetric geometry, allowing for the ansatz (7.2.5). Most importantly, it shows that 4D flatness is guaranteed by SI dilaton-brane couplings (7.2.4), and *not* by dilaton independent couplings ($\mathcal{A}'_b = \mathcal{T}'_b = 0$) in the presence of a BLF term as was previously claimed in the literature [BvN11, BvN13, Bur13]. If SI is broken, the right hand side of (7.2.24) does not vanish identically; however, since it explicitly depends on ϕ_b —which can generically diverge in this case—an actual evaluation requires to regularize the setup, see Sec. 7.3. In this case, we will find that there are additional contributions to $\hat{\mathcal{R}}$ caused by the finite brane width, which also breaks SI.

Alternatively, using the dilaton boundary condition (7.2.16), Eq. (7.2.24) can be written as

$$\hat{\mathcal{R}} = \frac{4\pi}{V} \sum_b [BW^4 \phi']_{\rho=\rho_b}, \quad (7.2.26)$$

saying that a necessary and sufficient condition for 4D flatness is a regular dilaton profile at the branes. This was already observed in [ABPQ04]. But in [BvN11, BvN13, Bur13],

⁹Here and henceforth, evaluation at $\rho = \rho_b$ is denoted by the corresponding subscript, e.g. $W_b \equiv W(\rho_b)$.

the wrong conclusion was drawn that this would be equivalent to dilaton independent brane couplings ($\mathcal{A}'_b = \mathcal{T}'_b = 0$).¹⁰ This is not the correct condition, because the BLF term leads to an additional, indirect dilaton coupling. This was explicitly shown in Sec. 7.2.4: Due to the bulk F^2 term the dilaton equation (7.2.13) obtains an $\delta^{(2)}$ -contribution proportional to \mathcal{A}_b (in addition to the \mathcal{A}'_b term). In other words, even if there is no *direct* dilaton-brane coupling, ϕ still gets sourced *indirectly* by the BLF term, because it couples to the bulk Maxwell field. Instead, we have proven that it is SI which ensures the brane dimensions to remain flat despite the presence of a brane vacuum energy.

7.2.7 Explicit 4D flat solutions

Let us now specialize to the case of 4D flat solutions, i.e. $\hat{\mathcal{R}} = 0$, which are the relevant candidates with respect to the CC problem. As shown above, this is guaranteed by brane-dilaton couplings of the form

$$\mathcal{T}_b(\phi) = \lambda_b, \quad \mathcal{A}_b(\phi) = \Phi_b e^{-\phi}, \quad (7.2.27)$$

with λ_b and Φ_b constant, which preserve the SI of the bulk theory. As we have seen, this also implies a regular dilaton profile, see Eq. (7.2.16). Incidentally, the most general solutions are explicitly known for this setup [GGP04]:¹¹

$$ds^2 = W^2(\xi) \left[\eta_{\mu\nu} dx^\mu dx^\nu + e^{-\phi_0} r_B^2 \left(d\xi^2 + \frac{\alpha_+ \alpha_-}{W^8(\xi)} \sin^2(\xi) d\theta^2 \right) \right], \quad (7.2.28a)$$

$$\phi(\xi) = \phi_0 - 2 \ln W(\xi), \quad (7.2.28b)$$

with

$$W^4(\xi) = \cosh(v) - \sinh(v) \cos(\xi). \quad (7.2.28c)$$

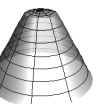
The constants r_B, α_\pm and v are fixed in terms of the model parameters via

$$r_B = \frac{\kappa}{2e}, \quad \alpha_\pm = 1 - \frac{\kappa^2}{2\pi} \lambda_\pm, \quad v = \frac{1}{2} \ln \left(\frac{\alpha_+}{\alpha_-} \right), \quad (7.2.29)$$

with \pm labeling the two branes, located at the poles $\xi_+ = 0$ and $\xi_- = \pi$. The dilaton constant ϕ_0 is not determined by any of the field equations, as is guaranteed by SI. Geometrically, the parameters $2\pi(1 - \alpha_\pm)$ correspond to the deficit angles at the branes that are created by their tensions. In the special case of equal tensions, the solution

¹⁰The error was caused by using the dilaton boundary condition from Ref. [BBvN10], which is only applicable in the case without BLF.

¹¹We use the coordinates introduced in [BvNW14a]. The metric could as well be brought into the form (7.2.5a) by changing to the normal coordinate $\rho \propto \int W d\xi$, but this transformation yields complicated expressions containing hypergeometric functions, which are not very useful.



simplifies to the rugby ball geometry. Otherwise, the warping W is nontrivial and the extra space looks like a deformed rugby ball. The extra space volume V is

$$V = 4\pi r_B^2 \sqrt{\alpha_+ \alpha_-} e^{-\phi_0}. \quad (7.2.30)$$

Furthermore, in these coordinates, the Maxwell field strength is given by

$$F_{\xi\theta} = \frac{r_B}{\kappa} \sqrt{\alpha_+ \alpha_-} \frac{\sin(\xi)}{W^8(\xi)} + \frac{1}{2\pi} \sum_b \Phi_b \delta(\xi - \xi_b). \quad (7.2.31)$$

The flux quantization condition (7.2.9) then becomes

$$\boxed{\frac{2\pi}{e} \sqrt{\alpha_+ \alpha_-} + \sum_b \Phi_b = \frac{2\pi n}{\tilde{e}}}. \quad (7.2.32)$$

7.2.8 Fine-tuning

Now the crucial point is that (7.2.32) does not contain any free integration constants, and therefore constitutes a tuning relation on model parameters. For parameters which do not fulfill this relation, there would be no static solution and we would expect some sort of runaway behavior. In particular, the brane tension (i.e. the 4D CC) must be fine-tuned in order to obtain this 4D flat solution. Therefore, the scale invariant SLED model cannot help with the CC problem.

Alternatively, we can understand this in the following way: Since the extra dimensions are compact, the low energy theory could also be studied from the Kaluza-Klein reduced, effective 4D point of view. In this case, Weinberg's general no-go theorem (cf. Sec. 1.2.1) applies, showing that SI is indeed sufficient to guarantee flat solutions, but only at the price of another fine-tuning; if the tuning were violated, there would only be runaway solutions.

For the original model without BLF, this problem was indeed realized from the very beginning [ABPQ04]. However, it was assumed that $\hat{\mathcal{R}} = 0$ would be guaranteed by the absence of dilaton-brane couplings, and not by SI. For pure tension branes, these two options are in fact indistinguishable ($\mathcal{T}'_b = 0$); furthermore, the expectation seemed reasonable because we know from (7.2.26) that $\hat{\mathcal{R}} = 0$ is ensured by a regular dilaton profile, which should be obtained for dilaton-independent brane couplings. Therefore, it was assumed [BvN11, BvN13] that a dilaton-independent BLF ($\mathcal{A}'_b = 0$)—which breaks SI—would still imply $\hat{\mathcal{R}} = 0$. In this case the flat dilaton potential would be lifted, and so the fine-tuning could be avoided. More explicitly, the BLF term in (7.2.32) would be dilaton dependent, and so flux quantization would simply fix the dilaton integration constant, and would not imply a tuning on model parameters.

However, as we have shown, this line of reasoning is flawed by the fact that it is *not* dilaton independence, but SI of the BLF term which guarantees 4D flat maximally symmetric solutions. The reason is that the dilaton is sourced indirectly (via the Maxwell sector), even if there is no direct BLF coupling, in precisely such a way that

ultimately SI guarantees a regular dilaton profile, cf. Sec. 7.2.6. But for SI couplings, the effective dilaton potential is flat again and we either have to fine-tune, or would be left with runaway solutions, in complete agreement with Weinberg's argument.

7.2.9 Constraint

Let us now turn to a peculiarity [BDW16] of the delta setup which was not discussed in [NS16a]. Multiplying the constraint (7.2.19b) by B^2 and taking the limit $\rho \rightarrow \rho_b$ yields (assuming that $B^2 e^\phi \rightarrow 0$)

$$\left\{ \frac{3}{8W^8} [B(W^4)']^2 + \frac{1}{W^4} [B(W^4)'] [B'] - \frac{1}{2} [B\phi']^2 \right\}_{\rho=\rho_b} = 0. \quad (7.2.33)$$

The terms in square brackets are those appearing in the boundary conditions (7.2.16), (7.2.21), and so we are led to (assuming that $[\mathcal{T}_b(\phi)]_{\rho=\rho_b}$ is finite, as it should be for physically relevant situations)

$$\mathcal{C}_b = 0. \quad (7.2.34)$$

This is in clear contradiction to the SI breaking expectation $\mathcal{C}_b \neq 0$. In [BDW16], it was argued that this uncovers an inconsistency of the delta analysis. The conclusion of [BDW16] was that one has to take into account an ad hoc metric dependence of the delta function, designed such that it results in a localized contribution to the angular Einstein equation (7.2.19c); in this case the constraint fixes the size of this term, and non SI couplings are possible. Let us summarize our point of view on this issue:

- (i) First of all, it should be emphasized that the SI case is completely insensitive to this issue, because then (7.2.34) is identically fulfilled. Thus, the important achievement of [NS16a], namely the first correct identification of those BLF couplings which unambiguously lead to $\hat{\mathcal{R}} = 0$ (and the resulting tuning relation), remains unaffected.
- (ii) Physically, the additional term proposed in [BDW16] corresponds to an angular pressure component. Since a codimension-two brane contains no direction this pressure could act in, such a construction seems ill-defined.
- (iii) If one still accepts this term, none of the conclusions of Sec. 7.2 would change. There would be an additional contribution to $\hat{\mathcal{R}}$ in (7.2.24) which also vanishes in the SI case.
- (iv) Alternatively, the impossibility to break SI consistently on a delta brane (in the case of 4D maximal symmetry) could be regarded as a prediction of this analysis. (Note that this does not preclude SI breaking couplings; SI could in principle also be restored dynamically by a runaway behavior.)



- (v) The latter case, however, also implies that the actual (nonzero) value of $\hat{\mathcal{R}}$ for broken SI cannot be inferred within the pure delta framework (which always¹² predicts $\hat{\mathcal{R}} = 0$), but requires studying a thick brane setup. This also has the advantage that potential singularities are regularized.
- (vi) By studying a regularized setup and properly taking the thin brane limit in Sec. 7.3, we will show that the latter option is indeed realized for a relevant class of couplings (of the form $\mathcal{C}_b \propto e^{\gamma\phi_b}$). While this means that $\hat{\mathcal{R}} \rightarrow 0$ despite these non SI couplings, it does not save the model because either one has to tune certain parameters or phenomenological bounds are violated.

7.3 Breaking scale invariance on thick branes

In Sec. 7.2, we showed that in the SLED model (with delta branes) solutions with vanishing 4D curvature $\hat{\mathcal{R}}$ are only guaranteed by SI and a fine-tuning of parameters (including the brane tension). While rather discouraging, this observation does not immediately rule out the SLED program as a candidate for addressing the CC problem. The remaining window of opportunity consists in breaking SI. In this case, Weinberg's argument does not tell us how large $\hat{\mathcal{R}}$ has to be, and the hope is that there might be SI breaking couplings for which it turns out to be small enough to be phenomenologically viable in a technically natural way.

In this section we will investigate this remaining possibility. Since we again restrict ourselves to 4D maximally symmetric solutions, we start with the effective theory that is obtained after the Maxwell field has been solved for (and the BLF divergence is removed by the appropriate counter term). The goal is to explicitly solve the resulting Einstein-dilaton system for given SI breaking couplings and analyze the tuning question and phenomenological bounds.

In fact, SI should be broken explicitly on the Standard Model brane (say, at the north pole) in any case, because otherwise the theory would predict a fifth force of gravitational strength [BvNW14b, BDW15c], which is clearly ruled out by solar system experiments [Wil06]. We will therefore consider a SI breaking contribution to the brane tension, but a SI BLF,¹³ parametrized as

$$\mathcal{T}_+(\phi) = \lambda_+ + \tau e^{\gamma\phi}, \quad \mathcal{A}_+(\phi) = \Phi_+ e^{-\phi}, \quad (7.3.1)$$

with constant λ_+ , τ , γ and Φ_+ . For simplicity, the southern brane will be assumed only to carry a SI tension $\mathcal{T}_- = \lambda_-$. For $\tau\gamma \neq 0$ SI is broken explicitly; but one virtue

¹²In the proposal of [BDW16] $\hat{\mathcal{R}} \neq 0$ would still be possible for delta branes, but only at the price of allowing $p_\theta \neq 0$.

¹³We could as well allow for a non SI BLF in a similar way. However, the discussion and physical implications would be completely analogous. Furthermore, such a term (unlike the tension) could presumably be taken to be arbitrarily small in a technically natural way, if the brane matter fields do not couple directly to the Maxwell sector [BDW15c].

of this class of couplings is that the contributions to $\hat{\mathcal{R}}$ which are $\propto \tau$ (which receives radiative corrections via SM loops) can be suppressed for ϕ_+ sufficiently negative.

Due to potential singularities, and for the reasons discussed in Sec. 7.2.9, it is not possible to solve the bulk equations and unambiguously predict the value of $\hat{\mathcal{R}}$ for delta branes with broken SI. We will therefore consider a finite brane width ℓ . Let us emphasize, though, that this should not be regarded as a mere technicality, but rather as another physical necessity: Any realistic brane would have a finite microscopic width, ultimately set by the underlying UV model. If the hierarchy between the 2D brane and bulk volume is large enough (if $\epsilon := \ell^2/V$ is sufficiently small) the brane could usually be treated as pointlike ($\epsilon \rightarrow 0$), as in Sec. 7.2. But in the present setup there is a subtlety. As we shall see, the nonzero width of the brane leads to an additional $\mathcal{O}(\epsilon)$ contribution to $\hat{\mathcal{R}}$ as compared to the delta setup. Now, since we are interested in situations in which all other contributions to $\hat{\mathcal{R}}$ are tremendously small (as compared to the bulk gravity scale), these $\mathcal{O}(\epsilon)$ can in fact become the dominant part and cannot be neglected. This will have crucial implications for the phenomenological viability of the model—even if the tension were SI.

7.3.1 Ring regularization

For simplicity, we will again (as in previous chapters) use the well-known ring regularization, in which the point in extra space (the north pole) is blown up to a circle of finite circumference ℓ . We assume that the low energy questions which we ask to be insensitive to this particular choice, and would expect to recover the same qualitative results in any other reasonable regularization (or UV model).¹⁴ The virtue of this regularization is its technical simplicity; the northern brane is moved to $\rho = \rho_+$ ($> \rho_0$), leaving behind a regular axis at $\rho = \rho_0$. (Without loss of generality, we will set $\rho_0 = 0$.) The corresponding extra space geometry is visualized in Fig. 7.1b above. The equations of motion are formally obtained from those presented in Sec. 7.2, viz. (7.2.14) and (7.2.19), by letting $\delta^{(2)}(y) \mapsto \delta(\rho - \rho_b)/2\pi$, and keeping in mind that now $B_+ \equiv \ell/2\pi > 0$ (whereas $B_0 = B_- = 0$). Furthermore, we will for convenience set $W_+ = 1$ by a (global) rescaling of the 4D coordinates.

However, as we already know from previous chapters, there is one further modification that is required in order to obtain a consistent regularization: the (θ) -component of the Einstein equations, i.e. the right hand side of Eq. (7.2.19c), has to be supplemented with a brane localized source of the form

$$\frac{\delta(\rho - \rho_+)}{2\pi B_+} p_\theta. \quad (7.3.2)$$

Physically, it corresponds to the angular pressure that is needed to prevent the ring from collapsing.¹⁵ Technically, it is required by and can be inferred from the constraint (7.2.19b), as will be explained in more detail below. Note that this is the same

¹⁴This could be checked explicitly by repeating our analysis e.g. in the UV model [BDW15a].

¹⁵A microscopic model that achieves this stabilization can be found e.g. in [BHdRT09].



term that was argued to be necessary also for unregularized delta branes in [BDW16], cf. Sec. 7.2.9. However, since a delta brane contains no direction this pressure could act in, we expect it to vanish in the thin brane limit $\epsilon \rightarrow 0$. This will later be verified explicitly (for the dilaton-brane couplings we consider).

7.3.2 Angular pressure and 4D curvature

This additional term has an important consequence, as it yields an additional contribution to $\hat{\mathcal{R}}$. This can be seen by repeating the calculation that led to (7.2.24), but taking (7.3.2) into account. We thereby obtain the thick brane result

$$V\hat{\mathcal{R}} = \kappa^2 (2\mathcal{C}_+ + p_\theta). \quad (7.3.3)$$

We can gain further insight by also expressing p_θ in terms of the brane couplings, following [BHdRT09]. First, the junction conditions across the brane read

$$[B\phi']_{\text{disc}} = \frac{\kappa^2}{2\pi} \mathcal{C}_+, \quad (7.3.4a)$$

$$4[B(\ln W)']_{\text{disc}} = \frac{\kappa^2}{2\pi} p_\theta, \quad (7.3.4b)$$

$$[B']_{\text{disc}} = -\frac{\kappa^2}{2\pi} \left(\mathcal{T}_+ + \frac{3}{4} p_\theta \right), \quad (7.3.4c)$$

where the discontinuity of a function f across the brane is denoted by $[f]_{\text{disc}} := f(\rho \searrow \rho_+) - f(\rho \nearrow \rho_+)$. Next, for a sufficiently large hierarchy between the brane width and bulk size, i.e. for $\epsilon \rightarrow 0$, the interior derivatives are expected to approach the (regular) values at the axis, viz.

$$\phi'(\rho \nearrow \rho_+) = \mathcal{O}(\epsilon), \quad W'(\rho \nearrow \rho_+) = \mathcal{O}(\epsilon), \quad B'(\rho \nearrow \rho_+) = 1 + \mathcal{O}(\epsilon). \quad (7.3.5)$$

These expectations will also be verified explicitly by the numerical analysis in Sec. 7.3.5. Using this, as well as $\epsilon \equiv (2\pi B_+)^2/V$, the constraint (7.2.19b) evaluated at $\rho \searrow \rho_+$ yields

$$\frac{3}{4} p_\theta^2 - 2 \left(\frac{2\pi}{\kappa^2} - \mathcal{T}_+ \right) p_\theta + \mathcal{C}_+^2 + \frac{\epsilon}{\kappa^4} \left[\kappa^2 V e^{\phi_+} \left(Q^2 - \frac{4e^2}{\kappa^4} \right) - V\hat{\mathcal{R}} \right] = \mathcal{O}(\epsilon). \quad (7.3.6)$$

The terms in square brackets are generically of the same order as the first terms in this equation,¹⁶ and so the factor ϵ allows to absorb them into $\mathcal{O}(\epsilon)$. Solving for p_θ , and choosing the branch that reproduces the GGP result $p_\theta = 0$ for a SI delta brane, we

¹⁶For $V\hat{\mathcal{R}}$ this follows from (7.3.3), for the first term from $V \sim e^{-\phi_+}$ —which will be confirmed below.

find

$$p_\theta = \frac{4}{3} \left[\left(\frac{2\pi}{\kappa^2} - \mathcal{T}_+ \right) - \sqrt{\left(\frac{2\pi}{\kappa^2} - \mathcal{T}_+ \right)^2 - \frac{3}{4} \mathcal{C}_+^2} \right] + \mathcal{O}(\epsilon) \quad (7.3.7a)$$

$$= \frac{1}{2} \left(\frac{2\pi}{\kappa^2} - \mathcal{T}_+ \right)^{-1} \mathcal{C}_+^2 + \mathcal{O}(\epsilon) + \mathcal{O}(\mathcal{C}_+^4). \quad (7.3.7b)$$

In the second line, we expanded around the SI case $\mathcal{C}_+ = 0$. Plugging this into the $\hat{\mathcal{R}}$ formula (7.3.3), we find that in the near SI limit ($\kappa^2 \mathcal{C}_+ \ll 1$) the leading contribution is given by

$$V \hat{\mathcal{R}} = 2\kappa^2 \mathcal{C}_+ + \mathcal{O}(\epsilon) + \mathcal{O}(\mathcal{C}_+^2). \quad (7.3.8)$$

Hence, the delta result (7.2.24) receives corrections that are suppressed in the near SI limit compared to the leading contribution $\propto \mathcal{C}_+$, and—more importantly— $\mathcal{O}(\epsilon)$ corrections which are caused by the finite brane width.

7.3.3 Volume dependence

Let us now focus on the dilaton coupling (7.3.1), for which

$$\mathcal{C}_+ = \tau\gamma e^{\gamma\phi_+}. \quad (7.3.9)$$

For the angular pressure this gives

$$p_\theta = \frac{\kappa^2}{4\pi\alpha_+} (\tau\gamma e^{\gamma\phi_+})^2 + \mathcal{O}(\epsilon) + \mathcal{O}(\mathcal{C}_+^3), \quad (7.3.10)$$

where still $\alpha_+ \equiv 1 - \frac{\kappa^2}{2\pi} \lambda_+$. In the near SI case which we are interested in, we expect the volume V to approach the GGP value (7.2.30), which can be written in terms of ϕ_+ as¹⁷

$$V \rightarrow V_{\text{GGP}} = \frac{\kappa^2}{e^2} \pi \alpha_+ e^{-\phi_+}. \quad (7.3.11)$$

Again, this expectation will later be confirmed explicitly by our numerics. The usefulness of this relation is that it allows to express ϕ_+ in terms of model parameters and V , which is constrained by observations. Crucially, it shows that if e^2 is not tuned much smaller than the bulk Planck scale κ , a phenomenologically necessary large volume ($V \gg \kappa$) is achieved if and only if $-\phi_+ \gg 1$.

For p_θ we thus obtain

$$p_\theta \propto \begin{cases} V^{-2\gamma} & (\text{for } 0 < \gamma < 1/2) \\ V^{-1} & (\text{for } \gamma = 0 \text{ or } \gamma > 1/2) \end{cases} \quad (7.3.12)$$

¹⁷This formula takes into account that we are now in the gauge $W_0 = 1$, which yields an additional factor $(W_+^{\text{GGP}})^{-2} = (\alpha_+/\alpha_-)^{1/4}$.



in the relevant large volume regime. The two cases discriminate which of the two leading terms in (7.3.10) dominates. As advertised, we see that within the class of exponential dilaton couplings (with $\gamma > 0$)¹⁸ $p_\theta \rightarrow 0$ in the thin brane limit $\epsilon \rightarrow 0$ (which can be realized via $V \rightarrow \infty$).

Finally, the leading contributions to the 4D curvature become

$$\boxed{V\hat{\mathcal{R}} = N_1 \left(\frac{V}{\kappa}\right)^{-\gamma} + N_2 \left(\frac{V}{\kappa}\right)^{-1}}, \quad (7.3.13)$$

where N_i are dimensionless coefficients, with

$$N_1 = 2\kappa^2\tau\gamma \left(\frac{\kappa\pi\alpha_+}{e^2}\right)^\gamma \quad \text{and} \quad N_2 \propto \frac{\ell^2}{\kappa}. \quad (7.3.14)$$

The unknown constant of proportionality for N_2 can be traced back to the unknown numerical coefficients of the $\mathcal{O}(\epsilon)$ terms in (7.3.5). Generically, we expect it to be ~ 1 , which will be confirmed explicitly by the numerical examples studied in Sec. 7.3.5. Let us point out that, while the N_1 contribution to $\hat{\mathcal{R}}$ is only present for SI breaking dilaton couplings (and depends on their details), the N_2 term is solely due to the finite thickness of the brane and thus insensitive to the dilaton-brane couplings. In particular, it is even present for SI couplings.

7.3.4 Phenomenology

Let us now discuss the phenomenological implications of our findings. The key point is that Eq. (7.3.13) provides a rigid relation between the 4D curvature and the size of the extra dimensions, both of which are constrained by observations: First, $\hat{\mathcal{R}}$ is measured by cosmography to be ~ 120 orders of magnitude smaller than M_{Pl}^2 . As usual in compact extra space models, the 4D Planck mass is related to the bulk gravity scale by [BDW15c]

$$M_{\text{Pl}}^2 = \frac{V}{\kappa^2}, \quad (7.3.15)$$

so this implies¹⁹

$$\frac{\kappa^2\hat{\mathcal{R}}}{V} \sim 10^{-120}. \quad (7.3.16)$$

¹⁸For $\gamma < 0$ the tension would become supercritical for large volumes; furthermore, the contribution to $\hat{\mathcal{R}}$ could not become small without fine-tuning. Thus, these couplings are not interesting.

¹⁹Actually, observations also tell us that $\hat{\mathcal{R}} < 0$, whereas we will find $\hat{\mathcal{R}} > 0$ (corresponding to *anti* de Sitter, in our present conventions) in the numerical solutions below, which might be regarded as an additional problem. However, it is also conceivable that natural solutions with the wrong sign but the correct magnitude of $\hat{\mathcal{R}}$ could become phenomenologically viable without spoiling naturalness, if quantum corrections (which are not studied here) would give additional negative contributions to $\hat{\mathcal{R}}$. In any case, we will find that the weaker requirement of demanding the correct magnitude for $\hat{\mathcal{R}}$ is already problematic.

And second, current upper bounds [KCA⁺07] on deviations from Newton’s inverse square law exclude extra dimensions larger than $\sim 10 \mu\text{m}$, which—again via (7.3.15)—requires

$$\frac{V}{\kappa} \lesssim 10^{28}. \quad (7.3.17)$$

Plugging these observational inputs into (7.3.13) then yields

$$N_1 \times 10^{-28\gamma} + N_2 \times 10^{-28} \lesssim 10^{-64}. \quad (7.3.18)$$

Unless there were an accidental cancellation between the two terms—which would require a careful tuning of parameters and should thus be dismissed when looking for a solution to the CC problem—they have to fulfill this bound separately. Let us discuss them in turn.

The first term $\propto N_1$ vanishes identically for SI dilaton-brane couplings. But as already mentioned, this would give rise to Brans-Dicke type 4D interactions which are ruled out by solar system observations. If SI is broken, Eq. (7.3.14) shows that N_1 will be of order unity for generic model parameters which are not tuned and do not introduce huge hierarchies. In this case, the bound (7.3.18) can only be satisfied for $\gamma \gtrsim 2.3$. However, the numerical analysis in the next section will allow us to infer the amount of tuning due to flux quantization, showing that this can be avoided only for $\gamma \lesssim 1/60$.

The second term is even more problematic. It implies that N_2 must be $\lesssim 10^{-36}$. From the discussion below Eq. (7.3.14), we know that this is only possible if the brane width ℓ were at least 18 orders of magnitude smaller than the fundamental bulk Planck length $\sqrt{\kappa}$. This would again correspond to the introduction of a huge hierarchy by hand, and—more importantly—question the applicability of a (semi-)classical analysis. On the other hand, for the natural (and classically accessible) scenario where the brane width is not smaller than the bulk Planck length, $N_2 \sim 1$ and so either the the 4D curvature or the size of the extra space volume would exceed their phenomenological bounds by (at least) 36 or 12 orders of magnitude, respectively.²⁰

7.3.5 Numerical results and fine-tuning

Note: This section is to large extent a verbatim reproduction of the corresponding section in [NS16b].

In this section we present the results of our numerical studies of the regularized model and discuss their physical implications for the SLED scenario. Since we derive the solutions of the full brane-bulk system without relying on any approximations, we will be able to explicitly test (and confirm) the analytical approximations and results of the last section. Furthermore, we will learn how much tuning is required by flux

²⁰More generally, $\hat{\mathcal{R}}$ and V exceed their bounds by m and n orders of magnitude, respectively, with $m + 3n = 36$.



quantization in order to achieve a small enough 4D curvature (or large enough 2D volume).

This section is divided into three parts: First, we will first briefly sketch the numerical algorithm. Next, we will discuss the simple case of SI brane couplings. In this case we know the exact analytic solutions for infinitely thin branes—the GGP solution, reviewed in Sec. 7.2.7 above—and so this provides a useful consistency check for our numerical solver. Finally, the last part addresses the actual case of interest: a SI breaking tension.

Throughout this section, we will for convenience set $\kappa = 1$, i.e. all dimensionful quantities are here measured in units of the bulk Planck scale.

Numerical algorithm and parameters

The goal is to determine the ρ -profiles of the dilaton ϕ and of the metric functions B and W for given model parameters. This requires solving the bulk ($\rho \neq \rho_b$) equations (7.2.14), (7.2.19), supplemented by the junction conditions (7.3.4) across $\rho = \rho_+$. Furthermore, we have to impose appropriate boundary conditions at the axes, viz.

$$\phi'_0 = 0, \quad W'_0 = 0, \quad B'_0 = 1, \quad B_0 = 0, \quad (7.3.19a)$$

$$\phi'_- = 0, \quad W'_- = 0, \quad B'_- = -\alpha_-, \quad B_- = 0. \quad (7.3.19b)$$

Our algorithm²¹ starts at the north pole ($\rho = 0$) and integrating outward using the second order equations. Since the constraint (7.2.19b) is analytically conserved, it only needs to be imposed initially at $\rho = 0$. For $\rho > 0$ it can then be used as a consistency check (or error estimator) of the numerical solution. At $\rho = \rho_+$, however, the constraint must be used once again, because it determines the stabilizing pressure p_θ . In other words, when the integration reaches $\rho \nearrow \rho_+$, the three junction conditions (7.3.4) must be supplemented by the constraint (evaluated at $\rho \searrow \rho_+$) in order to determine the three exterior ρ -derivatives and p_θ . Afterwards, the integration continues until $B \rightarrow 0$, defining the south pole $\rho = \rho_-$.

Before the equations can actually be integrated in this way, we need to specify the three a priori unknown integration constants ϕ_0 , Q and $\hat{\mathcal{R}}$. In general, however, all of them are ultimately fixed via (the SI case is exceptional, see Sec. 7.3.5)

- (i) flux quantization (7.2.9),
- (ii) regularity at the south pole, i.e., $\phi'_- = 0$,²²
- (iii) the correct conical defect at the south pole, i.e., $B'_- = -\alpha_-$.

Technically, this can be achieved by a standard shooting method: we choose some initial guesses for ϕ_0 , Q and $\hat{\mathcal{R}}$; after integrating the ODEs, the violations of (i)–(iii)

²¹It was implemented in Mathematica, using its “NDSolve” method.

²²The corresponding regularity condition for W is not independent thanks to the constraint, i.e., $W'_- = 0$ automatically whenever $\phi'_- = 0$.

can be computed, and finally be brought close to zero via an iterative root-finding algorithm.

In this way, since there are no integration constants left (in the non SI case), we also see that the full solution is uniquely determined for a given set of model parameters. These consist of the bulk couplings $\kappa = 1$ (in our present units), e , the regularization width ρ_+ , the brane couplings, parametrized by α_{\pm} , τ , γ and the BLF parameter Φ_+ , as well as the gauge coupling \tilde{e} . Since the latter only enters via flux quantization (7.2.9), it is convenient to introduce the abbreviation

$$\mathcal{N} := \frac{2\pi n}{\tilde{e}}, \quad (7.3.20)$$

so that flux quantization simply reads $\Phi_{\text{tot}} = \mathcal{N}$.

Note that the solution would *not* be determined uniquely if, for instance, the boundary conditions ensuring regularity at the south pole were neglected. In this case, it would not be possible to numerically predict the value of $\hat{\mathcal{R}}$, since it could be chosen freely. Thus, in order to *compute* this quantity numerically, it is crucial to find complete, regular bulk solutions. To our knowledge, this is done here for the first time.²³

The main question is whether it is possible to find solutions for which $\hat{\mathcal{R}}$ is small enough and V is large enough to be phenomenological viable without fine-tuning, i.e. for generic values of the model parameters. For definiteness, and in order not to introduce any large hierarchies into the model by hand, we will choose the following parameters,

$$e = 1, \quad \rho_+ = 1, \quad \Phi_+ = -0.6, \quad \tau = 0.9 \times 2\pi, \quad \alpha_+ = 0.9, \quad \text{and} \quad \alpha_- = 0.5. \quad (7.3.21)$$

(Somewhat different values would not change the main results, though.) The parameter \mathcal{N} , determining the total flux, will be varied, and used as a dial to achieve different values of $\hat{\mathcal{R}}$ and V .

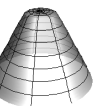
An exemplary numerical solution is shown in Fig. 7.2, where the three functions B, W, ϕ , as well as their ρ -derivatives are plotted, for $\gamma = 0.2$ and two different choices of \mathcal{N} , leading to two different values of V , as is evident from the profile of B . Since we chose $\alpha_+ \neq \alpha_-$, the solutions are warped—both W and ϕ have nontrivial profiles.²⁴

Furthermore, one can already see that the profiles inside the regularized brane ($\rho < \rho_+$) become more trivial as V increases, as expected. This trend continues, and all functions and their derivatives at $\rho \nearrow \rho_+$ were always found to approach the corresponding values at the regular axis ($\rho = 0$) like V^{-1} for $V \rightarrow \infty$, thereby confirming (7.3.5).

All of the ρ -derivatives are discontinuous at the regularized brane ($\rho = \rho_+$), as required by the junction conditions (7.3.4). B' consistently approaches $-\alpha_- = -0.5$

²³Analytically, the regularity condition also implicitly entered the derivation of (7.3.8) when integrating over the whole bulk. However, this equation for $\hat{\mathcal{R}}$ is not yet a prediction solely in terms of model parameters, since it still contains V and ϕ_+ (as well as the coefficient of $\mathcal{O}(\epsilon)$), which are a priori unknown. We were only able to infer the explicit value of $\hat{\mathcal{R}}$ numerically.

²⁴Note that here we chose the gauge $W_0 = 1$ for convenience, instead of $W_+ = 1$ as before. But this will not be relevant because $W_+ \rightarrow W_0$ in the thin brane limit.



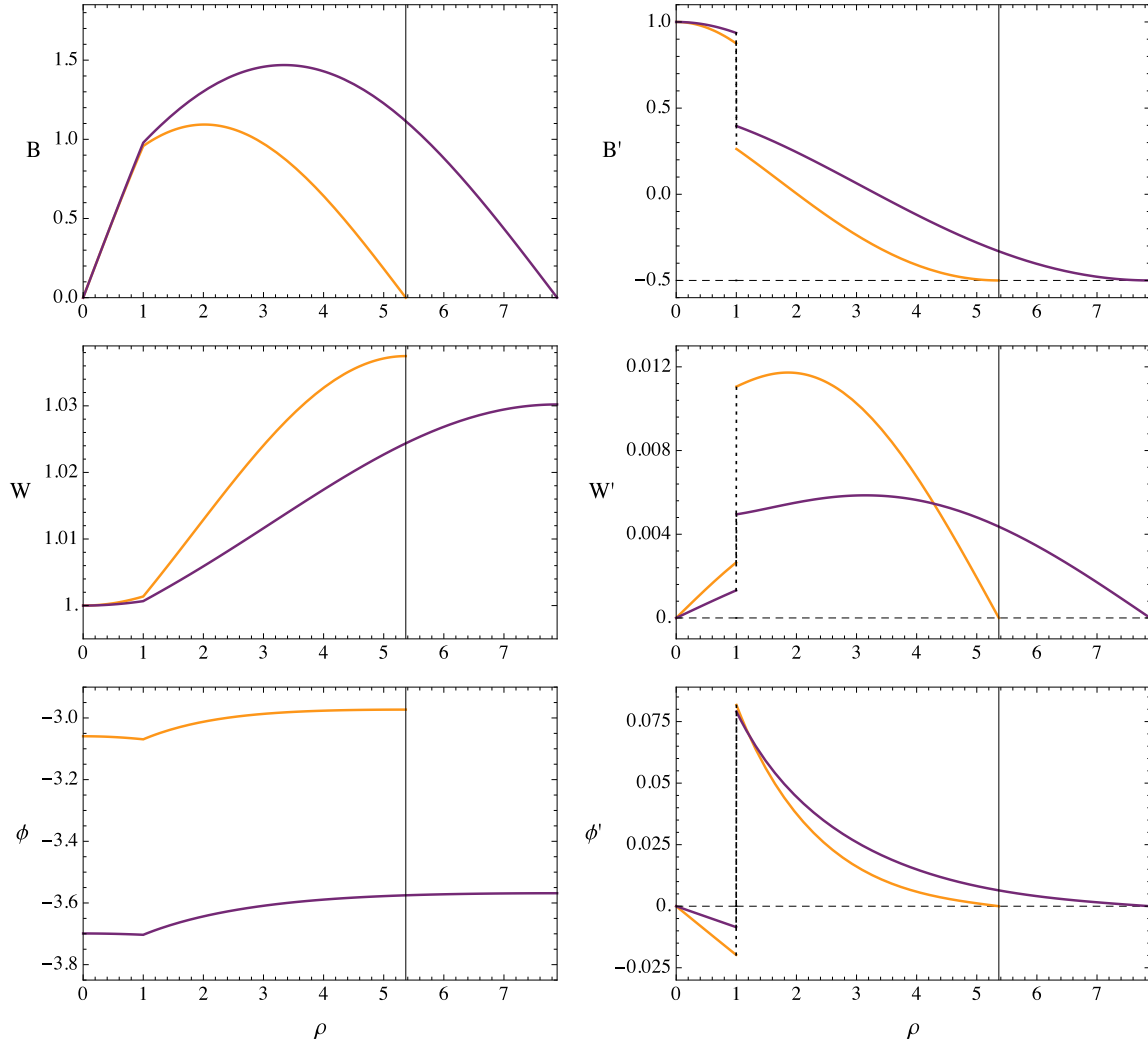


Figure 7.2: Complete numerical solutions of the coupled Einstein-dilaton system for the parameters (7.3.21) and $\gamma = 0.2$. The axis at the north pole ($\rho = 0$) is regular ($W' = \phi' = 0$) and elementary flat ($B' = 1$), while the axis at the south pole is regular but has a defect angle corresponding to the unregularized pure tension brane ($B' = -0.5$); the regularized brane sits at $\rho_+ = 1$ (in units of the bulk gravity scale), and produces jumps in the ρ -derivatives. The orange (light) and purple (dark) curves correspond to $V = 8\pi$ and $V = 16\pi$, respectively (which were obtained for $\mathcal{N} = -1.102$ and $\mathcal{N} = -0.885$). The required 4D curvature was $\hat{\mathcal{R}} = 0.0571$ and 0.0233 , respectively. The constraint violation, i.e. the numerical deviation of (7.2.19b) from zero, was always smaller than 10^{-10} in this example, and the numerical error bars would not exceed the line widths in the plots.

at the south pole and, most importantly, both W' and ϕ' vanish there, as required by regularity. By running the numerics similarly for different choices of γ and \mathcal{N} , we can now systematically learn how these model parameters determine $\hat{\mathcal{R}}$ and V .

Scale invariant couplings and thick branes

Let us first consider the case $\tau = 0$ corresponding to a SI tension $\mathcal{T}_+ = 2\pi(1 - \alpha_+)$. Incidentally, in this case the dilaton profile is regular, and so the solution can even be obtained for the idealized, infinitely thin brane, as already discussed in 7.2.7. It is given by the GGP solution [GGP04], for which $\hat{\mathcal{R}} = 0$. In that case, dilaton integration constant ϕ_0 drops out of all equations due to SI, and thus the above counting of constants does not add up. Instead, flux quantization results in the tuning relation (7.2.32) among model parameters. If we chose parameters which do not fulfill this equation, there would not be a static solution, in accordance with the expected runaway behavior à la Weinberg [Wei89]. In turn, the extra space volume V , which is $\propto e^{-\phi_0}$, cf. Eq. (7.2.30), can be chosen freely. As a result, this model could have a phenomenologically viable volume (although a vanishing 4D curvature is not compatible with observations), but only at the price of a new fine-tuning.

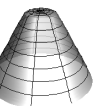
If SI is broken, things will change: on the one hand, ϕ_0 will be fixed, and thus the tuning relation is expected to disappear. On the other hand, the volume V will also be determined, and $\hat{\mathcal{R}}$ will be nonzero. The question then is if they can satisfy the phenomenological bounds presented in Sec. 7.3.4, and if so, whether this can be achieved without introducing yet another tuning.

Let us now present the numerical results for a regularized brane with SI couplings, i.e. $\tau = 0$ and all other parameters as in (7.3.21). One might expect that in this case still $\hat{\mathcal{R}} = 0$, because the brane coupling is SI. But this is in fact not the case, since SI is already broken by introducing a regularization scale ℓ . Thus, the above discussion applies here as well: ϕ_0 and V are fixed in terms of model parameters, and $\hat{\mathcal{R}}$ is nonvanishing.²⁵ However, if the thin brane limit is taken by letting $V \rightarrow \infty$ (which can be achieved by adjusting \mathcal{N} appropriately), these effects should become suppressed, and we expect to recover the GGP solution with $\hat{\mathcal{R}} = 0$. This is exactly what happens, as can be seen from Fig. 7.3a. Specifically, we find that $\hat{\mathcal{R}} \propto V^{-2}$ as $V \rightarrow \infty$. Furthermore, the angular pressure p_θ (not shown) is also nonvanishing, but goes to zero like V^{-1} . These findings are in complete agreement with the analytic predictions (7.3.13), (7.3.10) (with $\tau = 0$).

At the same time, the tuning relation (7.2.32) is also violated, and the static solutions exist for any choice of parameters. But again this violation,

$$\delta\Phi := \Phi_{\text{GGP}} - \mathcal{N}, \quad \text{with} \quad \Phi_{\text{GGP}} := \frac{2\pi}{e} \sqrt{\alpha_+ \alpha_-} + \Phi_+, \quad (7.3.22)$$

²⁵This is a qualitative difference to models with two *infinite* extra dimensions, where a regularized pure tension brane still has $\hat{\mathcal{R}} = 0$ [KK07, ENS15].



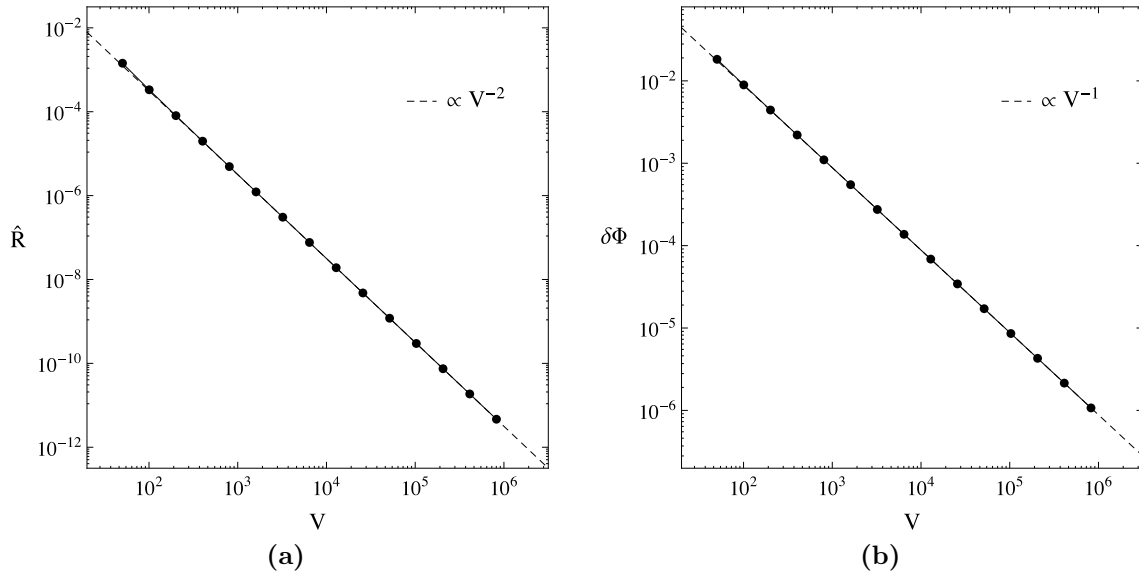


Figure 7.3: Numerical results for parameters (7.3.21) and $\tau = 0$, corresponding to SI brane couplings. For large volume V , the 4D curvature and the total flux both approach the corresponding GGP values which are valid for delta branes. The dashed lines are numerically inferred (and extrapolated) scaling laws.

vanishes (like V^{-1}) as $V \rightarrow \infty$, see Fig. 7.3b.²⁶

In summary, we explicitly confirmed that introducing a regularization (which breaks SI) leads to $\mathcal{O}(\epsilon)$ corrections of the GGP predictions ($\hat{\mathcal{R}} = 0$, $\Phi_{\text{GGP}} = \mathcal{N}$, $p_\theta = 0$), as should have been expected. In particular, this agrees with the analytic result of Sec. 7.2 that $\hat{\mathcal{R}} = 0$ is only guaranteed in the SLED model via SI (which is restored as $\epsilon \rightarrow 0$) and a tuning of model parameters ($\Phi_{\text{GGP}} = \mathcal{N}$). Furthermore, this simple example already shows that a stabilizing pressure p_θ is necessary for a thick brane, but also that $p_\theta \rightarrow 0$ as $\epsilon \rightarrow 0$, allowing for a consistent delta description as in Sec. 7.2.

But now we can even make a precise statement about the required tuning beyond the idealized delta brane limit. The phenomenological bound (7.3.16) requires (recall that we are working in units in which $\kappa = 1$)

$$10^{-120} \stackrel{!}{\sim} \frac{\hat{\mathcal{R}}}{V} \sim \delta\Phi^3, \quad (7.3.23)$$

where the second estimate used (and extrapolated) our numerically inferred scaling relations [neglecting the $\mathcal{O}(1)$ coefficients], cf. Fig. 7.3. Therefore, the parameter $\mathcal{N} \equiv 2\pi n/\tilde{e}$ must be tuned close to $\Phi_{\text{GGP}} \equiv \frac{2\pi}{\epsilon}\sqrt{\alpha_+\alpha_-} + \Phi_+$ with a precision of $\sim 10^{-40}$. This is clearly not better than the CC problem we started with. It is crucial to note

²⁶Incidentally, it turns out that without warping, i.e. for $\alpha_+ = \alpha_-$, the scalings are somewhat different: $\hat{\mathcal{R}} \propto V^{-3}$, $\delta\Phi \propto V^{-2}$ and $p_\theta \propto V^{-2}$. However, this does not help with the tuning problem discussed below.

that this can also directly be read as a tuning relation for the brane tension λ , since $\alpha_+ = 1 - \lambda/2\pi$.

But—as already anticipated in Sec. 7.3.4—there is also another problem regarding phenomenology, even if we allow for such a tuning: For $\delta\Phi \sim 10^{-40}$, the extra space volume would be $V \sim 10^{40}$, grossly violating the bound (7.3.17). Thus, by tuning $\hat{\mathcal{R}}$ small enough, we have at the same time tuned the extra space volume 12 orders of magnitude larger than allowed. Alternatively, if we require V to satisfy the observational bound (7.3.17), $\hat{\mathcal{R}}$ would still be 36 orders of magnitude larger than what is observed. Hence, as it stands, the model suffers not only from a tuning problem, but is not even phenomenologically viable.

This nicely agrees with the analytic discussion in Sec. 7.3.4. Explicitly, we confirmed the relation (7.3.13) (here for $\tau = 0$), finding the coefficient $N_2 = 3.16$ for this specific set of parameters, i.e. e , ρ_+ , Φ_+ and α_{\pm} as given in (7.3.21). Now, since the resulting failure to get both $\hat{\mathcal{R}}$ and V within their phenomenological bounds is the central result of this work, it is worthwhile to discuss its robustness.

First, it should be noted that the main reason for this result can be traced back to the $\mathcal{O}(\epsilon)$ contributions to the 4D curvature $\hat{\mathcal{R}}$, cf. Eq. (7.3.8), which are caused by endowing the brane with a finite width. Hence, they are unavoidable in a (realistic) thick brane setup; of course, we did our explicit calculations only in one particular regularization, but the standard EFT reasoning suggests that the qualitative answer would be the same for any other reasonable regularization.²⁷ While there are additional contributions to $\hat{\mathcal{R}}$ if the dilaton couplings break SI, see Eq. (7.3.13), they can only make things worse (unless there were a miraculous cancellation—a possibility that we dismiss in the search of a natural solution to the CC problem). Again, this will be explicitly confirmed in the following section. Next, we checked numerically that the scaling relation, as well as the order of magnitude of the coefficient N_2 do not change if different tensions (i.e. other generic²⁸ values for α_{\pm}) are chosen. Furthermore, the parameters Φ_+ and e have no influence on the result at all; this is obvious for the BLF Φ_+ , but also easily seen for the gauge coupling e as follows: For the SI couplings we are considering here, the full (regularized) equations of motion enjoy the exact symmetry

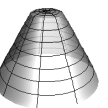
$$e \mapsto ae, \quad Q \mapsto aQ, \quad e^{\phi} \mapsto \frac{1}{a^2} e^{\phi}, \quad (7.3.24)$$

for any constant a . Hence, after changing e , the new solution is simply obtained from the old one by rescaling Q and e^{ϕ} appropriately. Since the metric is unaltered, this leaves $\hat{\mathcal{R}}$ and V unchanged.²⁹ Hence, the only parameter that could change things is ρ_+ , determining the regularization scale $\ell \approx 2\pi\rho_+$, in accordance with the discussion below Eq. (7.3.18).

²⁷One could test this assumption by repeating our analysis e.g. in the UV model proposed in [BDW15a].

²⁸A counterexample is provided by unwarped solutions which are achieved by tuning both tensions equal; in this case the contributions to $\hat{\mathcal{R}}$ would only be $\mathcal{O}(\epsilon^2)$.

²⁹Note that the (bulk) flux transforms as $\Phi \mapsto \Phi/a$, and so \mathcal{N} has to be readjusted accordingly. This, however, does not affect the relation between $\hat{\mathcal{R}}$ and V .



Non scale invariant couplings

We now turn to the case $\tau \neq 0$ (and $\gamma > 0$),³⁰ where SI is broken explicitly via the tension term. The hope is to find values of γ for which no tuning is required in order to achieve a large volume and small curvature. As argued above, this suggests focusing on $\gamma > 0$, because then $V \rightarrow \infty$ drives the model towards the SI case which in turn implies $\hat{\mathcal{R}} \rightarrow 0$. While this case was already discussed in Sec. 7.3.4 under certain reasonable assumptions, the numerical analysis independently confirms the previous results and allows to quantify the amount of tuning necessary to get a viable 4D curvature.

Figure 7.4 shows the numerical results for different values of $\gamma > 0$. Again, small $\hat{\mathcal{R}}$ and large V are generically realized for $\delta\Phi \rightarrow 0$, i.e. if Φ_{GFP} is tuned close to \mathcal{N} . Evidently, both quantities again show a power law dependence on $\delta\Phi$, with exponents which now depend on γ . Empirically, we find the following laws,

$$\hat{\mathcal{R}} \propto \begin{cases} \delta\Phi^{1+1/\gamma} \\ \delta\Phi^2 \end{cases}, \quad V \propto \begin{cases} \delta\Phi^{-1/\gamma} & (\text{for } 0 < \gamma < 1) \\ \delta\Phi^{-1} & (\text{for } 1 < \gamma) \end{cases}, \quad (7.3.25)$$

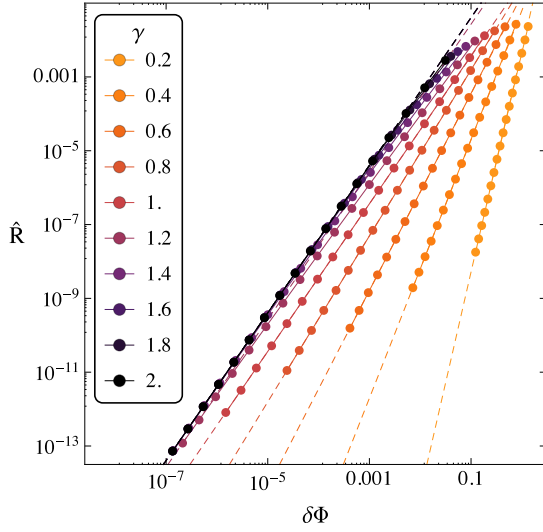
as $\delta\Phi \rightarrow 0$. These are plotted in Figs. 7.4a and 7.4b as dashed lines, and evidently provide very good fits to the numerical data points. Note that the scalings for $\gamma > 1$ are the same as the ones obtained in the SI case $\tau = 0$. The transition to this generic scaling law occurs because for $\gamma > 1$ the finite width effects (which are independent of γ) dominate, cf. Sec. 7.3.3. Also note that combining the scaling relations for $\hat{\mathcal{R}}$ and V exactly reproduces the analytic prediction (7.3.13). For completeness, let us mention that the corresponding numerical coefficient N_1 was found to agree with the analytic prediction (7.3.14) within the numerical uncertainties. Likewise, the scaling relations (7.3.12) for p_θ , which are drawn as dashed lines in Fig. 7.4c, again agree very well with the data. Finally, Fig. 7.4d shows the relation between the dilaton evaluated at the brane and the volume, confirming (7.3.11).

With these results, we can now turn to the tuning question. For $\gamma > 1$, the discussion is exactly the same as for the SI case ($\tau = 0$) above, because the scaling relations are the same. But for $\gamma < 1$ there is a modification: Using the scaling relations (7.3.25), the phenomenological bound (7.3.16) now implies

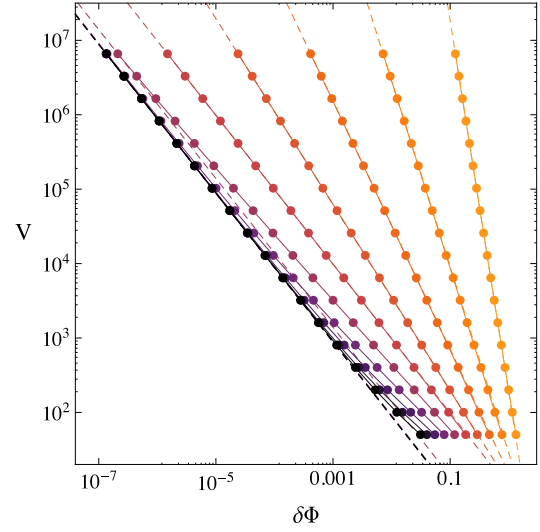
$$10^{-120} \sim \delta\Phi^{1+2/\gamma}. \quad (7.3.26)$$

For $\gamma \lesssim 1$, $\delta\Phi$ still has to be tuned tremendously close to zero; but for $\gamma \ll 1$, this is not the case anymore. Specifically, if we choose $\gamma \approx 1/60$ (which is not hierarchically small), this relation is already fulfilled if $\delta\Phi \sim 0.1$, i.e. without any fine-tuning of model parameters. So we find the remarkable result that the near-SI tension is capable of producing a small 4D curvature and a large volume (as compared to the fundamental bulk scale) without fine-tuning, although this was not possible for a SI tension ($\tau = 0$). At first sight, this looks very promising. However, on closer inspection, there is an even bigger problem with the volume bound (7.3.17) than before, since $\gamma \sim 1/60$ and

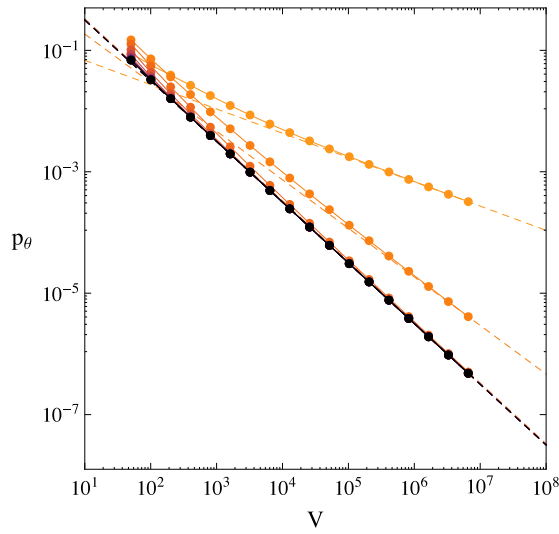
³⁰The case $\gamma = 0$ is still SI and identical to the discussion above after renaming $\lambda + \tau \rightarrow \lambda$.



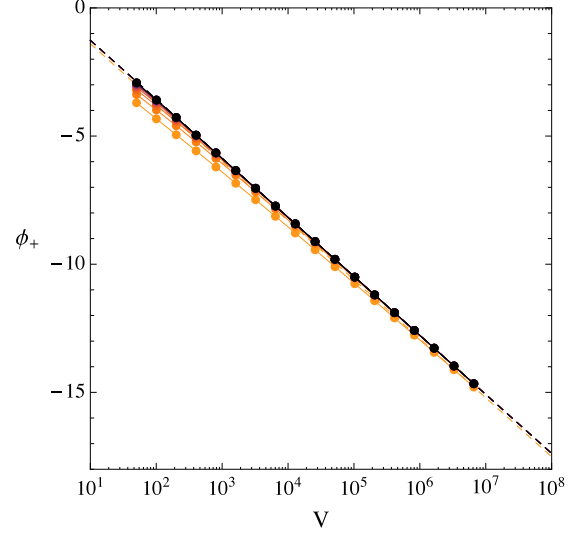
(a) A small 4D curvature $\hat{\mathcal{R}}$ is realized for a small violation $\delta\Phi$ of the GGP tuning relation.



(b) A large extra space volume V is achieved for a small $\delta\Phi$.



(c) The angular pressure p_θ vanishes in the thin brane limit in accordance with the EFT expectation.



(d) The dilaton evaluated at the brane ϕ_+ controls the extra space volume V via (7.3.11).

Figure 7.4: Numerical results for the parameters (7.3.21) and different values of the SI breaking parameter γ . Each dot corresponds to a separate run; the numerical uncertainties were always smaller than the point sizes. The dashed lines show power law fits with exponents as given in (7.3.25) and (7.3.12), as well as the exact analytic prediction (7.3.11), which are always approached as $V \rightarrow \infty$. Whenever the scaling is γ independent, there are several data points which lie on top of each other.



$\delta\Phi \sim 0.1$ now yields $V \sim 10^{60}$, exceeding the bound by 32 orders of magnitude. In turn, if we chose $\gamma \sim 1/28$, so that the volume satisfies the bound for $\delta\Phi \sim 0.1$, then $\hat{\mathcal{R}} \sim 10^{-57} M_{\text{Pl}}^2$, which is 63 orders of magnitude larger than its observational bound.

In summary, while it is possible to get small $\hat{\mathcal{R}}$ and large V without tuning Φ_{GGP} extremely close to \mathcal{N} , it is not possible for both of them to satisfy their phenomenological bounds, in accordance with the general discussion in Sec. 7.3.4.

Let us note that this possibility of getting a large volume without large parameter hierarchies was also recently observed in [BDW15c], where the same model was studied in a dimensionally reduced, effective 4D theory. However, there it was also assumed that it would at the same time be possible to have $\hat{\mathcal{R}}$ within its bounds (possibly via some independent fine-tuning), so that the model could in this way at least address the electroweak hierarchy problem (albeit not the CC problem). Here we found that this is not possible, because $\hat{\mathcal{R}}$ and V are not independent, and so one cannot tune $\hat{\mathcal{R}}$ without at the same time ruining the value of V .

7.4 Conclusion

In this chapter, we investigated the question whether the codimension-two degravitation mechanism can be successfully used to solve the CC problem in the case of *compact* extra dimensions, focusing on the SLED model [ABPQ04]. A major difficulty is that the flux quantization condition, which is necessary to stabilize the compact extra space, reintroduces a fine-tuning of the brane tension in order to obtain degravitating, i.e. 4D flat solutions. The idea of [BvN11, BvN13] was to circumvent this problem by introducing a BLF. If this term does not couple to the dilaton, it adds a dilaton-dependent contribution to the total magnetic flux, so that flux quantization fixes the dilaton zero mode (which can readjust dynamically) instead of imposing a tuning relation.

In the first part, we revealed the problem with this BLF proposal: The crucial feature with respect to the CC problem, namely the existence of 4D flat solutions, is only preserved if the BLF is *scale invariant*—and not if it is dilaton independent as was previously claimed [BvN11, BvN13]. But in this case, the dilaton drops out of the flux quantization condition, and the tuning problem gets restored. In other words, the BLF does not add anything new to the story; in fact, the exact same picture would have emerged without BLF, if SI were broken by a dilaton dependent tension.

The crucial technical ingredient in our derivation was the addition of a counter term that is necessary (and sufficient) to dispose of divergences which are caused by the BLF. As a consistency check, we found agreement of our result with a recent analysis based on a specific UV model [BDW15a], as expected from an EFT point of view.

Our result can nicely be reconciled with Weinberg’s argument (cf. Sec. 1.2.1): Since the extra space is compact,³¹ one can always construct a Kaluza-Klein reduced effective 4D theory. From this point of view, Weinberg tells us that scale invariance can be used

³¹Note that this is a crucial difference to the BIG scenario.

to guarantee flat solutions, but only at the price of yet another fine-tuning—otherwise there would only be runaway solutions.

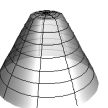
The remaining hope for the SLED program then lies within brane couplings which break SI. While these will not lead to 4D flat solutions, it is not a priori clear how large the 4D Ricci scalar $\hat{\mathcal{R}}$ will be, and it might still turn out (due to the degravitation mechanism) to be small enough to comply with observations for natural values of the model parameters. We therefore investigated the model with a SI breaking brane tension³² in the second part of this chapter; specifically, we focused on a tension of the form $\propto e^{\gamma\phi}$, which allows to have both small $\hat{\mathcal{R}}$ and large extra dimensions at the same time. A thorough treatment of this case required to regularize the brane by giving it a finite thickness, which presented the second difference to part I (where only delta branes were studied).

By performing an analytical, as well as a complementary numerical analysis, we were able to infer the impact of the SI breaking tension on $\hat{\mathcal{R}}$, confirming the delta result at leading order. Furthermore, we were able to pin down the amount of tuning due to flux quantization that is required to achieve small values of $\hat{\mathcal{R}}$. While affirming the delta prediction that a fine-tuning is required for 4D flatness, we also found that if $\gamma \ll 1$, $\mathcal{O}(1)$ violations of this tuning can indeed still result in $\hat{\mathcal{R}}$ small enough to be phenomenologically viable. However, all these solutions yielded an extra space volume V way above its current upper limits, unless some model parameters were tuned again.

But an even more important result of our analysis was that the nonzero brane width ℓ led to an additional contribution $\approx \epsilon/V$ to $\hat{\mathcal{R}}$, where $\epsilon \equiv \ell^2/V$. This contribution cannot be seen by studying delta branes, but should be taken into account for any realistic model, because a brane ultimately always comes with some finite microscopic width. The trouble with this unavoidable term is that—if ℓ is not smaller than the bulk Planck length, and the size of the extra dimensions is within current experimental bounds—it gives a contribution to $\hat{\mathcal{R}}$ which is already 36 orders of magnitude above its measured value. Thus, the model (with a super-Planckian brane width) is ruled out phenomenologically, unless there are additional contributions to $\hat{\mathcal{R}}$ which are fine-tuned in order to achieve the required cancellation. But the latter option would presumably not present progress regarding the CC problem. Since this result does not depend at all on the nature of the dilaton-brane couplings (and the corresponding breaking of SI) it provides the most serious challenge for the SLED program. In fact, it is reasonable to expect it also to apply to any other concrete braneworld model with two large extra dimensions, not just to SLED.

Finally, let us note that we performed a purely classical analysis, based on the assumption that all model parameters take generic values set by the fundamental bulk Planck scale. While this makes sure that we do not introduce a priori hierarchies or tunings into the model by hand, it is in principle still possible that some choices which we would regard as “tuned” might in fact not be spoiled by quantum corrections, and

³²We also checked that a SI breaking BLF leads to the same conclusions, in accordance with the expectation from part I.



thus be technically natural.³³ This option can only be checked by performing loop calculations in an explicit brane matter theory, which is beyond the scope of our work; but at the moment we do not see any indications why or how it could be realized. It should be emphasized, however, that our findings are valuable in any case, as they already tell us *which* tunings have to be realized, and would need to be protected against radiative corrections.

³³For instance, we always assumed two different values of the (dilaton independent) brane tensions; if, instead, asymptotically unwarped solutions were possible in a technically natural way, the brane width contributions to $V\hat{\mathcal{R}}$ would only be $\mathcal{O}(\epsilon^2)$. However, even in this most optimistic scenario, these brane width contribution to $\hat{\mathcal{R}}$ would still be 8 orders of magnitude too large.

APPENDIX TO CHAPTER 7

Note: This appendix is to large extend a verbatim reproduction of the corresponding appendix in [NS16a].

7.A Agreement with a specific UV model

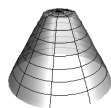
A crucial step in our analysis was the introduction of the counter term in Sec. 7.2.3, which was necessary to handle delta-like branes in the presence of BLF terms. As argued in Sec. 7.2.3, this term is uniquely fixed in the sense that it is necessary and sufficient to remove all divergences, and has all the required symmetries. However, in order to gain more confidence in our approach, it is instructive to compare our results with the ones obtained in a recently proposed UV model [BDW15a]. There, the microscopic degrees of freedom creating the branes are resolved, and the branes have a finite thickness, thus avoiding all divergences. The BLF is modeled by introducing a kinetic mixing of the Maxwell field to another U(1) field. In [BDW15a], only the non-supersymmetric case (without dilaton) was studied. This case is also covered by our analysis, and can be recovered by setting the dilaton to zero ($\phi \equiv 0$), discarding its equation of motion, Sec. 7.2.4, and replacing $2e^2/\kappa^4$ by a bulk CC Λ .

The main result of [BDW15a] was that the BLF “does not gravitate”. This result is recovered in our analysis by noticing that \mathcal{A}_b does not appear in the Einstein equations (7.2.19). Note that in the original equation (7.2.18) it *does* appear; it only drops out after plugging in the solution for the Maxwell field, i.e. it is canceled by the localized contributions from F_{MN} . This is exactly the cancellation mechanism which is describes in the paragraph below Eq. (3.71) in [BDW15a]. In summary, there is no contribution of the localized flux to the 4D Ricci on the brane in the non-SUSY case.

Reference [BDW15a] also discusses how the UV results can be understood in a low energy EFT in which the branes look delta-like. It is also found that a renormalization is necessary to avoid divergent terms in the 4D action. Remarkably, this renormalization is *exactly* the same subtraction scheme we suggested here in Sec. 7.2.3.³⁴ Indeed, Eq. (3.50) in [BDW15a] subtracts exactly our term S_{div} defined in (7.2.11).³⁵ All in all,

³⁴Let us emphasize, though, that our technique and results were communicated to the authors of [BDW15a] long before [BDW15a] appeared.

³⁵However, this subtraction is called a renormalization of the tension in [BDW15a]. As discussed



our EFT analysis is in great agreement with the thorough and detailed UV analysis in [BDW15a], proving once again the usefulness and power of EFT reasoning.

above, we disagree with this statement, because a tension would not have the additional metric dependence $1/\sqrt{g_2}$. Consequently, the counter term enters in the Einstein equation (7.2.18) differently than \mathcal{T}_b .

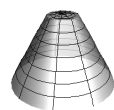
BIBLIOGRAPHY

- [A⁺06] A. Albrecht et al. Report of the Dark Energy Task Force. 2006. [arXiv:astro-ph/0609591](#).
- [A⁺14] P.A.R. Ade et al. Planck 2013 results. XVI. Cosmological parameters. *Astron. Astrophys.*, 571:A16, 2014. [arXiv:1303.5076](#), [doi:10.1051/0004-6361/201321591](#).
- [A⁺15a] P. A. R. Ade et al. Planck 2015 results. XIII. Cosmological parameters. 2015. [arXiv:1502.01589](#).
- [A⁺15b] P. A. R. Ade et al. Planck 2015 results. XX. Constraints on inflation. 2015. [arXiv:1502.02114](#).
- [ABPQ04] Y. Aghababaie, C. P. Burgess, S. L. Parameswaran, and F. Quevedo. Towards a naturally small cosmological constant from branes in 6-D supergravity. *Nucl. Phys.*, B680:389–414, 2004. [arXiv:hep-th/0304256](#), [doi:10.1016/j.nuclphysb.2003.12.015](#).
- [ADM61] R. Arnowitt, S. Deser, and C. W. Misner. Wave Zone in General Relativity. *Phys. Rev.*, 121:1556–1566, Mar 1961. [doi:10.1103/PhysRev.121.1556](#).
- [AG83] P. A. Amundsen and Ø. Grøn. General static plane-symmetric solutions of the Einstein-Maxwell equations. *Phys. Rev.*, D27:1731–1739, Apr 1983. [doi:10.1103/PhysRevD.27.1731](#).
- [AGH00] Bradley Alpert, Leslie Greengard, and Thomas Hagstrom. Rapid Evaluation of Nonreflecting Boundary Kernels for Time-Domain Wave Propagation. *SIAM Journal on Numerical Analysis*, 37(4):1138–1164, 2000. [doi:10.1137/S0036142998336916](#).
- [AGK09] Niayesh Afshordi, Ghazal Geshnizjani, and Justin Khoury. Do observations offer evidence for cosmological-scale extra dimensions? *JCAP*, 0908:030, 2009. [arXiv:0812.2244](#), [doi:10.1088/1475-7516/2009/08/030](#).



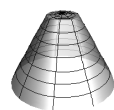
- [AHDD98] Nima Arkani-Hamed, Savas Dimopoulos, and G. R. Dvali. The Hierarchy problem and new dimensions at a millimeter. *Phys. Lett.*, B429:263–272, 1998. [arXiv:hep-ph/9803315](#), [doi:10.1016/S0370-2693\(98\)00466-3](#).
- [AHDDG02] Nima Arkani-Hamed, Savas Dimopoulos, Gia Dvali, and Gregory Gabadadze. Nonlocal modification of gravity and the cosmological constant problem. 2002. [arXiv:hep-th/0209227](#).
- [AHDKS00] Nima Arkani-Hamed, Savas Dimopoulos, Nemanja Kaloper, and Raman Sundrum. A Small cosmological constant from a large extra dimension. *Phys. Lett.*, B480:193–199, 2000. [arXiv:hep-th/0001197](#), [doi:10.1016/S0370-2693\(00\)00359-2](#).
- [AS65] Milton Abramowitz and Irene Stegun. *Handbook of Mathematical Functions with Formulas, Graphs, and Mathematical Tables*. Dover Publications, New York, 1965.
- [AS82] Andreas Albrecht and Paul J. Steinhardt. Cosmology for Grand Unified Theories with Radiatively Induced Symmetry Breaking. *Phys. Rev. Lett.*, 48:1220–1223, Apr 1982. [doi:10.1103/PhysRevLett.48.1220](#).
- [AT92] Theocharis A. Apostolatos and Kip S. Thorne. Rotation halts cylindrical, relativistic gravitational collapse. *Phys. Rev.*, D46:2435–2444, Sep 1992. [doi:10.1103/PhysRevD.46.2435](#).
- [B⁺14] M. Betoule et al. Improved cosmological constraints from a joint analysis of the SDSS-II and SNLS supernova samples. *Astron. Astrophys.*, 568:A22, 2014. [arXiv:1401.4064](#), [doi:10.1051/0004-6361/201423413](#).
- [Bae06] John Baez. What exactly is wrong with Huygens’ principle in two dimensions?, December 2006. URL: <http://sci.physics.research.narkive.com/RdBW05TY/what-exactly-is-wrong-with-huygens-principle-in-two-dimensions#post7>.
- [BB02] Christopher Beetle and Lior M. Burko. A Radiation Scalar for Numerical Relativity. *Phys. Rev. Lett.*, 89:271101, Dec 2002. [doi:10.1103/PhysRevLett.89.271101](#).
- [BBvN10] Allan Bayntun, C. P. Burgess, and Leo van Nierop. Codimension-2 Brane-Bulk Matching: Examples from Six and Ten Dimensions. *New J. Phys.*, 12:075015, 2010. [arXiv:0912.3039](#), [doi:10.1088/1367-2630/12/7/075015](#).
- [BDEL00] Pierre Binétruy, Cedric Deffayet, Ulrich Ellwanger, and David Langlois. Brane cosmological evolution in a bulk with cosmological constant. *Phys. Lett.*, B477:285–291, 2000. [arXiv:hep-th/9910219](#), [doi:10.1016/S0370-2693\(00\)00204-5](#).

- [BDL00] Pierre Binetruy, Cedric Deffayet, and David Langlois. Nonconventional cosmology from a brane universe. *Nucl. Phys.*, B565:269–287, 2000. [arXiv:hep-th/9905012](#), [doi:10.1016/S0550-3213\(99\)00696-3](#).
- [BDW15a] C. P. Burgess, R. Diener, and M. Williams. The Gravity of Dark Vortices: Effective Field Theory for Branes and Strings Carrying Localized Flux. *JHEP*, 11:049, 2015. [arXiv:1506.08095](#), [doi:10.1007/JHEP11\(2015\)049](#).
- [BDW15b] C. P. Burgess, Ross Diener, and M. Williams. EFT for Vortices with Dilaton-dependent Localized Flux. *JHEP*, 11:054, 2015. [arXiv:1508.00856](#), [doi:10.1007/JHEP11\(2015\)054](#).
- [BDW15c] C. P. Burgess, Ross Diener, and M. Williams. Self-Tuning at Large (Distances): 4D Description of Runaway Dilaton Capture. *JHEP*, 10:177, 2015. [arXiv:1509.04209](#), [doi:10.1007/JHEP10\(2015\)177](#).
- [BDW16] C. P. Burgess, Ross Diener, and M. Williams. A problem with delta-functions: stress-energy constraints on bulk-brane matching (with comments on arXiv:1508.01124). *JHEP*, 01:017, 2016. [arXiv:1509.04201](#), [doi:10.1007/JHEP01\(2016\)017](#).
- [BH10] B. Bassett and R. Hlozek. Baryon acoustic oscillations. In P. Ruiz-Lapuente, editor, *Dark Energy: Observational and Theoretical Approaches*, pages 246–278. Cambridge University Press, 2010.
- [BHdRT09] C.P. Burgess, D. Hoover, C. de Rham, and G. Tasinato. Effective Field Theories and Matching for Codimension-2 Branes. *JHEP*, 0903:124, 2009. [arXiv:0812.3820](#), [doi:10.1088/1126-6708/2009/03/124](#).
- [BHN12] Felix Berkhahn, Stefan Hofmann, and Florian Niedermann. Brane Induced Gravity: From a No-Go to a No-Ghost Theorem. *Phys. Rev.*, D86:124022, 2012. [arXiv:1205.6801](#), [doi:10.1103/PhysRevD.86.124022](#).
- [BHS05] Gianfranco Bertone, Dan Hooper, and Joseph Silk. Particle dark matter: Evidence, candidates and constraints. *Phys. Rept.*, 405:279–390, 2005. [arXiv:hep-ph/0404175](#), [doi:10.1016/j.physrep.2004.08.031](#).
- [BPRSU14] Jose J. Blanco-Pillado, Borja Reina, Kepa Sousa, and Jon Urrestilla. Supermassive Cosmic String Compactifications. *JCAP*, 1406:001, 2014. [arXiv:1312.5441](#), [doi:10.1088/1475-7516/2014/06/001](#).
- [Bri25] H. W. Brinkmann. Einstein spaces which are mapped conformally on each other. *Math. Ann.*, 94:119–145, 1925.
- [Bro15] Kevin Brown. Huygens’ principle, 1994–2015. URL: <http://www.mathpages.com/home/kmath242/kmath242.htm>.



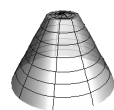
- [BST83] James M. Bardeen, Paul J. Steinhardt, and Michael S. Turner. Spontaneous creation of almost scale-free density perturbations in an inflationary universe. *Phys. Rev.*, D28:679–693, Aug 1983. doi:10.1103/PhysRevD.28.679.
- [Bur04] C. P. Burgess. Quantum gravity in everyday life: General relativity as an effective field theory. *Living Rev. Rel.*, 7:5–56, 2004. arXiv:gr-qc/0311082, doi:10.12942/lrr-2004-5.
- [Bur13] C. P. Burgess. The Cosmological Constant Problem: Why it’s hard to get Dark Energy from Micro-physics. In *100e Ecole d’Ete de Physique: Post-Planck Cosmology Les Houches, France, July 8-August 2, 2013*, 2013. URL: <http://inspirehep.net/record/1254422/files/arXiv:1309.4133.pdf>, arXiv:1309.4133.
- [BvN11] C. P. Burgess and L. van Nierop. Large Dimensions and Small Curvatures from Supersymmetric Brane Back-reaction. *JHEP*, 04:078, 2011. arXiv:1101.0152, doi:10.1007/JHEP04(2011)078.
- [BvN13] C.P. Burgess and Leo van Nierop. Technically Natural Cosmological Constant From Supersymmetric 6D Brane Backreaction. *Phys. Dark Univ.*, 2:1–16, 2013. arXiv:1108.0345, doi:10.1016/j.dark.2012.10.001.
- [BvNW14a] C. P. Burgess, L. van Nierop, and M. Williams. Distributed SUSY breaking: dark energy, Newton’s law and the LHC. *JHEP*, 07:034, 2014. arXiv:1311.3911, doi:10.1007/JHEP07(2014)034.
- [BvNW14b] C. P. Burgess, L. van Nierop, and M. Williams. Gravitational Forces on a Codimension-2 Brane. *JHEP*, 04:032, 2014. arXiv:1401.0511, doi:10.1007/JHEP04(2014)032.
- [C⁺11] A. Conley et al. Supernova Constraints and Systematic Uncertainties from the First Three Years of the Supernova Legacy Survey. *The Astrophysical Journal Supplement Series*, 192(1):1, 2011. URL: <http://stacks.iop.org/0067-0049/192/i=1/a=1>.
- [Car04] Sean Carroll. *Spacetime and Geometry. An introduction to General Relativity*. Addison Wesley, San Francisco, California, 2004.
- [CFPS12] Timothy Clifton, Pedro G. Ferreira, Antonio Padilla, and Constantinos Skordis. Modified Gravity and Cosmology. *Phys. Rept.*, 513:1–189, 2012. arXiv:1106.2476, doi:10.1016/j.physrep.2012.01.001.
- [CG03] Sean M. Carroll and Monica M. Guica. Sidestepping the cosmological constant with football shaped extra dimensions. 2003. arXiv:hep-th/0302067.

- [CGKP06] Christos Charmousis, Ruth Gregory, Nemanja Kaloper, and Antonio Padilla. DGP Spectroscopy. *JHEP*, 10:066, 2006. [arXiv:hep-th/0604086](#), [doi:10.1088/1126-6708/2006/10/066](#).
- [Cho98] Inyong Cho. Inflation and nonsingular space-times of cosmic strings. *Phys. Rev.*, D58:103509, 1998. [arXiv:gr-qc/9804086](#), [doi:10.1103/PhysRevD.58.103509](#).
- [CHT03] Sean M. Carroll, Mark Hoffman, and Mark Trodden. Can the dark energy equation - of - state parameter w be less than -1? *Phys. Rev.*, D68:023509, 2003. [arXiv:astro-ph/0301273](#), [doi:10.1103/PhysRevD.68.023509](#).
- [CLP00] Jiunn-Wei Chen, Markus A. Luty, and Eduardo Ponton. A Critical cosmological constant from millimeter extra dimensions. *JHEP*, 09:012, 2000. [arXiv:hep-th/0003067](#), [doi:10.1088/1126-6708/2000/09/012](#).
- [CLV99] M. Christensen, A. L. Larsen, and Y. Verbin. Complete classification of the string - like solutions of the gravitating Abelian Higgs model. *Phys. Rev.*, D60:125012, 1999. [arXiv:gr-qc/9904049](#), [doi:10.1103/PhysRevD.60.125012](#).
- [CMPP04] A. Coley, R. Milson, Vojtech Pravda, and A. Pravdova. Classification of the Weyl tensor in higher dimensions. *Class. Quant. Grav.*, 21:L35-L42, 2004. [arXiv:gr-qc/0401008](#).
- [dB10] W. J. G. de Blok. The Core-Cusp Problem. *Advances in Astronomy*, 2010:5, 2010. [arXiv:0910.3538](#), [doi:10.1155/2010/789293](#).
- [DD00] Nathalie Deruelle and Tomas Dolezel. Brane versus shell cosmologies in Einstein and Einstein-Gauss-Bonnet theories. *Phys. Rev.*, D62:103502, 2000. [arXiv:gr-qc/0004021](#), [doi:10.1103/PhysRevD.62.103502](#).
- [DDG02] Cedric Deffayet, G.R. Dvali, and Gregory Gabadadze. Accelerated universe from gravity leaking to extra dimensions. *Phys. Rev.*, D65:044023, 2002. [arXiv:astro-ph/0105068](#), [doi:10.1103/PhysRevD.65.044023](#).
- [DDGV02] Cedric Deffayet, G. R. Dvali, Gregory Gabadadze, and Arkady I. Vainshtein. Nonperturbative continuity in graviton mass versus perturbative discontinuity. *Phys. Rev.*, D65:044026, 2002. [arXiv:hep-th/0106001](#), [doi:10.1103/PhysRevD.65.044026](#).
- [Def01] Cedric Deffayet. Cosmology on a brane in Minkowski bulk. *Phys. Lett.*, B502:199-208, 2001. [arXiv:hep-th/0010186](#), [doi:10.1016/S0370-2693\(01\)00160-5](#).
- [DG01] G. R. Dvali and Gregory Gabadadze. Gravity on a brane in infinite volume extra space. *Phys. Rev.*, D63:065007, 2001. [arXiv:hep-th/0008054](#), [doi:10.1103/PhysRevD.63.065007](#).



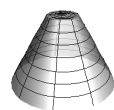
- [DGHS03] Gia Dvali, Gregory Gabadadze, Xin-rui Hou, and Emiliano Sefusatti. Seesaw modification of gravity. *Phys. Rev.*, D67:044019, 2003. [arXiv:hep-th/0111266](#), [doi:10.1103/PhysRevD.67.044019](#).
- [DGI06] Cedric Deffayet, Gregory Gabadadze, and Alberto Iglesias. Perturbations of Self-Accelerated Universe. *JCAP*, 0608:012, 2006. [arXiv:hep-th/0607099](#), [doi:10.1088/1475-7516/2006/08/012](#).
- [DGP00] G. R. Dvali, Gregory Gabadadze, and Massimo Porrati. 4-D gravity on a brane in 5-D Minkowski space. *Phys. Lett.*, B485:208–214, 2000. [arXiv:hep-th/0005016](#), [doi:10.1016/S0370-2693\(00\)00669-9](#).
- [DGS02] Gia Dvali, Gregory Gabadadze, and M. Shifman. Diluting cosmological constant via large distance modification of gravity. pages 566–581, 2002. [arXiv:hep-th/0208096](#).
- [DGS03] Gia Dvali, Gregory Gabadadze, and M. Shifman. Diluting cosmological constant in infinite volume extra dimensions. *Phys. Rev.*, D67:044020, 2003. [arXiv:hep-th/0202174](#), [doi:10.1103/PhysRevD.67.044020](#).
- [DHK07] Gia Dvali, Stefan Hofmann, and Justin Khoury. Degravitation of the cosmological constant and graviton width. *Phys. Rev.*, D76:084006, 2007. [arXiv:hep-th/0703027](#), [doi:10.1103/PhysRevD.76.084006](#).
- [Don94a] John F. Donoghue. General relativity as an effective field theory: The leading quantum corrections. *Phys. Rev.*, D50:3874–3888, 1994. [arXiv:gr-qc/9405057](#), [doi:10.1103/PhysRevD.50.3874](#).
- [Don94b] John F. Donoghue. Leading quantum correction to the Newtonian potential. *Phys. Rev. Lett.*, 72:2996–2999, 1994. [arXiv:gr-qc/9310024](#), [doi:10.1103/PhysRevLett.72.2996](#).
- [DPPR10] Mark Durkee, Vojt Pravda, Alena Pravdova, and Harvey S. Reall. Generalization of the Geroch-Held-Penrose formalism to higher dimensions. *Class. Quant Grav.*, 27:215010, 2010. [arXiv:1002.4826](#), [doi:10.1088/0264-9381/27/21/215010](#).
- [DR03] S. L. Dubovsky and V. A. Rubakov. Brane-induced gravity in more than one extra dimension: Violation of equivalence principle and ghost. *Phys. Rev.*, D67:104014, May 2003. [doi:10.1103/PhysRevD.67.104014](#).
- [dRHKT08] Claudia de Rham, Stefan Hofmann, Justin Khoury, and Andrew J. Tolley. Cascading Gravity and Degravitation. *JCAP*, 0802:011, 2008. [arXiv:0712.2821](#), [doi:10.1088/1475-7516/2008/02/011](#).
- [Dva06] Gia Dvali. Predictive Power of Strong Coupling in Theories with Large Distance Modified Gravity. *New J. Phys.*, 8:326, 2006. [arXiv:hep-th/0610013](#), [doi:10.1088/1367-2630/8/12/326](#).

- [Ech93] Fernando Echeverria. Gravitational collapse of an infinite, cylindrical dust shell. *Phys. Rev.*, D47:2271–2282, Mar 1993. doi:[10.1103/PhysRevD.47.2271](https://doi.org/10.1103/PhysRevD.47.2271).
- [Ein16a] Albert Einstein. Die Grundlage der allgemeinen Relativitätstheorie. *Ann. Phys.*, 49:769–822, 1916. doi:[10.1002/andp.200590044](https://doi.org/10.1002/andp.200590044).
- [Ein16b] Albert Einstein. Hamiltonsches Prinzip und allgemeine Relativitätstheorie. *Preuss. Akad. Wiss. Berlin, Sitzungsber.*, pages 1111–1116, 1916. URL: <http://echo.mpiwg-berlin.mpg.de/MPIWG:90NOCB46>.
- [ENS15] Ludwig Eglseer, Florian Niedermann, and Robert Schneider. Brane induced gravity: Ghosts and naturalness. *Phys. Rev.*, D92(8):084029, 2015. arXiv:[1506.02666](https://arxiv.org/abs/1506.02666), doi:[10.1103/PhysRevD.92.084029](https://doi.org/10.1103/PhysRevD.92.084029).
- [ER37] A. Einstein and N. Rosen. On gravitational waves. *Journal of the Franklin Institute*, 223(1):43 – 54, 1937. doi:[10.1016/S0016-0032\(37\)90583-0](https://doi.org/10.1016/S0016-0032(37)90583-0).
- [Fix09] D. J. Fixsen. The Temperature of the Cosmic Microwave Background. *The Astrophysical Journal*, 707(2):916, 2009. URL: <http://stacks.iop.org/0004-637X/707/i=2/a=916>.
- [Fre82] Peter G.O. Freund. Kaluza-Klein Cosmologies. *Nucl. Phys.*, B209:146, 1982. doi:[10.1016/0550-3213\(82\)90106-7](https://doi.org/10.1016/0550-3213(82)90106-7).
- [Fri22] A. Friedmann. Über die Krümmung des Raumes. *Zeitschrift für Physik*, 10(1):377–386, 1922. doi:[10.1007/BF01332580](https://doi.org/10.1007/BF01332580).
- [Fri24] A. Friedmann. Über die Möglichkeit einer Welt mit konstanter negativer Krümmung des Raumes. *Zeitschrift für Physik*, 21(1):326–332, 1924. doi:[10.1007/BF01328280](https://doi.org/10.1007/BF01328280).
- [FWH⁺08] Wenjuan Fang, Sheng Wang, Wayne Hu, Zoltan Haiman, Lam Hui, and Morgan May. Challenges to the DGP Model from Horizon-Scale Growth and Geometry. *Phys. Rev.*, D78:103509, 2008. arXiv:[0808.2208](https://arxiv.org/abs/0808.2208), doi:[10.1103/PhysRevD.78.103509](https://doi.org/10.1103/PhysRevD.78.103509).
- [GGP04] G. W. Gibbons, Rahmi Gueven, and C. N. Pope. 3-branes and uniqueness of the Salam-Sezgin vacuum. *Phys. Lett.*, B595:498–504, 2004. arXiv:[hep-th/0307238](https://arxiv.org/abs/hep-th/0307238), doi:[10.1016/j.physletb.2004.06.048](https://doi.org/10.1016/j.physletb.2004.06.048).
- [GH77] G. W. Gibbons and S. W. Hawking. Action integrals and partition functions in quantum gravity. *Phys. Rev.*, D15:2752–2756, May 1977. doi:[10.1103/PhysRevD.15.2752](https://doi.org/10.1103/PhysRevD.15.2752).
- [Giv91] Dan Givoli. Non-reflecting Boundary Conditions. *J. Comput. Phys.*, 94(1):1–29, May 1991. doi:[10.1016/0021-9991\(91\)90135-8](https://doi.org/10.1016/0021-9991(91)90135-8).



- [GKMP07] Ruth Gregory, Nemanja Kaloper, Robert C. Myers, and Antonio Padilla. A New perspective on DGP gravity. *JHEP*, 0710:069, 2007. [arXiv:0707.2666](#), [doi:10.1088/1126-6708/2007/10/069](#).
- [GKS06] Dmitry Gorbunov, Kazuya Koyama, and Sergei Sibiryakov. More on ghosts in DGP model. *Phys. Rev.*, D73:044016, 2006. [arXiv:hep-th/0512097](#), [doi:10.1103/PhysRevD.73.044016](#).
- [Got85] III Gott, J. Richard. Gravitational lensing effects of vacuum strings: Exact solutions. *Astrophys. J.*, 288:422–427, 1985. [doi:10.1086/162808](#).
- [Gow71] Robert H. Gowdy. Gravitational Waves in Closed Universes. *Phys. Rev. Lett.*, 27:826–829, Sep 1971. [doi:10.1103/PhysRevLett.27.826](#).
- [GP82] Alan H. Guth and So-Young Pi. Fluctuations in the New Inflationary Universe. *Phys. Rev. Lett.*, 49:1110–1113, Oct 1982. [doi:10.1103/PhysRevLett.49.1110](#).
- [GP04] Jaume Garriga and Massimo Porrati. Football shaped extra dimensions and the absence of self-tuning. *JHEP*, 08:028, 2004. [arXiv:hep-th/0406158](#), [doi:10.1088/1126-6708/2004/08/028](#).
- [Gre96] Ruth Gregory. Cosmic p-branes. *Nucl. Phys.*, B467:159–182, 1996. [arXiv:hep-th/9510202](#), [doi:10.1016/0550-3213\(96\)00089-2](#).
- [Gre03] Ruth Gregory. Inflating p-branes. *JHEP*, 0306:041, 2003. [arXiv:hep-th/0304262](#), [doi:10.1088/1126-6708/2003/06/041](#).
- [Gru05] Andrei Gruzinov. On the graviton mass. *New Astron.*, 10:311–314, 2005. [arXiv:astro-ph/0112246](#), [doi:10.1016/j.newast.2004.12.001](#).
- [Gut81] Alan H. Guth. Inflationary universe: A possible solution to the horizon and flatness problems. *Phys. Rev.*, D23:347–356, Jan 1981. [doi:10.1103/PhysRevD.23.347](#).
- [Had52] Jacques Hadamard. *Lectures on Cauchy's Problem in Linear Partial Differential Equations*. Dover Publications, Inc., New York, 1952.
- [Haw82] S. W. Hawking. The development of irregularities in a single bubble inflationary universe. *Phys. Lett.*, B115(4):295 – 297, 1982. [doi:10.1016/0370-2693\(82\)90373-2](#).
- [HGLM03] Peter Hoflich, C. Gerardy, E. Linder, and H. Marion. Models for Type Ia supernovae and cosmology. *Lect. Notes Phys.*, 635:203, 2003. [arXiv:astro-ph/0301334](#), [doi:10.1007/978-3-540-39882-0_11](#).

- [HHvS11] S.F. Hassan, Stefan Hofmann, and Mikael von Strauss. Brane Induced Gravity, its Ghost and the Cosmological Constant Problem. *JCAP*, 1101:020, 2011. [arXiv:1007.1263](#), [doi:10.1088/1475-7516/2011/01/020](#).
- [Hil15] David Hilbert. Grundlagen der Physik, Erste Mitteilung, vorgelegt in der Sitzung vom 20. November 1915. *Königl. Gesell. Wiss. Göttingen, Nachr., Math.-Physik. Kl.*, pages 395–407, 1915. URL: <http://echo.mpiwg-berlin.mpg.de/MPIWG:234X0D0W>.
- [His85] W. A. Hiscock. Exact Gravitational Field of a String. *Phys. Rev.*, D31:3288–3290, 1985. [doi:10.1103/PhysRevD.31.3288](#).
- [HNS13] Stefan Hofmann, Florian Niedermann, and Robert Schneider. Interpretation of the Weyl tensor. *Phys. Rev.*, D88:064047, 2013. [arXiv:1308.0010](#), [doi:10.1103/PhysRevD.88.064047](#).
- [Hub29] Edwin Hubble. A relation between distance and radial velocity among extra-galactic nebulae. *Proceedings of the National Academy of Sciences*, 15(3):168–173, 1929. [doi:10.1073/pnas.15.3.168](#).
- [IMM⁺09] Fabio Iocco, Gianpiero Mangano, Gennaro Miele, Ofelia Pisanti, and Pasquale D. Serpico. Primordial Nucleosynthesis: from precision cosmology to fundamental physics. *Phys. Rept.*, 472:1–76, 2009. [arXiv:0809.0631](#), [doi:10.1016/j.physrep.2009.02.002](#).
- [Isr66] W. Israel. Singular hypersurfaces and thin shells in general relativity. *Il Nuovo Cimento B Series 10*, 44(1):1–14, 1966. [doi:10.1007/BF02710419](#).
- [Isr67] W. Israel. Singular hypersurfaces and thin shells in general relativity. *Il Nuovo Cimento B Series 10*, 48(2):463–463, 1967. [doi:10.1007/BF02712210](#).
- [K⁺10] P. Kroupa et al. Local-Group tests of dark-matter concordance cosmology . Towards a new paradigm for structure formation. *Astronomy and Astrophysics*, 523:A32, November 2010. [arXiv:1006.1647](#), [doi:10.1051/0004-6361/201014892](#).
- [Kal21] Theodor Kaluza. Zum Unitätsproblem der Physik. *Sitzungsber. Preuss. Akad. Wiss. Berlin (Math. Phys.)*, 1921:966–972, 1921.
- [KCA⁺07] D. J. Kapner, T. S. Cook, E. G. Adelberger, J. H. Gundlach, B. R. Heckel, C. D. Hoyle, and H. E. Swanson. Tests of the Gravitational Inverse-Square Law below the Dark-Energy Length Scale. *Phys. Rev. Lett.*, 98:021101, Jan 2007. [doi:10.1103/PhysRevLett.98.021101](#).



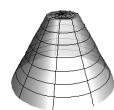
- [KG89] J. B. Keller and D. Givoli. Exact Non-reflecting Boundary Conditions. *J. Comput. Phys.*, 82(1):172–192, May 1989. doi:[10.1016/0021-9991\(89\)90041-7](https://doi.org/10.1016/0021-9991(89)90041-7).
- [KK07] Nemanja Kaloper and Derrick Kiley. Charting the landscape of modified gravity. *JHEP*, 0705:045, 2007. arXiv:[hep-th/0703190](https://arxiv.org/abs/hep-th/0703190), doi:[10.1088/1126-6708/2007/05/045](https://doi.org/10.1088/1126-6708/2007/05/045).
- [Kle26] Oskar Klein. Quantum Theory and Five-Dimensional Theory of Relativity. (In German and English). *Z. Phys.*, 37:895–906, 1926. doi:[10.1007/BF01397481](https://doi.org/10.1007/BF01397481).
- [Koy05] Kazuya Koyama. Are there ghosts in the self-accelerating brane universe? *Phys. Rev.*, D72:123511, 2005. arXiv:[hep-th/0503191](https://arxiv.org/abs/hep-th/0503191), doi:[10.1103/PhysRevD.72.123511](https://doi.org/10.1103/PhysRevD.72.123511).
- [KP14] Nemanja Kaloper and Antonio Padilla. Vacuum Energy Sequestering: The Framework and Its Cosmological Consequences. *Phys. Rev.*, D90(8):084023, 2014. arXiv:[1406.0711](https://arxiv.org/abs/1406.0711), doi:[10.1103/PhysRevD.90.084023](https://doi.org/10.1103/PhysRevD.90.084023), [10.1103/PhysRevD.90.109901](https://doi.org/10.1103/PhysRevD.90.109901).
- [KPSS15] Nemanja Kaloper, Antonio Padilla, Paul Saffin, and David Stefanyszyn. Unitarity and the Vainshtein Mechanism. *Phys. Rev.*, D91(4):045017, 2015. arXiv:[1409.3243](https://arxiv.org/abs/1409.3243), doi:[10.1103/PhysRevD.91.045017](https://doi.org/10.1103/PhysRevD.91.045017).
- [KS07] Kazuya Koyama and Fabio P. Silva. Non-linear interactions in a cosmological background in the DGP braneworld. *Phys. Rev.*, D75:084040, 2007. arXiv:[hep-th/0702169](https://arxiv.org/abs/hep-th/0702169), doi:[10.1103/PhysRevD.75.084040](https://doi.org/10.1103/PhysRevD.75.084040).
- [KSS00] Shamit Kachru, Michael B. Schulz, and Eva Silverstein. Selftuning flat domain walls in 5-D gravity and string theory. *Phys. Rev.*, D62:045021, 2000. arXiv:[hep-th/0001206](https://arxiv.org/abs/hep-th/0001206), doi:[10.1103/PhysRevD.62.045021](https://doi.org/10.1103/PhysRevD.62.045021).
- [Lev18] T. Levi-Civita. ds^2 einsteiniani in campi newtoniani. V: Il sottocaso B_2 : Soluzioni longitudinali ($\xi = 0$). *Rom. Acc. L. Rend. (5)*, 27(2):240–248, 1918.
- [Lev19] T. Levi-Civita. IX: L’analogo del potenziale logaritmico. *Rom. Acc. L. Rend. (5)*, 28(1):101–109, 1919.
- [LG89] P. Laguna and D. Garfinkle. Space-time of Supermassive U(1) Gauge Cosmic Strings. *Phys. Rev.*, D40:1011–1016, 1989. doi:[10.1103/PhysRevD.40.1011](https://doi.org/10.1103/PhysRevD.40.1011).
- [Lin82] A.D. Linde. A new inflationary universe scenario: A possible solution of the horizon, flatness, homogeneity, isotropy and primordial monopole problems. *Phys. Lett.*, B108(6):389 – 393, 1982. doi:[10.1016/0370-2693\(82\)91219-9](https://doi.org/10.1016/0370-2693(82)91219-9).

- [Lin90] B. Linet. On the supermassive U(1) gauge cosmic strings. *Class. Quant. Grav.*, 7:L75–L79, 1990. doi:10.1088/0264-9381/7/3/002.
- [Lin96] Andrei D. Linde. Monopoles as big as a universe and the universe inside a bubble. *Int. J. Mod. Phys.*, D5:845–867, 1996. doi:10.1142/S0218271896000515.
- [LL94] Andrei D. Linde and Dmitri A. Linde. Topological defects as seeds for eternal inflation. *Phys. Rev.*, D50:2456–2468, 1994. arXiv:hep-th/9402115, doi:10.1103/PhysRevD.50.2456.
- [LPR03] Markus A. Luty, Massimo Porrati, and Riccardo Rattazzi. Strong interactions and stability in the DGP model. *JHEP*, 09:029, 2003. arXiv:hep-th/0303116, doi:10.1088/1126-6708/2003/09/029.
- [Mar58] L. Marder. Gravitational Waves in General Relativity. I. Cylindrical Waves. *Proceedings of the Royal Society of London. Series A, Mathematical and Physical Sciences*, 244(1239):pp. 524–537, 1958. URL: <http://www.jstor.org/stable/100266>.
- [MC81] V. F. Mukhanov and G. V. Chibisov. Quantum fluctuations and a non-singular universe. *JETP Letters*, 33:532 – 535, May 1981.
- [MGG+99] B. Moore, S. Ghigna, F. Governato, G. Lake, Thomas R. Quinn, et al. Dark matter substructure within galactic halos. *Astrophys. J.*, 524:L19–L22, 1999. arXiv:astro-ph/9907411, doi:10.1086/312287.
- [MK10] Roy Maartens and Kazuya Koyama. Brane-World Gravity. *Living Rev. Rel.*, 13(5), 2010. doi:10.1007/lrr-2010-5.
- [MS93] Marc Mars and Jose M. M. Senovilla. Axial symmetry and conformal Killing vectors. *Class. Quant. Grav.*, 10:1633–1647, 1993. arXiv:gr-qc/0201045, doi:10.1088/0264-9381/10/8/020.
- [MSBdB00] Stacy S. McGaugh, Jim M. Schombert, Greg D. Bothun, and W.J.G. de Blok. The Baryonic Tully-Fisher relation. *Astrophys. J.*, 533:L99–L102, 2000. arXiv:astro-ph/0003001, doi:10.1086/312628.
- [MTW73] Charles W. Misner, Kip S. Thorne, and John Archibald Wheeler. *Gravitation*. W. H. Freeman and Company, New York, 1973.
- [Muk05] Viatcheslav Mukhanov. *Physical Foundations of Cosmology*. Cambridge University Press, New York, 2005.
- [Nav03a] Ignacio Navarro. Codimension two compactifications and the cosmological constant problem. *JCAP*, 0309:004, 2003. arXiv:hep-th/0302129, doi:10.1088/1475-7516/2003/09/004.



- [Nav03b] Ignacio Navarro. Spheres, deficit angles and the cosmological constant. *Class. Quant. Grav.*, 20:3603–3612, 2003. [arXiv:hep-th/0305014](#), [doi:10.1088/0264-9381/20/16/306](#).
- [NBBR06] Andrea Nerozzi, Marco Bruni, Lior M. Burko, and Virginia Re. Towards a novel wave-extraction method for numerical relativity. *AIP Conf. Proc.*, 861:702–707, 2006. [arXiv:gr-qc/0607066](#), [doi:10.1063/1.2399646](#).
- [NE08] Andrea Nerozzi and Oliver Elbracht. Using curvature invariants for wave extraction in numerical relativity. 2008. [arXiv:0811.1600](#).
- [NO73] Holger Bech Nielsen and P. Olesen. Vortex Line Models for Dual Strings. *Nucl. Phys.*, B61:45–61, 1973. [doi:10.1016/0550-3213\(73\)90350-7](#).
- [Nol04] Brien C. Nolan. Physical interpretation of gauge invariant perturbations of spherically symmetric space-times. *Phys. Rev.*, D70:044004, Aug 2004. [doi:10.1103/PhysRevD.70.044004](#).
- [NPT04] Hans-Peter Nilles, Antonios Papazoglou, and Gianmassimo Tasinato. Selftuning and its footprints. *Nucl. Phys.*, B677:405–429, 2004. [arXiv:hep-th/0309042](#), [doi:10.1016/j.nuclphysb.2003.11.003](#).
- [NR04] Alberto Nicolis and Riccardo Rattazzi. Classical and quantum consistency of the DGP model. *JHEP*, 06:059, 2004. [arXiv:hep-th/0404159](#), [doi:10.1088/1126-6708/2004/06/059](#).
- [NS05] Ignacio Navarro and José Santiago. Gravity on codimension 2 brane worlds. *JHEP*, 2005(02):007, 2005. URL: <http://stacks.iop.org/1126-6708/2005/i=02/a=007>.
- [NS15a] Florian Niedermann and Robert Schneider. Cosmology on a cosmic ring. *JCAP*, 2015(03):050, 2015. URL: <http://stacks.iop.org/1475-7516/2015/i=03/a=050>.
- [NS15b] Florian Niedermann and Robert Schneider. Radially stabilized inflating cosmic strings. *Phys. Rev.*, D91(6):064010, 2015. [arXiv:1412.2750](#), [doi:10.1103/PhysRevD.91.064010](#).
- [NS16a] Florian Niedermann and Robert Schneider. Fine-tuning with Brane-Localized Flux in 6D Supergravity. *JHEP*, 02:025, 2016. [arXiv:1508.01124](#), [doi:10.1007/JHEP02\(2016\)025](#).
- [NS16b] Florian Niedermann and Robert Schneider. SLED Phenomenology: Curvature vs. Volume. *JHEP*, 03:130, 2016. [arXiv:1512.03800](#), [doi:10.1007/JHEP03\(2016\)130](#).

- [NSHK15] Florian Niedermann, Robert Schneider, Stefan Hofmann, and Justin Khoury. Universe as a cosmic string. *Phys. Rev.*, D91(2):024002, 2015. [arXiv:1410.0700](#), [doi:10.1103/PhysRevD.91.024002](#).
- [OGP09] Eimear O’Callaghan, Ruth Gregory, and Alkistis Pourtsidou. The Cosmology of Asymmetric Brane Modified Gravity. *JCAP*, 0909:020, 2009. [arXiv:0904.4182](#), [doi:10.1088/1475-7516/2009/09/020](#).
- [Ort91] Miguel E. Ortiz. A New look at supermassive cosmic strings. *Phys. Rev.*, D43:2521–2526, 1991. [doi:10.1103/PhysRevD.43.2521](#).
- [P+12] S. Perlmutter et al. Supernova Cosmology Project. <http://supernova.lbl.gov/Union/>, July 2012.
- [Pad05a] Antonio Padilla. Cosmic acceleration from asymmetric branes. *Class. Quant. Grav.*, 22:681–694, 2005. [arXiv:hep-th/0406157](#), [doi:10.1088/0264-9381/22/4/003](#).
- [Pad05b] Antonio Padilla. Infra-red modification of gravity from asymmetric branes. *Class. Quant. Grav.*, 22:1087–1104, 2005. [arXiv:hep-th/0410033](#), [doi:10.1088/0264-9381/22/6/011](#).
- [Pad07] Antonio Padilla. A Short review of ‘DGP spectroscopy’. *J. Phys.*, A40:6827–6834, 2007. [arXiv:hep-th/0610093](#), [doi:10.1088/1751-8113/40/25/S26](#).
- [Pir56] F. A. E. Pirani. On the physical significance of the Riemann tensor. *Acta Physica Polonica*, 15:389–405, 1956.
- [Pir57] F. A. E. Pirani. Invariant Formulation of Gravitational Radiation Theory. *Phys. Rev.*, 105:1089–1099, Feb 1957. [doi:10.1103/PhysRev.105.1089](#).
- [Pir09] Felix A. E. Pirani. Republication of: On the physical significance of the Riemann tensor. *General Relativity and Gravitation*, 41(5):1215–1232, 2009. [doi:10.1007/s10714-009-0787-9](#).
- [Por02] M. Porrati. Fully covariant van Dam-Veltman-Zakharov discontinuity, and absence thereof. *Phys. Lett.*, B534:209–215, 2002. [arXiv:hep-th/0203014](#), [doi:10.1016/S0370-2693\(02\)01656-8](#).
- [PQ77a] R. D. Peccei and Helen R. Quinn. Constraints imposed by CP conservation in the presence of pseudoparticles. *Phys. Rev.*, D16:1791–1797, Sep 1977. [doi:10.1103/PhysRevD.16.1791](#).
- [PQ77b] R. D. Peccei and Helen R. Quinn. CP Conservation in the Presence of Pseudoparticles. *Phys. Rev. Lett.*, 38:1440–1443, Jun 1977. [doi:10.1103/PhysRevLett.38.1440](#).



- [PS12] Jiri Podolsky and Robert Svarc. Interpreting spacetimes of any dimension using geodesic deviation. *Phys. Rev.*, D85:044057, 2012. [arXiv:1201.4790](#), [doi:10.1103/PhysRevD.85.044057](#).
- [PTVF92] William H. Press, Saul A. Teukolsky, William T. Vetterling, and Brian P. Flannery. *Numerical Recipes in C: The Art of Scientific Computing*. Cambridge University Press, New York, NY, USA, 2 edition, 1992.
- [PW65] A. A. Penzias and R. W. Wilson. A Measurement of Excess Antenna Temperature at 4080 Mc/s. *Astrophysical Journal*, 142:419–421, 1965. [doi:10.1086/148307](#).
- [R⁺11] Adam G. Riess et al. A 3Space Telescope and Wide Field Camera 3. *The Astrophysical Journal*, 730(2):119, 2011. URL: <http://stacks.iop.org/0004-637X/730/i=2/a=119>.
- [RDSS83] S. Randjbar-Daemi, Abdus Salam, and J. Strathdee. Spontaneous compactification in six-dimensional Einstein-Maxwell theory. *Nucl. Phys.*, B214(3):491 – 512, 1983. [doi:10.1016/0550-3213\(83\)90247-X](#).
- [RS83] V. A. Rubakov and M. E. Shaposhnikov. Do We Live Inside a Domain Wall? *Phys. Lett.*, B125:136–138, 1983. [doi:10.1016/0370-2693\(83\)91253-4](#).
- [RS99a] Lisa Randall and Raman Sundrum. A Large mass hierarchy from a small extra dimension. *Phys. Rev. Lett.*, 83:3370–3373, 1999. [arXiv:hep-ph/9905221](#), [doi:10.1103/PhysRevLett.83.3370](#).
- [RS99b] Lisa Randall and Raman Sundrum. An Alternative to compactification. *Phys. Rev. Lett.*, 83:4690–4693, 1999. [arXiv:hep-th/9906064](#), [doi:10.1103/PhysRevLett.83.4690](#).
- [RT60] Ivor Robinson and A. Trautman. Spherical Gravitational Waves. *Phys. Rev. Lett.*, 4:431–432, Apr 1960. [doi:10.1103/PhysRevLett.4.431](#).
- [Rub03] V. A. Rubakov. Strong coupling in brane induced gravity in five-dimensions. 2003. [arXiv:hep-th/0303125](#).
- [S⁺12] Morag I. Scrimgeour et al. The WiggleZ Dark Energy Survey: the transition to large-scale cosmic homogeneity. *Monthly Notices of the Royal Astronomical Society*, 425(1):116–134, 2012. [doi:10.1111/j.1365-2966.2012.21402.x](#).
- [Sbi15] Fulvio Sbisà. Classical and quantum ghosts. *Eur. J. Phys.*, 36:015009, 2015. [arXiv:1406.4550](#), [doi:10.1088/0143-0807/36/1/015009](#).

- [SKM⁺03] Hans Stephani, Dietrich Kramer, Malcolm MacCallum, Cornerlius Hoenselaers, and Eduard Herlt. *Exact Solutions of Einstein's Field Equations*. Cambridge University Press, second edition, 2003.
- [Sta82] A. A. Starobinsky. Dynamics of phase transition in the new inflationary universe scenario and generation of perturbations. *Phys. Lett.*, B117(3-4):175 – 178, 1982. doi:[10.1016/0370-2693\(82\)90541-X](https://doi.org/10.1016/0370-2693(82)90541-X).
- [Ste03] Gary Steigman. Big bang nucleosynthesis: Probing the first 20 minutes. *Measuring and Modeling the Universe*, pages 169–195, 2003. arXiv:[astro-ph/0307244](https://arxiv.org/abs/astro-ph/0307244).
- [Sun99] Raman Sundrum. Compactification for a three-brane universe. *Phys. Rev.*, D59:085010, 1999. arXiv:[hep-ph/9807348](https://arxiv.org/abs/hep-ph/9807348), doi:[10.1103/PhysRevD.59.085010](https://doi.org/10.1103/PhysRevD.59.085010).
- [SYPB09] Prakash Sarkar, Jaswant Yadav, Biswajit Pandey, and Somnath Bhadravaj. The scale of homogeneity of the galaxy distribution in SDSS DR6. *Monthly Notices of the Royal Astronomical Society: Letters*, 399(1):L128–L131, 2009. doi:[10.1111/j.1745-3933.2009.00738.x](https://doi.org/10.1111/j.1745-3933.2009.00738.x).
- [Sze65] P. Szekeres. The Gravitational compass. *J. Math. Phys.*, 6:1387–1391, 1965.
- [Tau51] A. H. Taub. Empty Space-Times Admitting a Three Parameter Group of Motions. *Annals of Mathematics*, 53(3):pp. 472–490, 1951. URL: <http://www.jstor.org/stable/1969567>.
- [Tho65] Kip S. Thorne. Energy of Infinitely Long, Cylindrically Symmetric Systems in General Relativity. *Phys. Rev.*, 138:B251–B266, Apr 1965. doi:[10.1103/PhysRev.138.B251](https://doi.org/10.1103/PhysRev.138.B251).
- [Vai72] A. I. Vainshtein. To the problem of nonvanishing gravitation mass. *Phys. Lett.*, B39:393–394, 1972. doi:[10.1016/0370-2693\(72\)90147-5](https://doi.org/10.1016/0370-2693(72)90147-5).
- [vDV70] H. van Dam and M. J. G. Veltman. Massive and massless Yang-Mills and gravitational fields. *Nucl. Phys.*, B22:397–411, 1970. doi:[10.1016/0550-3213\(70\)90416-5](https://doi.org/10.1016/0550-3213(70)90416-5).
- [Vil81] A. Vilenkin. Gravitational Field of Vacuum Domain Walls and Strings. *Phys. Rev.*, D23:852–857, 1981. doi:[10.1103/PhysRevD.23.852](https://doi.org/10.1103/PhysRevD.23.852).
- [Vil94] Alexander Vilenkin. Topological inflation. *Phys. Rev. Lett.*, 72:3137–3140, 1994. arXiv:[hep-th/9402085](https://arxiv.org/abs/hep-th/9402085), doi:[10.1103/PhysRevLett.72.3137](https://doi.org/10.1103/PhysRevLett.72.3137).
- [Wal84] Robert M. Wald. *General Relativity*. The University of Chicago Press, Chicago and London, 1984.



- [Wan91] Anzhong Wang. Gravitational Faraday rotation induced from interacting gravitational plane waves. *Phys. Rev.*, D44:1120–1131, 1991. doi:10.1103/PhysRevD.44.1120.
- [Wei72] Steven Weinberg. *Gravitation and Cosmology. Principles and Applications of the General Theory of Relativity*. John Wiley & Sons, Inc., New York, 1972.
- [Wei89] Steven Weinberg. The Cosmological Constant Problem. *Rev. Mod. Phys.*, 61:1–23, 1989. doi:10.1103/RevModPhys.61.1.
- [Wei96] Steven Weinberg. Theories of the cosmological constant. In *Critical dialogues in cosmology. Proceedings, Celebration of the 250th Anniversary of Princeton University, Princeton, USA, June 24-27, 1996*, 1996. URL: <http://alice.cern.ch/format/showfull?sysnb=0234881>, arXiv:astro-ph/9610044.
- [Wei08] Steven Weinberg. *Cosmology*. Oxford University Press, New York, 2008.
- [Wil06] Clifford M. Will. The Confrontation between general relativity and experiment. *Living Rev. Rel.*, 9:3, 2006. arXiv:gr-qc/0510072, doi:10.12942/lrr-2006-3.
- [Wit82] Edward Witten. Instability of the Kaluza-Klein vacuum. *Nucl. Phys.*, B195(3):481 – 492, 1982. doi:10.1016/0550-3213(82)90007-4.
- [Woo07] Richard P. Woodard. Avoiding dark energy with $1/r$ modifications of gravity. *Lect. Notes Phys.*, 720:403–433, 2007. arXiv:astro-ph/0601672, doi:10.1007/978-3-540-71013-4_14.
- [Xu14] Lixin Xu. Confronting DGP braneworld gravity with cosmic observations after Planck data. *JCAP*, 1402:048, 2014. arXiv:1312.4679, doi:10.1088/1475-7516/2014/02/048.
- [Yor72] James W. York. Role of Conformal Three-Geometry in the Dynamics of Gravitation. *Phys. Rev. Lett.*, 28:1082–1085, Apr 1972. doi:10.1103/PhysRevLett.28.1082.
- [Zak70] V. I. Zakharov. Linearized gravitation theory and the graviton mass. *JETP Lett.*, 12:312, 1970. [Pisma Zh. Eksp. Teor. Fiz.12,447(1970)].

ACKNOWLEDGMENTS

First, I want to thank my supervisor Stefan Hofmann for his great support and encouragement over the past years. He has been an amazing mentor, and I am deeply grateful for the many inspiring, open-minded discussions about physics, but also about music, sci-fi, life, the universe and everything. I will truly miss our lunchtime at the “Lo”.

I also would like to express my gratitude to Gia Dvali for agreeing to be the second supervisor, for many helpful discussions and for sharing his inspiring, unique view and understanding of theoretical physics. Furthermore, I thank Jochen Weller and Otmar Biebel for completing my PhD committee.

I am indebted to my friend and colleague Florian Niedermann for an outstanding and enormously fruitful collaboration, as well as countless discussions and insights about physics. Basically none of the results would have been obtained without this teamwork, neither would the time at the LMU, UPenn and PI have been as enjoyable as it was.

A special thanks goes to Justin Khoury, whose collaboration initiated a major breakthrough in the cosmic string project. Moreover, I thank him for the opportunity to visit the UPenn, and for numerous inspiring and enlightening discussions and a stimulating exchange of ideas. I am also grateful to Cliff Burgess for hosting me at the PI, and I thank him, Ross Diener and Matt Williams for a vivid communication. Let me also thank Stanley Deser for his interest in our Weyl paper and for an interesting subsequent discussion about gravitational waves.

Furthermore, I would like to thank all of my colleagues at the LMU, in particular Felix Berkhahn, Michael Kopp, Cora Uhlemann, Tehseen Rug, Dennis Schimmel, Sophia Müller, Parvin Moyassari, Cristiano Germani, Slava Emelyanov, Thomas Haugg, Ludwig Eglseer and Marc Schneider for many interesting and helpful discussions, and for making the LMU a great place to work at. I especially appreciate Tehseen and Florian proofreading parts of this thesis. I also thank Herta Wiesbeck-Yonis for her administrative support, and I acknowledge the financial support by the DFG cluster of excellence “Origin and Structure of the Universe”.

My deepest gratitude goes to my parents, for supporting me in any possible way throughout my life, and to my wonderful girlfriend Judith, for always being there for me, encouraging me and for filling my life with joy.